NEUROMECHANICS IN MOVEMENT AND DISEASE WITH PHYSIOLOGICAL AND PATHOPHYSIOLOGICAL IMPLICATIONS: FROM FUNDAMENTAL EXPERIMENTS TO BIO-INSPIRED TECHNOLOGIES

EDITED BY: Ramona Ritzmann, Christoph Centner, Alessandro Del Vecchio, Albert Gollhofer, Marco Vincenzo Narici, Nicolas Place and Stéphane Baudry

PUBLISHED IN: Frontiers in Physiology, Frontiers in Bioengineering and Biotechnology and Frontiers in Human Neuroscience

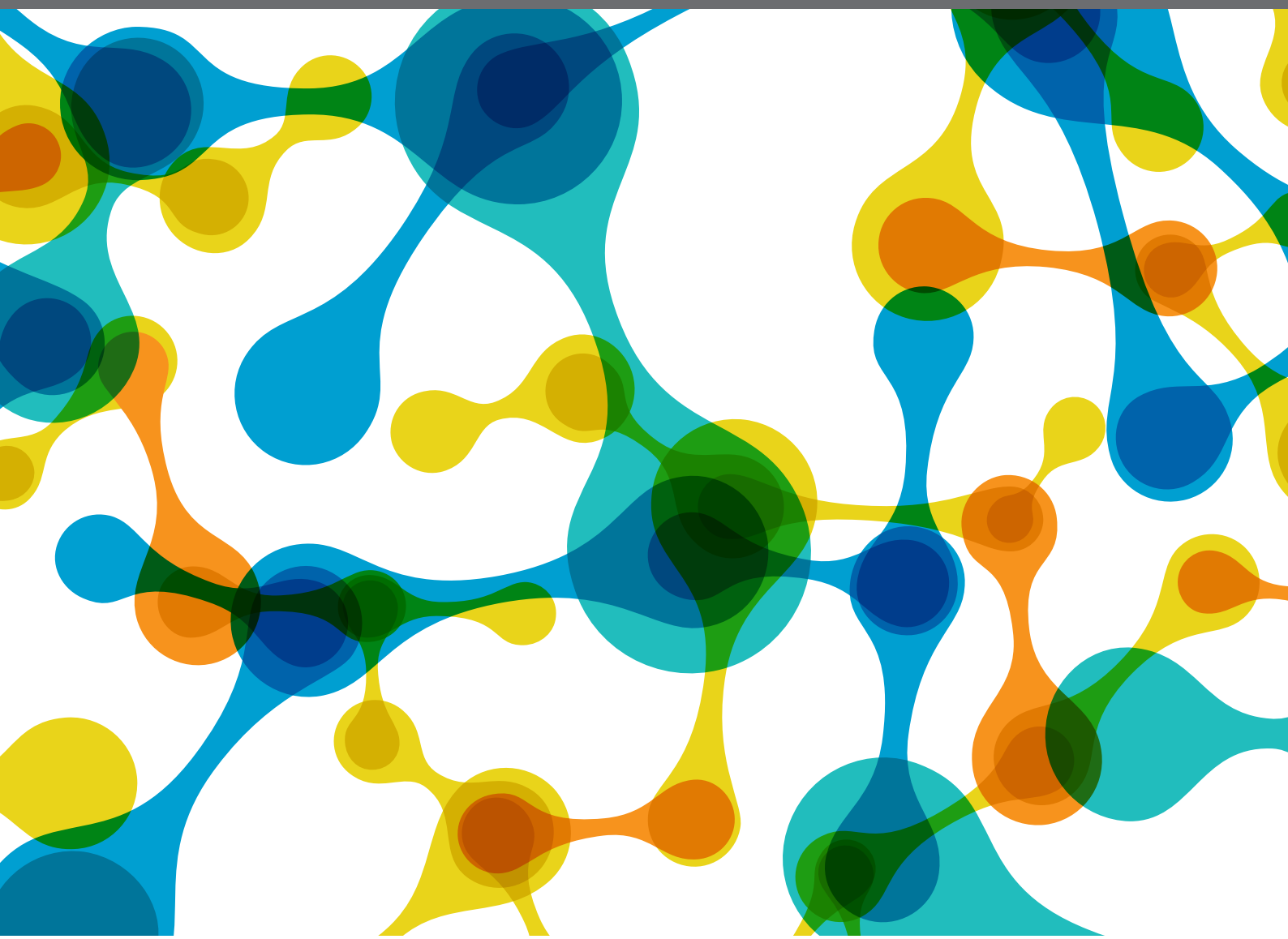

frontiers Research Topics

ISSN 1664-8714
ISBN 978-2-88976-119-7
DOI 10.3389/978-2-88976-119-7

About Frontiers

Frontiers is more than just an open-access publisher of scholarly articles: it is a pioneering approach to the world of academia, radically improving the way scholarly research is managed. The grand vision of Frontiers is a world where all people have an equal opportunity to seek, share and generate knowledge. Frontiers provides immediate and permanent online open access to all its publications, but this alone is not enough to realize our grand goals.

Frontiers Journal Series

The Frontiers Journal Series is a multi-tier and interdisciplinary set of open-access, online journals, promising a paradigm shift from the current review, selection and dissemination processes in academic publishing. All Frontiers journals are driven by researchers for researchers; therefore, they constitute a service to the scholarly community. At the same time, the Frontiers Journal Series operates on a revolutionary invention, the tiered publishing system, initially addressing specific communities of scholars, and gradually climbing up to broader public understanding, thus serving the interests of the lay society, too.

Dedication to Quality

Each Frontiers article is a landmark of the highest quality, thanks to genuinely collaborative interactions between authors and review editors, who include some of the world's best academicians. Research must be certified by peers before entering a stream of knowledge that may eventually reach the public - and shape society; therefore, Frontiers only applies the most rigorous and unbiased reviews.
Frontiers revolutionizes research publishing by freely delivering the most outstanding research, evaluated with no bias from both the academic and social point of view. By applying the most advanced information technologies, Frontiers is catapulting scholarly publishing into a new generation.

What are Frontiers Research Topics?

Frontiers Research Topics are very popular trademarks of the Frontiers Journals Series: they are collections of at least ten articles, all centered on a particular subject. With their unique mix of varied contributions from Original Research to Review Articles, Frontiers Research Topics unify the most influential researchers, the latest key findings and historical advances in a hot research area! Find out more on how to host your own Frontiers Research Topic or contribute to one as an author by contacting the Frontiers Editorial Office: frontiersin.org/about/contact

NEUROMECHANICS IN MOVEMENT AND DISEASE WITH PHYSIOLOGICAL AND PATHOPHYSIOLOGICAL IMPLICATIONS: FROM FUNDAMENTAL EXPERIMENTS TO BIO-INSPIRED TECHNOLOGIES

Topic Editors:
Ramona Ritzmann, Clinic Rennbahn AG, Switzerland
Christoph Centner, University of Freiburg, Germany
Alessandro Del Vecchio, University of Erlangen Nuremberg, Germany
Albert Gollhofer, University of Freiburg, Germany
Marco Vincenzo Narici, University of Padua, Italy
Nicolas Place, University of Lausanne, Switzerland
Stéphane Baudry, Université libre de Bruxelles, Belgium

Citation: Ritzmann, R., Centner, C., Del Vecchio, A., Gollhofer, A., Narici, M. V., Place, N., Baudry, S., eds. (2022). Neuromechanics in Movement and Disease With Physiological and Pathophysiological Implications: From Fundamental Experiments to Bio-Inspired Technologies. Lausanne: Frontiers Media SA.
doi: 10.3389/978-2-88976-119-7

Table of Contents

frontiers | Frontiers in Physiology

EDITORIAL
published: 14 April 2022
doi: 10.3389/fphys.2022.895968

Editorial: Neuromechanics in Movement and Disease With Physiological and Pathophysiological Implications: From Fundamental Experiments to Bio-Inspired Technologies

Ramona Ritzmann[1], Alessandro Del Vecchio[2], Stéphane Baudry[3], Nicolas Place[4], Albert Gollhofer[1], Marco Narici[5] and Christoph Centner[1]*

[1]Department of Sport and Sport Science, University of Freiburg, Freiburg, Germany, [2]Department of AI in Biomedical Engineering, University of Erlangen-Nuernberg, Erlangen, Germany, [3]Laboratory of Applied Biololgy and Research Unit in Applied Neurophysiology (LABNeuro), Faculty of Motor Sciences, Université Libre de Bruxelles, Bruxelles, Belgium, [4]Institut des Sciences du Sport, University of Lausanne, Lausanne, Switzerland, [5]Neuromuscular Physiology Laboratory, Department of Biomedical Sciences, University of Padua, Padua, Italy

Keywords: sensory, muscle, tendon, computational neuroscience, simulation, robotic, brain

Editorial on the Research Topic

Neuromechanics in Movement and Disease With Physiological and Pathophysiological Implications: From Fundamental Experiments to Bio-Inspired Technologies

OPEN ACCESS

Edited and reviewed by:
Giuseppe D'Antona, University of Pavia, Italy

****Correspondence:***
Ramona Ritzmann
ramona.ritzmann@sport.uni-freiburg.de

Specialty section:
This article was submitted to Exercise Physiology, a section of the journal Frontiers in Physiology

Received: *14 March 2022*
Accepted: *24 March 2022*
Published: *14 April 2022*

Citation:
Ritzmann R, Del Vecchio A, Baudry S, Place N, Gollhofer A, Narici M and Centner C (2022) Editorial: Neuromechanics in Movement and Disease With Physiological and Pathophysiological Implications: From Fundamental Experiments to Bio-Inspired Technologies. Front. Physiol. 13:895968. doi: 10.3389/fphys.2022.895968

NEUROMECHANICS: THE WHY AND THE HOW

Coordinated motor function in humans is characterized by a complex interplay between neuromuscular Kalc et al. and musculoskeletal elements Smart et al. Within the field of neuromechanics, neuroscience (e.g., assessment of neural control mechanisms *via* neuroimaging or neurophysiology for spinal and supraspinal areas), biomechanics (e.g., architectural muscle and tendon physiology, kinematics, kinetic characteristics), physiology (e.g., electromyography, *in vivo* bio-imagery) and technical approaches (e.g., computational neuroscience, humanoid robotics and bionic modelling) are combined to contribute to an holistic understanding of human movement Mohr et al.; Fauvet et al.; Ogasawara et al., through its underlying physiological processes and its adaptations to physical activity or chronic disuse Divjak et al. Transdisciplinary methodological techniques and integrative approaches exist to unravel paradigms of coordinated sensorimotor control, interventions and technologies to restore motor function, rehabilitation or movement optimization (**Figure 1**). These paradigms are used to predict the pattern of muscle activation Munoz-Martel et al. and the transmission of force *via* tendons to the skeleton Smart et al. They allow understanding how movement is anticipated Munoz-Martel et al., proactively generated and controlled in humans. Their clinical applications include easing health problems and designing and controlling bio-inspired robotic systems. Importantly, biological actuators are different from their mechatronic counterparts in terms of form and function Morasso; therefore coherence is achieved throughout progressive scientific evidence at the transdisciplinary conjunction. In this context, neuromechanics is not restricted to studying movement control Hofstetter et al., motor learning Morasso, in healthy individuals, but also helps to explain motor deficits in clinically relevant areas with reference to diseases and injuries.

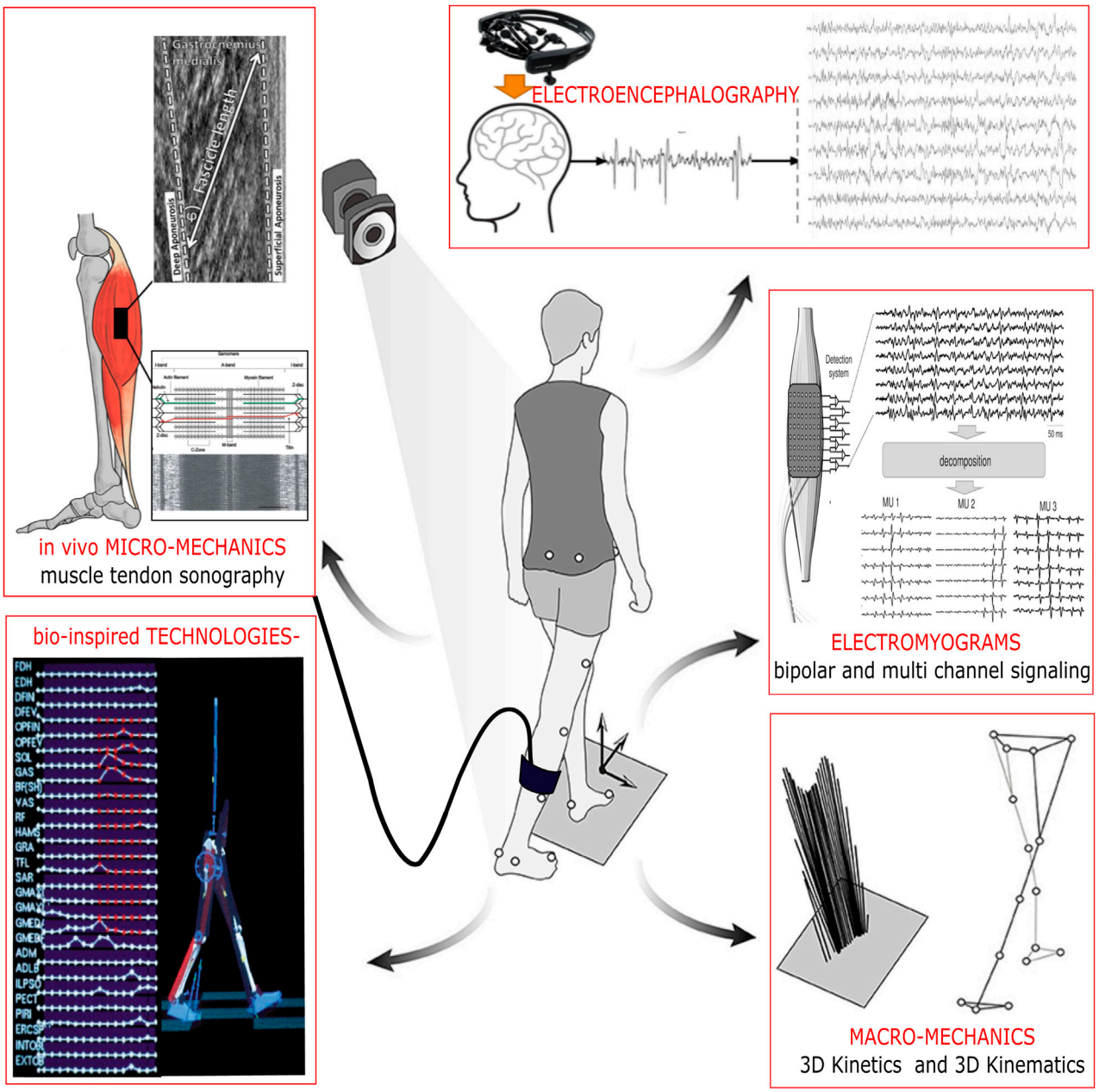

FIGURE 1 | The neural control of human movement is characterized by the resulting micro- and micromechanics. Scientific evidence from holistic experiments is aiding in the development of new therapeutic approaches and bio-inspired technologies to improve motor control in healthy individuals and patients and trigger long-term adaptations.

PHYSIOLOGICAL AND PATHOPHYSIOLOGICAL IMPLICATIONS

Examining the interplay between neural, and biomechanical and environmental dynamics serves as a unique approach for understanding the holistic framework of motor behaviors in both healthy and diseased individuals. Previous evidence indicates that biological and technical systems cannot be interpreted independently but must be integrated in a coherent context to allow to fully capture the complexity of movements (Ting et al., 2015). Several articles in this Research Topic tie in evidence about neuromuscular adaptations and deepen understanding about synergistic and agonistic muscle coordination with an impact on muscle-tendon interaction. For example, changes in micro- and macro-mechanical stress and strain Smart et al. were demonstrated to non-linearly affect monoarticular and complex motion of the entire body. Muscle pre-activation and synergies adopted to changes in movement

anticipation Munoz-Martel et al., spinal excitability decreased with tissue flossing Kalc et al. and antagonistic co-activation Divjak et al. in the lower extremities was sensitive to the level of physical activity and life span in healthy humans. These neuromuscular modulations further took impact on myotendinous conjunction. Smart et al. and Stäudle et al. investigated muscle-tendon interaction and found that mechanical properties and energy management of the tendinous tissue is determined by neuronal innervation, contractile and architectural attributes of the attached muscle. In the transition between micro and macro mechanics and with an emphasis on more complex movements Hofstetter et al. showed that cervical spinal stiffness is segment and load dependent and Mohr et al. specified that upper body and pelvic rotation are sex-specific.

To contribute to the understanding of the pathogenesis of rapid eye movement sleep behavior disorder, Peng et al. analyzed electroencephalography (EEG) microstate characteristics with the aim of validating EEG microstate as an early-stage marker of this disorder. Their findings pointed towards abnormalities in resting-state EEG microstates and indicated that such neurophysiological analyses might complement current clinical concepts in the early detection of rapid eye movement sleep behavior disorder. Through the combined use of EEG, electromyographic (EMG) and kinematic measures, Fauvet et al. investigated the temporal dynamic of cortico-muscular coherence in post-stroke patients in order to investigate whether alterations of the functional coupling between brain and muscles contributes to impairments of motor function. The findings revealed that cortico-muscular coherence in antagonist muscles was higher for post-stroke patients compared to controls during the acceleration phase. The authors propose that this might reflect the loss of sensitivity of motor command occurring after stroke.

High-density EMG decomposition techniques allow an accurate and non-invasive evaluation of MU behavior in various populations and paradigms (Del Vecchio et al., 2020). In a study by Divjak et al., the authors compared the change in MU discharge patterns following 14-days of immobilization in young and older individuals. After analyzing isometric coactivations of the triceps surae and tibialis muscles, the authors demonstrated that changes in MU discharge rates and muscle coactivation patterns seem to be person-specific and dependent on the level of isometric loading. These results also highlighted that before immobilization, younger individuals demonstrated substantially higher inter-person variability in coactivation patterns, which have equalized following 14-days of immobilization.

BIO-INSPIRED TECHNOLOGICAL IMPLICATIONS

In the light of the rapid progress in the field of advanced technological applications and robotics, bio-inspired assistive devices have been successfully designed and integrate physiological inputs to aid human movements Yang and Lee and compensate for impairments in human motor control. With the use of brain computer interfaces (BCIs), neural signals can be implemented to directly operate external devices with real-time feedback. In neurorehabilitation, signals from motor units convey important information about motor control which can be extracted and used to control robotic rehabilitation devices. Besides assessing motor unit behavior *via* invasive needle techniques (Adam et al., 1998), recent advances which use modern decomposition techniques (Del Vecchio et al., 2020) have been demonstrated as valid measures of the circuitries underlying the motor unit and thus motor behavior (Nordstrom et al., 1992; Heckman et al., 2005). From one side, motor unit and EMG properties during synergistic tasks such as locomotion or isometric contractions represent an interface with the neurorehabilitation intervention and supplementary characterization of the pathology, from another side it is possible to use the spared EMG activity after injury (e.g., spinal cord injury or stroke), for controlling assistive devices.

With this regard, BCIs (Collinger et al., 2013), electrical stimulation of the spinal cord (Wenger et al., 2016), and motor neuron interfaces (Farina et al., 2017) have shown the greatest potential in enabling the voluntary control of several degrees of freedom. Recently, Ting et al. (Ting et al., 2021) reported that it is possible to observe distinct patterns of EMG activity in a subject with complete spinal cord injury. Despite voluntary movement of the individual hand digits was not possible, the subject was able to control the activity of a few MUs that were unique for each finger. Future bio-inspired technologies can take advantage of these discharge patterns and novel finding being implemented in neuro-rehabilitation Munoz-Martel et al.

PROSPECT

The present Research Topic aimed to overcome conventional boundaries of physiology, neuroscience and biomechanics to emphasize the interaction between the brain and muscles to produce adequate motor behavior in humans. The understanding of the underlying mechanisms coupled with bio-inspired application technologies will further empower us to revisit current approaches of robotic systems to produce human-like physical behavior or feasible applications in clinical or therapeutic environments. Given the high relevance of this topic, the Research Topic emphasizes fundamental practical applications useful for clinicians and exercise scientists.

AUTHOR CONTRIBUTIONS

All authors listed have made a substantial, direct, and intellectual contribution to the work and approved it for publication.

REFERENCES

Adam, A., Luca, C. J. D., and Erim, Z. (1998). Hand Dominance and Motor Unit Firing Behavior. *J. Neurophysiol.* 80 (3), 1373–1382. doi:10.1152/jn.1998.80.3.1373

Collinger, J. L., Boninger, M. L., Bruns, T. M., Curley, K., Wang, W., and Weber, D. J. (2013). Functional Priorities, Assistive Technology, and Brain-Computer Interfaces after Spinal Cord Injury. *Jrrd* 50 (2), 145–160. doi:10.1682/jrrd.2011.11.0213

Del Vecchio, A., Holobar, A., Falla, D., Felici, F., Enoka, R. M., and Farina, D. (2020). Tutorial: Analysis of Motor Unit Discharge Characteristics from High-Density Surface EMG Signals. *J. Electromyogr. Kinesiol.* 53, 102426. doi:10.1016/j.jelekin.2020.102426

Farina, D., Vujaklija, I., Sartori, M., Kapelner, T., Negro, F., Jiang, N., et al. (2017). Man/machine Interface Based on the Discharge Timings of Spinal Motor Neurons after Targeted Muscle Reinnervation. *Nat. Biomed. Eng.* 1 (2), 0025. doi:10.1038/s41551-016-0025

Heckman, C. J., Gorassini, M. A., and Bennett, D. J. (2005). Persistent Inward Currents in Motoneuron Dendrites: Implications for Motor Output. *Muscle Nerve* 31 (2), 135–156. doi:10.1002/mus.20261

Nordstrom, M. A., Fuglevand, A. J., and Enoka, R. M. (1992). Estimating the Strength of Common Input to Human Motoneurons from the Cross-Correlogram. *J. Physiol.* 453, 547–574. doi:10.1113/jphysiol.1992.sp019244

Ting, J. E., Vecchio, A. D., Sarma, D., Colachis, S. C., Annetta, N. V., Collinger, J. L., et al. (2021). Sensing and Decoding the Neural Drive to Paralyzed Muscles during Attempted Movements of a Person with Tetraplegia Using a Sleeve Array. *medRxiv* 126 (6), 2104–2118. doi:10.1152/jn.00220.2021

Ting, L. H., Chiel, H. J., Trumbower, R. D., Allen, J. L., McKay, J. L., Hackney, M. E., et al. (2015). Neuromechanical Principles Underlying Movement Modularity and Their Implications for Rehabilitation. *Neuron* 86 (1), 38–54. doi:10.1016/j.neuron.2015.02.042

Wenger, N., Moraud, E. M., Gandar, J., Musienko, P., Capogrosso, M., Baud, L., et al. (2016). Spatiotemporal Neuromodulation Therapies Engaging Muscle Synergies Improve Motor Control after Spinal Cord Injury. *Nat. Med.* 22 (2), 138–145. doi:10.1038/nm.4025

Conflict of Interest: The authors declare that the research was conducted in the absence of any commercial or financial relationships that could be construed as a potential conflict of interest.

Publisher's Note: All claims expressed in this article are solely those of the authors and do not necessarily represent those of their affiliated organizations, or those of the publisher, the editors and the reviewers. Any product that may be evaluated in this article, or claim that may be made by its manufacturer, is not guaranteed or endorsed by the publisher.

frontiers in Bioengineering and Biotechnology

ORIGINAL RESEARCH
published: 21 June 2021
doi: 10.3389/fbioe.2021.657357

Sex-Specific Hip Movement Is Correlated With Pelvis and Upper Body Rotation During Running

Maurice Mohr, Robin Pieper, Sina Löffler, Andreas R. Schmidt and Peter A. Federolf*

Department of Sport Science, University of Innsbruck, Innsbruck, Austria

There is a sex bias for common overuse running injuries that are associated with sex-specific hip kinematics. Gait retraining programs aimed at altering hip kinematics may be more efficient if they incorporated an understanding of how hip kinematics are correlated with the movement of the remaining body segments. We applied a principal component analysis to structure the whole-body running kinematics of 23 runners (12 ♀) into k = 12 principal movements (PM_k), describing correlated patterns of upper and lower body movements. We compared the time-dependent movement amplitudes with respect to each PM_k between males and females using a waveform analysis and interpreted our findings according to stick figure animations. The movement amplitudes of two PMs (PM_6 and PM_8) showed statistically significant effects of "sex," which were independent of running speed. According to PM_8, females showed more hip adduction, which correlated with increased transverse rotation of the pelvis and upper body compared to men. We propose that increased hip adduction and upper body rotation in female runners may be a strategy to compensate for a less efficient arm and upper body swing compared to men. Gait interventions aimed at reducing hip adduction and running-related injuries in female runners should consider instructions for both upper and lower body to maximize training efficacy.

Keywords: running injury, knee pain, gender differences, principal component analysis (PCA), gait retraining, patellofemoral pain (PFP), iliotibial band syndrome

OPEN ACCESS

Edited by:
Stéphane Baudry,
Université libre de Bruxelles, Belgium

Reviewed by:
Claudio Pizzolato,
Griffith University, Australia
João Abrantes,
Universidade Lusófona, Portugal

****Correspondence:***
Maurice Mohr
maurice.mohr@uibk.ac.at

Specialty section:
This article was submitted to Biomechanics, a section of the journal Frontiers in Bioengineering and Biotechnology

Received: *22 January 2021*
Accepted: *26 May 2021*
Published: *21 June 2021*

Citation:
Mohr M, Pieper R, Löffler S, Schmidt AR and Federolf PA (2021) Sex-Specific Hip Movement Is Correlated With Pelvis and Upper Body Rotation During Running. Front. Bioeng. Biotechnol. 9:657357. doi: 10.3389/fbioe.2021.657357

INTRODUCTION

Women and men perform many athletic tasks in a sex-specific manner. One important motivation to study sex-specific movement strategies is a range of musculoskeletal sport injuries, which exhibit a bias such that some injuries are more prevalent in women compared to men and vice versa (Taunton et al., 2002; Emery and Tyreman, 2009; Ristolainen et al., 2009). In running, patellofemoral pain (PFP) and iliotibial band syndrome (ITBS) are among the most common injuries and both injuries are more prevalent in women compared to men (Taunton et al., 2002; Boling et al., 2010).

Many authors have investigated sex-specific running kinematics with the most consistent finding that females show a more adducted hip during the stance phase of running (Ferber et al., 2003; Schache et al., 2003; Chumanov et al., 2008; Phinyomark et al., 2014; Sakaguchi et al., 2014;

Willson et al., 2015; Almonroeder and Benson, 2017; Boyer et al., 2017). Traditionally, a more adducted hip is thought to result from sex-specific anthropometrics, especially a greater pelvis width to femoral length ratio in women (Ferber et al., 2003; Chumanov et al., 2008) and has been suggested to contribute to the higher prevalence of PFP in women (Noehren et al., 2007; Neal et al., 2016). Consequently, the goal of several recent interventions in individuals with PFP has been to reduce hip adduction and thereby reduce knee pain (Neal et al., 2016).

While some of these prospective studies have achieved promising pain reductions through hip strengthening and biofeedback-guided gait retraining (Earl and Hoch, 2011; Noehren et al., 2011; Willy et al., 2012), none of the current interventions considers the movement of the upper body during running. Of all cross-sectional studies comparing running kinematics between males and females, only two investigations considered upper body movement and both demonstrated larger oscillations in pelvic and lumbar axial rotation in female compared to male runners (Schache et al., 2003; Bruening et al., 2020). The authors of the most recent report on sex-specific running kinematics speculated that there may be a functional relationship between observed differences in hip, pelvis, and upper body movement but acknowledged that this relationship remains poorly understood (Bruening et al., 2020). A better understanding of sex-specific whole-body movement during running, including the correlation between upper and lower body movement, could enhance the design and effectiveness of gait retraining programs aimed at injury prevention or treatment.

In running, the interaction between lower and upper body motion controls the whole-body angular momentum, particularly in the transverse plane (Hinrichs, 1987; Willwacher et al., 2016). Therefore, we can expect that sex-specific differences in lower extremity movement, such as increased hip adduction in females, are correlated with sex-specific compensatory upper body movements. One powerful approach to investigate whole-body movement patterns is to apply a principal component analysis (PCA) to the marker trajectories resulting from 3D motion analysis (Federolf et al., 2013; Federolf, 2016; Werner et al., 2020). This technique allows to structure the movement into individual movement components, i.e., principal movements (PM), which shed light on patterns of correlated segment movements. The advantages of applying a PCA directly to marker trajectories rather than the more traditional 3D joint angles are (1) that the former does not require assumptions on the orientation of joint axes thus avoiding a potential source of error (Della Croce et al., 2005) and (2) that the movement components dominating each PM can be easily visualized in intuitive stick figure animations (Troje, 2002). Two previous studies successfully applied a kinematic PCA to resolve sex-specific running kinematics but did not use a full-body marker set-up and/or did not report on upper body movement (Maurer et al., 2012; Nigg et al., 2012).

The aim of the current study was to investigate sex differences in whole-body movement patterns during running as quantified by a kinematic PCA. We hypothesized, that sex-specific lower extremity motion, e.g., greater hip adduction in women, would be correlated with sex-specific upper body movements to maintain a balanced and stable gait pattern. The correlation between specific lower and upper body movements would be evident through their joint expression in individual principal movements.

MATERIALS AND METHODS

Study Design and Participants

This was a cross-sectional study to compare whole-body movement patterns between healthy males and females during running. An *a priori* power analysis was conducted based on 10 previously published studies investigating sex-specific movement patterns during running (Malinzak et al., 2001; Ferber et al., 2003; Chumanov et al., 2008; Maurer et al., 2012; Phinyomark et al., 2014, 2015; Sakaguchi et al., 2014; Willson et al., 2015; Almonroeder and Benson, 2017; Boyer et al., 2017). A pooled analysis of these studies yielded an average effect size (Cohen's d) for kinematic comparisons between males and females of 1.25. With a significance level of $\alpha = 0.05$ and a desired power = 0.8, the required sample size was calculated as $N = 24$. Exclusion criteria were (1) age outside the range of 18–35 years old, (2) no experience with treadmill running, and (3) lower extremity injuries in the last 6 months prior to study participation. Injuries were defined as events that required medical consultation and/or disruption of sport participation for longer than 2 weeks.

A convenience sample of 24 healthy, physically active adults (12 males, 12 females) volunteered to participate in this study. All participants indicated to be physically active for a duration of at least 1–5 h per week. About 90% (21 out of 24) of participants were physically active at least 5 h per week and dedicated one or more hours to activities involving running. The remaining participants were equally physically active and reported previous running experience but were not involved in a running routine at the time of testing. There were no competitive runners in this sample. Therefore, study participants are considered novice and/or recreational runners (Honert et al., 2020). The data from one male participant had to be excluded due to poor recording quality, yielding a final sample size of $n = 23$. This study was approved by the local ethics board of the University of Innsbruck (Certificate 70/2019) in accordance with the ethical principles of the Helsinki Declaration. Prior to study participation, all individuals provided written informed consent and filled out a Physical Readiness Questionnaire.

Experimental Protocol

All participants completed a treadmill running protocol while their three-dimensional movement patterns were recorded using an 8-camera Vicon system with a sample rate of 250 Hz (Vicon Motion Systems Ltd., Oxford, United Kingdom). Individuals were equipped with 39 retro-reflective markers according to the Vicon Plug-in Gait full body model. Next, an incremental method was used to determine the participants' preferred speed (Jordan et al., 2007) with the specific instruction to select a comfortable speed for a 40-min training run. Then, each individual completed a warm-up period consisting of 5 min of brisk walking and 5 min of running at the test speed. Next, we recorded the 3D marker trajectories for 30 s yielding 35–40 full gait cycles per

participant, which has been shown to be sufficient for accurately estimating kinematic running patterns (Dingenen et al., 2018; García-Pinillos et al., 2018). Throughout the entire treadmill protocol, participants were wearing a safety harness to avoid the risk of injury in the case of a fall or slip.

Data Processing and Analysis

Marker Trajectories

For this analysis, the marker set was reduced to 30 markers, neglecting all markers that are not symmetric between the left and right sides of the body. The marker trajectories were reconstructed and labeled using Vicon Nexus software (v. 2.9.2). Gap-filling in marker trajectories was performed using Nexus software for small gaps in pelvis and head markers and a validated marker reconstruction technique (Federolf, 2013; Gløersen and Federolf, 2016) based on a PCA for small gaps in other marker trajectories.

Principal Movement Analysis

Processed marker trajectories were further analyzed using the publicly available *PMAnalyzer* (Haid et al., 2019). This Matlab-based software implements all steps for conducting a kinematic PCA with the goal to structure the complex whole-body running movement into its main movement components, the PMs (Federolf, 2016).

The PMAnalyzer achieved the following pre-processing steps: (1) Filter marker trajectories using a 4th-order Butterworth low-pass filter with a cut-off frequency at 15 Hz; (2) Build one 7,500 [250 Hz × 30 s] row × 90 marker coordinates matrix for each individual. Each row of these matrices is interpreted as a "posture vector," containing the posture of a given participant at a given point in time; (3) Subtract the mean posture (mean across rows) from each subject-specific matrix; (4) Normalize the posture vectors of each individual to their mean Euclidean norm to minimize the influence of anthropometric differences between individuals on movement amplitudes (Federolf, 2016); (5) Concatenate all subject-specific matrices row-wise yielding one PCA-input matrix with 172,500 rows [7,500 samples × 23 participants] and 90 columns.

Next, the PMAnalyzer performed a PCA on the input matrix providing a new set of 90 orthogonal base vectors (eigenvectors v_k) along with their eigenvalues ev_k to fully describe the running movement. Specifically, each eigenvector represents one principal movement while the corresponding eigenvalue indicates the amount of variance accounted for by this principal movement. The projection of the PCA-input data onto v_k defines the time-dependent principal positions $PP_k(t)$, which quantify the movement amplitudes of a given individual at a given point in time with respect to each principal movement. For this analysis, the number of included v_k were selected such that the corresponding $PP_k(t)$ explained 99% of the total movement variance.

Gait Cycle Segmentation

The principal positions were segmented and time-normalized according to the instances of foot contact. The time points of right and left foot contact were detected according to the first negative peak in the vertical acceleration profile of the toe marker following a maximum in the pelvis height marking the end of the flight phase. This detection algorithm was modified from a technique described by Schache et al. (2001). In comparison to the toe velocity profile used in Schache et al. (2001) we found the acceleration profile to yield a more consistent detection of ground contact. Time-normalized principal positions for each full gait cycle i were computed in three steps: PP_k were resampled to 101 data points for the duration between a right foot strike $FS_{i,R}$ and the next left foot strike $FS_{i,L}$. Next, PP_k were resampled to 101 data points for the duration between the current left foot strike $FS_{i,L}$ and the next right foot strike $FS_{i+1,R}$. Lastly, the two resampled PP_k were concatenated to form one full gait cycle.

Principal Positions—Visual Comparison

Subject-average PP_k waveforms for each individual were computed as the mean over the time-normalized PP_k of 34 full gait cycles. Subject-average waveforms were further averaged to create one average male and one average female principal movement pattern (±1SD).

Principal Positions—Video Animations

Principal movements were visualized in 2D videos using the PMAnalyzer video function "PM trials/subject." For one randomly selected participant, this function reconstructs the pattern of correlated 3D marker trajectories for a given principal movement and is computed by multiplying $PP_k(t)$ and v_k. After reversing the normalization to Euclidean distance and adding the mean posture of the exemplary participant, the principal movement videos can be displayed in the original units of measurement (mm). Due to the smaller movement amplitudes explained by the higher-order principal movements, we amplified the respective $PP_k(t)$ with a manually selected amplification factor *AmpFac*. Note that this analysis step is simply for visualizing and interpreting the correlated kinematic patterns described by each PM.

The principal movements, which showed statistical differences between males and females were inspected in further detail. First, one gait cycle of a male and a female average running pattern was reconstructed based on the first 20 v_k and the average, time-normalized $PP_k(t)$ of either all males or all females, respectively (sex-specific mean of subject-average $PP_k(t)$ waveforms, see section "Principal Positions—Visual Comparison"). The movement in the original coordinate system was derived by reversing the normalization to Euclidean distance (using the average of all norm factors) and adding the mean posture (using the average of all mean postures). For the last two steps, we used grand averages rather than sex-specific averages to isolate differences in the movement pattern from anatomical differences. Second, to visualize the differences in the running movement between males and females explained by one specific principal movement, we amplified the respective $PP_k(t)$ with a manually selected amplification factor *AmpFac*. In addition, the created videos were used to generate image sequences illustrating the sex-specific differences in movement patterns at specific time points during the first half of the gait cycle: 5% (right foot early

stance), 15% (mid stance), 30% (late stance/push-off), and 45% (early swing).

Principal Positions—Waveform Analysis

To investigate quantitatively whether the time-normalized $PP_k(t)$ waveforms were different between male and female runners, a second PCA analysis was conducted. Comparing waveforms with the help of a PCA has the advantage that the entire waveform shape and amplitude can be compared between conditions rather than limiting the analysis to discrete time points such as minima or maxima. This waveform-PCA was computed separately for each $PP_k(t)$. As a first step, the time-normalized waveforms of all gait cycles and individuals (34 gait cycles × 23 participants = 782 waveforms) were concatenated into a (782 rows × 201 time points) PCA-input matrix. The second PCA yielded a new set of eigenvectors w_k where the eigenvector w_1 with the highest corresponding eigenvalue ew_1 represented the largest variation in shape and/or amplitude of the analyzed gait cycle waveforms. The projection of the principal position input matrix onto w_1 yielded a score $s_{i,p}$ for each gait cycle i and participant p, indicating the extent (positive or negative), to which the analyzed waveform shows the pattern described by w_1. These waveform (w_1) scores $s_{i,p,k}$ for each $PP_k(t)$ were then averaged across gait cycles, yielding one average score per individual and principal movement $s_{p,k}$, which served as dependent variables for the statistical analyses.

Comparison of PM-Based and Joint Angular Representations of Running Kinematics

While the PM-based representation of whole-body movement has been validated to accurately represent the mechanics of the movement system (Federolf, 2016), the research and clinical community is more familiar with the description of running kinematics using 3D joint angles. To provide reference values and illustrate how the PM-based waveform scores relate to a joint angle framework, we investigated the peak-to-peak oscillations (i.e., the joint range of motion, ROM) for selected joint angle profiles. Specifically, we used a full-body musculoskeletal model and a standard inverse kinematics procedure in OpenSim (v. 4.1) to determine the peak-to-peak oscillation in knee flexion/extension and hip adduction/abduction of the left leg during each full gait cycle (Delp et al., 2007; Rajagopal et al., 2016). We selected those joint angles because our analysis yielded two PMs—PM_6 and PM_8—that contained sex-specific movement components and visual inspection of those PMs suggested sex-specific knee movement (PM_6) and hip movement (PM_8), respectively (see sections "Description of Principal Movements" and "Sex Differences in Running Movement Components"). A more detailed description of the joint angle analysis is provided in the **Supplementary Material**.

Statistical Analysis

Descriptive statistics of participant age, height, weight, and running speed were determined according to the sex-specific means and standard deviations. The goal of the primary statistical analysis was to investigate whether the waveform scores s corresponding to the shapes of $PP_k(t)$ differed between males and females independent of the running speed. Therefore, we performed a set of univariate analyses of covariance (ANCOVA) with "sex" as the independent variable, "running speed" as the covariate, and the scores $s_{p,k}$ for a specific principal movement PM_k as the dependent variable. Running speed did not differ significantly between males and females according to an independent t-test and there was no significant interaction of "sex" and "running speed" on any of the PP scores, justifying the inclusion of running speed as a covariate (Field, 2009). Further assumptions of ANCOVA were confirmed based on a Shapiro–Wilk test (approximate normal distribution of residuals) and a Levene's test (homogeneity of variances). *Post hoc* tests of the running speed-adjusted scores were conducted to investigate mean differences between males and females. Effect sizes were reported as partial Eta squared.

As described in the "Results" section, k = 1,..,12 principal movements were included in this analysis while PM_4 and PM_5 were not included in the statistical analysis, yielding m = 10 ANCOVAS. To control for the expected proportion of false discoveries (type I error), we used the Benjamini-Hochberg procedure to adjust our significance level for each ANCOVA according to Eq. 1:

$$\alpha_{adj} = \frac{l}{m} \cdot \alpha, \tag{1}$$

where l is the rank of each ANCOVA, ordered according to their p-values with respect to the independent variable "sex" (from lowest to highest) (Benjamini and Hochberg, 1995). The same procedure was performed to evaluate the effects of the covariate "running speed."

In a secondary statistical analysis, we used two general linear regression models to investigate the association between (1) joint ROM in knee flexion/extension and PM_6 waveform scores (model 1) and (2) joint ROM in hip adduction/abduction and PM_8 waveform scores (model 2). In both models, the outcome variable was the PM waveform score and the predictor variables included "sex," the "joint ROM," and the respective interaction term. Confounding by running speed was assessed but was not present. All assumptions for linear regression (normality of residuals, homogeneity of variance, absence of outliers) were assessed and met. The joint angle analysis was limited to the left leg since the right leg showed nearly identical outcomes.

All statistical analyses were carried out in IBM SPSS Statistics for Windows (v25, IBM Corp., Armonk, NY, United States) at an *a-priori* significance level of $\alpha = 0.05$.

RESULTS

Participant Characteristics

Age, height, mass, and preferred running speed of the male and female participants are presented in **Table 1**

Description of Principal Movements

The first three principal movements explained ∼90% of the variance contained in the overall running movement. The first 12 principal movements explained 99% of the total variance. The full

TABLE 1 | Participant age, mass, height, and preferred running speed.

	Female (n = 12)	Male (n = 11)
Age (years, mean ± SD)	25 ± 4	27 ± 3
Height (cm, mean ± SD)	170 ± 7	181 ± 5*
Mass (kg, mean ± SD)	61 ± 5	75 ± 7*
Preferred running speed (km/h, mean ± SD)	10.1 ± 0.8	10.7 ± 1.0

**Significantly higher compared to females according to an independent t-test, alpha = 0.05.*

description of the dominating movement patterns in each PM is summarized in **Table 2**. PM_{1-8} are additionally visualized based on the stick figure animations in the **Supplementary Videos 1, 2**.

The first three components explain the main features of the running gait, including the leg swing (PM_1), the arm swing (PM_1, PM_2), corresponding upper body rotation (PM_1, PM_2), the stepping motion (PM_2), and the vertical bouncing motion (PM_3). PM_4 and PM_5 explain the anterior-posterior and medio-lateral whole-body positioning on the treadmill belt. Since the absolute position of the body on the treadmill was not of interest in this study, PM_4 and PM_5 were excluded from all further analyses. The functional interpretation of higher-order PMs becomes increasingly difficult since these patterns represent compensatory or complementary balancing movements and postural adjustments, not necessarily visible to the eye when watching a runner. For example, PM_6 appears to complement PM_2 and PM_3 by additionally describing leg extension and upper body forward lean. PM_8 in contrast seems to represent a medio-lateral balancing strategy including the medio-lateral placement of the feet (i.e., hip adduction-abduction) as well as pelvis and upper body movement in the transverse and frontal planes.

Note that for some PMs, e.g., PM_6 and PM_7, the stick figure animations seem to suggest length changes of the thigh and/or shank (**Supplementary Video 2**). This is a phenomenon created by the fact that the PC vectors form an orthonormal coordinate system for the changes in posture; if rotations of body segments are projected onto only one of the PM-dimensions, then they will appear as length changes of these segments. For comparison, leg or arm swing in gait also appear as segment length changes if observed as a frontal plane projection only. Similarly, segment rotations such as the circular motion path of the feet during running, must be described by the combination of movement along multiple PC vectors with some containing virtual segment deformations that appear unnatural if only one PM is considered (especially after amplification). In general, PMs should not be understood as actual movements but as a coordinate system for the movements of all body segments. **Table 2** thus describes the movement aspects that dominate each of the PM_k coordinate axes (Federolf, 2016).

TABLE 2 | Description of principal movements (PMs) and their cumulative, explained variance relative to the total movement variance (var.).

PM_k [var.]	Principal movement description
PM_1 [73.7%]	**Anterior–posterior arm and leg swing** Forward and backward swing of the arms and leg correlated with an upper body rotation and lateral pelvic drop
PM_2 [83.2%]	**Stepping motion ("Butt-kick exercise")** Knee, hip, and ankle extension-flexion correlated with pelvis and upper body rotation around vertical axis. Pelvis and upper body rotate in opposite direction
PM_3 [90.5%]	**Bouncing movement** Bouncing movement of the entire body, predominantly through knee flexion and extension
PM_4 [94.9%]	**Whole-body position** Anterior-posterior movement on the treadmill belt including a slight forward lean of the upper body
PM_5 [96.6%]	**Whole-body position** Medio-lateral movement on the treadmill belt
PM_6 [97.3%]	**Leg extension coupled with upper body lean** Hip and knee and flexion-extension correlated with forward lean of the upper body
PM_7 [97.8%]	**Stepping motion ("Skipping exercise")** Hip and knee flexion-extension correlated with anti-phasic arm swing motion
PM_8 [98.1%]	**Medio-lateral balancing** Medio-lateral position of feet (hip adduction-abduction) correlated with pelvis rotation, upper body rotation and side lean, arm balancing motion, and knee and ankle flexion-extension
PM_9 [98.4%]	**Leg flexion-extension** Hip, knee, and ankle flexion-extension
PM_{10} [98.6%]	**Asymmetric movement during left foot strike** Balancing movement related to arm and head motion
PM_{11} [98.8%]	**Head movement** Lifting and lowering the head
PM_{12} [99.0%]	**Medio-lateral positioning** Whole-body movement to correct the medio-lateral position on the treadmill belt

Sex Differences in Running Movement Components

Figure 1 shows the sex-specific averages of the time-normalized principal position waveforms for the first 12 PMs (excluding, as discussed earlier, PM_4 and PM_5) where the time points 0 and 50% of gait cycle correspond to right and left foot strikes, respectively. Particularly PM_6 at 10 and 60% of the gait cycle and PM_8 throughout suggested that males and females showed sex-specific PP(t)-waveforms (**Figures 1D,F**). The dashed and solid black lines in **Figure 1** illustrate the features extracted by the waveform analysis conducted on the principal positions. Specifically, the lines represent the two individual gait cycles that scored lowest and highest on the first waveform principal component (w_1) across all individuals and gait cycles. For example, a high score for PP_8 resulted from a more male-like waveform shape (start with valley and end with peak) and vice versa for a low score (**Figure 1F**). Across PMs, **Figure 1** demonstrates that the waveform features described by the first waveform principal component coincide with the features that also appear different between males and females. **Figure 2** presents the statistical comparison of PP-waveform scores between males and females while considering running speed as a covariate.

Medio-Lateral Balancing Strategy (PM_8)

The most obvious sex-specific difference in principal positions was observed in PM_8, where males and females showed a mirrored waveform shape. Accordingly, there was a significant, effect of "sex" on PP_8 scores [$F(1,20) = 8.54$, $p = 0.008$, partial

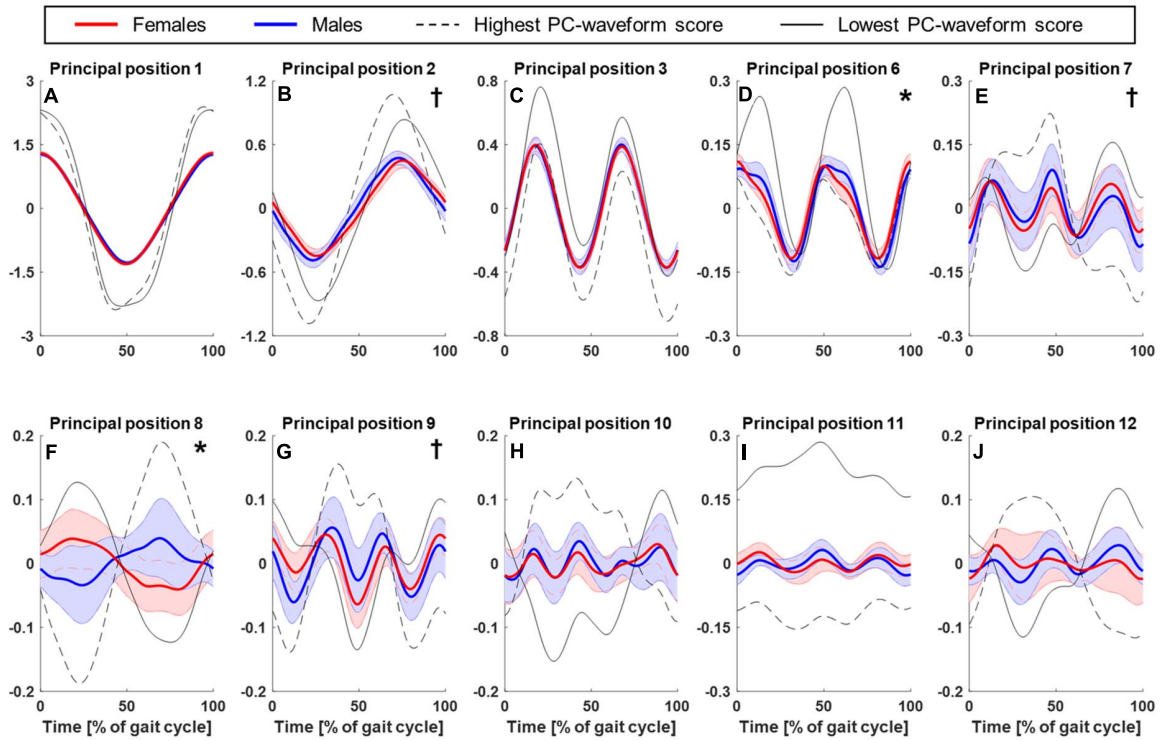

FIGURE 1 | Comparison of principal position waveforms between males and females. Mean and standard deviation (shaded areas) of time-normalized principal position waveforms corresponding to PM1–3 **(A–C)** and 6–12 **(D–J)** for females (red, n = 12) and males (blue, n = 11). Time point 0% corresponds to a heel strike of the right foot, 50% to a heel strike of the left foot, thus one full gait cycle is shown. Overlaid are those PP-waveforms that scored lowest (solid, black lines) and highest (dashed, black lines) on the first waveform principal components across all participants and gait cycles (see section "Principal Positions—Waveform Analysis"). These waveforms illustrate the main features described by the waveform scores, which were analyzed statistically: "*" and "†" indicate a statistically significant effect of "sex" or "running speed" on the principal position scores, respectively.

η^2 = 0.299] without a significant influence of running speed [F(1,20) = 0.17, p = 0.684, partial η^2 = 0.008]. Corresponding running-speed adjusted means (±1SD) of PP8-scores were −0.39 ± 0.53 and 0.29 ± 0.53 for females and males, respectively (**Figure 2**). According to **Figures 3A–D** and **Supplementary video 3** (amplification factor 10), females tended to place their stance foot more medially (indicative of larger hip adduction ROM) while males strike the ground more laterally. At the same time, females showed a larger relative rotation between the pelvis and leg segments and a larger excursion of upper body rotation, both in the transverse plane.

Knee Flexion (PM_6)

A second difference in principal positions was apparent for PM_6. Specifically, males showed wider PP_6 maxima (∼10 and 60% of gait cycle) and lower PP_6 minima (∼30 and 80% of gait cycle). These PP_6 shape differences were reflected in a significant effect of "sex" on PP_6 scores [F(1,20) = 11.06, p = 0.003, partial η^2 = 0.356]. There was no significant influence of running speed [F(1,20) = 1.78, p = 0.197, partial η^2 = 0.082]. Corresponding running-speed adjusted means (±1SD) of PP_6-scores were −0.18 ± 0.15 and −0.39 ± 0.15 for females and males, respectively. **Figures 3E–H** and **Supplementary Video 4** (amplification factor 5) suggest that this difference originated from variations in knee flexion angle between males and females. Specifically, compared to males, females tended to show a more flexed knee during mid stance (**Figures 3E,F**) but less knee flexion of the swing leg. In addition, sex-specific variations in the ankle angle around ground contact and push-off were visible in **Figures 3E,H**.

Stepping Motion (PM_2)

Of the first three PMs, only the second component showed a visibly different shape of the average principal positions between males and females; specifically females showed an average waveform that is shifted to the right and smaller in amplitude (∼25 and 75% of gait cycle). These differences, reflected by PP_2 scores, were influenced by a significant effect of running speed [F(1,20) = 11.65, p = 0.003, partial η^2 = 0.368]. The effect of "sex" on PP_2 scores [F(1,20) = 5.62, p = 0.028, partial η^2 = 0.220] did not reach the adjusted significance level of α_{adj} = 0.015 (l = 3 in Eq. 1). **Figures 3I–L** and **Supplementary Video 5** (amplification factor 2) indicate that the observed differences in PP_2 were mostly related to a difference in swing leg knee flexion. **Supplementary Video 5** further suggests that the timing of push-off was affected by the combined influence of running speed and sex.

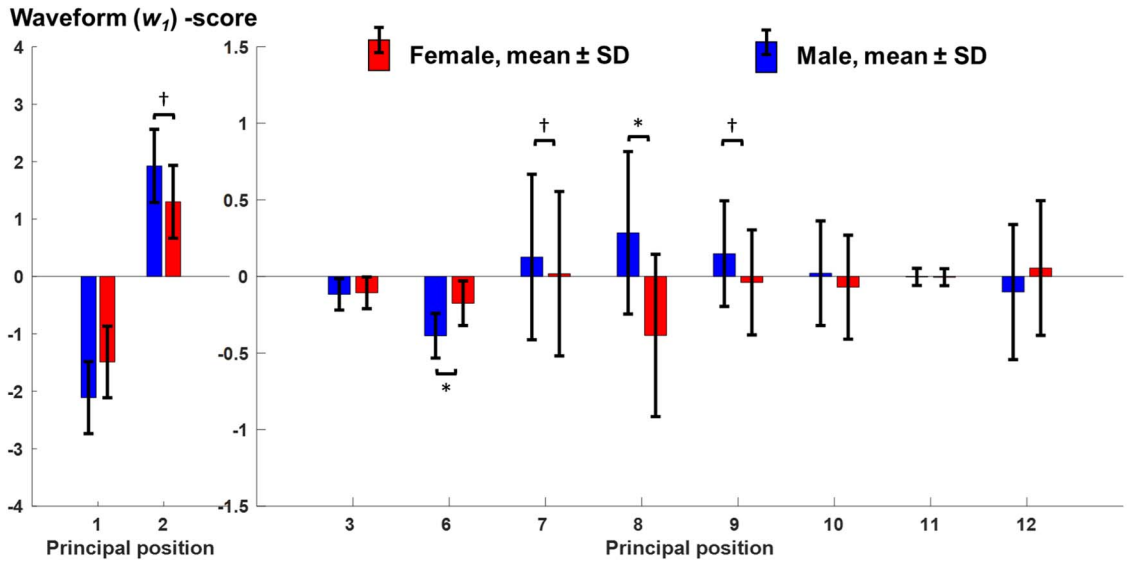

FIGURE 2 | Comparison of PCA-based principal position scores between males and females. Mean and standard deviation of principal position scores regarding waveform PC1 (w_1) for females (red, n = 12) and males (blue, n = 11). These values represent the adjusted means with respect to the covariate running speed. "*" and "†" mark significant effects of "sex" or "running speed" on the principal position scores after adjusting for multiple comparisons.

The Influence of Speed on Running Movement Components

Further PP scores that showed a significant effect of running speed but no significant sex effect were PP_7 [speed: $F(1,20) = 7.82$, $p = 0.011$, partial $\eta^2 = 0.281$; sex: $F(1,20) = 0.22$, $p = 0.646$, partial $\eta^2 = 0.011$] and PP_9 [speed: $F(1,20) = 10.3$, $p = 0.004$, partial $\eta^2 = 0.340$; sex: $F(1,20) = 1.61$, $p = 0.219$, partial $\eta^2 = 0.075$]. PP_1 scores showed a trend for an effect of both sex [$F(1,20) = 5.30$, $p = 0.032$, partial $\eta^2 = 0.210$] and speed [$F(1,20) = 4.80$, $p = 0.041$, partial $\eta^2 = 0.193$] but did not reach the adjusted significance level.

Association With Joint Angle Range of Motion

Joint ROM in hip adduction/abduction was a significant predictor of PM_8 waveform scores (B [95% CI] = −0.07 [−0.10, −0.04], $t(22) = -4.37$, $p < 0.001$) and joint ROM in knee flexion/extension was a significant predictor of PM_6 waveform scores (B [95% CI] = −0.02 [−0.03, −0.01], $t(22) = -5.58$, $p < 0.001$). Both associations are illustrated in **Supplementary Figure 1**. In model 2 (PM_8 vs. hip adduction/abduction), the interaction term with "sex" was a significant predictor of PM_8 waveform scores, indicating a stronger association in males compared to females (B [95% CI] = 0.08 [0.01, 0.15], $t(22) = 2.56$, $p = 0.02$). A similar interaction was observed in model 1 (PM_6 vs. knee flexion/extension) but the corresponding coefficient was not statistically significant (B [95% CI] = −0.01 [0.00, 0.02], $t(22) = 1.99$, $p = 0.06$). On average and compared to males, female runners showed a larger ROM in hip adduction/abduction by 7° and a smaller ROM in knee flexion/extension by 6°.

DISCUSSION

This study tested the hypothesis that the correlated motion of the upper and lower body differs systematically between males and females during running. A kinematic PCA yielded principal movements and corresponding principal positions, i.e., the time-dependent whole-body posture changes associated with each principal movement for either males or females. In support of our hypothesis, we showed distinct visually and statistically significant differences between men and women with respect to the shape and/or amplitude of the principal positions in PM_8 and PM_6. For these movement components, there was no evidence for an influence of running speed and they represented a sex-specific balancing strategy including medio-lateral foot placement correlated with pelvis and upper body rotation during stance (PM_8) as well as sex-specific stance and swing leg kinematics (PM_6).

Increased hip adduction in female compared to male runners is the most consistent finding related to sex differences in running kinematics (Ferber et al., 2003; Schache et al., 2003; Chumanov et al., 2008; Sakaguchi et al., 2014; Willson et al., 2015; Phinyomark et al., 2016; Almonroeder and Benson, 2017; Boyer et al., 2017). In contrast to the traditional clinical gait analysis, the PCA approach does not express the running movement in terms of 3D joint rotations but creates a new, movement-specific coordinate system where each axis describes correlated movements of body segments. Although conceptually different, the traditional and PCA approach should result in similar observations. The principal positions related to PM_8 indicated a clear difference in movement strategies between the sexes and the corresponding video animations were indicative of more hip adduction in females, which agrees with previous reports

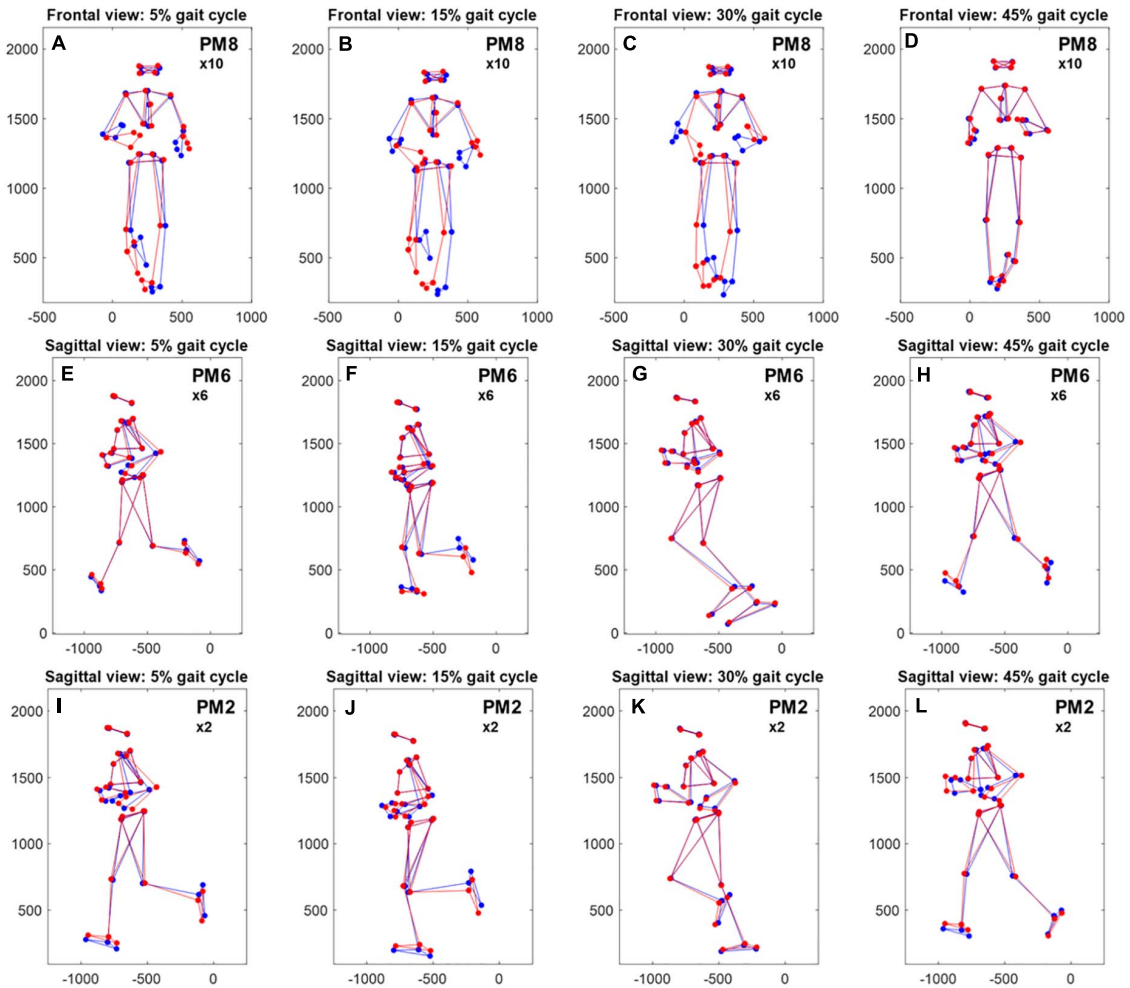

FIGURE 3 | Reconstructed, average movement patterns of males and females. Comparison of reconstructed, average movement patterns of females (red) and males (blue) with amplification of specific principal movements **[(A–D)**, 10 × PM_8—frontal plane; **(E–H)**, 6 × PM_6—sagittal plane, **(I–L)**, 2 × PM_2—sagittal plane]. Reconstructions are based on the first 20 eigenvectors $v_{1\text{-}20}$, the average, time-normalized female and male principal position waveforms (see **Figure 1**), and the grand average of the mean posture and Euclidean distance normalization factors. x- and y-axes show the distance in mm; the axis labels were removed for better readability.

(Ferber et al., 2003; Schache et al., 2003, 2005; Chumanov et al., 2008; Sakaguchi et al., 2014; Willson et al., 2015; Phinyomark et al., 2016; Almonroeder and Benson, 2017; Boyer et al., 2017). Further, our observations confirmed the previous findings that females show more axial rotation of their pelvis (=internal hip rotation) (Ferber et al., 2003; Chumanov et al., 2008; Sakaguchi et al., 2014; Almonroeder and Benson, 2017) and a larger excursion of upper body rotation (Schache et al., 2003; Bruening et al., 2020), although some conflicting evidence exists for these movement features (Malinzak et al., 2001; Maurer et al., 2012; Phinyomark et al., 2014). The regression analysis partially validated our interpretation of the PM animations, revealing that a larger ROM in hip adduction/abduction predicts smaller PP_8 waveform scores and smaller ROM in knee flexion/extension predicts higher PP_6 waveform scores (i.e., a more female-like pattern). Currently, we are unsure why these associations were stronger in male runners compared to female runners. Given that our waveform analysis considered only the scores of the first waveform principal component (explaining about 50% of the waveform variance depending on the PM), we speculate that some additional information related to female runners may be contained in higher waveform principal components that were not considered.

The new information, that the current study provides is that sex-specific hip movement is inherently linked to pelvis and upper body rotation, which confirms an assumption of previous investigators (Noehren et al., 2007; Bruening et al., 2020). There may be at least three factors to explain a sex-specific whole-body running movement: (1) anthropometrics, (2) muscle strength, or (3) whole-body dynamics, i.e., the interaction of forces and motion across all body segments. There is little evidence, however, for a consistent association between the anthropometrics and kinematics of the pelvis and hip joint during running (Schache et al., 2005; Chumanov et al., 2008).

Further, although women do show lower normalized strength of the hip abductors (Claiborne et al., 2006), successful muscle strengthening did not significantly alter hip or pelvic motion in runners (Earl and Hoch, 2011; Willy and Davis, 2011; Neal et al., 2016). These observations suggest that sex-specific whole-body dynamics may be the predominant factor to explain the current findings.

The whole-body angular momentum during running has to be controlled by coordinated movement of leg, pelvis, trunk, arm, and head motion, particularly in the transverse plane (rotation about vertical body axis) (Hinrichs, 1987; Willwacher et al., 2016). During the stance phase, the ground reaction force (GRF) under the stance leg and the concurrent motion of the swing leg generate a transverse moment, the "free moment" that rotates the runner's pelvis and upper body towards the stance leg (Hinrichs, 1987; Li et al., 2001). Among other factors, the magnitude of the free moment decreases with a more medial placement of the foot (more hip adduction) and/or with a larger opposite angular momentum generated by upper body sway and arm swing (Hinrichs, 1987). Li and colleagues showed that walking with restricted arm motion had a larger influence on the free moment in men compared to women (Li et al., 2001). Furthermore, men show a higher relative upper body muscle mass in comparison to women (Janssen et al., 2000). We thus assume that upper body rotation of female runners may be less effective in balancing the free moment due to narrower shoulders and less mass distributed across arms and upper body (Li et al., 2001). Therefore, women may control the free moment by more hip adduction and a larger upper body swing excursion compared to males. The combination of more hip adduction and pelvis rotation has been shown to put more stress on the patellofemoral joint as well as on the iliotibial band and may thus expose women to a higher risk of injuries of these structures (Ferber et al., 2010; Willy and Davis, 2011). In contrast, males can potentially afford to land with more hip abduction and balance the resulting transverse free moment with more angular momentum of the upper body. Taken together, these findings suggest that gait-retraining interventions with the goal of preventing knee injuries in female runners with excessive hip adduction should include instructions to actively increase arm und upper body swing in order to allow landing with a less adducted hip. Given the correlational evidence provided by the kinematic PCA in this study, however, the proposed relationship should be confirmed in a subsequent study that experimentally manipulates either arm and trunk sway or segment inertial properties and determines the effect on hip movement. Either way, displaying PM-based stick figure animations to the learner to visualize their own as well as a desired movement pattern could provide a powerful tool in a gait retraining setting given the finding that learning is enhanced when individuals try to imitate model movements rather than following instructions related to joint kinematics (Benjaminse et al., 2015).

In contrast to sex-specific hip adduction during running, previous findings for other joints and in other planes of movement are less consistent. For example, some authors have reported that during the running stance phase, females show more knee flexion compared to men (Boyer et al., 2017) while others showed the opposite (Malinzak et al., 2001; Phinyomark et al., 2014), or no significant difference in knee flexion angles (Ferber et al., 2003; Almonroeder and Benson, 2017). Our findings based on PM6 extend those of Boyer et al. (2017) that women tend to bend their knees more during mid-stance. The conflicting findings between investigations of sex-specific leg flexion/extension may arise from variations in study designs with respect to the tested running speeds, i.e., either pre-determined or self-selected speeds. It is known that faster speeds lead to adaptations in the running gait with most pronounced adaptations in basic sagittal plane kinematics (Maurer et al., 2012). This is reflected in our analysis, showing a significant influence of running speed on PM_2 principal positions and a trend of an effect of speed on PM_1 principal positions. These movement components mainly describe leg and arm motion in the sagittal plane. If male and female movements are compared at a constant speed, e.g., 3.5 m/s, the relative speed (with respect to their maximum) is likely faster for females compared to males, which could confound the kinematic comparison. On the other hand, if running kinematics are compared at a self-selected pace, a lower preferred speed in the female group could equally confound the kinematic analysis. Our solution to this issue was to compare men and women at their preferred running speed and include speed as a covariate in the analysis. This approach allowed us to differentiate between the effects of speed, which are generally present in the basic movement components of running (e.g., PM_2) (Maurer et al., 2012; Nigg et al., 2012), and the effects of sex, which we identified in PM_6 and PM_8. Our findings of more knee flexion during stance in women as well as sex-specific ankle angles at ground contact (see **Figures 3F,H**) suggest that women may use a modified foot strike pattern from men. This finding further adds to the body of literature concerning sex differences in running kinematics but was not the main focus of this analysis and will not be further discussed.

A limitation of this study is the relatively small sample size when compared to other analyses of sex differences in running kinematics with 100 or more participants (Nigg et al., 2012; Phinyomark et al., 2014). Our literature review, however, resulted in expected large effects and thus justified our sample size. Further, the holistic approach of the kinematic PCA and waveform analysis is likely more sensitive (Federolf et al., 2013) compared to traditional approaches in detecting sex differences in running kinematics since it takes into account all measured marker trajectories as a function of time instead of picking discrete outcome variables. A second limitation is that our sample consisted of physically active, young adults but not necessarily trained runners and thus, our results may not be generalized to other running populations such as elite/experienced or elderly runners. Nevertheless, our findings are applicable to (1) novice runners who are an interesting population due to their relatively high risk of running injury (Nielsen et al., 2012) and (2) recreational runners who form the largest running population (Hoitz et al., 2020). Third, part of our discussion revolves around whole-body rotational moments, which we did not assess directly in this study. Although they should be considered speculative, our arguments appear reasonable given previous evidence of sex differences in free vertical moments during walking, which are closely related to whole-body angular momentum in the

transverse plane (Li et al., 2001). Nevertheless, the proposed relationship between a sex-specific body mass distribution, whole-body angular momentum, hip joint movement, and ultimately the risk of running-related injury should be considered a hypothesis to be tested in a future prospective study, which includes a biomechanical model based on sex-specific anthropometrics and segment masses to quantify segment inertial properties. Lastly, the qualitative PM descriptions in **Table 2** are interpretations, which are susceptible to observer bias or misinterpretations, marking a limitation of our approach. However, the PMs themselves, including their representation as animations, are objective and purely data-driven outcomes in the current study. By amplifying the influence of individual PMs on the overall movement in **Supplementary Videos 1, 2**, we attempted to make the movement aspects dominating each PM more obvious. Our approach is strengthened by the result of a significant association between the PM waveform scores and the ROM with respect to those joint angular movements that were evident from the corresponding PM animations.

Based on a whole-body movement analysis, this study confirmed that women demonstrate more hip adduction and pelvis rotation during running compared to men. As a novel finding, we showed that sex-specific hip motion correlates with sex-specific pelvis and upper body movement. Specifically, women use a larger range of motion with respect to pelvis and upper body rotation. We suggest that female runners employ this strategy of hip adduction coupled with more upper body rotation to maintain a whole-body angular momentum of close to zero in the transverse plane, potentially compensating for a less efficient arm swing and trunk sway. The correlation between lower body and upper body mechanics should be considered when designing interventions aimed at reducing hip adduction and internal rotation as risk factors for overuse injuries during running.

DATA AVAILABILITY STATEMENT

The datasets presented in this study can be found in online repositories. The names of the repository/repositories and accession number(s) can be found below: Mohr et al., 2021.

ETHICS STATEMENT

The studies involving human participants were reviewed and approved by local ethics board of the University of Innsbruck (Certificate 70/2019). The patients/participants provided their written informed consent to participate in this study.

AUTHOR CONTRIBUTIONS

MM, RP, SL, and AS conducted pilot tests and recruited participants. RP, SL, and AS carried out measurements. MM, RP, and SL processed the marker trajectories. MM analyzed the data and wrote the first manuscript draft. All authors conceived the study and its design, revised the manuscript, and read and approved the final manuscript version.

SUPPLEMENTARY MATERIAL

The Supplementary Material for this article can be found online at: https://www.frontiersin.org/articles/10.3389/fbioe.2021.657357/full#supplementary-material

REFERENCES

Almonroeder, T. G., and Benson, L. C. (2017). Sex differences in lower extremity kinematics and patellofemoral kinetics during running. *J. Sports Sci.* 35, 1575–1581.

Benjamini, Y., and Hochberg, Y. (1995). Controlling the false discovery rate: a practical and powerful approach to multiple testing. *J. R. Stat. Soc. Series B Stat. Methodol.* 57, 289–300. doi: 10.1111/j.2517-6161.1995.tb02031.x

Benjaminse, A., Gokeler, A., Dowling, A. V., Faigenbaum, A., Ford, K. R., Hewett, T. E., et al. (2015). Optimization of the anterior cruciate ligament injury prevention paradigm: novel feedback techniques to enhance motor learning and reduce injury risk. *J. Orthop. Sports Phys. Ther.* 45, 170–182. doi: 10.2519/jospt.2015.4986

Boling, M., Padua, D., Marshall, S., Guskiewicz, K., Pyne, S., and Beutler, A. (2010). Gender differences in the incidence and prevalence of patellofemoral pain syndrome. *Scand. J. Med. Sci. Sports* 20, 725–730. doi: 10.1111/j.1600-0838.2009.00996.x

Boyer, K. A., Freedman Silvernail, J., and Hamill, J. (2017). Age and sex influences on running mechanics and coordination variability. *J. Sports Sci.* 35, 2225–2231. doi: 10.1080/02640414.2016.1265139

Bruening, D. A., Baird, A. R., Weaver, K. J., and Rasmussen, A. T. (2020). Whole body kinematic sex differences persist across non-dimensional gait speeds. *PLoS One* 15:e0237449. doi: 10.1371/journal.pone.0237449

Chumanov, E. S., Wall-Scheffler, C., and Heiderscheit, B. C. (2008). Gender differences in walking and running on level and inclined surfaces. *Clin. Biomech.* 23, 1260–1268. doi: 10.1016/j.clinbiomech.2008.07.011

Claiborne, T. L., Armstrong, C. W., Gandhi, V., and Pincivero, D. M. (2006). Relationship between hip and knee strength and knee valgus during a single leg squat. *J. Appl. Biomech.* 22, 41–50. doi: 10.1123/jab.22.1.41

Della Croce, U., Leardini, A., Chiari, L., and Cappozzo, A. (2005). Human movement analysis using stereophotogrammetry: part 4: assessment of anatomical landmark misplacement and its effects on joint kinematics. *Gait Posture* 21, 226–237. doi: 10.1016/j.gaitpost.2004.05.003

Delp, S. L., Anderson, F. C., Arnold, A. S., Loan, P., Habib, A., John, C. T., et al. (2007). OpenSim: open-Source software to create and analyze dynamic simulations of movement. *IEEE Trans. Biomed. Eng.* 54, 1940–1950. doi: 10.1109/tbme.2007.901024

Dingenen, B., Barton, C., Janssen, T., Benoit, A., and Malliaras, P. (2018). Test-retest reliability of two-dimensional video analysis during running. *Phys. Ther. Sport* 33, 40–47. doi: 10.1016/j.ptsp.2018.06.009

Earl, J. E., and Hoch, A. Z. (2011). A proximal strengthening program improves pain, function, and biomechanics in women with patellofemoral pain syndrome. *Am. J. Sports Med.* 39, 154–163. doi: 10.1177/0363546510379967

Emery, C., and Tyreman, H. (2009). Sport participation, sport injury, risk factors and sport safety practices in Calgary and area junior high schools. *Paediatr. Child Health* 14, 439–444. doi: 10.1093/pch/14.7.439

Federolf, P. A. (2013). A novel approach to solve the "missing marker problem" in marker-based motion analysis that exploits the segment coordination patterns in multi-limb motion data. *PLoS One* 8:e78689. doi: 10.1371/journal.pone.0078689

Federolf, P. A. (2016). A novel approach to study human posture control: "principal movements" obtained from a principal component analysis of

kinematic marker data. *J. Biomech.* 49, 364–370. doi: 10.1016/j.jbiomech.2015.12.030

Federolf, P. A., Boyer, K. A., and Andriacchi, T. P. (2013). Application of principal component analysis in clinical gait research: identification of systematic differences between healthy and medial knee-osteoarthritic gait. *J. Biomech.* 46, 2173–2178. doi: 10.1016/j.jbiomech.2013.06.032

Ferber, R., Davis, I. M., and Williams, D. S. III (2003). Gender differences in lower extremity mechanics during running. *Clin. Biomech.* 18, 350–357. doi: 10.1016/s0268-0033(03)00025-1

Ferber, R., Noehren, B., Hamill, J., and Davis, I. S. (2010). Competitive female runners with a history of iliotibial band syndrome demonstrate atypical hip and knee kinematics. *J. Orthop. Sports Phys. Ther.* 40, 52–58. doi: 10.2519/jospt.2010.3028

Field, A. P. (2009). *Discovering Statistics Using SPSS: (and Sex, Drugs and Rock "n" Roll)*, 3rd Edn. Los Angeles, CA: SAGE Publications.

García-Pinillos, F., Latorre-Román, P. A., Ramírez-Campillo, R., Párraga-Montilla, J. A., and Roche-Seruendo, L. E. (2018). Minimum time required for assessing step variability during running at submaximal velocities. *J. Biomech.* 80, 186–195. doi: 10.1016/j.jbiomech.2018.09.005

Gløersen, Ø, and Federolf, P. (2016). Predicting missing marker trajectories in human motion data using marker intercorrelations. *PLoS One* 11:e0152616. doi: 10.1371/journal.pone.0152616

Haid, T. H., Zago, M., Promsri, A., Doix, A.-C. M., and Federolf, P. A. (2019). PManalyzer: a software facilitating the study of sensorimotor control of whole-body movements. *Front. Neuroinform.* 13:24. doi: 10.3389/fninf.2019.00024

Hinrichs, R. N. (1987). Upper extremity function in running. II: angular momentum considerations. *J. Appl. Biomech.* 3, 242–263. doi: 10.1123/ijsb.3.3.242

Hoitz, F., Mohr, M., Asmussen, M., Lam, W.-K., Nigg, S., and Nigg, B. (2020). The effects of systematically altered footwear features on biomechanics, injury, performance, and preference in runners of different skill level: a systematic review. *Footwear Sci* 12, 193–215. doi: 10.1080/19424280.2020.1773936

Honert, E. C., Mohr, M., Lam, W.-K., and Nigg, S. (2020). Shoe feature recommendations for different running levels: a Delphi study. *PLoS One* 15:e0236047. doi: 10.1371/journal.pone.0236047

Janssen, I., Heymsfield, S. B., Wang, Z. M., and Ross, R. (2000). Skeletal muscle mass and distribution in 468 men and women aged 18-88 yr. *J. Appl. Physiol.* 89, 81–88. doi: 10.1152/jappl.2000.89.1.81

Jordan, K., Challis, J. H., and Newell, K. M. (2007). Speed influences on the scaling behavior of gait cycle fluctuations during treadmill running. *Hum. Mov. Sci.* 26, 87–102. doi: 10.1016/j.humov.2006.10.001

Li, Y., Wang, W., Crompton, R. H., and Gunther, M. M. (2001). Free vertical moments and transverse forces in human walking and their role in relation to arm-swing. *J. Exp. Biol.* 204, 47–58. doi: 10.1242/jeb.204.1.47

Malinzak, R. A., Colby, S. M., Kirkendall, D. T., Yu, B., and Garrett, W. E. (2001). A comparison of knee joint motion patterns between men and women in selected athletic tasks. *Clin. Biomech.* 16, 438–445. doi: 10.1016/s0268-0033(01)00019-5

Maurer, C., Federolf, P., von Tscharner, V., Stirling, L., and Nigg, B. M. (2012). Discrimination of gender–, speed–, and shoe–dependent movement patterns in runners using full-body kinematics. *Gait Posture* 36, 40–45. doi: 10.1016/j.gaitpost.2011.12.023

Mohr, M., Pieper, R., Löffler, S., Schmidt, A., and Federolf, P. (2021), "Sex-specific whole-body running kinematics: data, code, and supplemental files," in *Mendeley Data*, V2, doi: 10.17632/ndvj69k7bx.2

Neal, B. S., Barton, C. J., Gallie, R., O'Halloran, P., and Morrissey, D. (2016). Runners with patellofemoral pain have altered biomechanics which targeted interventions can modify: a systematic review and meta-analysis. *Gait Posture* 45, 69–82. doi: 10.1016/j.gaitpost.2015.11.018

Nielsen, R. O., Buist, I., Sørensen, H., Lind, M., and Rasmussen, S. (2012). Training errors and running related injuries: a systematic review. *Int. J. Sports Phys. Ther.* 7, 58–75.

Nigg, B. M., Baltich, J., Maurer, C., and Federolf, P. (2012). Shoe midsole hardness, sex and age effects on lower extremity kinematics during running. *J. Biomech.* 45, 1692–1697. doi: 10.1016/j.jbiomech.2012.03.027

Noehren, B., Davis, I., and Hamill, J. (2007). ASB clinical biomechanics award winner 2006: prospective study of the biomechanical factors associated with iliotibialband syndrome. *Clin. Biomech.* 22, 951–956. doi: 10.1016/j.clinbiomech.2007.07.001

Noehren, B., Scholz, J., and Davis, I. (2011). The effect of real-time gait retraining on hip kinematics, pain and function in subjects with patellofemoral pain syndrome. *Br. J. Sports Med.* 45, 691–696. doi: 10.1136/bjsm.2009.069112

Phinyomark, A., Hettinga, B. A., Osis, S. T., and Ferber, R. (2014). Gender and age-related differences in bilateral lower extremity mechanics during treadmill running. *PLoS One* 9:e105246. doi: 10.1371/journal.pone.0105246

Phinyomark, A., Osis, S., Hettinga, B. A., Leigh, R., and Ferber, R. (2015). Gender differences in gait kinematics in runners with iliotibial band syndrome. *Scand. J. Med. Sci. Sports* 25, 744–753. doi: 10.1111/sms.12394

Phinyomark, A., Osis, S. T., Hettinga, B. A., Kobsar, D., and Ferber, R. (2016). Gender differences in gait kinematics for patients with knee osteoarthritis. *BMC Musculoskelet. Disord.* 17:157. doi: 10.1186/s12891-016-1013-z

Rajagopal, A., Dembia, C., DeMers, M., Delp, D., Hicks, J., and Delp, S. (2016). Full body musculoskeletal model for muscle-driven simulation of human gait. *IEEE Trans. Biomed. Eng.* 63, 2068–2079. doi: 10.1109/tbme.2016.2586891

Ristolainen, L., Heinonen, A., Waller, B., Kujala, U. M., and Kettunen, J. A. (2009). Gender differences in sport injury risk and types of inju-ries: a retrospective twelve–month study on cross-country skiers, swimmers, long–distance runners and soccer players. *J. Sports Sci. Med.* 8, 443–451.

Sakaguchi, M., Ogawa, H., Shimizu, N., Kanehisa, H., Yanai, T., and Kawakami, Y. (2014). Gender differences in hip and ankle joint kinematics on knee abduction during running. *Eur. J. Sport Sci.* 14(Suppl. 1), S302–S309.

Schache, A. G., Blanch, P., Rath, D., Wrigley, T., and Bennell, K. (2003). Differences between the sexes in the three-dimensional angular rotations of the lumbo-pelvic-hip complex during treadmill running. *J. Sports Sci.* 21, 105–118. doi: 10.1080/0264041031000070859

Schache, A. G., Blanch, P. D., Rath, D. A., Wrigley, T. V., and Bennell, K. L. (2005). Are anthropometric and kinematic parameters of the lumbo-pelvic-hip complex related to running injuries? *Res. Sports Med.* 13, 127–147. doi: 10.1080/15438620590956133

Schache, A. G., Blanch, P. D., Rath, D. A., Wrigley, T. V., Starr, R., and Bennell, K. L. (2001). A comparison of overground and treadmill running for measuring the three-dimensional kinematics of the lumbo-pelvic-hip complex. *Clin. Biomech.* 16, 667–680. doi: 10.1016/s0268-0033(01)00061-4

Taunton, J. E., Ryan, M. B., Clement, D. B., McKenzie, D. C., Lloyd-Smith, D. R., and Zumbo, B. D. (2002). A retrospective case-control analysis of 2002 running injuries. *Br. J. Sports Med.* 36, 95–101. doi: 10.1136/bjsm.36.2.95

Troje, N. F. (2002). Decomposing biological motion: a framework for analysis and synthesis of human gait patterns. *J. Vis.* 2, 371–387.

Werner, I., Szelenczy, N., Wachholz, F., and Federolf, P. (2020). How do movement patterns in weightlifting (clean) change when using lighter or heavier barbell loads? – A comparison of two principal component analysis-based approaches to studying technique. *Front. Psychol.* 11: 606070. doi: 10.3389/fpsyg.2020.606070

Willson, J. D., Loss, J. R., Willy, R. W., and Meardon, S. A. (2015). Sex differences in running mechanics and patellofemoral joint kinetics following an exhaustive run. *J. Biomech.* 48, 4155–4159. doi: 10.1016/j.jbiomech.2015.10.021

Willwacher, S., Goetze, I., Fischer, K. M., and Brüggemann, G.-P. (2016). The free moment in running and its relation to joint loading and injury risk. *Footwear Sci.* 8, 1–11. doi: 10.1080/19424280.2015.1119890

Willy, R. W., and Davis, I. S. (2011). The effect of a hip-strengthening program on mechanics during running and during a single-leg squat. *J. Orthop. Sports Phys. Ther.* 41, 625–632. doi: 10.2519/jospt.2011.3470

Willy, R. W., Scholz, J. P., and Davis, I. S. (2012). Mirror gait retraining for the treatment of patellofemoral pain in female runners. *Clin. Biomech.* 27, 1045–1051. doi: 10.1016/j.clinbiomech.2012.07.011

Conflict of Interest: The authors declare that the research was conducted in the absence of any commercial or financial relationships that could be construed as a potential conflict of interest.

frontiers in Human Neuroscience

ORIGINAL RESEARCH
published: 23 July 2021
doi: 10.3389/fnhum.2021.682080

Temporal Dynamics of Corticomuscular Coherence Reflects Alteration of the Central Mechanisms of Neural Motor Control in Post-Stroke Patients

*Maxime Fauvet[1], David Gasq[1,2], Alexandre Chalard[1,3,4], Joseph Tisseyre[1] and David Amarantini[1]**

[1] ToNIC—Toulouse NeuroImaging Center, Université de Toulouse, Inserm, UPS, Toulouse, France, [2] Department of Functional Physiological Explorations, University Hospital of Toulouse, Hôpital Rangueil, Toulouse, France, [3] Department of Neurology, University of California, Los Angeles, Los Angeles, CA, United States, [4] California Rehabilitation Institute, Los Angeles, CA, United States

The neural control of muscular activity during a voluntary movement implies a continuous updating of a mix of afferent and efferent information. Corticomuscular coherence (CMC) is a powerful tool to explore the interactions between the motor cortex and the muscles involved in movement realization. The comparison of the temporal dynamics of CMC between healthy subjects and post-stroke patients could provide new insights into the question of how agonist and antagonist muscles are controlled related to motor performance during active voluntary movements. We recorded scalp electroencephalography activity, electromyography signals from agonist and antagonist muscles, and upper limb kinematics in eight healthy subjects and seventeen chronic post-stroke patients during twenty repeated voluntary elbow extensions and explored whether the modulation of the temporal dynamics of CMC could contribute to motor function impairment. Concomitantly with the alteration of elbow extension kinematics in post-stroke patients, dynamic CMC analysis showed a continuous CMC in both agonist and antagonist muscles during movement and highlighted that instantaneous CMC in antagonist muscles was higher for post-stroke patients compared to controls during the acceleration phase of elbow extension movement. In relation to motor control theories, our findings suggest that CMC could be involved in the online control of voluntary movement through the continuous integration of sensorimotor information. Moreover, specific alterations of CMC in antagonist muscles could reflect central command alterations of the selectivity in post-stroke patients.

Keywords: electroencephalography, electromyography, brain muscle functional connectivity, agonist and antagonist muscles, elbow extension

OPEN ACCESS

Edited by:
Christoph Centner, University of Freiburg, Germany

Reviewed by:
Francesco Felici, Foro Italico University of Rome, Italy
Alessandro Del Vecchio, University of Erlangen Nuremberg, Germany

***Correspondence:**
David Amarantini
david.amarantini@inserm.fr

Specialty section:
This article was submitted to Motor Neuroscience, a section of the journal Frontiers in Human Neuroscience

Received: *17 March 2021*
Accepted: *21 June 2021*
Published: *23 July 2021*

Citation:
Fauvet M, Gasq D, Chalard A, Tisseyre J and Amarantini D (2021) Temporal Dynamics of Corticomuscular Coherence Reflects Alteration of the Central Mechanisms of Neural Motor Control in Post-Stroke Patients. Front. Hum. Neurosci. 15:682080. doi: 10.3389/fnhum.2021.682080

INTRODUCTION

Understanding how agonist and antagonist muscles activity is controlled during goal-directed and precise movements is an ongoing challenge in understanding neural control of human movement. In motor control and related fields, it has been demonstrated that muscular contraction is generated by an efferent motor command sent from the motor cortex to the muscles based

on somatotopic organization in the central nervous system (Jasper and Penfield, 1949; Penfield, 1954). Moreover, movement control implies continuous integration of afferent and efferent information (Campfens et al., 2013) during both preparatory and online control phases of movement execution (Buneo and Andersen, 2006). This argues for the involvement of continuous communication between the brain and muscles to drive efficiently the activity of both agonist and antagonist muscles activated during the movement. The analysis of the brain's oscillatory rhythms through event-related desynchronization (Pfurtscheller, 1992) in the beta frequency band (β, 13–30 Hz) enables characterizing increased cortical excitability during movement, thought to reflect an "activated (cortical) state with enhanced processing" (Pfurtscheller, 2001) related to motor control (Pfurtscheller and Lopes da Silva, 1999). The interactions between brain and muscles can be further analyzed through corticomuscular coherence (CMC), the use of which has been in continuous development for two decades in the fields of motor control and neuroscience. CMC can be taken as a descriptor of the brain-muscle functional connectivity, defined as a measure of the functional coupling between sensorimotor cortex and muscular activity obtained from electroencephalography (EEG) and electromyography (EMG) during muscular contraction (Conway et al., 1995; Halliday et al., 1998; Mima and Hallett, 1999; Salenius and Hari, 2003; Baker, 2007). CMC would result from the interaction between the motor cortex and contracting muscles via efferent descending motor pathways and afferent ascending somatosensory pathways (Baker, 2007; Witham et al., 2011; Campfens et al., 2013), which is consistent with evidence of the efferent and afferent components in CMC (Riddle and Baker, 2005). Even if it still remains to clearly understand the functional role of such a synchronization between the brain and muscle oscillatory signals (Bourguignon et al., 2019), most studies on CMC in motor control endorse the consensus that CMC takes part in the regulation of agonist and antagonist muscles activity (Cremoux et al., 2017; Dal Maso et al., 2017), and is related to sensorimotor integration (Baker, 2007; Witham et al., 2011). CMC is thus thought to reflect a direct regulation process occurring in the motor system via the corticospinal pathway (Conway et al., 1995; Kristeva et al., 2007).

Most of the results on the contribution of CMC to motor control have been obtained during isometric muscular contractions (Conway et al., 1995; Mima et al., 1999; Salenius and Hari, 2003). In healthy subjects, these results have highlighted that the value of significant CMC can vary according to the force level (Mima et al., 1999; Omlor et al., 2007), experimental design (von Carlowitz-Ghori et al., 2014) and the frequency band even if it occurs mainly at ∼20 Hz (i.e., in the β frequency band). The first studies analyzing CMC during dynamic contractions have shown that CMC was present during the pre- and post-movement phases, but was absent during movement (Kilner et al., 1999, 2003). However, more recent studies conducted on isokinetic (Liu et al., 2019) or cyclical (Yoshida et al., 2017) contractions have shown that the CMC magnitude is not constant over the time-period corresponding to movement, and a recent study performed on healthy subjects engaged in a squat-like task revealed that the level of CMC was different according to either the concentric, eccentric or isometric movement phases (Kenville et al., 2020). Similarly, a recent study from our group (Glories et al., 2021) showed that CMC decreased in lengthening compared to isometric contractions. Taken together, these results raise an important methodological concern regarding CMC evaluation—namely the need for a novel dynamic analysis framework to account for the time-varying changes in CMC during the time course of movement execution – and hence the need to refine and enhance our understanding of its involvement in the functional coupling between brain and muscles. This is also in agreement with the recent findings from Nijhuis et al. (2021) who highlighted dynamic modulations of CMC in healthy subjects involved in finger tapping, thus suggesting "an important role of beta band neural oscillations in [. . .] sensorimotor synchronization."

In line with the approach used by Chen et al. (2018) to investigate the brain mechanisms underlying the control of inter-joint synergies in post-stroke patients, the relevance of analyzing the temporal evolution of CMC is assumed to be not only fundamental, but also clinical. Indeed, previous studies have found lower CMC in stroke patients compared to healthy subjects (Mima et al., 2001; Fang et al., 2009), and have also shown that CMC peaks are more widely distributed over the scalp in post-stroke subjects (Rossiter et al., 2013). These findings may be at least partly explained by the numerous neuronal reorganizations and adaptive mechanisms that occur following stroke (Grefkes and Ward, 2014): as a consequence of the alteration of the corticospinal tract (Chollet et al., 1991) and other neuronal circuits (Ward et al., 2003), stroke implies increased activity in contralesional motor cortex or ipsilesional non-sensorimotor regions (Chollet et al., 1991; Ward et al., 2003; Gerloff, 2006) and decreased intercortical inhibitions (Grefkes et al., 2008). These impairments lead to less efficient neural drive to paretic muscles and may alter the flow of afferent and efferent information required for fine motor control, to the detriment of limb motor function and patient's autonomy (Langhorne et al., 2011). Previous studies proposed that the remaining CMC in patients could reflect the degree of recovery after stroke (Graziadio et al., 2012; Zheng et al., 2018). The examination of temporal dynamics of CMC in stroke patients could open new insights on what extent the alteration of the neural information flow along the motor tracts contributes to motor function impairment. Referring to the perspectives offered by the analysis of the temporal evolution of corticomuscular interactions after stroke (Chen et al., 2018), a comparison of CMC dynamics during voluntary movement between healthy subjects and post-stroke patients could further help understanding the roles of CMC in motor control with potential application for the use of brain computer interfaces for rehabilitation (Tung et al., 2013).

Using a novel analysis framework, the present study compares time-varying changes in CMC during sub-movement phases of active elbow extension between control subjects and post-stroke patients, exploring possible association between alterations of motor performances and alterations of the brain-muscles communication. Such links would help understand the functional role of CMC in the control of agonist and antagonist muscles during voluntary active movements. In line both with previous

results (Yoshida et al., 2017; Liu et al., 2019; Nijhuis et al., 2021) and the hypothesis of constant integration of afferent and efferent information in CMC, we first hypothesized that CMC would vary with movement time for both control subjects and post-stroke patients. We also expected to find differences in either average or instantaneous CMC parameters between control subjects and post-stroke patients, which could reflect a deficit of motor control after stroke resulting from an alteration of afferent and efferent information flows. The significance of these findings are discussed in relation to motor control theories to better understand to what extent temporal dynamics of CMC could reflect adaptive mechanisms contributing to motor performance after stroke.

MATERIALS AND METHODS

Participants

Eight healthy control volunteers (43 ± 21 years, three females) and seventeen post-stroke patients in chronic phase (58.2 ± 12.7 years, four females), none of which was specifically trained to the task, were recruited from two different ongoing prospective studies (see **Table 1** for detailed patient demographics). Patients with cognitive disorders preventing simple instruction comprehension, with an active elbow extension angle less than 20 degrees or suffering from painful movement of the paretic arm were excluded from the study. The first study, approved by the Research Ethical Committee of Toulouse University Hospitals (No. 07-0716), included five post-stroke patients and all healthy controls, and the second study, approved by Research Ethics Board (No. ID-RCB: 2017-A01616-47), included the remaining subjects. Both studies were conducted in accordance with the Declaration of Helsinki and all participants gave written informed consent.

Experimental Procedure

The experimental procedure was the same as described in Chalard et al. (2020). Briefly, in the initial position, subjects were comfortably seated, their arms resting on a table with shoulders 80° flexed, the elbow 90° flexed and the forearm placed in front of the thorax. They were instructed to perform two series of ten full elbow extension/flexion cycles at a self-selected speed, returning to the initial position once the flexion movement has ended. Each movement cycle was preceded with an audible stimulus, with at least 10 s rest between each elbow extension and flexion. The experimental procedure was performed on both the dominant and the non-dominant arms for control subjects and on both the paretic and the non-paretic arms for post-stroke patients.

Materials

Kinematics

Upper limb kinematics were recorded at 125 Hz with eight infrared cameras (model S250e, Optitrack, NaturalPoint, Corvallis, Oregon, United States). Reflective markers were placed upon breastbone, C7 vertebra, and both acromion, lateral epicondyle, ulnar styloid and second metacarpal. Arm et forearm segments were defined by acromion-lateral epicondyle and lateral epicondyle-ulnar styloid markers, respectively.

Electroencephalography

EEG data were continuously recorded at 1024 Hz using a 64-channel EEG cap (ActiveTwo System, Biosemi, Amsterdam, Netherlands) placed according to the international 10–20 system. Reference electrodes were included in the cap and impedance of all electrodes was maintained below 30 kΩ before the experiment start.

Electromyography

Surface EMG signals from triceps brachii (TB), biceps brachii (BB), brachialis (BA), and brachioradialis (BR) were recorded at 1000 Hz using disposable Ag-AgCl electrodes in bipolar configuration with an inter-electrode distance of 2 cm, by using the MP150 system with EMG100C amplifier (Biopac Systems Inc., Goleta, CA, United States). After standard skin preparation procedures (Hermens et al., 2000), the pairs of electrodes were placed over the belly of each muscle, identified from palpations and few blank tests of elbow extension, in a same manner was done in Charissou et al. (2017) for surface EMG of hand and wrist muscles. The reference electrode was placed on the right mastoid. Additionally, the EMG signals were monitored online before the experiment start to assess the good positioning of electrodes and the recordings quality.

Synchronization

Kinematic, EEG, and EMG data were synchronized with a common Transistor-Transistor Logic (TTL) pulse generated from the Biopac MP150 system.

Analysis

Data preprocessing and analysis were performed offline with MATLAB 2017b (The MathWorks Inc., Natick, MA, United States). In this study, only elbow extensions of the dominant arm in controls and of the paretic arm in post-stroke patients were considered, mainly because the non-paretic arm is known to be also affected in post-stroke patients (Graziadio et al., 2012), suggesting that it may not be a suitable control for our analysis. It is noteworthy that no significant differences were found between dominant and non-dominant arms in controls.

Data Preprocessing

Kinematic data were low-pass filtered at 6 Hz. Elbow joint angle was calculated as the two-dimensional angle between the arm and forearm segments. Elbow angular velocity and acceleration profiles were obtained from elbow angular displacement data by finite differentiation. An angular velocity threshold over 0.01 degrees.s^{-1} was chosen to identify the beginning and end of each elbow extension movement (Chalard et al., 2020).

Continuous EMG and EEG data were 3–100 Hz band-pass and 45–55 Hz notch filtered, all filters being zero-lag fourth order Butterworth filters.

Kinematic, EMG and EEG data were segmented into epochs from −3 s prior to the beginning and + 3 s after the end of each movement.

TABLE 1 | Participants' demographics (M, Male; F, Female; FMA, Fugl-Meyer Assessment for upper extremity; WFMT, Wolf Function Motor Test; MCA, Middle Cerebral Artery).

Subjects	Age/Sex	Time since stroke (months)	Stroke type	Localization	FMA	WFMT
S1	61/M	51	Hemorrhage	Right, basal ganglia and corona radiata	38	33
S2	59/F	18	Ischemia	Right, cortical and subcortical territories of MCA	46	34
S3	69/M	19	Ischemia	Right, pons	44	46
S4	65/M	75	Ischemia	Right, cortical and subcortical territories of MCA	32	50
S5	50/M	30	Hemorrhage	Left, basal ganglia and internal capsule	42	42
S6	57/M	14	Ischemia	Left, posterior limb of the internal capsule	45	46
S7	75/M	26	Ischemia	Left, cortical and subcortical territories of MCA	26	10
S8	46/M	8	Ischemia	Left, cortical and subcortical territories of MCA	53	49
S9	65/M	116	Ischemia	Right, cortical and subcortical territories of MCA	30	36
S10	49/M	13	Ischemia	Right, pons	53	50
S11	33/F	13	Ischemia	Left, pons middle cerebral peduncles	45	48
S12	33/F	12	Ischemia	Left, subcortical territories of MCA	21	25
S13	57/M	18	Ischemia	Right, cortical and subcortical territories of MCA	41	42
S14	56/M	34	Ischemia	Right, cortical and subcortical territories of MCA	29	29
S15	75/M	12	Ischemia	Left, subcortical territories of MCA and hippocampus uncus	50	54
S16	74/M	34	Ischemia	Right, pons	23	28
S17	66/M	6	Ischemia	Left, subcortical territories of MCA	47	47
Controls (n = 8)	43 ± 21/3F	–	–	–	–	–

EMG signals were visually inspected to reject epochs with movement artifacts. Additionally, for each subject, the epochs with outlier values for which EMG root mean square (RMS) was larger than twice the standard error were also rejected in order to exclude potential unexpected movements. EEG data were common average referenced and visually inspected to reject epochs with eye-blinks or face and neck muscles contractions artifacts.

The average number of remaining elbow extensions for analysis was similar between control subjects and post-stroke patients [13.9 ± 4.6 vs. 14.2 ± 3.5; $t(20) = 0.18$, $p > 0.05$].

Kinematic Analysis

Active elbow extension angle was calculated from the difference of the elbow joint angle between the initial and the fully extended arm positions.

As recommended by Rohrer et al. (2002), movement smoothness was quantified as the number of peaks of the acceleration profile analysis, further normalized by the mean angular velocity (de los Reyes-Guzmán et al., 2014; Chalard et al., 2020).

Corticomuscular Coherence Analysis

Corticomuscular Coherence Calculation

CMC between EEG signals and unrectified EMG signals was first computed in the time-frequency domain using wavelet analysis with the *WaveCrossSpec* package proposed in Bigot et al. (2011) and previously used for corticomuscular coherence analysis (Cremoux et al., 2017; Dal Maso et al., 2017). In the ongoing debate on EMG rectification for coherence analysis, we clearly advocate the non-rectification of EMG signals to satisfy both theoretical arguments (Bigot et al., 2011; McClelland et al., 2012) and experimental evidence showing that EMG rectification is not suitable for coherence analysis (Ruiz-Gonzalez et al., 2019). In *WaveCrossSpec*, the wavelet parameters "nvoice," "J1" and "wavenumber" were, respectively, set to 7, 30 and 10 to yield time-frequency transforms of full signals in the 0.002–48 Hz frequency range. These parameters set the time-frequency precision compromise to a 0.1 s – 3 Hz precision window within the β (13–30 Hz) frequency band. To cope with the issue of inter-trial duration variability that can lead to power spectrum cancelation, a normalization procedure was used to obtain EEG and EMG time-frequency power and EEG-EMG coherence spectra with time expressed as a percentage of elbow extension movement time (Fauvet et al., 2019). This normalization step is designed as to preserve frequency content of signals and enable point-wise comparison between trials of different durations. Typical recordings of kinematics, EMG from TB electrode, EEG from C3 electrode and CMC obtained in control (left) and patient (right) are presented in **Figure 1**.

Corticomuscular Coherence Detection and Quantification

In order to consider the functional reorganization of motor networks following stroke (Grefkes and Ward, 2014), the choice of interest EEG electrodes was individualized among participants. Then, for each subject, CMC was analyzed with the EEG electrode where event-related desynchronization in the β band was highest among the electrodes covering bilateral sensorimotor areas (Krauth et al., 2019) (FC1, FC3, FC5, C1, C3, C5, CP1, CP3, CP5, FCz, Cz, CPz, FC2, FC4, FC6, C2, C4, C6, CP2, CP4, CP6). The choice of the EEG electrodes showing the maximum event-related desynchronization values during movement ensures that CMC is computed from the sensorimotor regions with the maximum cortical activity. Only these selected and personalized sets of EEG electrodes were used in the following steps of analysis.

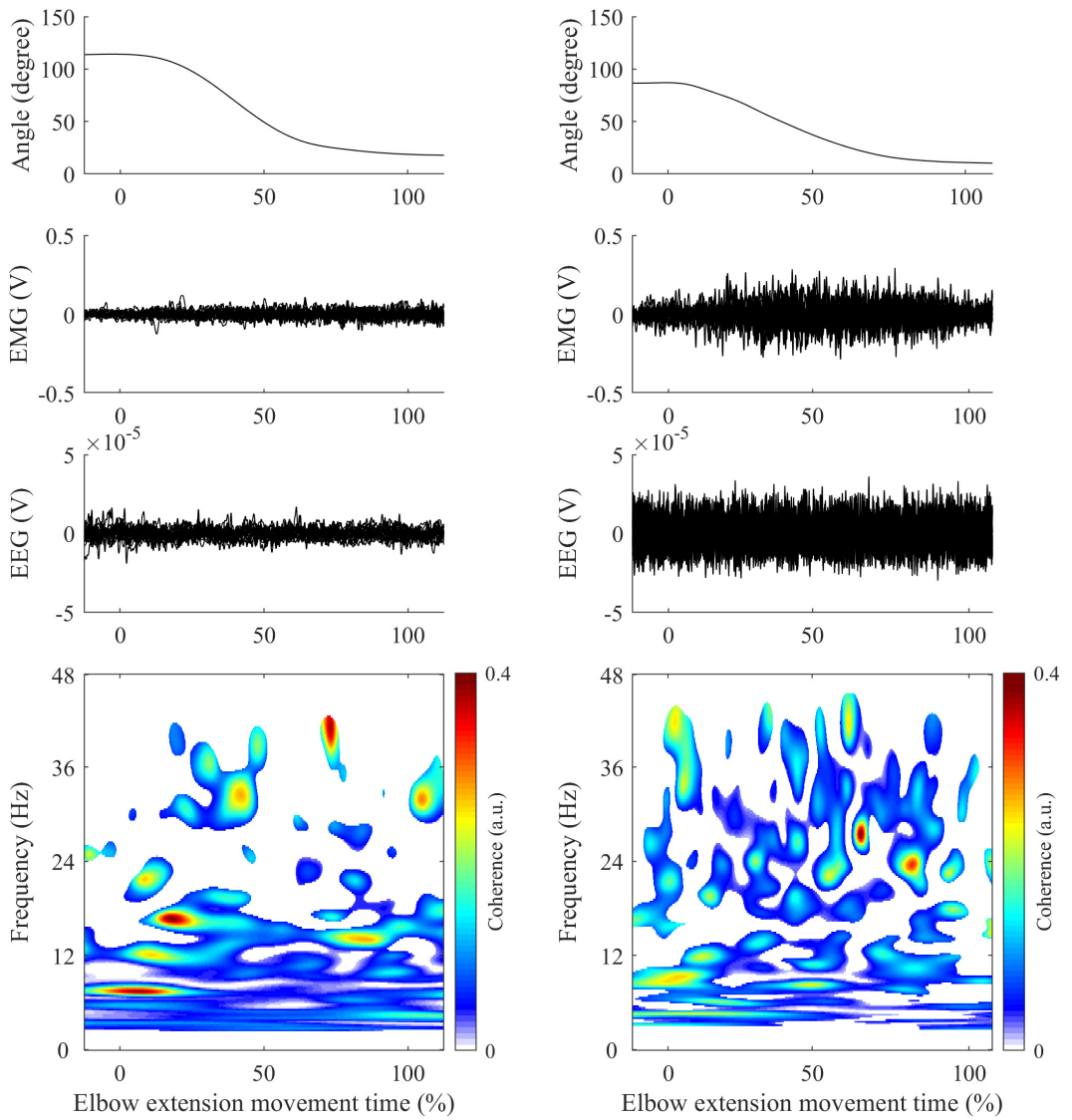

FIGURE 1 | Illustration of typical recordings obtained in control (left panels) and patient (right panels) during elbow extension movement. First row: Elbow joint kinematics. Second row: Mean EMG signals from Triceps Brachii. Third row: Mean EEG signals from C3/C4 electrodes (depending on the studied arm). Fourth row: CMC computed between EMG (Triceps Brachii) and EEG signals following steps described in methods. All-time series are represented in percent of elbow extension.

For each subject and each muscle separately, CMC was finally quantified from EEG-EMG coherence values where the interactions between the EEG and EMG was significant in the time-frequency plane with two key approaches:

- First approach: Average CMC was computed as the mean of magnitude-squared coherence values in the β band where a significant correlation between EEG and EMG was detected on the wavelet cross-spectrum (Bigot et al., 2011) over (i) the whole elbow extension movement duration, (ii) the acceleration phase of elbow extension and (iii) the deceleration phase of elbow extension. This distinction between the acceleration and deceleration phases, as indicated by the time to peak elbow angular velocity, has been made to consider the changes in the coordination and the functional role of agonist and antagonist muscles between the two phases (Chiovetto et al., 2013).
- Second approach: To investigate temporal dynamics of CMC, instantaneous CMC was computed at each time instant t as the mean of the magnitude-squared coherence values in the β band where a significant correlation between EEG and EMG was detected on the wavelet cross-spectrum (Bigot et al., 2011).

Statistics

Statistical analyses were performed with Matlab built-in functions. Generalized linear models were used to test the group effect (i.e., controls vs. patients) on the mean values of

active elbow extension angle, peak angular velocity, movement smoothness and average CMC computed over the entire movement and in both the acceleration and deceleration phases. Models' results are presented as mean ± standard error (SE) difference between patients and controls, with the corresponding explained variance (R^2) and p-value. The models' quality was graphically assessed by visual evaluation of residuals normality and variance homogeneity (Anscombe, 1973). It is noteworthy that all models showed normal residuals distribution and explained at least half of the total variance. For all tests, significance was accepted at $p < 0.05$.

Inter-group instantaneous differences in angular kinematic and CMC profiles were assessed with Tmax non-parametric tests (Wilcoxon signed-rank-based) using 2000 permutations as implemented in EEGLAB, 2019 version, function *statcond* (Delorme and Makeig, 2004). As performed by Castelhano et al. (2017), p-values were corrected for multiple comparisons with a successive use of False Discovery Rate (Benjamini and Hochberg, 1995) and cluster-based (Maris and Oostenveld, 2007) methods.

The same statistical procedure was used to determine instantaneous differences from either the mean or the null value on CMC profiles, and to inspect the inter-group differences in the instantaneous CMC of each EEG/EMG electrode pairs. For the antagonist muscles, the periods showing significant CMC with BA, BB, and BR were pooled for this analysis.

RESULTS

Elbow Angular Kinematics

For the same functional task of elbow extension performed by both healthy controls and post-stroke patients, the analysis revealed between-groups differences in motor performance. The mean amplitude of active elbow extension was 91 ± 11 degrees for controls and 60 ± 12 degrees for patients, indicating that a significant decrease (−32 ± 2.3 degrees, $R^2 = 0.61$, $p < 0.01$) was found in the patient group when compared to the control group. Similarly, the peak angular velocity was -0.86 ± 0.02 degrees.s^{-1} for controls and -0.58 ± 0.02 degrees.s^{-1} for patients, leading to a significant velocity peak decrease in patients (-0.28 ± 0.02 degrees.s^{-1}, $R^2 = 0.50$, $p < 0.01$). Moreover, the analysis of sub-phases of movement revealed that movement smoothness was significantly altered in patients compared with controls during the deceleration phase only (+ 0.60 ± 0.23, $R^2 = 0.22$, $p = 0.02$; **Figure 2**).

Average and Instantaneous CMC

Average CMC computed over the whole elbow extension movement duration with elbow extensor or each flexor did not significantly differ between groups ($0.01 < R^2 < 0.08$, all $p > 0.12$). Likewise, no significant inter-group differences were observed on average CMC during either the acceleration or deceleration ($0.01 < R^2 < 0.06$, all $p > 0.30$; and $0.01 < R^2 < 0.04$, all $p > 0.35$, respectively). Detailed average CMC of each group are presented in **Table 2**. Nevertheless, the results provided by the analysis of CMC dynamics showed differences between the two groups, revealing the substantial interest of such analyses:

- The instantaneous CMC magnitude for BA of each group is represented in **Figure 3**. Point-wise comparison of CMC to zero showed a biphasic pattern for healthy controls: CMC was not significantly different from zero during the first 25% of movement duration (CMC < 0.02, all $t < 2.32$, all corrected $p > 0.05$), while it was significantly above zero during the remaining time of movement ($0.02 < \text{CMC} < 0.07$, $2.33 < t < 5.91$, all corrected $p < 0.05$). Conversely, instantaneous CMC remained continuously above zero during the whole movement duration for post-stroke patients ($0.03 < \text{CMC} < 0.09$, $2.74 < t < 7.30$, all corrected $p < 0.05$).
  The comparison of instantaneous CMC to mean CMC values of each group showed a biphasic pattern for both healthy controls and post-stroke patients. However, CMC was significantly below the mean for the first 25% of movement duration for healthy controls (CMC < 0.02, $2.13 < t < 3.52$, all corrected $p < 0.05$), while it was significantly below the mean during only the first 15% of movement duration for post-stroke patients (CMC < 0.035, $2.23 < t < 7.94$, all corrected $p < 0.05$). Noteworthy, the same pattern for both groups was observed in the two other antagonist muscles (i.e., BB and BR), whereas it was not observed in the agonist muscle (i.e., TB) (results not shown).
- The inter-group comparisons of instantaneous CMC magnitude are shown in **Figure 4**. In reference to the inter-group differences of the amplitude of active elbow extension, point-wise comparison of the mean CMC with TB—i.e., with the agonist muscle—between the two groups did not reveal any difference ($0.00 < \text{CMC difference} < 0.04$, $0.01 < t < 2.17$, all corrected $p > 0.05$). Similarly, the dynamic analysis of CMC with BA muscle did not reveal differences of CMC magnitude between the two groups ($0.00 < \text{CMC difference} < 0.03$, $0.01 < t < 2.43$, all corrected $p > 0.05$). However, when compared to healthy controls, higher CMC was observed and subsequently confirmed by the effect size analysis ($0.23 < \text{Hedges' g} < 0.94$) in post-stroke patients during the acceleration phase of elbow extension only. Noteworthy is that the same results were observed for the two other antagonist muscles (i.e., BB and BR) (results not shown).

DISCUSSION

This study originally investigated temporal dynamics of CMC in healthy subjects and post-stroke patients involved in a self-paced elbow extension movement to provide an understanding of whether the alteration of the functional coupling between brain and muscles contributes to motor function impairment. We analyzed kinematic data and changes of CMC magnitude over time during both the acceleration and deceleration phases of elbow extensions. Observed alterations of movement kinematics after stroke and changes in CMC compared to controls are discussed in relation to motor control theories in order to better understand the functional significance of CMC parameters in

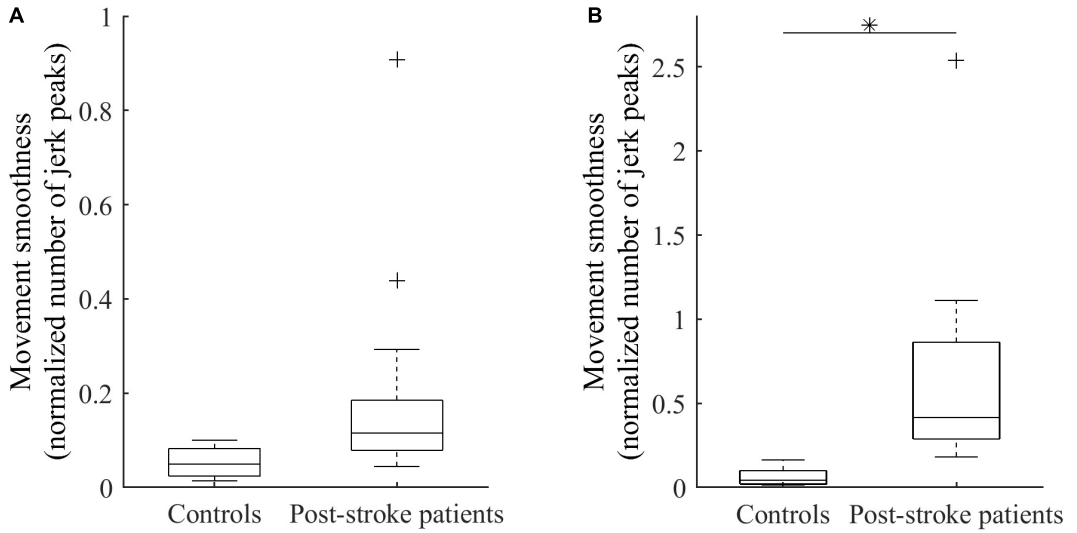

FIGURE 2 | Smoothness of elbow extension for controls and patients during the acceleration phase **(A)** and the deceleration phase **(B)**. *Indicates a significant between-group difference ($p < 0.05$).

TABLE 2 | Average CMC magnitude ± SE of each group in all muscles and all movement phases.

	Full movement		Acceleration phase		Deceleration phase	
Muscle	**Controls**	**Patients**	**Controls**	**Patients**	**Controls**	**Patients**
TB	0.04 ± 0.01	0.04 ± 0.01	0.04 ± 0.02	0.03 ± 0.03	0.06 ± 0.02	0.05 ± 0.03
BA	0.03 ± 0.02	0.04 ± 0.03	0.02 ± 0.02	0.03 ± 0.03	0.07 ± 0.02	0.06 ± 0.03
BB	0.03 ± 0.02	0.04 ± 0.02	0.03 ± 0.02	0.03 ± 0.03	0.04 ± 0.02	0.05 ± 0.04
BR	0.03 ± 0.02	0.04 ± 0.03	0.02 ± 0.03	0.02 ± 0.05	0.03 ± 0.02	0.03 ± 0.04

Statistical analyses did not reveal any inter-group differences.

the neural motor control of agonist and antagonist muscles. The higher CMC levels observed in patients during the acceleration phase of the elbow extension is proposed to reflect the loss of selectivity of motor command occurring after stroke.

In line with the findings of previous studies (Murphy et al., 2011; Chalard et al., 2020), our results showed alteration of kinematic elbow extension performance parameters in post-stroke patients compared to healthy subjects. As expected, active elbow extension angle and extension angular velocity decreased in post-stroke patients. Besides these well-known motor function alterations (Parker et al., 1986), our results further confirmed that movement smoothness was also altered in post-stroke patients, but this group difference was specific to the deceleration phase of elbow extension. This finding complements previous results which have highlighted that stroke patients' movement amplitude was related to movement smoothness (Murphy et al., 2011), and suggests an alteration of the central nervous mechanisms involved in the control of agonist or antagonist muscles during the braking phase of elbow extension. Indeed, even if it has been largely demonstrated that stretch reflex is increased in post-stroke patients (McPherson et al., 2018), i.e., a lower stretch sensitivity threshold leads to increased muscle contraction when the muscle is stretched, this hypothesis is supported by several key pieces of evidence. Among these evidence of increased antagonist muscle activity in post-stroke patients during voluntary movements, an association was found between altered beta cortical activity and excessive antagonist muscle activation (Chalard et al., 2020), and it has been shown that a less smooth movement is associated with recruitment of secondary motor areas of the brain during reaching and grasping after stroke (Buma et al., 2016). Referring to the single joint movement model proposed by Gottlieb et al. (1989) in the speed-insensitive condition which argues that only the duration of the excitation pulse to each muscle group is modified in a given task, herein we also saw evidence to suggest that the control of antagonist muscles may be less stationary after stroke compared to the situation in healthy subjects. We cannot exclude that agonist muscles weakening (Tang and Rymer, 1981) or inter-joint synergies impairment (Kisiel-Sajewicz et al., 2011) may take part in the alteration of movement smoothness. However, based on the assumption that agonist and antagonist muscles are controlled through the emission of continuous pulses triggering the agonists in acceleration phase and the antagonists in deceleration phase, we propose that post-stroke patients present sporadic excessive motor command to the antagonist

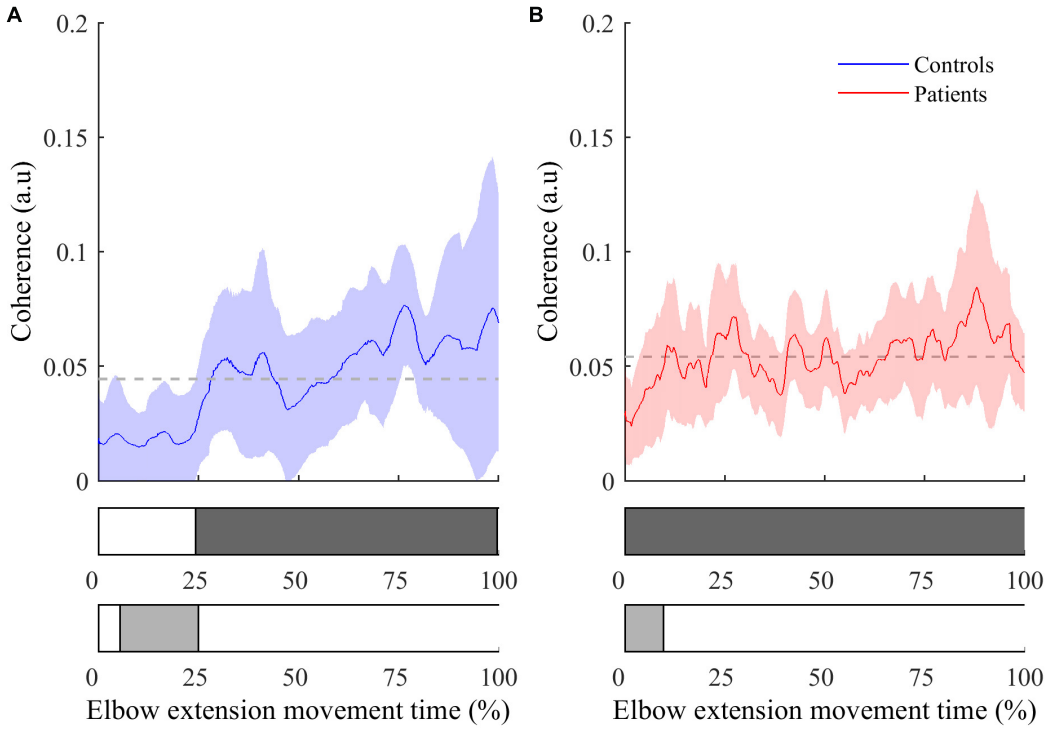

FIGURE 3 | Instantaneous CMC with BA muscle (mean ± 95% CI) as a function of time expressed in percent for controls **(A)** and patients **(B)**. The colored areas inside the horizontal bars beneath the graphs indicate time periods where CMC is significantly different from mean instantaneous CMC (light gray areas) or from null value (dark gray areas). In both graphs, the dashed lines represent the average CMC computed over the whole movement duration.

muscles during the deceleration phase, which may at least partly contribute to altering the smoothness and, *in fine*, the performance of their movement (Chalard et al., 2020).

Both the average and instantaneous CMC analyses employed here clearly showed a significant amount of CMC during movement in all muscles for both healthy subjects and post-stroke patients. CMC is known to be highly dependent on experimental design (von Carlowitz-Ghori et al., 2014), task difficulty (McClelland et al., 2012) or computation method (Bigot et al., 2011), and the actual presence of CMC during movements is still controversial. While some studies showed a total disappearance of CMC during lever displacement (Kilner et al., 2000, 2003), others highlighted significant CMC during either ankle cyclical (Yoshida et al., 2017) or isokinetic arm movements (Liu et al., 2019). In light of this debate, our results lend support to the idea that the detection of significant CMC occurs during both isometric contraction tasks and dynamic movements. In the same way as the conclusions drawn from isometric contraction paradigms, the presence of CMC during dynamic movements could indicate that it reflects central mechanisms involvement in control of agonist and antagonist muscles. Besides the detection of significant CMC during the whole elbow extension movement, the analysis of the temporal dynamics of CMC revealed the presence of CMC magnitude variations during movement in antagonist muscles for both healthy and post-stroke subjects, suggesting non-constant coupling between cortical and muscular pools of neurons. Beyond the evident methodological interest of such an analysis of CMC, this finding reveals that the flow of afferent or efferent information reflected through CMC (Riddle and Baker, 2005; Witham et al., 2011) varies over movement duration. From a functional point of view, the presence of variable CMC during movement might thus reflect a movement-phase dependent sensorimotor integration participating in the online motor control along the visual control of trajectory (Elliott et al., 1999).

The intra-group analysis (see **Figure 3**) revealed that the temporal dynamics of CMC were different between controls and post-stroke patients in the acceleration phase. Compared to controls, patients showed a shorter period of non-significant CMC relatively to the total acceleration phase, suggesting an earlier functional coupling.

Even though the absence of significant instantaneous differences of CMC magnitude in the dynamic inter-group analysis may challenge this finding, some convincing evidence allow us to consider inter-group differences of CMC in antagonist muscles as meaningful differences of the functional coupling between brain and muscles. Firstly, the lack of significant differences can be related to the high variability of instantaneous CMC (see **Figure 4**). Given the massive number of observations in the dynamic analysis (> 2000), the correction for multiple comparisons, although mandatory, required less CMC variability

and our analysis lacked statistical power allowing existing small differences to withstand the FDR correction. Secondly, by performing an instantaneous estimation of Hedges' g (Hedges and Olkin, 2014) as a complementary analysis to evaluate the magnitude of the difference of CMC between both groups in antagonist muscles, we highlighted medium to large effect size reflecting meaningful differences (Cohen, 2013). Effect size analyses are thought to overcome the inherent limitations of the *p*-values and may reveal meaningful differences even if the statistical power of the study is relatively weak (Sullivan and Feinn, 2012). These complemental results are presented in the third panel of **Figure 4** as a horizontal bar representing the instantaneous values of Hedges' g in a cyan-magenta spectrum. According to the common interpretation of Cohen's *d*-values (Cohen, 2013), the effect size of the difference in CMC magnitude ranges from medium to large effect (from 0.5 to 0.94) in roughly the same period highlighted in **Figure 3** and does not exceed medium effect (< 0.5) during the remaining movement time.

In light of those converging arguments, the observed inter-group meaningful differences of CMC in antagonist muscles provide valuable additional evidence for the alteration of antagonist muscles control at the beginning of the movement in post-stroke patients. Indeed, these findings suggest an increase in the efferent and afferent information flow, which may be interpreted in different ways. Firstly, one may suggest that the presence of a premature CMC during the acceleration phase in post-stroke patients could be explained by the previously reported hypothesis from Witham et al. (2011): an earlier increase of afferent information flow in patients would be reflected in CMC quantification. Secondly, one may argue that the task of elbow extension does not involve the same motor control strategy in healthy subjects and post-stroke patients since patients may use compensatory strategies involving more than one joint while controls can easily perform the task with a single joint strategy. Even though the relationship between muscular synergy and CMC remains unclear in the literature (Reyes et al., 2017; Chen et al., 2018), the earlier emergence of CMC in post-stroke patients might reflect these different strategies. However, we rather explain the earlier detection of functional coupling between the cortex and the antagonist muscles during the acceleration phase in post-stroke patients by the fact that the central command to antagonist muscles could be altered during the acceleration phase with a concomitant trigger of both agonist and antagonist commands. Referring to the λ model of the equilibrium-point theory (Feldman, 1986), this interpretation appears consistent with the well-documented impairment of muscle selectivity in post-stroke patients, which has already been correlated to the loss of motor function (Lang and Schieber, 2004; Schieber et al., 2009). This model proposes that the central mechanisms are represented through two commands: the reciprocal command (R) which regulates the net torque production around the joint from agonist and antagonist activities and the coactivation command (C) which controls the simultaneous activity of agonist and antagonist muscles. In line with the study of Levin and Dimov (1997) on agonist/antagonist coactivation in healthy subjects and post-stroke subjects, the observed modulation of CMC may reflect that post-stroke patients present a modification of the temporal representation of the C-command, leading to an altered control of the concomitant activity of elbow extensor and flexor muscles and, *in fine*, an alteration of the co-contraction dynamics to the detriment of their motor function. Even though the activation of alternate motor fibers in patients (Rüber et al., 2012) could induce a concomitant noise, disturbing the synchronization through corticospinal pathways, we rather

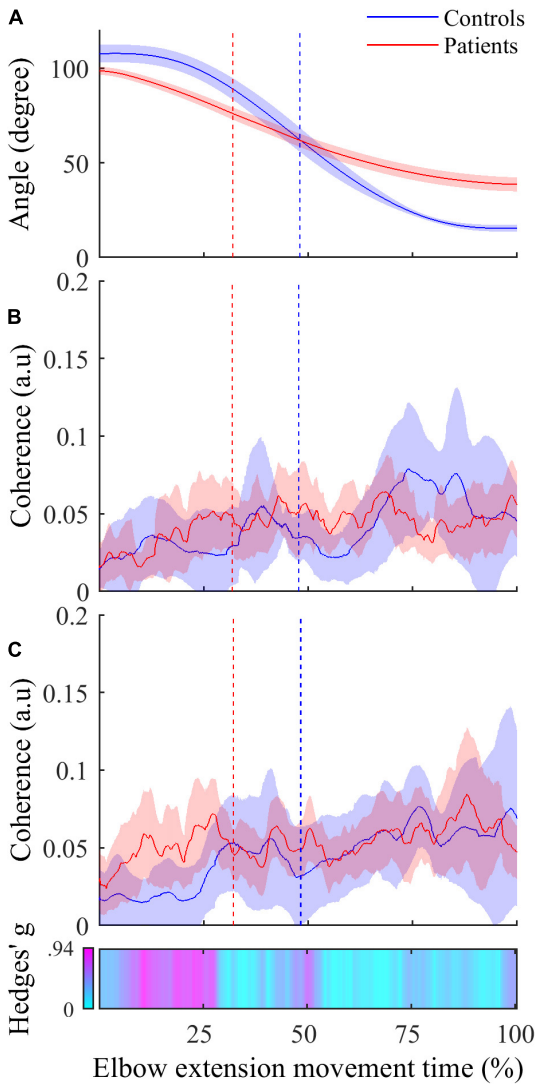

FIGURE 4 | (A) Active elbow extension angle (mean ± 95% CI) as a function of time expressed in percent for controls (in blue) and patients (in red). **(B)** Mean instantaneous CMC with agonist TB muscle (mean ± 95% CI) as a function of time expressed in percent for controls (in blue) and patients (in red). **(C)** Instantaneous CMC with antagonist BA muscle (mean ± 95% CI) as a function of time expressed in percent for controls (in blue) and patients (in red). In **(C)**, CMC is higher in patients in more than half the acceleration phase and not different in deceleration phase when using non-corrected *p*-values ($\alpha = 0.05$). Instantaneous Hedges' g, representing effect size of the CMC difference are shown as a horizontal bar with values ranging from 0 (cyan) to magenta (0.94). In all graphs, the vertical dashed lines represent the boundary between the acceleration and the deceleration phases for controls (in blue) and patients (in red).

explain that the major mechanism underlying such alteration is the discrepancy observed in inhibitory mechanisms in post-stroke patients, both in the brain (Grefkes et al., 2008) and in the spinal cord (Katz and Pierrot-Deseilligny, 1982).

LIMITS AND PERSPECTIVES

One could point out few limits of this work. Firstly, a relatively small number of control subjects have been included, potentially reducing the probability of finding inter-group differences. However, the choice of strict statistical analyses reduced the possible biases and allowed for strongly supported discussion. The number of patients and the presence of antagonist co-contractions motivated the non-separation of the different patients according to their motor functions during movements even in patients with a good recovery level. Nevertheless, the individualized analysis of the association between the alteration of temporal patterns of CMC and the alteration of motor function would be interesting to support the hypothesis of the potential role of CMC as a marker of motor recovery (Krauth et al., 2019). Secondly, the EMG signals recordings and investigations could reflect a small degree of crosstalk between the EMG electrodes, mainly for antagonist muscles as BA and BR electrodes were located relatively close to each other. However, special care was taken to locate EMG sensors on the desired target muscle, and the potential impact of crosstalk between EMG electrodes can be regarded as low given that the intermuscular interactions were not studied in the present work. Nevertheless, further data collection should favor the use of intramuscular electrodes for an accurate measure of individual muscle activity. Thirdly, the high dynamicity of the task may have induced EEG contaminations from muscular contractions of the upper body. However, as was done in all previous studies by our group on EEG during upper limb contraction (Cremoux et al., 2013; Tisseyre et al., 2019; Chalard et al., 2020), each trial was visually inspected to remove trials where EEG signals were contaminated by muscle artifacts. Finally, even though the experimental task is the same for all participants, strategies to achieve the elbow extension may vary between subjects, especially for stroke patients. Given that our CMC magnitude comparison between healthy subjects and post-stroke patients might reveal different muscular synergies rather than actual alterations of the same central motor control mechanisms (Chen et al., 2018), the present results may require further investigations with more controlled dynamic tasks (and then less degrees of freedom for unexpected movement) to fully understand the part of the central motor control mechanisms supplied by CMC analyses.

The dynamic CMC analysis showed discontinuous levels of CMC magnitudes during elbow extension in both groups and suggested the presence of a fluctuating mix of afferent and efferent information taking part in voluntary movement control. The earlier functional coupling in the antagonist muscles during the acceleration phase of paretic elbow extension fits well to existing motor control models and to the contribution of the lack of motor selectivity to the loss of motor function in post-stroke patients. In line with recent neurophysiological studies (e.g., Coffey et al., 2021), our study supports the view that CMC, especially when considering its temporal dynamics for analysis, can be regarded as an appropriate tool for exploring the mechanisms underlying the online control of voluntary movements in healthy subjects and post-stroke patients, and can also provide a relevant ground for further analyses involving effective connectivity quantifications and dynamic causal modeling.

DATA AVAILABILITY STATEMENT

The raw data supporting the conclusions of this article will be made available by the authors, without undue reservation.

ETHICS STATEMENT

The studies involving human participants were reviewed and approved by Research Ethics Board (No. ID-RCB: 2017-A01616-47) and Research Ethical Committee of Toulouse University Hospitals (No. 07-0716). The patients/participants provided their written informed consent to participate in this study.

AUTHOR CONTRIBUTIONS

MF co-wrote the manuscript, performed analyses, and discussed the results. AC and JT revised the manuscript, performed data acquisition, and discussed the results. DG and DA designed the study, co-wrote and revised the manuscript, and discussed the results. All authors contributed to the article and approved the submitted version.

REFERENCES

Anscombe, F. J. (1973). Graphs in statistical analysis. *Am. Stat.* 27, 17–21. doi: 10.2307/2682899

Baker, S. N. (2007). Oscillatory interactions between sensorimotor cortex and the periphery. *Curr. Opin. Neurobiol.* 17, 649–655. doi: 10.1016/j.conb.2008.01.007

Benjamini, Y., and Hochberg, Y. (1995). Controlling the false discovery rate: a practical and powerful approach to multiple testing. *J. R. Stat. Soc. Series B Stat. Methodol.* 57, 289–300. doi: 10.1111/j.2517-6161.1995.tb02031.x

Bigot, J., Longcamp, M., Dal Maso, F., and Amarantini, D. (2011). A new statistical test based on the wavelet cross-spectrum to detect time-frequency dependence between non-stationary signals: application to the analysis of cortico-muscular interactions. *Neuroimage* 55, 1504–1518. doi: 10.1016/j.neuroimage.2011.01.033

Bourguignon, M., Jousmäki, V., Dalal, S. S., Jerbi, K., and De Tiège, X. (2019). Coupling between human brain activity and body movements: insights from non-invasive electromagnetic recordings. *Neuroimage* 203:116177. doi: 10.1016/j.neuroimage.2019.116177

Buma, F. E., van Kordelaar, J., Raemaekers, M., van Wegen, E. E. H., Ramsey, N. F., and Kwakkel, G. (2016). Brain activation is related to smoothness of upper limb movements after stroke. *Exp. Brain Res.* 234, 2077–2089. doi: 10.1007/s00221-015-4538-8

Buneo, C. A., and Andersen, R. A. (2006). The posterior parietal cortex: sensorimotor interface for the planning and online control of visually guided

movements. *Neuropsychologia* 44, 2594–2606. doi: 10.1016/j.neuropsychologia.2005.10.011

Campfens, S. F., Schouten, A. C., van Putten, M. J. A. M., and van der Kooij, H. (2013). Quantifying connectivity via efferent and afferent pathways in motor control using coherence measures and joint position perturbations. *Exp. Brain Res.* 228, 141–153. doi: 10.1007/s00221-013-3545-x

Castelhano, J., Duarte, I. C., Abuhaiba, S. I., Rito, M., Sales, F., and Castelo-Branco, M. (2017). Cortical functional topography of high-frequency gamma activity relates to perceptual decision: an intracranial study. *PloS One* 12:e0186428. doi: 10.1371/journal.pone.0186428

Chalard, A., Amarantini, D., Tisseyre, J., Marque, P., and Gasq, D. (2020). Spastic co-contraction is directly associated with altered cortical beta oscillations after stroke. *Clin. Neurophysiol.* 131, 1345–1353. doi: 10.1016/j.clinph.2020.02.023

Charissou, C., Amarantini, D., Baurès, R., Berton, E., and Vigouroux, L. (2017). Effects of hand configuration on muscle force coordination, co-contraction and concomitant intermuscular coupling during maximal isometric flexion of the fingers. *Eur. J. Appl. Physiol.* 117, 2309–2320. doi: 10.1007/s00421-017-3718-6

Chen, X., Xie, P., Zhang, Y., Chen, Y., Cheng, S., and Zhang, L. (2018). Abnormal functional corticomuscular coupling after stroke. *Neuroimage Clin.* 19, 147–159. doi: 10.1016/j.nicl.2018.04.004

Chiovetto, E., Berret, B., Delis, I., Panzeri, S., and Pozzo, T. (2013). Investigating reduction of dimensionality during single-joint elbow movements: a case study on muscle synergies. *Front. Comput. Neurosci.* 7:11. doi: 10.3389/fncom.2013.00011

Chollet, F., Dipiero, V., Wise, R. J. S., Brooks, D. J., Dolan, R. J., and Frackowiak, R. S. J. (1991). The functional anatomy of motor recovery after stroke in humans: a study with positron emission tomography. *Ann. Neurol.* 29, 63–71. doi: 10.1002/ana.410290112

Coffey, A., Bista, S., Fasano, A., Buxo, T., Mitchell, M., Giglia, E. R., et al. (2021). Altered supraspinal motor networks in survivors of poliomyelitis: a cortico-muscular coherence study. *Clin. Neurophysiol.* 132, 106–113. doi: 10.1016/j.clinph.2020.10.011

Cohen, J. (2013). *Statistical Power Analysis for the Behavioral Sciences*. Burlington, VT: Academic Press.

Conway, B. A., Halliday, D. M., Farmer, S. F., Shahani, U., Maas, P., Weir, A. I., et al. (1995). Synchronization between motor cortex and spinal motoneuronal pool during the performance of a maintained motor task in man. *J. Physiol.* 489, 917–924. doi: 10.1113/jphysiol.1995.sp021104

Cremoux, S., Tallet, J., Berton, E., Dal Maso, F., and Amarantini, D. (2013). Motor-related cortical activity after cervical spinal cord injury: multifaceted EEG analysis of isometric elbow flexion contractions. *Brain Res.* 1533, 44–51. doi: 10.1016/j.brainres.2013.08.008

Cremoux, S., Tallet, J., Maso, F. D., Berton, E., and Amarantini, D. (2017). Impaired corticomuscular coherence during isometric elbow flexion contractions in humans with cervical spinal cord injury. *Eur. J. Neurosci.* 46, 1991–2000. doi: 10.1111/ejn.13641

Dal Maso, F., Longcamp, M., Cremoux, S., and Amarantini, D. (2017). Effect of training status on beta-range corticomuscular coherence in agonist vs. Antagonist muscles during isometric knee contractions. *Exp. Brain Res.* 235, 3023–3031. doi: 10.1007/s00221-017-5035-z

de los Reyes-Guzmán, A., Dimbwadyo-Terrer, I., Trincado-Alonso, F., Monasterio-Huelin, F., Torricelli, D., and Gil-Agudo, A. (2014). Quantitative assessment based on kinematic measures of functional impairments during upper extremity movements: a review. *Clin. Biomech.* 29, 719–727. doi: 10.1016/j.clinbiomech.2014.06.013

Delorme, A., and Makeig, S. (2004). EEGLAB: an open source toolbox for analysis of single-trial EEG dynamics including independent component analysis. *J. Neurosci. Methods.* 134, 9–21. doi: 10.1016/j.jneumeth.2003.10.009

Elliott, D., Binsted, G., and Heath, M. (1999). The control of goal-directed limb movements: correcting errors in the trajectory. *Hum. Mov. Sci.* 18, 121–136. doi: 10.1016/S0167-9457(99)00004-4

Fang, Y., Daly, J. J., Sun, J., Hvorat, K., Fredrickson, E., Pundik, S., et al. (2009). Functional corticomuscular connection during reaching is weakened following stroke. *Clin. Neurophysiol.* 120, 994–1002. doi: 10.1016/j.clinph.2009.02.173

Fauvet, M., Cremoux, S., Chalard, A., Tisseyre, J., Gasq, D., and Amarantini, D. (2019). "A novel method to generalize time-frequency coherence analysis between EEG or EMG signals during repetitive trials with high intra-subject variability in duration," in *Proceedings of the 2019 9th International IEEE/EMBS Conference on Neural Engineering (NER)* (San Francisco, CA), 437–440. doi: 10.1109/NER.2019.8716973

Feldman, A. G. (1986). Once more on the equilibrium-point hypothesis (λ model) for motor control. *J. Mot. Behav.* 18, 17–54. doi: 10.1080/00222895.1986.10735369

Gerloff, C. (2006). Multimodal imaging of brain reorganization in motor areas of the contralesional hemisphere of well recovered patients after capsular stroke. *Brain* 129, 791–808. doi: 10.1093/brain/awh713

Glories, D., Soulhol, M., Amarantini, D., and Duclay, J. (2021). Specific modulation of corticomuscular coherence during submaximal voluntary isometric, shortening and lengthening contractions. *Sci. Rep.* 11:6322. doi: 10.1038/s41598-021-85851-w

Gottlieb, G. L., Corcos, D. M., and Agarwal, G. C. (1989). Organizing principles for single-joint movements. I. A speed-insensitive strategy. *J. Neurophysiol.* 62, 342–357. doi: 10.1152/jn.1989.62.2.342

Graziadio, S., Tomasevic, L., Assenza, G., Tecchio, F., and Eyre, J. A. (2012). The myth of the 'unaffected' side after unilateral stroke: is reorganisation of the non-infarcted corticospinal system to re-establish balance the price for recovery? *J. Exp. Neurol.* 238, 168–175. doi: 10.1016/j.expneurol.2012.08.031

Grefkes, C., Nowak, D. A., Eickhoff, S. B., Dafotakis, M., Küst, J., Karbe, H., et al. (2008). Cortical connectivity after subcortical stroke assessed with functional magnetic resonance imaging. *Ann. Neurol.* 63, 236–246. doi: 10.1002/ana.21228

Grefkes, C., and Ward, N. S. (2014). Cortical reorganization after stroke: how much and how functional? *Neuroscientist* 20, 56–70. doi: 10.1177/1073858413491147

Halliday, D. M., Conway, B. A., Farmer, S. F., and Rosenberg, J. R. (1998). Using electroencephalography to study functional coupling between cortical activity and electromyograms during voluntary contractions in humans. *Neurosci. Lett.* 241, 5–8. doi: 10.1016/S0304-3940(97)00964-6

Hedges, L. V., and Olkin, I. (2014). *Statistical Methods for Meta-Analysis*. Cambridge, MA: Academic Press.

Hermens, H. J., Freriks, B., Disselhorst-Klug, C., and Rau, G. (2000). Development of recommendations for SEMG sensors and sensor placement procedures. *J. Electromyogr. Kinesiol.* 10, 361–374. doi: 10.1016/S1050-6411(00)00027-4

Jasper, H., and Penfield, W. (1949). Electrocorticograms in man: effect of voluntary movement upon the electrical activity of the precentral gyrus. *Arch. Psychiatr. Nervenkr.* 183, 163–174. doi: 10.1007/BF01062488

Katz, R., and Pierrot-Deseilligny, E. (1982). Recurrent inhibition of alpha-motoneurons in patients with upper motor neuron lesions. *Brain* 105(Pt 1), 103–124. doi: 10.1093/brain/105.1.103

Kenville, R., Maudrich, T., Vidaurre, C., Maudrich, D., Villringer, A., Nikulin, V. V., et al. (2020). Corticomuscular interactions during different movement periods in a multi-joint compound movement. *Sci. Rep.* 10:5021. doi: 10.1038/s41598-020-61909-z

Kilner, J. M., Baker, S. N., Salenius, S., Hari, R., and Lemon, R. N. (2000). Human cortical muscle coherence is directly related to specific motor parameters. *J. Neurosci.* 20, 8838–8845.

Kilner, J. M., Baker, S. N., Salenius, S., Jousmäki, V., Hari, R., and Lemon, R. N. (1999). Task-dependent modulation of 15-30 Hz coherence between rectified EMGs from human hand and forearm muscles. *J. Physiol.* 516, 559–570. doi: 10.1111/j.1469-7793.1999.0559v.x

Kilner, J. M., Salenius, S., Baker, S. N., Jackson, A., Hari, R., and Lemon, R. N. (2003). Task-dependent modulations of cortical oscillatory activity in human subjects during a bimanual precision grip task. *Neuroimage* 18, 67–73. doi: 10.1006/nimg.2002.1322

Kisiel-Sajewicz, K., Fang, Y., Hrovat, K., Yue, G. H., Siemionow, V., Sun, C.-K., et al. (2011). Weakening of synergist muscle coupling during reaching movement in stroke patients. *Neurorehabil. Neural Repair.* 25, 359–368. doi: 10.1177/1545968310388665

Krauth, R., Schwertner, J., Vogt, S., Lindquist, S., Sailer, M., Sickert, A., et al. (2019). Cortico-muscular coherence is reduced acutely post-stroke and increases bilaterally during motor recovery: a pilot study. *Front. Neurol.* 10:126. doi: 10.3389/fneur.2019.00126

Kristeva, R., Patino, L., and Omlor, W. (2007). Beta-range cortical motor spectral power and corticomuscular coherence as a mechanism for effective corticospinal interaction during steady-state motor output. *Neuroimage* 36, 785–792. doi: 10.1016/j.neuroimage.2007.03.025

Lang, C. E., and Schieber, M. H. (2004). Reduced muscle selectivity during individuated finger movements in humans after damage to the motor cortex

or corticospinal tract. *J. Neurophysiol.* 91, 1722–1733. doi: 10.1152/jn.00805.2003

Langhorne, P., Bernhardt, J., and Kwakkel, G. (2011). Stroke rehabilitation. *Lancet* 377, 1693–1702. doi: 10.1016/S0140-6736(11)60325-5

Levin, M. F., and Dimov, M. (1997). Spatial zones for muscle coactivation and the control of postural stability. *Brain Res.* 757, 43–59. doi: 10.1016/S0006-8993(97)00204-7

Liu, J., Sheng, Y., Zeng, J., and Liu, H. (2019). Corticomuscular coherence for upper arm flexor and extensor muscles during isometric exercise and cyclically isokinetic movement. *Front. Neurosci.* 13:522. doi: 10.3389/fnins.2019.00522

Maris, E., and Oostenveld, R. (2007). Nonparametric statistical testing of EEG- and MEG-data. *J. Neurosci. Methods* 164, 177–190. doi: 10.1016/j.jneumeth.2007.03.024

McClelland, V. M., Cvetkovic, Z., and Mills, K. R. (2012). Rectification of the EMG is an unnecessary and inappropriate step in the calculation of corticomuscular coherence. *J. Neurosci. Methods* 205, 190–201. doi: 10.1016/j.jneumeth.2011.11.001

McPherson, J. G., Stienen, A. H., Drogos, J. M., and Dewald, J. P. (2018). Modification of spastic stretch reflexes at the elbow by flexion synergy expression in individuals with chronic hemiparetic stroke. *Arch. Phys. Med. Rehabil.* 99, 491–500. doi: 10.1016/j.apmr.2017.06.019

Mima, T., and Hallett, M. (1999). Corticomuscular coherence: a review. *J. Clin. Neurophysiol.* 16:501.

Mima, T., Simpkins, N., Oluwatimilehin, T., and Hallett, M. (1999). Force level modulates human cortical oscillatory activities. *Neurosci. Lett.* 275, 77–80. doi: 10.1016/S0304-3940(99)00734-X

Mima, T., Toma, K., Koshy, B., and Halett, M. (2001). Coherence between cortical and muscular activities after subcortical stroke. *Stroke* 32, 2597–2601. doi: 10.1161/hs1101.098764

Murphy, M. A., Willén, C., and Sunnerhagen, K. S. (2011). Kinematic variables quantifying upper-extremity performance after stroke during reaching and drinking from a glass. *Neurorehabil. Neural Repair* 25, 71–80. doi: 10.1177/1545968310370748

Nijhuis, P., Keller, P. E., Nozaradan, S., and Varlet, M. (2021). Dynamic modulation of cortico-muscular coupling during real and imagined sensorimotor synchronisation. *Neuroimage* 238:118209. doi: 10.1016/j.neuroimage.2021.118209

Omlor, W., Patino, L., Hepp-Reymond, M.-C., and Kristeva, R. (2007). Gamma-range corticomuscular coherence during dynamic force output. *Neuroimage* 34, 1191–1198. doi: 10.1016/j.neuroimage.2006.10.018

Parker, V. M., Wade, D. T., and Hewer, R. L. (1986). Loss of arm function after stroke: measurement, frequency, and recovery. *Int. Rehabil. Med.* 8, 69–73. doi: 10.3109/03790798609166178

Penfield, W. (1954). Mechanisms of voluntary movement. *Brain* 77, 1–17. doi: 10.1093/brain/77.1.1

Pfurtscheller, G. (1992). Event-related synchronization (ERS): an electrophysiological correlate of cortical areas at rest. *Electroencephalogr. Clin. Neurophysiol.* 83, 62–69. doi: 10.1016/0013-4694(92)90133-3

Pfurtscheller, G. (2001). Functional brain imaging based on ERD/ERS. *Vision Res.* 41, 1257–1260. doi: 10.1016/S0042-6989(00)00235-2

Pfurtscheller, G., and Lopes da Silva, F. H. (1999). Event-related EEG/MEG synchronization and desynchronization: basic principles. *Clin. Neurophysiol.* 110, 1842–1857. doi: 10.1016/S1388-2457(99)00141-8

Reyes, A., Laine, C. M., Kutch, J. J., and Valero-Cuevas, F. J. (2017). Beta band corticomuscular drive reflects muscle coordination strategies. *Front. Comput. Neurosci.* 11:17. doi: 10.3389/fncom.2017.00017

Riddle, C. N., and Baker, S. N. (2005). Manipulation of peripheral neural feedback loops alters human corticomuscular coherence. *J. Physiol.* 566(Pt 2), 625–639. doi: 10.1113/jphysiol.2005.089607

Rohrer, B., Fasoli, S., Krebs, H. I., Hughes, R., Volpe, B., Frontera, W. R., et al. (2002). Movement smoothness changes during stroke recovery. *J. Neurosci.* 22, 8297–8304. doi: 10.1523/JNEUROSCI.22-18-08297.2002

Rossiter, H. E., Eaves, C., Davis, E., Boudrias, M.-H., Park, C., Farmer, S., et al. (2013). Changes in the location of cortico-muscular coherence following stroke. *Neuroimage Clin.* 2, 50–55. doi: 10.1016/j.nicl.2012.11.002

Rüber, T., Schlaug, G., and Lindenberg, R. (2012). Compensatory role of the cortico-rubro-spinal tract in motor recovery after stroke. *Neurology* 79, 515–522. doi: 10.1212/WNL.0b013e31826356e8

Ruiz-Gonzalez, Y., Velázquez-Pérez, L., Rodríguez-Labrada, R., Torres-Vega, R., and Ziemann, U. (2019). "Role of EMG rectification for corticomuscular and intermuscular coherence estimation of spinocerebellar ataxia type 2 (SCA2)," in *Progress in Pattern Recognition, Image Analysis, Computer Vision, and Applications*, eds I. Nyström, Y. Hernández Heredia, and V. Milián Núñez (Cham: Springer International Publishing), 306–315. doi: 10.1007/978-3-030-33904-3_28

Salenius, S., and Hari, R. (2003). Synchronous cortical oscillatory activity during motor action. *Curr. Opin. Neurobiol.* 13, 678–684. doi: 10.1016/j.conb.2003.10.008

Schieber, M., Lang, C., Reilly, K., McNulty, P., and Sirigu, A. (2009). Selective activation of human finger muscles after stroke or amputation. *Adv. Exp. Med. Biol.* 629, 559–575. doi: 10.1007/978-0-387-77064-2_30

Sullivan, G. M., and Feinn, R. (2012). Using effect size—or why the p value is not enough. *J. Grad. Med. Educ.* 4, 279–282. doi: 10.4300/JGME-D-12-00156.1

Tang, A., and Rymer, W. Z. (1981). Abnormal force—EMG relations in paretic limbs of hemiparetic human subjects. *J. Neurol. Neurosurg. Psychiatry.* 44, 690–698.

Tisseyre, J., Marquet-Doléac, J., Barral, J., Amarantini, D., and Tallet, J. (2019). Lateralized inhibition of symmetric contractions is associated with motor, attentional and executive processes. *Behav. Brain Res.* 361, 65–73. doi: 10.1016/j.bbr.2018.12.034

Tung, S. W., Guan, C., Ang, K. K., Phua, K. S., Wang, C., Zhao, L., et al. (2013). "Motor imagery BCI for upper limb stroke rehabilitation: an evaluation of the EEG recordings using coherence analysis," in *Proceedings of the 2013 35th Annual International Conference of the IEEE Engineering in Medicine and Biology Society (EMBC)* (Osaka: IEEE), 261–264. doi: 10.1109/EMBC.2013.6609487

von Carlowitz-Ghori, K., Bayraktaroglu, Z., Hohlefeld, F. U., Losch, F., Curio, G., and Nikulin, V. V. (2014). Corticomuscular coherence in acute and chronic stroke. *Clin. Neurophysiol.* 125, 1182–1191. doi: 10.1016/j.clinph.2013.11.006

Ward, N. S., Brown, M. M., Thompson, A. J., and Frackowiak, R. S. J. (2003). Neural correlates of motor recovery after stroke: a longitudinal fMRI study. *Brain* 126, 2476–2496. doi: 10.1093/brain/awg245

Witham, C. L., Riddle, C. N., Baker, M. R., and Baker, S. N. (2011). Contributions of descending and ascending pathways to corticomuscular coherence in humans. *J. Physiol.* 589, 3789–3800. doi: 10.1113/jphysiol.2011.211045

Yoshida, T., Masani, K., Zabjek, K., Chen, R., and Popovic, M. R. (2017). Dynamic increase in corticomuscular coherence during bilateral, cyclical ankle movements. *Front. Hum. Neurosci.* 11:155. doi: 10.3389/fnhum.2017.00155

Zheng, Y., Peng, Y., Xu, G., Li, L., and Wang, J. (2018). Using corticomuscular coherence to reflect function recovery of paretic upper limb after stroke: a case study. *Front. Neurol.* 8:728. doi: 10.3389/fneur.2017.00728

Conflict of Interest: The authors declare that the research was conducted in the absence of any commercial or financial relationships that could be construed as a potential conflict of interest.

Publisher's Note: All claims expressed in this article are solely those of the authors and do not necessarily represent those of their affiliated organizations, or those of the publisher, the editors and the reviewers. Any product that may be evaluated in this article, or claim that may be made by its manufacturer, is not guaranteed or endorsed by the publisher.

frontiers in Physiology

ORIGINAL RESEARCH
published: 27 September 2021
doi: 10.3389/fphys.2021.654231

Resting Tendon Cross-Sectional Area Underestimates Biceps Brachii Tendon Stress: Importance of Measuring During a Contraction

Rowan R. Smart[1], *Brian O'Connor*[2] *and Jennifer M. Jakobi*[1]*

[1] *Healthy Exercise and Aging Laboratory, School of Health and Exercise Sciences, University of British Columbia Okanagan, Kelowna, BC, Canada,* [2] *Department of Psychology, Faculty of Arts and Social Sciences, University of British Columbia Okanagan, Kelowna, BC, Canada*

Force produced by the muscle during contraction is applied to the tendon and distributed through the cross-sectional area (CSA) of the tendon. This ratio of force to the tendon CSA is quantified as the tendon mechanical property of stress. Stress is traditionally calculated using the resting tendon CSA; however, this does not take into account the reductions in the CSA resulting from tendon elongation during the contraction. It is unknown if calculating the tendon stress using instantaneous CSA during a contraction significantly increases the values of *in vivo* distal biceps brachii (BB) tendon stress in humans compared to stress calculated with the resting CSA. Nine young (22 ± 1 years) and nine old (76 ± 4 years) males, and eight young females (21 ± 1 years) performed submaximal isometric elbow flexion tracking tasks at force levels ranging from 2.5 to 80% maximal voluntary contraction (MVC). The distal BB tendon CSA was recorded on ultrasound at rest and during the submaximal tracking tasks (instantaneous). Tendon stress was calculated as the ratio of tendon force during contraction to CSA using the resting and instantaneous measures of CSA, and statistically evaluated with multi-level modeling (MLM) and Johnson–Neyman regions of significance tests to determine the specific force levels above which the differences between calculation methods and groups became statistically significant. The tendon CSA was greatest at rest and decreased as the force level increased ($p < 0.001$), and was largest in young males (23.0 ± 2.90 mm^2) followed by old males (20.87 ± 2.0 mm^2) and young females (17.08 ± 1.54 mm^2) ($p < 0.001$) at rest and across the submaximal force levels. Tendon stress was greater in the instantaneous compared with the resting CSA condition, and young males had the greatest difference in the values of tendon stress between the two conditions (20 ± 4%), followed by old males (19 ± 5%), and young females (17 ± 5%). The specific force at which the difference between the instantaneous and resting CSA stress values became statistically significant was 2.6, 6.6, and 10% MVC for old males, young females, and young males, respectively. The influence of using the instantaneous compared to resting CSA for tendon stress is sex-specific in young adults, and age-specific in the context of males. The instantaneous CSA should be used to provide a more accurate measure of *in vivo* tendon stress in humans.

Keywords: ultrasound, aging, tendon mechanics, *in vivo*, elbow flexion, sex differences

OPEN ACCESS

Edited by:
Stéphane Baudry,
Université libre de Bruxelles, Belgium

Reviewed by:
Stefano Longo,
University of Milan, Italy
Ramona Ritzmann,
Clinic Rennbahn AG, Switzerland

***Correspondence:**
Jennifer M. Jakobi
jennifer.jakobi@ubc.ca

Specialty section:
This article was submitted to Exercise Physiology, a section of the journal Frontiers in Physiology

Received: *15 January 2021*
Accepted: *09 August 2021*
Published: *27 September 2021*

Citation:
Smart RR, O'Connor B and Jakobi JM (2021) Resting Tendon Cross-Sectional Area Underestimates Biceps Brachii Tendon Stress: Importance of Measuring During a Contraction. Front. Physiol. 12:654231. doi: 10.3389/fphys.2021.654231

INTRODUCTION

Producing movement and torque around a joint requires the transfer of force from the muscle to the bone *via* the tendon. As the muscle shortens, forces placed on the tendon are distributed through the cross-sectional area (CSA) of the tendon, and this ratio of force to the CSA is quantified as the tendon's mechanical property of stress (Vergari et al., 2011; Eriksen et al., 2018; Lepley et al., 2018; Ristaniemi et al., 2018; Smart et al., 2018a). Stress is dependent on the amount of force applied to the tendon and the CSA of the tendon, such that greater amounts of applied force and smaller tendon CSA culminate in the higher stress.

Human *in vivo* studies evaluating the tendon stress traditionally rely on the measure of engineering stress which assumes that CSA is constant from rest to the maximal forces, and uses the resting tendon CSA for all the calculations of stress (Stenroth et al., 2012; Eriksen et al., 2018; Lepley et al., 2018). This experimental approach is appealing, as resting CSA measures are relatively easy to acquire (Stenroth et al., 2012; Eriksen et al., 2018). Since the tendon CSA decreases as the applied force increases (Vergari et al., 2011; Obst et al., 2014b; Smart et al., 2018b), utilizing this singular resting CSA measure for all the contraction intensities likely underestimates the tendon stress, and the magnitude of the underestimation is likely greater at higher relative forces when the decrease in tendon CSA is the greatest (Smart et al., 2017, 2018a,b). Therefore, applying resting CSA in the calculation of tendon stress fails to account for the dynamic nature of the tendon and likely misrepresents the true amount of stress experienced by the tendon across various force levels.

In an *ex vivo* equine tendon model, Vergari et al. (2011) demonstrated that when increasing the tendon strain (elongating the tendon by a percentage of its resting length), CSA decreased linearly while the stress increased in a non-linear fashion. Over the tested strain levels, Vergari et al. (2011) found that the tendon stress was 7–14% greater when calculated using the instantaneous compared with resting CSA. This underestimation that occurs when resting CSA is used, has not been investigated *in vivo* for human tendons. The technique of *ex vivo* studies evaluating the tendon stress as the tendon is lengthened to a given amount of strain is not experimentally viable for *in vivo* human tendons. Notwithstanding the potential to use multiple ultrasound probes, which in some tendons is anatomically impossible, this technique would require real-time monitoring of the tendon elongation and CSA during the contraction. Current two-dimensional (2D) ultrasound technology does not allow for real-time simultaneous recordings of *in vivo* elongation and CSA.

To understand the effects of strength and tendon size on the increase in *in vivo* tendon stress values from the resting to instantaneous CSA calculation, we evaluated the sex- and age-group differences at relative force levels. Prior studies of the Achilles tendon showed greater stress in young compared with old (Stenroth et al., 2012) and males compared with females (Stenroth et al., 2012; Lepley et al., 2018) when calculated using the resting tendon CSA, and we showed that distal BB tendon stress is greater in young males as compared with old males when calculated using the instantaneous CSA (Smart et al., 2018a). Young males are stronger than young females and old males (Pereira et al., 2015; Smart et al., 2018a), and have greater distal biceps brachii (BB) tendon elongation and CSA than the old males (Smart et al., 2018a) and presumably young females. The higher strength in young males would generate greater pull on the tendon and augment elongation and CSA reductions at relative force levels, increasing the difference in tendon stress values between the resting and instantaneous CSA calculations to a greater extent than the old males and young females.

The purpose of this study was to compare calculations of tendon stress values for the distal BB tendon using the resting and instantaneous measures of tendon CSA across different force levels. We evaluated sex- and age-related differences in the two measures of tendon stress with the multi-level statistical modeling procedures. The use of modeling is beneficial for answering the unique research questions across multiple research fields, such as neuromuscular physiology (Taylor and Enoka, 2004; Tibold and Fuglevand, 2015; Potvin and Fuglevand, 2017). We hypothesized that the tendon CSA would decrease during a contraction due to tendon elongation, leading to higher tendon stress calculated using the instantaneous CSA compared with the resting CSA and that the difference would be greater at higher forces. Second, we hypothesized that due to a combination of greater strength and the decrease in tendon CSA, the difference in tendon stress values from the resting to instantaneous CSA conditions would be highest in young males, followed by old males and young females, and that the difference between stress values would become statistically significant at lower forces in young males.

MATERIALS AND METHODS

Participants

Tendon stress was determined for nine young males and nine old males using a previously published data set (Smart et al., 2018a), and for eight young females using unpublished data (**Table 1**). The experimental set-ups and procedures were identical for both datasets apart from the submaximal force levels as described in the protocol section below. All participants were recreationally active, and the old males were non-frail, community dwelling, and functionally independent. Most spoke of engagement with outdoor activities, such as gardening and golfing. All the participants self-identified as right-hand dominant. The exclusion criteria for this study were orthopedic surgery or injury to the right shoulder or arm in the prior 6 months, participation in high levels of upper body strength training, or conditions that influence the muscle and tendon beyond typical age-related changes. Written informed consent was obtained from all participants prior to their participation and ethics approval was granted from the University of British Columbia Okanagan's Behavioral Research Ethics Board.

Experimental Set-Up

Participants were seated in a custom-built isometric dynamometer chair (Brown et al., 2010; Harwood et al., 2010; Smart et al., 2017, 2018a,b) with their right arm positioned at 110° of elbow flexion (full extension being 180°), the

TABLE 1 | Subject characteristics.

	Young-males	Old-males	Young-females	Group effect
Age (yrs)	22 ± 1[#]	76 ± 4*	21 ± 1[#]	$F_{(2,25)} = 849.66$, $\eta^2 = 0.99$, $p < 0.01$
Height (cm)	180.0 ± 7.0	173.9 ± 6.9	167.0 ± 7.6*	$F_{(2,25)} = 7.06$, $\eta^2 = 0.38$, $p < 0.01$
Body mass (kg)	79.4 ± 8.3	78.0 ± 10.9	61.0 ± 5.5*[#]	$F_{(2,25)} = 11.68$, $\eta^2 = 0.50$, $p < 0.01$
MVC (N)	250.7 ± 31.0[#]	200.1 ± 28.5*	149.8 ± 27.0*[#]	$F_{(2,25)} = 25.7$, $\eta^2 = 0.69$, $p < 0.01$
Moment arm (mm)	56.1 ± 4.7	55.9 ± 4.1	53.6 ± 4.6	$H_{(2)} = 3.98$, $p = 0.14$
Lever arm (mm)	354.3 ± 11.6	348.6 ± 16.1	322.3 ± 18.9*[#]	$F_{(2,25)} = 9.92$, $\eta^2 = 0.46$; $p < 0.01$
Stiffness (N/mm)	170 ± 132.9	113.0 ± 55.1	55.8 ± 43.3*	$H_{(2)} = 6.857$, $p = 0.032$

MVC, maximal voluntary contraction; N, Newtons.
**Differs from young males; [#]differs from old males. Values are mean ± SD.*

shoulder forward flexed 15°, and the right hand grasping the manipulandum with the wrist in a neutral position halfway between full supination and pronation. The force transducer (MLP-150, Transducer Techniques, Temecula, CA, USA) was located directly below the hand. Force was sampled at 2,381 Hz, converted from analog-to-digital format using a power 1401 plus [Cambridge Electronic Designs (CED), Cambridge, England], and stored for offline analysis using Spike 2 v7.12 (CED, Cambridge, England). The real-time visual feedback of the force signal was displayed on a 52 cm monitor positioned 1-m in front of participants. A B-mode ultrasound probe (ML6-15, 4–15 MHz, GE LOGIQ E9; General Electric, Fairfield, CT, USA) was placed in a custom-made probe holder and secured over the distal BB tendon. The probe was positioned in transverse orientation at the mid-point of the BB tendon to visualize the tendon in cross-section (**Figure 1**). For tendon elongation, the probe was secured in a longitudinal orientation to visualize the muscle-tendon junction (MTJ) of the long head of the BB (**Figure 2**). Visual representation of the experimental set-up has been previously published (Smart et al., 2017).

Anatomical Measures

Anatomical measures were performed as previously described (Smart et al., 2017, 2018a,b). Briefly, lever arm length was measured on the skin surface as the distance from the head of the radius to the force transducer. The moment arm was obtained by locating the distal MTJ of the BB and the insertion of the distal BB tendon onto the radius using ultrasound and indicating these points on the skin. A linear edge was placed between these points and the moment arm was measured as the perpendicular distance from this linear edge to the lateral epicondyle of the humerus.

Protocol

Participants performed three isometric elbow flexion maximal voluntary contractions (MVCs). In the experiment involving young and old males, the submaximal forces of 2.5, 5, 10, 20, 40, 60, and 80% MVC were calculated, while force levels of 5, 10, 25, 50, and 75% MVC were used in the study of young females. The submaximal contractions consisted of a 3-s ramp to the target force level, a 5–10 s plateau, and a 3-s ramp down to the baseline. Following each contraction, 2-min rest was provided to ensure that there was no fatigue. The feedback of the force signal during the submaximal contractions was scaled according to the MVC of the participant to provide similar visual feedback across participants and force levels (Harwood et al., 2014). Ultrasound videos of tendon CSA (**Figure 1**) and elongation were recorded during the contractions at a frame rate of 31 Hz. Each submaximal contraction level was performed four times to obtain the two recordings of tendon CSA and two of elongation. The force levels were randomized within the CSA and elongation blocks, and the average of the two contractions are reported for elongation, tendon force, CSA, and stress. Following the submaximal contractions, participants performed a final MVC that was within 5% of their initial MVC to ensure fatigue did not occur as a result of the protocol.

Data Analysis

Tendon CSA and elongation were captured using ultrasonography through the video recordings of the tendon in a cross-sectional or longitudinal view, respectively. Tendon CSA was measured at rest and at the mid-point of the steady-state plateau of the submaximal contractions by tracing the outer border of the tendon using the inherent measurement tool platform of the ultrasound (GE LOGIQ E9). For tendon elongation, it was measured as the difference in length from the distal BB MTJ to the edge of the ultrasound field of view in the resting state and the mid-point of the plateau in the contracted state. The distance to a hyperechoic marker was also measured to ensure that the probe did not move during the contractions (Smart et al., 2017, 2018a,b). The high repeatability of ultrasound measurements for the distal BB tendon has been previously published by our lab group (Smart et al., 2017). The force was analyzed as the mean force produced during the middle 3–5 s of the plateau phase of the contractions. The tendon stiffness was calculated as detailed in the prior studies on the distal BB tendon (Smart et al., 2018a,b) as the slope of the tendon force/elongation relationship between low (∼20%) and high (∼80%) submaximal forces. Tendon stress was calculated at each force level using the resting and instantaneous CSA. Following determination of the muscle moment (Equation 1), tendon force was computed using moment arm length (Equation 2). This was subsequently used in the calculation of tendon stress (Equation 3) for the two conditions of resting and instantaneous tendon CSA. The calculation of tendon stress has been described for various tendons using resting (Stenroth et al., 2012; Eriksen et al., 2018;

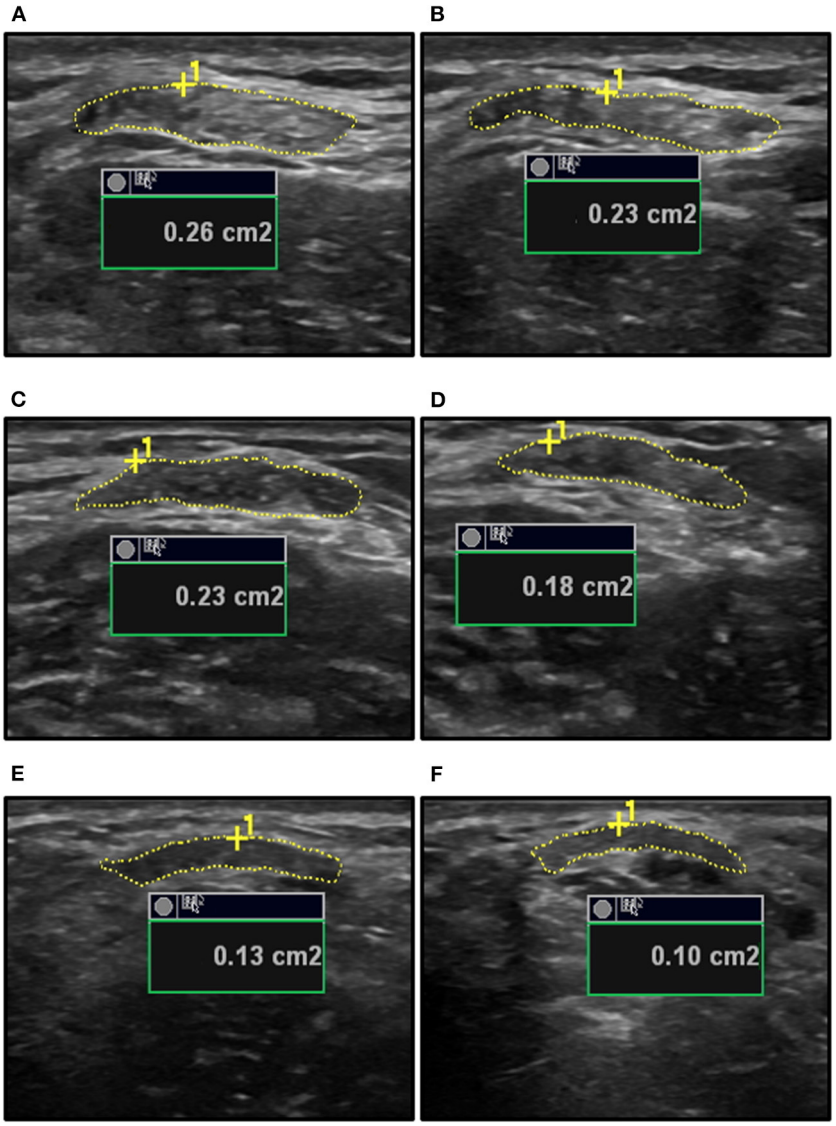

FIGURE 1 | The ultrasound measurements of biceps brachii (BB) tendon cross-sectional area (CSA) for a young male at rest **(A)** and during a 20% MVC contraction **(B)**, an old male at rest **(C)** and during a 20% MVC contraction **(D)**, and a young female at rest **(E)** and during a 25% MVC contraction **(F)**. The inherent measurement platform of the ultrasound provides the area in square centimeters (cm^2) and this was converted to square millimeter (mm^2) prior to the calculations of tendon stress using the resting and the instantaneous tendon CSA measures. MVC, maximal voluntary contraction.

Lepley et al., 2018) and instantaneous CSA (Smart et al., 2017, 2018a,b).

$$\text{Force}\,(N) * \textit{Lever arm length}\,(mm) = \textit{Muscle moment}\,(N * mm) \quad (1)$$

$$\frac{\textit{Muscle moment}\,(N * mm)}{\textit{Moment arm length}\,(mm)} = \textit{Tendon force}\,(N) \quad (2)$$

$$\frac{\textit{Tendon force}\,(N)}{\textit{Tendon CSA}\,(mm^2)} = \textit{Tendon stress}\,(MPa) \quad (3)$$

Statistical Analysis

Tests of Normality and Mixed-Model ANOVAs

The tests of normality were conducted for all variables. Shapiro–Wilk's test indicated that the moment arm and tendon stiffness were not normally distributed for old males ($p = 0.020$, $p = 0.024$) and young females ($p = 0.003$, $p = 0.035$). In young males, the moment arm was not normally distributed ($p = 0.032$) and the tendon stiffness approached significance ($p = 0.061$) in not being normally distributed. For non-normally distributed variables, the Kruskal–Wallis test was used to compare the groups. For significant effects, *post-hoc* Mann–Whitney *U*-tests were applied to determine the differences between the groups. MVC and

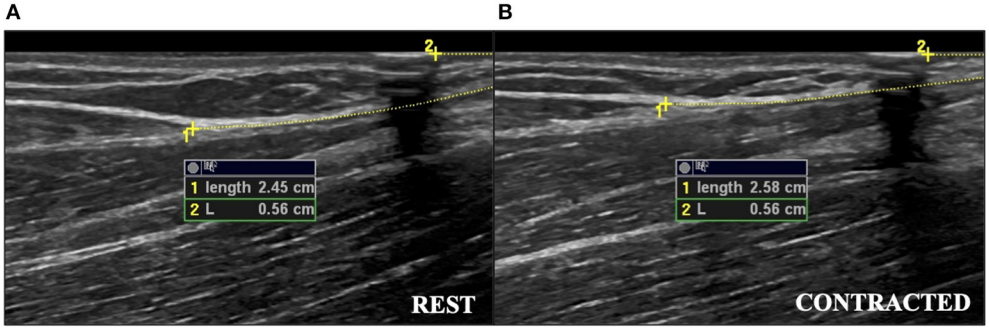

FIGURE 2 | The ultrasound measurements of tendon elongation in a young female during a 25% MVC contraction. **(A)** Measurement at rest of distance from muscle-tendon junction to edge of ultrasound field of view (Length 1), and measurement of distance from hyperechoic marker to the edge of ultrasound field of view (L2). **(B)** Measurement during the contracted state. The difference between the measurements during the contracted and resting states was used as the measure of tendon elongation. Images have been cropped for reproduction, but analysis captured the full length of the tendon. MVC, maximal voluntary contraction.

lever arm were compared between the groups using one-way ANOVAs with Tukey's *post-hoc* tests. In order to compare among all the three groups and across all force levels, tendon CSA was evaluated using a 3 (group: young males, old males, young females) × 11 (resting, 2.5, 5, 10, 20, 25, 40, 50, 60, 75, and 80% MVC) mixed-model ANOVA, while tendon force and elongation were evaluated with a 3 (group: young males, old males, young females) × 10 (force level: 2.5, 5, 10, 20, 25, 40, 50, 60, 75, and 80% MVC) ANOVA. When significant interactions occurred, one-way ANOVAs with Tukey's *post-hoc* tests were used to compare among the groups at each force level. The statistical analyses for the ANOVAs were performed using SPSS version 25 (IBM, Amrok, NY, USA). The effect sizes are reported as eta squared (η^2) for one-way ANOVAs, and partial eta squared (η_p^2) for the two-way ANOVAs. Data are reported as means ± SD, and the alpha level was set at 0.05.

Multi-Level Modeling and Johnson–Neyman Analysis

The data were also evaluated using growth curve analyses *via* multi-level modeling (MLM), which allows comparisons among the groups when the levels of repeated measurements are not the same for all persons. The analyses also provided a broader picture of the differences in tendon stress across conditions (the resting or instantaneous CSA), sex-age, and force levels.

The MLM growth curve analyses of tendon stress were conducted using the nlm package in R (Pinhero and Bates, 2000; Snijders and Bosker, 2012; Verbeke, 2013; Hox et al., 2018; Humphrey and LeBreton, 2019). In this procedure, a curve was fit for every participant for the relationship between force level (on the *x*-axis) and tendon stress (on the *y*-axis). The tests were then conducted to determine whether there was significant variation in the intercepts and slopes of the curves. When there was significant variation in either of these parameters, the predictor variables were introduced in an effort to account for the variation. The first predictor variable (sex-age) was examined as a categorical variable representing the three groups: young males, old males, and young females. The second predictor variable was instantaneous-resting, representing the two tendon CSA states. After testing for interactions between the predictor variables in the MLM, the Johnson–Neyman regions of significance procedure (Johnson and Fay, 1950; Bauer et al., 2005; Lazar and Zerbe, 2011; Rast et al., 2014; Hayes, 2018) was conducted to identify the precise force levels at which there were statistically significant differences in tendon stress between the two resting-instantaneous conditions and among the three sex-age groups within the resting and instantaneous conditions, with the probability of significance placed at 0.05.

The use of MLM and the Johnson–Neyman regions of significance procedure are novel statistical procedures in the study of tendon mechanics. They provide a more precise determination, compared with the traditional methods, of the point at which group and condition differences begin to occur, based on the simultaneous analyses of all available data.

RESULTS

Subject Characteristics

Young males were the strongest followed by old males and young females ($p < 0.01$). There was no difference in the tendon moment arm among the groups ($p = 0.14$). The lever arm did not differ between young and old males but was shorter in young females compared with both the young and old males ($p < 0.01$). Tendon stiffness did not differ between young and old males ($p = 0.49$) and between old males and young females (0.064) but was significantly greater in young males compared with young females ($p = 0.012$) (**Table 1**).

Multi-level Modeling for Resting and Instantaneous Tendon CSA

The MLM method of testing for the significant differences between the lines, and for group differences in the slopes of the lines, involves examining the fit levels for a sequence of models. The likelihood ratio (LR) test established that permitting the intercepts to vary across participants did not improve the model fit (LR = 0.00000048, $p = 0.9994$), and therefore, the intercepts were fixed (not permitted to vary) for all the subsequent analyses. In contrast, permitting the slopes to vary across participants did increase the model fit relative to a fixed slope model,

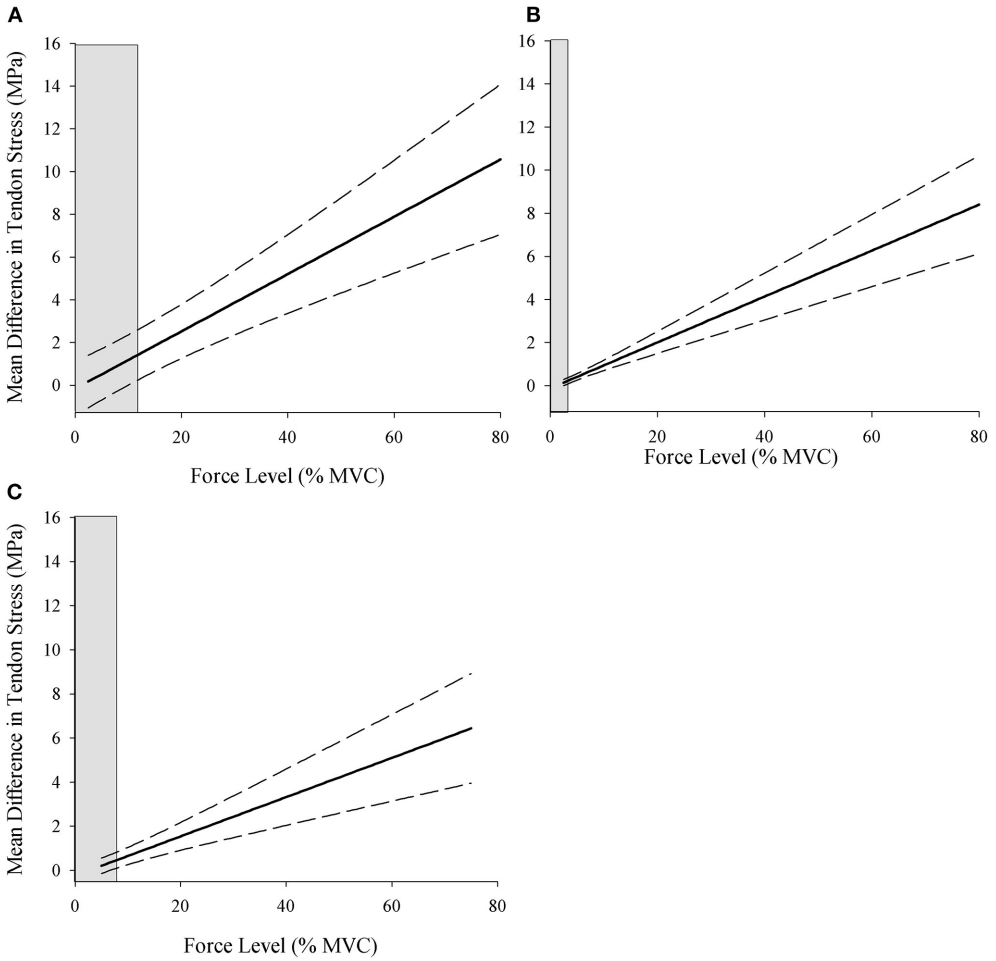

FIGURE 3 | Johnson–Neyman regions of significance for the difference in stress calculated using the resting and instantaneous CSA for young males **(A)**, old males **(B)**, and young females **(C)**. Values to the right of the shaded areas indicate the statistically significant differences between stress values calculated using the resting and instantaneous tendon CSA ($p < 0.05$). MVC, maximal voluntary contraction; MPa, megapascals.

LR = 1091.35, $p < 0.0001$. This means that there was statistically significant variation in the slopes, but not in the intercepts. A model with the interaction between the sex-age predictor and force level for the slopes fit the data better than a model without the interactions (LR = 76.7, $p < 0.0001$). Similarly, for the instantaneous-resting predictor, a model that included the interaction between instantaneous-resting and force level fit the data more appropriately (LR = 56.83, $p < 0.0001$) than a model that did not include the interaction, and thus both the expected two-way interactions were significant. Finally, a test for the possible three-way interaction (young males, old males, and young females × instantaneous-resting × force level) indicated an improvement in fit over a model that contained all the possible two-way interactions, LR = 479.65, $p < 0.0001$, but none of the individual three-way terms in the model were significant. This was likely due to the small sample size for the three-way interactions. The subsequent analyses, therefore, focused on the two-way interactions.

Johnson–Neyman Regions of Significance

The Johnson–Neyman regions of significance analysis was conducted to determine the force-level above which the difference values for tendon stress became statistically significant for comparisons between (1) the instantaneous and resting CSA conditions for each of the three sex-age groups, and (2) each of the three sex-age groups within the resting and instantaneous conditions separately. The differences between stress calculated with the resting and instantaneous CSA are plotted across the force levels for young males, old males, and young females (**Figure 3**), and the mean difference was greatest in young males (0.64–11.19 MPa), followed by old males (0.15–9.3 MPa), and young females (0.21–7.37 MPa).

The difference value at the relative force level where the shaded gray area ends is the point at which the stress values become significantly different between the resting and instantaneous CSA calculations for each sex-age group. The shaded gray area on the left side of the plots represents the region of non-significance,

TABLE 2 | Johnson–Neyman regions of significance.

	Comparison	Force level (% MVC) at which differences in stress become significantly different
Young-males	Resting vs. instantaneous	9.98
Old-males	Resting vs. instantaneous	2.56
Young-females	Resting vs. instantaneous	6.63
Resting	Young-males vs. old-males	9.94
Resting	Young-males vs. young-females	3.47
Resting	Old-males vs. young-females	1.91
Instantaneous	Young-males vs. old-males	5.95
Instantaneous	Young-males vs. young-females	2.64
Instantaneous	Old-males vs. young-females	15.07

and the non-shaded area is the region of significant differences between the calculations. The region of significance began at lower force levels in old males (>2.56% MVC) followed by young females (>6.63% MVC) and young males (>9.98% MVC) (**Table 2**, **Figure 3**), indicating that the point at which tendon stress is significantly greater using the instantaneous CSA is both age- and sex-specific.

The Johnson–Neyman analysis also evaluated the group differences in tendon stress within the resting and instantaneous CSA conditions separately in order to better understand the influence of tendon condition on the population differences in tendon stress. This comparison evaluated the differences between the groups within the resting and instantaneous CSA conditions separately. In the resting CSA condition, young males had significantly greater tendon stress than old males at 9.94% MVC and above. However, this threshold decreased to 5.95% MVC in the instantaneous CSA condition, highlighting that the age-related difference in stress between the young and old males became statistically significant at a lower relative force level when stress was calculated from the instantaneous CSA measure. Similarly, young males had greater tendon stress than young females above 3.47% MVC in the resting CSA condition, and this decreased to 2.64% MVC in the instantaneous condition, and thus the sex-related difference in tendon stress also occurred at a lower force when the instantaneous CSA is used in the calculation. The decrease in significance threshold for the age- and sex comparisons demonstrates that the higher stress values in the instantaneous condition led to the significant group differences in tendon stress at lower relative force levels. However, the comparison between old males and young females did not follow this expected trend. The threshold actually increased from 1.91 to 15.07% MVC between the resting and instantaneous calculations, and this is in part due to data variability as well as the physiological oddity of comparing young females to old males (**Table 2**).

Supplemental ANOVA Results

There was a force level by group interaction for tendon force [$F_{(7,147)} = 6.34$; $\eta_p^2 = 0.22$; $p < 0.001$]. Tendon force increased from 2.5% MVC (40.83 ± 6.65 N) to 80% MVC (1126.22 ± 221.40 N) [force main effect: $F_{(9,147)} = 340.63$; $\eta_p^2 = 0.95$; $p < 0.001$], and the interaction occurred from the tendon force being the greatest in young males (492 ± 80.75 N), followed by old males (384.3 ± 51.4 N) and young females (292.66 ± 42.86 N) ($p < 0.001$) at 5 and 10% MVC, and greater in young males than the old males from 20 to 80% MVC (**Figure 4A**). Tendon CSA had main effects of force [$F_{(10,169)} = 9.01$; $\eta_p^2 = 0.35$; $p < 0.001$] and group [$F_{(2,169)} = 78.85$; $\eta_p^2 = 0.48$; $p < 0.001$]. CSA values during the active muscle contraction decreased across the submaximal force levels, and was greatest in young males (23.0 ± 2.90 mm^2) followed by old males (20.87 ± 2.0 mm^2) and young females (17.08 ± 1.54 mm^2) ($p < 0.001$) (**Figure 4B**). There was a force by group interaction for elongation [$F_{(7,152)} = 2.01$; $\eta_p^2 = 0.099$; $p = 0.049$]. The tendon elongated 14.1 mm (1.37 ± 0.82 to 15.47 ± 4.38 mm) in young males, 8.81 mm (2.45 ± 1.27 to 11.26 ± 3.50 mm) in old males, and 6.21 mm (2.50 ± 2.58 to 8.79 ± 7.51 mm) in young females [$F_{(9,152)} = 23.77$; $\eta_p^2 = 0.62$; $p < 0.001$]. The elongation did not differ among the three groups at 5% MVC (2.78 ± 1.94 mm, $p = 0.11$) and 10% MVC (3.98 ± 2.42 mm, $p = 0.23$), but was greater in young males than the old males at 60% MVC (13.88 ± 4.15, 9.78 ± 2.27 mm, $p = 0.028$) and 80% MVC (15.47 ± 4.38, 11.26 ± 3.50 mm, $p = 0.047$).

DISCUSSION

The present study showed significant variation in the rate of increase in distal BB tendon stress values among young males, old males, and young females as well as between the resting and instantaneous CSA conditions, and that the tendon stress values were significantly greater in the instantaneous compared with the resting CSA condition. The use of MLM and Johnson–Neyman regions of significance tests allowed for a more precise and comprehensive analysis of the tendon stress data to establish the specific force levels of statistical differences, regardless of the submaximal force levels performed. The Johnson–Neyman regions of significance tests showed that (1) the difference between the resting and instantaneous CSA stress values became greater as the submaximal force levels increased, (2) this difference was greatest in young males, followed by old males and young females, and (3) sex- and age-group differences in tendon stress occurred at lower relative forces when instantaneous CSA was used in the calculations. Overall, calculating the distal BB tendon stress with resting CSA significantly underestimated *in vivo* tendon stress compared to the calculations using CSA measured during the muscle contraction, and the extent of underestimation was both age- and sex-specific.

Tendon Stress Across Submaximal Forces

The MLM growth curve analyses were beneficial in determining the rate of increase in distal BB tendon stress values across the relative force levels was greater using the instantaneous compared with the resting CSA, and that young males had the fastest rate of increase followed by old males and young females (**Figure 5**). The condition and group differences in tendon stress were evident through an improvement in model fit of the slopes

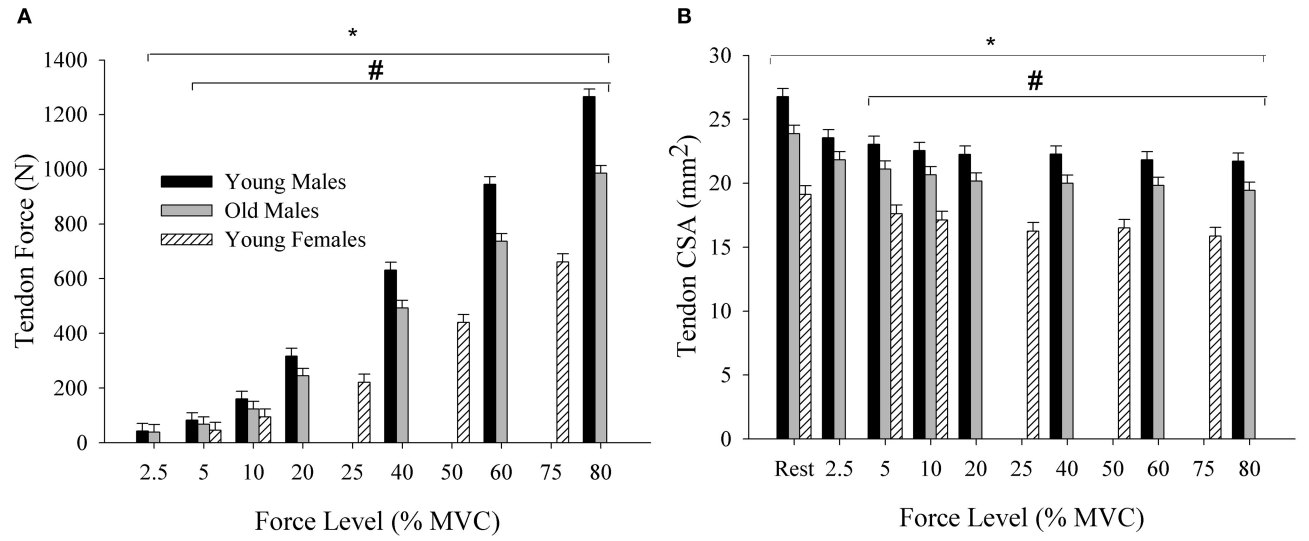

FIGURE 4 | (A) Tendon force across the submaximal force levels for young and old males and young females. Tendon force increased with the contraction intensity and was greater in young males compared with the old males and young females. **(B)** Tendon CSA at rest and across the submaximal force levels. CSA, cross-sectional area; MVC, Maximal voluntary contraction; N, Newtons. *differs across force levels; #differs between all the three groups at 5% and 10% MVC, and between young and old males at 20, 40, 60, and 80% MVC ($p < 0.05$).

when interaction terms were included for the instantaneous-resting predictors and sex-age predictors. The increase in slope of tendon stress from the resting to instantaneous condition resulted from the progressive decrease in CSA due to the constant volume of tendon being lengthened as the submaximal force increased. This contributed to the ratio of tendon force to CSA becoming greater at a faster rate in the instantaneous compared with the resting condition. The decrease in CSA resulting from tendon lengthening has been previously reported for the distal BB tendon (Smart et al., 2018a,b), Achilles tendon (Obst et al., 2014b), as well as *ex vivo* equine tendon (Vergari et al., 2011). The age- and sex-related differences in the rate at which tendon stress increased across the force levels resulted from young males being the strongest, followed by old males and young females. The greater strength in young males led them to apply more absolute force to the tendon at the relative force levels, culminating in greater tendon force in young males, followed by old males and young females. When combined with the reduction in CSA, the higher tendon force in young males contributes to a faster rate of increase in tendon stress values (steeper slope), followed by old males and young females.

Resting and Instantaneous Tendon CSA

In support of the first hypothesis, the Johnson–Neyman analysis demonstrated that tendon stress differed between the resting and instantaneous CSA calculations within each group. Old males had the lowest relative force level at which differences between the resting and instantaneous CSA stress calculations became statistically significant, followed by young females and young males (**Table 2**, **Figure 3**). This does not align with the second hypothesis as we expected that young males would show statistical differences at lower forces because they were the strongest and would have the largest ratio of tendon force to CSA. However, old males had a greater decrease in tendon CSA (5%) at the lower force levels (2.5–10%) compared with young females (3%) and young males (4%) (see **Figure 4**), and this likely amplified the ratio of tendon force to the instantaneous CSA leading to significantly greater stress at the lower force levels in the old males. The order effect of the groups in the determination of tendon stress between calculation methods emphasizes the importance of considering the study sample under investigation. The comparison between age or sex groups, for example, provides an opportunity to consider the contribution of population differences in the mechanical (Stenroth et al., 2012; Lepley et al., 2018; Smart et al., 2018a) and material (Thorpe et al., 2017) properties of the tendon to CSA. A prior study of the medial gastrocnemius of young and old females showed that fascicle slack and tendon stiffness were greater in young females compared with old (Csapo et al., 2014). If young males of the present study exhibited greater fascicle slack for the BB, fascicles would need to shorten to a greater extent prior to the tendon lengthening. The greater fascicle slack in young males, combined with their stiffer tendon, could explain why their tendon CSA did not decrease as much at the lower force levels and led to significantly greater tendon stress in the instantaneous condition occurring at a higher relative force level; however, sex- and age-related differences in the BB muscle slack and tendon stiffness require further study.

Sex- and Age-Related Differences in Stress Underestimation

In support of the second hypothesis, young males had the greatest increase in stress values between the resting and instantaneous CSA calculations, followed by old males and young females

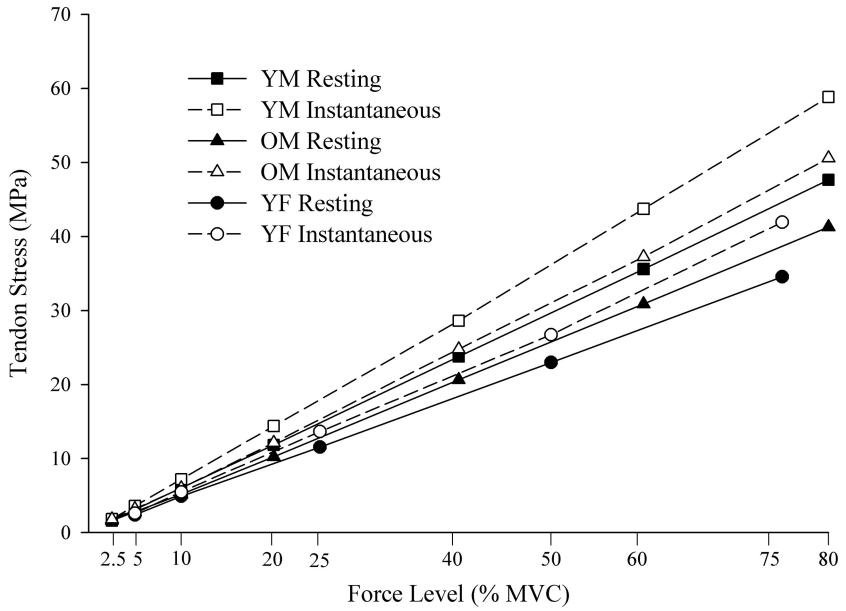

FIGURE 5 | Stress values calculated using the resting and instantaneous tendon CSA. CSA, cross-sectional area YM, young males; OM, old males; YF, young females. MPa, megapascals; MVC, maximal voluntary contraction.

(**Figure 5**). In the resting CSA condition, the sex and age-related differences in tendon stress resulted from young males being the strongest, followed by old males and young females, and this aligns with prior reports on the age-related and sex-specific differences in elbow flexion strength (Brown et al., 2010; Pereira et al., 2015; Smart et al., 2018a). The greater strength in young males resulted in more absolute force being placed on the tendon at the submaximal relative force levels, and this generated a higher ratio of tendon force to CSA. The higher applied forces in young males would also lead to greater reductions in tendon CSA relative to rest, thereby, further amplifying the difference in the resting and instantaneous CSA stress values (the ratio of tendon force to CSA).

When comparing tendon stress calculated with the resting CSA across the three groups and comparing tendon stress calculated with the instantaneous CSA across the three groups, tendon stress in young males became statistically greater than the old males and young females at a lower relative force level in the instantaneous compared with the resting CSA condition (**Table 2**). This was likely due to the decrease in CSA amplifying the rate of increase in tendon stress values, creating larger group differences at the lower relative force levels. Overall, the Johnson–Neyman analysis demonstrated that the difference between resting and instantaneous CSA stress values is age and sex-specific. The underestimation of tendon stress arising from the use of resting CSA needs to be contextualized within the population of study and may lead to age- and sex-related differences in the tendon stress being overlooked or erroneously diminished.

The underestimation of tendon stress generated by the use of resting CSA in the calculation has also been shown in an *ex vivo* equine tendon model by Vergari et al. (2011) where stress at tendon failure was 10.9% greater using the instantaneous compared with the resting CSA. Our findings in humans show ∼20% higher tendon stress during the submaximal contractions of 75–80% MVC, when instantaneous CSA was used, suggesting that failure stress for human tendons is likely higher than previously reported (Lewis and Shaw, 1997; Wren et al., 2001). Although the differences in stress we observed between the instantaneous and resting calculations (0.15–11.19 MPa) were small relative to the total stress experienced by the tendon (41.28–58.84 MPa), it may be consequential to production of steady elbow flexion force control (Smart et al., 2018a), tendon injury, and rehabilitation. Not accounting for the decrease in tendon CSA that occurs during the muscle contraction could lead to excessive stress on the tendon and increase the risk of tendon injury, and the underestimations shown in the present study suggests that this risk of injury may be sex- and age-specific.

Choices of Statistical Approaches

Multi-level modeling growth curve analysis is a modern, widely recommended analytical method for repeated measures analysis when the measurement levels repeated factors are not exactly the same across persons. Between the two datasets used in the current study, the tendon stress data were obtained at 10 different force levels, however, data were not available for all of the sex-age groups at each of the 10 force levels (young and old males: 2.5, 5, 10, 20, 40, 60, and 80% MVC; young females: 5, 10, 25, 50, and 75% MVC). Using the individual data, growth curves were computed for each participant and further analyses focused on the slopes and intercepts of the computed curves. As the curves were computed for all the three groups using MLM, evaluating the characteristics of the curves among the groups and conditions allowed for comparisons not bound by the

individual force levels. MLM also has the benefit of not requiring homoscedasticity within the data, and the heteroscedasticity often present within human physiology data can be incorporated into the MLM analyses *via* weights that are based on the differing variances for more accurate estimates (see Pinhero and Bates, 2000). Models generated in the present study show condition (resting-instantaneous) and sex-age differences for the increase in tendon stress values across the relative forces and highlight the importance of using instantaneous CSA in the determination of stress.

The Johnson–Neyman analysis was used to determine (1) the force levels in which stress values were significantly greater when instantaneous CSA was used compared with the resting CSA within each group, and (2) the force level where stress values became significantly different between groups within the resting and instantaneous CSA conditions. As evidenced by the values in **Table 2** and the visual representations in **Figure 3**, the thresholds for significant differences were not aligned with the submaximal force levels executed and demonstrate that the traditional ANOVA analyses may miss the precise point of the continuous variable at which significant differences start to occur.

LIMITATIONS

From the resting to instantaneous CSA conditions, the higher stress values using instantaneous CSA were expected to lower the force level at which the greater tendon stress in old males became statistically significant from young females, following similar trends as the comparisons to young males. This was not the case as the force level for significant differences between old males and young females increased from the resting to instantaneous CSA conditions, and may have been a result of low sample size increasing variability within the data, as well as this comparison not being physiologically relevant. Future studies examining the influence of resting or instantaneous CSA on the measures of tendon stress should include a sample of old females to allow for a more appropriate sex-related comparison to the old males. To fully appreciate the application of instantaneous compared with the resting tendon CSA, ultrasonography measures should be made along the entirety of the distal BB tendon. Tendon CSA was obtained from the approximate mid-length of the tendon, and may not account for the potential changes in CSA along the entire length of the tendon as seen for the Achilles (Obst et al., 2014a,b) and patellar tendons (Mersmann et al., 2020). Additionally, the measurements of whole BB muscle length along with aponeurosis length would aid in understanding fascicle to aponeurosis ratios of the BB, and future studies should explore this possibility. We performed measures of tendon CSA at relative force levels in contrast to the known strain levels conducted by Vergari et al. (2011). Real-time two-dimensional ultrasound limits the recording to either longitudinal or cross-sectional views making the simultaneous acquisition of tendon elongation and CSA to estimate the stress at a specific strain not feasible. Simultaneous recordings of elongation and CSA could be undertaken in long tendons, e.g., Achilles tendon with two ultrasound probes; however, the anatomy of the elbow limits this possibility.

Conclusion

The MLM demonstrated that tendon stress values increased at a faster rate across the force levels when calculated using the instantaneous compared with the resting CSA. The difference between resting and instantaneous calculations was greatest in young males followed by old males and young females. Further, statistical modeling through the use of the Johnson–Neyman regions of significance test revealed that the force level at which values became significantly greater in the instantaneous compared with the resting condition depended both on sex and age. These findings suggest that the tendon stress underestimation arising from the use of resting CSA is age- and sex-specific. Future *in vivo* human studies should consider the use of instantaneous tendon CSA for evaluating tendon stress to obtain a true representation of the ability of tendon to distribute force from the muscle to the bone in the production and control of human movement.

DATA AVAILABILITY STATEMENT

The raw data supporting the conclusions of this article will be made available by the authors, without undue reservation.

ETHICS STATEMENT

The studies involving human participants were reviewed and approved by University of British Columbia Okanagan's Behavioral Research Ethics Board. The patients/participants provided their written informed consent to participate in this study.

AUTHOR CONTRIBUTIONS

RS designed study, collected and analyzed data, performed statistical analysis, and prepared manuscript. BO'C performed statistical analysis and prepared manuscript. JJ designed study and prepared manuscript. All authors contributed to the article and approved the submitted version.

FUNDING

RS was supported by a Natural Sciences and Engineering Research Council doctoral award and JJ was supported by a Natural Sciences and Engineering Research Council grant (Grant No: 312038).

ACKNOWLEDGMENTS

The tendon stress data used in the present study for young and old males have been previously published (Smart et al., 2018a). We would like to thank Johanne Rosnick, Samantha Kuyzk, and Andrey Federov who assisted in the data collection for the datasets used in the present study.

REFERENCES

Bauer, D. J., Curran, P. J., and Thurstone, L. L. (2005). Probing interactions in fixed and multilevel regression: inferential and graphical techniques. *Multivariate Behav. Res.* 40, 373–400. doi: 10.1207/s15327906mbr4003_5

Brown, R. E., Edwards, D. L., and Jakobi, J. M. (2010). Sex differences in force steadiness in three positions of the forearm. *Eur. J. Appl. Physiol.* 110, 1251–1257. doi: 10.1007/s00421-010-1600-x

Csapo, R., Malis, V., Hodgson, J., and Sinha, S. (2014). Age-related greater Achilles tendon compliance is not associated with larger plantar flexor muscle fascicle strains in senior women. *J Appl. Physiol.* 116, 961–969. doi: 10.1152/japplphysiol.01337.2013

Eriksen, C. S., Henkel, C., Svensson, R. B., Agergaard, A.-S., Couppé, C., Kjaer, M., et al. (2018). Lower tendon stiffness in very old compared with old individuals is unaffected by short-term resistance training of skeletal muscle. *J. Appl. Physiol.* 125, 205–214. doi: 10.1152/japplphysiol.00028.2018

Harwood, B., Cornett, K. M. D., Edwards, D. L., Brown, R. E., and Jakobi, J. M. (2014). The effect of tendon vibration on motor unit activity, intermuscular coherence and force steadiness in the elbow flexors of males and women. *Acta Physiol.* 211, 597–608. doi: 10.1111/apha.12319

Harwood, B., Edwards, D. L., and Jakobi, J. M. (2010). Age independent and position-dependent alterations in motor unit activity of the biceps brachii. *Eur. J. Appl. Physiol.* 110, 27–38. doi: 10.1007/s00421-010-1438-2

Hayes, A. F. (2018). *Introduction to Mediation, Moderation, and Conditional Process Analysis: A Regression-Based Approach, 2nd Edn*. New York, NY: Guilford Press.

Hox, J. J., Moerbeek, M., and van de Schoot, R. (2018). *Multilevel Analysis: Techqniues and Applications, 2nd Edn*. New York, NY: Routledge.

Humphrey, S., and LeBreton, J. (2019). *The Handbook of Multilevel Theory, Measurement, and Analysis*. Washington, DC: American Physiological Society.

Johnson, P. O., and Fay, L. C. (1950). The Johnson-Neyman technique, it's theory and applications. *Psychometrika* 15, 349–367. doi: 10.1007/BF02288864

Lazar, A. A., and Zerbe, G. O. (2011). Solutions for determining the significance region using the Johnson-Neyman type procedure in generalized linear (mixed) models. *J. Educ. Behav. Stat.* 36, 699–719. doi: 10.3102/1076998610396889

Lepley, A. S., Joseph, M. F., Daigle, N. R., Digiacomo, J. E., Galer, J., Rock, E., et al. (2018). Sex differences in mechanical properties of the Achilles tendon: longitudinal response to repetitive loading exercise. *J. Strength Cond. Res.* 32, 3070–3079. doi: 10.1519/JSC.0000000000002386

Lewis, G., and Shaw, K. M. (1997). Tensile properties of human tendo Achillis: effect of donor age and strain rate. *J. Foot Ankle Surg.* 36, 435–445. doi: 10.1016/S1067-2516(97)80096-8

Mersmann, F., Laube, G., Bohm, S., and Arampatzis, A. (2020). Muscle and tendon morphology in early-adolescent athletes and untrained peers. *Front. Physiol.* 11:1029. doi: 10.3389/fphys.2020.01029

Obst, S. J., Newsham-West, R., and Barrett, R. S. (2014a). *In vivo* measurement of human Achilles tendon morphology using freehand 3-D ultrasound. *Ultrasound Med. Biol.* 40, 62–70. doi: 10.1016/j.ultrasmedbio.2013.08.009

Obst, S. J., Renault, J.-B., Newsham-West, R., and Barrett, R. S. (2014b). Three-dimensional deformation and transverse rotation of the human free Achilles tendon *in vivo* during isometric plantarflexion contraction. *J. Appl. Physiol.* 116, 376–384. doi: 10.1152/japplphysiol.01249.2013

Pereira, H. M., Spears, V. C., Schlinder-Delap, B., Yoon, T., Nielson, K. A., and Hunter, S. K. (2015). Age and sex differences in steadiness of elbow flexor muscles with imposed cognitive demand. *Eur. J. Appl. Physiol.* 115, 1367–1379. doi: 10.1007/s00421-015-3113-0

Pinhero, J., and Bates, D. M. (2000). *Mixed-Effects Models in S and S- PLUS*. New York, NY: Springer.

Potvin, J. R., and Fuglevand, A. J. (2017). A motor unit-based model of muscle fatigue. *PLoS Comput. Biol.* 13, 1–30. doi: 10.1371/journal.pcbi.1005581

Rast, P., Rush, J., Piccinin, A., and Hofer, S. M. (2014). The identification of regions of significance in the effect of multimorbidity on depressive symptoms using longitudinal data: an application of the Johnson-Neyman technique. *Gerontology* 60, 274–281. doi: 10.1159/000358757

Ristaniemi, A., Stenroth, L., Mikkonen, S., and Korhonen, R. K. (2018). Comparison of elastic, viscoelastic and failure tensile material properties of knee ligaments and patellar tendon. *J. Biomech.* 79, 31–38. doi: 10.1016/j.jbiomech.2018.07.031

Smart, R., Baudry, S., Fedorov, A., Kuzyk, S., and Jakobi, J. M. (2018a). Influence of biceps brachii tendon mechanical properties on elbow flexor force steadiness in young and old males. *Scand J. Med. Sci. Sport* 28, 983–991. doi: 10.1111/sms.13024

Smart, R. R., Kohn, S., Richardson, C. M., and Jakobi, J. M. (2018b). Influence of forearm orientation on biceps brachii tendon mechanics and elbow flexor force steadiness. *J. Biomech.* 76, 129–135. doi: 10.1016/j.jbiomech.2018.05.039

Smart, R. R., Richardson, C. M., and Jakobi, J. M. (2017). Repeatability of ultrasound in assessment of distal biceps brachii tendon. *Int. J. Diagnostic Imaging* 4, 1–8. doi: 10.5430/ijdi.v4n2p1

Snijders, T. A., and Bosker, R. J. (2012). *Multilevel Analysis: An Introduction to Basic and Advanced Multilevel Modeling*. Los Angeles, CA: SAGE Publications Inc.

Stenroth, L., Peltonen, J., Cronin, N. J., Sipilä, S., and Finni, T. (2012). Age-related differences in Achilles tendon properties and triceps surae muscle architecture *in vivo*. *J. Appl. Physiol.* 113, 1537–1544. doi: 10.1152/japplphysiol.00782.2012

Taylor, A. M., and Enoka, R. M. (2004). Optimization of input patterns and neuronal properties to evoke motor neuron synchronization. *J. Comput. Neurosci.* 16, 139–157. doi: 10.1023/B:JCNS.0000014107.16610.2e

Thorpe, C. T., Riley, G. P., Birch, H. L., Clegg, P. D., and Screen, H. R. C. (2017). Fascicles and the interfascicular matrix show decreased fatigue life with ageing in energy storing tendons. *Acta Biomater.* 56, 58–64. doi: 10.1016/j.actbio.2017.03.024

Tibold, R., and Fuglevand, A. J. (2015). Prediction of muscle activity during loaded movements of the upper limb. *J. Neuroeng. Rehabil.* 12, 1–12. doi: 10.1186/1743-0003-12-6

Verbeke, G. (2013). *Linear Mixed Models for Longitudinal Data*. New York, NY: Springer-Verlag.

Vergari, C., Pourcelot, P., Holden, L., Ravary-Plumioën, B., Gerard, G., Laugier, P., et al. (2011). True stress and Poisson's ratio of tendons during loading. *J. Biomech.* 44, 719–724. doi: 10.1016/j.jbiomech.2010.10.038

Wren, T., Yerby, S., Beaupré, G. S., and Carter, D. R. (2001). Mechanical properties of the human Achilles tendon, *in vivo*. *Clin. Biomech.* 16, 245–251. doi: 10.1016/S0268-0033(00)00089-9

Conflict of Interest: The authors declare that the research was conducted in the absence of any commercial or financial relationships that could be construed as a potential conflict of interest.

frontiers in Physiology

ORIGINAL RESEARCH
published: 15 October 2021
doi: 10.3389/fphys.2021.752641

Effects of Different Tissue Flossing Applications on Range of Motion, Maximum Voluntary Contraction, and H-Reflex in Young Martial Arts Fighters

Miloš Kalc[1], Samo Mikl[1], Franci Žökš[1], Matjaž Vogrin[1,2] and Thomas Stöggl[3,4]*

[1] Institute of Sports Medicine, Faculty of Medicine, University of Maribor, Maribor, Slovenia, [2] Department of Orthopaedics, University Medical Centre Maribor, Maribor, Slovenia, [3] Department of Sport and Exercise Science, University of Salzburg, Salzburg, Austria, [4] Athlete Performance Center, Red Bull Sports, Thalgau, Austria

OPEN ACCESS

Edited by:
Christoph Centner,
University of Freiburg, Germany

Reviewed by:
Patrick Wiegel,
University of Freiburg, Germany
Emiliano Cè,
University of Milan, Italy
Benedikt Lauber,
University of Fribourg, Switzerland

****Correspondence:***
Miloš Kalc
milos.kalc@um.si
orcid.org/0000-0001-7002-2924

Specialty section:
This article was submitted to Exercise Physiology, a section of the journal Frontiers in Physiology

Received: *03 August 2021*
Accepted: *21 September 2021*
Published: *15 October 2021*

Citation:
Kalc M, Mikl S, Žökš F, Vogrin M and Stöggl T (2021) Effects of Different Tissue Flossing Applications on Range of Motion, Maximum Voluntary Contraction, and H-Reflex in Young Martial Arts Fighters. Front. Physiol. 12:752641. doi: 10.3389/fphys.2021.752641

The purpose of this study was to investigate the effects of tissue flossing applied to the ankle joint or to the calf muscles, on ankle joint flexibility, plantarflexor strength and soleus H reflex. Eleven young (16.6 ± 1.2 years) martial arts fighters were exposed to three different intervention protocols in distinct sessions. The interventions consisted of wrapping the ankle (ANKLE) or calf (CALF) with an elastic band for 3 sets of 2 min (2 min rest) to create vascular occlusion. A third intervention without wrapping the elastic band served as a control condition (CON). Active range of motion for ankle (AROM), plantarflexor maximum voluntary contraction (MVC), and soleus H reflex were assessed before (PRE), after (POST), and 10 min after (POST10) the intervention. The H reflex, level of pain (NRS) and wrapping pressure were also assessed during the intervention. Both CALF and ANKLE protocols induced a significant drop in H reflex during the intervention. However, the CALF protocol resulted in a significantly larger H reflex reduction during and after the flossing intervention (medium to large effect size). H reflexes returned to baseline levels 10 min after the intervention in all conditions. AROM and MVC were unaffected by any intervention. The results of this study suggest that tissue flossing can decrease the muscle soleus H reflex particularly when elastic band is wrapped around the calf muscles. However, the observed changes at the spinal level did not translate into higher ankle joint flexibility or plantarflexor strength.

Keywords: vascular occlusion, motoneuron excitability, ankle, joint, muscle, elastic band

INTRODUCTION

Martial arts are dynamic activities where the athletes require muscular power, strength, and joint flexibility (Bridge et al., 2014). Static stretching has largely been demonstrated to be an effective method to increase flexibility around a joint (Opplert and Babault, 2018); however, it significantly reduces maximal voluntary strength, which could originate from various neural and peripheral mechanisms (Power et al., 2004; Opplert et al., 2016). The importance of generating high dynamic strength and flexibility is functionally important to support the technical demands in martial arts

(Bridge et al., 2014). Thus, static stretching should be used carefully or even avoided during warm-up to prevent subsequent potentially deleterious effects on muscular performance. In the last decade, the interest has focused on the effects of different stretching modalities such as dynamic stretching or foam rolling, which have the potential to increase joint flexibility and maintain muscle power (Opplert and Babault, 2018). Tissue flossing is a novel method, which consists of wrapping part of a limb with a thick elastic band, thus increasing pressure and producing vascular occlusion in a part of that limb distal from the band. Some studies have recently recognized the value of this technique as a way of increasing joint range of motion (ROM) while maintaining or even increasing muscle strength and power (Driller and Overmayer, 2017).

In clinical practice as well as in the current published literature, there are two main band application modes: the joint technique, where the elastic band is wrapped around a joint, and the muscle technique, where the band is wrapped around the muscles of the limb (Konrad et al., 2021). To the best of our knowledge, the effects of tissue flossing on joint ankle ROM and torque of the plantarflexors using the joint and muscle technique have never been compared in a single study on the same pool of participants.

Studies investigating the effects of both techniques have found conflicting results. Studies where the elastic band was wrapped around the ankle joint of recreationally trained individuals, reported an increase in ROM (Driller and Overmayer, 2017), a decrease in muscle tone (Vogrin et al., 2020b), as well as positive effects on muscle strength, jump and sprint performance (Driller et al., 2017; Driller and Overmayer, 2017). However, tissue flossing seems to be less effective when applied to athletes (Mills et al., 2020). The effects of tissue flossing when wrapped around the muscle have produced ambiguous results. Konrad et al. (2021) as well as Vogrin et al. (2020a) wrapped the thigh, reporting an increase in maximal isometric torque of the knee extensors, but no increase in ROM measured by the active straight leg raise (ASLR) test. In contrast, Kaneda et al. (2020) reported a substantial increase in ASLR. Gorny and Stöggl (2018) lacked to find any effect of tissue flossing on DOMS (Delayed Onset Muscle Soreness) reduction.

Despite the increased interest in this field, only a handful of studies investigated the physiological mechanisms responsible for the observed functional changes in ROM and MVC (Konrad et al., 2021). There are different possible mechanisms of action involved in the observed increase in ROM: Kaneda et al. (2020) reported an increased passive torque at the end of the ROM after tissue flossing, which might indicate higher tolerance to stretch. Moreover, the increased ROM was not accompanied by changes in muscle stiffness (Kaneda et al., 2020; Vogrin et al., 2020a). The effects of tissue flossing on ROM can be compared to those elicited via self-myofascial release, which is created by applying pressure on muscles and fascia using foam rollers. Even though the physiological mechanisms responsible for the effects of foam rolling are still part of a scientific debate, the mechanisms can be divided into mechanical, focused on the alteration of the fascia (Schleip and Müller, 2013) and neurophysiological (Schleip, 2003). In this regard, it has been suggested that pressure applied by the tissue flossing on muscle, skin, and fascia could impact fluid viscosity, which could lead to less resistance to movement (Konrad et al., 2021).

Increased muscular strength and power after tissue flossing could be explained by increased sympathetic outflow and a facilitation of the short-latency stretch reflex (Konrad et al., 2020). It is well known that afferent signals from muscle spindles contribute to different voluntary muscle contractions (Macefield et al., 1991), and thus an increase in spinal excitability can induce an increase in performance. Furthermore, Vogrin et al. (2020a) reported a reduction in contraction time in the rectus femoris after tissue flossing, which was interpreted as neuromuscular potentiation.

Besides the effects caused by pressure on muscle, skin and fascia, tissue flossing induces vascular occlusion, which can be compared with ischemic preconditioning (Driller and Overmayer, 2017). Ischemic preconditioning is a technique where sub-lethal local acute ischemia is induced by arterial occlusion. It is thought that ischemic preconditioning can prevent or attenuate future ischemic reperfusion injuries in the exposed tissue (Murry et al., 1986). Recently, this method was tested in other applications, resulting in enhanced exercise performance (Cocking et al., 2018), delayed time to fatigue (Halley et al., 2018) and improvements in postural control (Cherry-Allen et al., 2015). Due to differences in protocol conditions and durations between ischemic preconditioning studies, is it still unclear if ischemic preconditioning induces an increase or depression of neuromuscular performance. Both methods, ischemic preconditioning and tissue flossing, create vascular occlusion, thus limiting oxygen availability to the wrapped body part. This is borne out by a recent study by Pavlů et al. (2021) that confirmed a drastic drop in blood flow during 2 min flossing application.

Oxygen availability as well as afferent inputs from muscle spindles and other pressure-sensitive receptors, play an essential role in the function of the central nervous system (CNS). A reduction in oxygen supply (hypoxia) quickly affects neural mechanisms, especially their metabolic requirements and excitability (Neubauer and Sunderram, 2004). On the other hand, afferent signaling from mechanoreceptors might stimulate the nervous system and thereby lead to reduced muscle stiffness (Schleip, 2003). There is some evidence that pressure exerted by foam rolling treatment decreases neural modulation of spinal excitability (Young et al., 2018). Studies suggest that changes in the CNS are peripherally mediated central effects via III and IV afferents from within the muscle (Verges et al., 2012), skin and fascia (Schleip, 2003). At the spinal level, neural impairment can be partially linked to the inhibition or excitability of the alpha motoneuron pool (Garland and McComas, 1990). We, therefore, believe it is worth exploring the effects of tissue flossing on the excitability of the motoneuron pool employing a widely accepted technique like the H reflex (Zehr, 2002). The H reflex is electrically evoked and considered the analog of the stretch reflex since both share the same monosynaptic reflex pathway (Zehr, 2002). However, the H reflex bypasses the muscle spindle; thus, its amplitude depends not only on motoneuron excitability (Schieppati, 1987) but also on the level

of presynaptic inhibition affecting the Ia afferents (Knikou, 2008). Earlier literature describes the effects of systemic hypoxia on H reflex in ambiguous terms, showing increased (Delliaux and Jammes, 2006), decreased (Willer et al., 1987), or unchanged H reflex amplitude (Kayser et al., 1993). Tissue flossing using joint and muscle wrapping techniques might have different effects on neuromuscular parameters in respect of unique receptors present in both the muscle and joint capsule tissue (Taylor, 2009).

Based on previous studies, we hypothesize an increase in ankle joint ROM after the joint application, an increase in plantarflexion MVC after the muscle application and a higher reduction of the H-reflex using the muscle application compared to the joint application. Therefore, the aim of the study was to investigate the effects of tissue flossing applied to the ankle joint or to the calf muscles on ankle ROM, plantarflexor MVC and muscle soleus H reflex.

MATERIALS AND METHODS

Study Design

The present study followed a cross-over repeated measures design, where each participant was randomly exposed to three intervention protocols, one per visit. At each visit, following warm-up and pretest assessments, an elastic band (Medical Flossing Band, Germany, 1.3 mm thick, 50 mm wide, 150 mm long) was used to wrap the ankle (ANKLE condition) or calf (CALF condition) of the left leg. The third visit without elastic band wrapping was used as the control condition (CON). During each visit, participants underwent the same assessments prior to (PRE), immediately after (POST) and 10 min after (POST10) the intervention (floss band application or control). The following lower-leg assessments were conducted: (i) muscle soleus H-reflex (HM); (ii) plantarflexion MVC; (iii) active ankle range of motion (AROM). In addition, H-reflexes were elicited while the band was applied (F1, F2, F3) and during the rest period between applications (R1, R2) (see **Figure 1A**). The same procedure was applied in the CON condition without band application. There were 48-h between consecutive visits to avoid between-session influences.

Participants

Eleven young elite non-Olympic martial arts fighters (Biological sex: 5 men, 6 women, Age: 16.6 ± 1.2 years, Weight: 62.3 ± 7.9 kg, Height: 171.3 ± 9.0 cm) participated in this study (power 0.6). Participants undertook regular training (Weekly training session: 7.7 ± 5.0; Weekly training volume: 9.3 ± 1.0 h) and participated in international and domestic Taekwondo and Kickbox tournaments. Recent competitive achievements were 3 World and 4 European champions in their age group; 6 fighters were classified in the world top 5 rank in their age group. All participants were free of acute locomotor, nerve, or known cardiovascular and metabolic diseases. Prior to the first visit, the participants completed a modified risk assessment questionnaire (Kacin et al., 2015), to exclude possible safety risks while inducing vascular occlusion. Among the exclusion criteria were family history of clotting disorders (e.g., lupus, hemophilia, high platelets), level 1 hypertension (SAP ≥ 140 mmHg), hypertension (SAP 120–140 mmHg), history of deep vein thrombosis, pulmonary embolism, history of hemorrhagic or thrombotic stroke, smokers, medication including the contraceptive pill, history of nerve injury (including back or neck injury), history of injury to arteries or veins, diabetes, metalwork *in situ*, undiagnosed groin or calf pain, compartment syndrome, surgery within the previous 4 weeks, a journey lasting more than 4 h or a flight in the previous 7 days and any other medical conditions including a history of synovitis.

The participants were familiarized with the experimental procedure and their voluntary cooperation was confirmed by written informed consent on the first testing day. The study was approved by the Research Ethics Committee of the University Medical Centre Maribor, Slovenia. All procedures were performed according to the Declaration of Helsinki.

Assessment Procedures

Maximum Voluntary Contraction Assessment

To assess the MVC of ankle plantarflexors, participants were instructed to sit on an ankle dynamometer equipped with a force sensor (S2P, Ljubljana, Slovenia) with a sampling rate of 1,000 Hz. Their hips, knees and ankles were flexed at 90°. The lateral malleolus of the tibia was aligned with the dynamometer's axis of rotation and plantarflexion movement was restricted using the dynamometer fixation system, which uses a rigid brace pressed to the thigh, just above the knee joint (**Figure 1B**). At the beginning of each visit, the participants were familiarized with the MVC technique and asked to contract their plantarflexors seven times for 5 s (30 s between contractions). They were instructed to exert a medium effort (subjectively defined) at the first contraction and progressively increase effort at every consecutive contraction until reaching a maximal contraction at the last trial. This procedure also served as a warm-up. At each time point (PRE, POST, POST10), the participants were instructed to progressively contract their plantarflexors until the maximum torque was reached (within 2 s approximately), maintaining the maximum isometric contraction for approximately 4 s. Participants were verbally encouraged to perform the tests with maximal effort. No visual feedback was provided (Verges et al., 2009). Two repetitions with 30 s rest were permitted at each time point.

Range of Motion Assessment

The ROM of the left ankle was assessed using a G-Walk (BTS, Bioengineering, Italy) digital goniometer with a sampling rate of 1,000 Hz. Participants were instructed to lie supine on a (standard) therapeutic table, with arms alongside the body. In order to permit unrestricted ankle motion, the left ankle extended past the edge of the table, with the edge supporting the lower leg just above the malleoli on the distal third. In addition, a cushion was placed below the knee joint allowing 30° knee flexion. The contralateral leg was flexed in the hip and knee and in contact with the table. The goniometer was placed just below the lateral malleolus of the ankle, with the *y*-axis lined up through the lateral aspect of the fibula and the *x*-axis lined up with the 5th metatarsophalangeal joint. The goniometer was attached to the skin using bandaging tapes and additionally fixed in

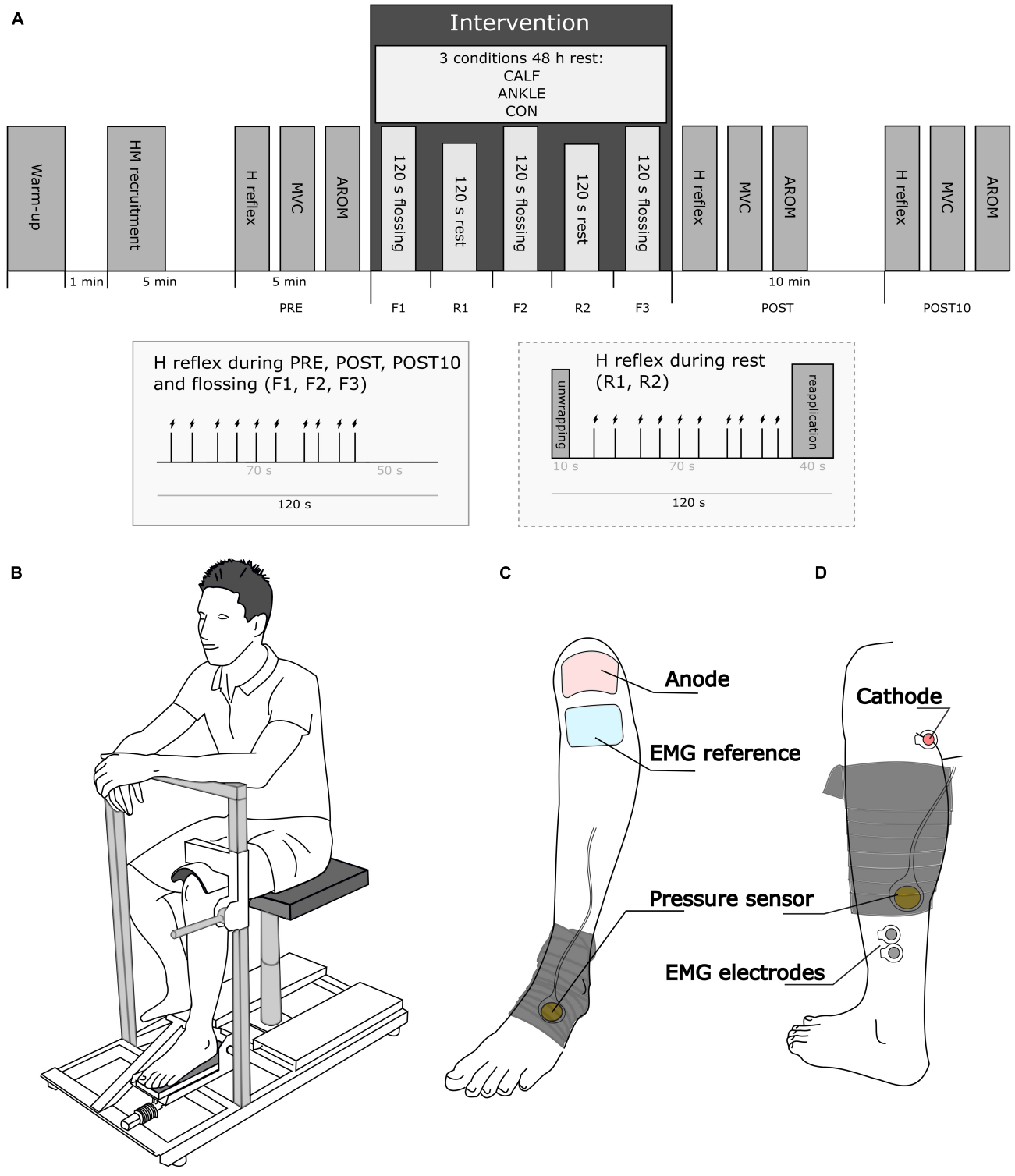

FIGURE 1 | (A) Graphical representation of the study design. AROM and MVC were assessed before (PRE) and after the intervention (POST and POST10). The H reflex was assessed during the flossing and control intervention (F1, F2, F3) and in the rest periods between flossing and control interventions (R1, R2). The small box captions represent the timeline of nerve stimulation during PRE, F1, F2, F3, POST, POST10, and R1, R2, respectively. **(B)** Schematic of the position of the subject during the neuromuscular assessment. **(C)** Flossing band wrapping during the ANKLE condition; **(D)** flossing band during the CALF condition. **(C,D)** Show the placement of the pressure sensor probe, EMG and stimulation electrodes.

position with an elastic bandage. The position of the goniometer at the PRE time point was marked using a skin marker to allow accurate repositioning at POST and POST10 time points. At each measuring time (PRE, POST, and POST10), the participants were instructed to slowly (within 2 s approximately) extend the left ankle (plantarflexion) and maintain that position for approximately 1 s before slowly flexing the ankle (dorsal flexion). Once maximum dorsiflexion was reached, participants maintained the final position for approximately 1 s before slowly (approx. 2 s) returning to the starting position. The procedure was repeated twice for each time point.

Surface Electromyography

Participants were prepared for surface electromyographic (EMG) recording of the soleus muscle (SOL) using a standard procedure: the skin was shaved and slightly rubbed using an abrasive paste. Electrodes (Covidien 24 mm, Walpole, Massachusetts, United States) for recording the H reflex from the SOL muscle were placed in a standard bipolar configuration at an interelectrode distance of 20 mm. The reference electrode (50 × 100 mm, 00734, Compex, Guildford, Surrey, United Kingdom) was placed over the tuberositas tibiae. The EMG signal was collected using a PowerLab data acquisition toolbox and LabChart 8 software (both ADInstruments, Bella Vista, New South Wales, Australia) at 4,000 Hz sampling frequency and filtered using a 10–500 Hz band-pass filter.

Electrical Stimulation

All stimulations were performed with the participants in the same position for measuring MVC. H reflex and respective M waves measured in SOL were elicited by a custom-built, constant current high voltage electrical stimulator (NeoStim 1, FE Furlan, Ljubljana, Slovenia) delivering single rectangular electrical impulses (1 ms) to the tibial nerve in 5–8 s pseudo-random interstimulus intervals. This interstimuli interval minimized the possibility of post-activation depression (Zehr, 2002; Burke, 2016). The anode (50 × 90 mm, MyoTrode PLUS, Globus, Italy) was placed over the patella and the cathode (Covidien 24 mm, Walpole, Massachusetts, United States) was placed in the popliteal fossa at the position that provided the greatest M wave at 20 mA intensity. Such high intensity was used only to detect the best stimulation position. The cathode position was marked with a skin marker and additionally fixed using an elastic band. In the preparatory phase of each visit (before PRE time point), an H reflex—M wave recruitment (HM recruitment) curve was assessed starting at 10 mA, increasing the stimulation intensity by 1 mA every successive stimulation until the H reflex clearly reached its descending phase. Stimulation intensities were then increased in 5 mA steps until a maximal M wave was reached (Mmax). Stimulation intensity during experimental measuring was adjusted to obtain a value where the H reflex would fall on the ascending part of the HM recruitment curve with an M wave value of approximately 10% Mmax amplitude (M10). 10 stimuli at M10 intensity were delivered at each time point (PRE, F1, R1, F2, R2, F3, POST, POST10). Particular attention was made to starting the stimulation protocol within 5 s from the start of each time point. The intensity was slightly adjusted during the experiment to elicit a consistent M10 amplitude.

Level of Pain

The level of pain was assessed using an 11-point numerical rating scale (NRS), where 0 indicates "no pain" and 10 indicates the "worst imaginable pain." 60 s after the floss band was applied, participants were instructed to choose a single number from the scale that best indicated their level of pain (Hjermstad et al., 2011). The level of pain was not assessed during the CON condition.

Kikuhime Pressure Control Sensor Measurement

A flat balloon-like pressure control sensor (35 mm in diameter; Kikuhime, TT Meditrade, Sorø, Denmark) was used to control the pressure exerted by the floss band to the wrapped ankle or calf. This device represents a validated (ICC = 0.99, CV = 1.1%) and reliable (CV = 4.9%) tool to be used in the sports medicine setting (Brophy-Williams et al., 2013). The pressure control sensor was fixed with a tape patch over the tube of the sensor. During the CALF visit, the sensor was placed on the triceps surae aponeurosis just below the gastrocnemius bulk, while during the ANKLE visit, the sensor was placed on the cuneiform bones. To ensure precise pressure measurements, the tube attaching the sensor to the digital display was always set facing proximally toward the knee while the sensor itself was set toward the floss band and progressively compressed by the band application (**Figures 1C,D**).

Floss Band Application

Following pre-tests, participants were instructed to sit on the ankle dynamometer. To facilitate wrapping and unwrapping of the floss band, they were asked to extend their left knee, placing the lower part of the leg on a pillow. The leg position (wrapping position) was slightly different between CALF and ANKLE conditions. During the ANKLE visit, the pillow was placed at the middle-third of the lower leg on the medial gastrocnemius muscle, while during the CALF and CON visits, the pillow supporting the leg was placed in the distal third of the lower leg, just above the calcaneus. In visits where banding was applied (ANKLE and CALF), the floss band, comprising a thick latex elastic band, was wrapped around the ankle joint (ANKLE) or the calf muscles (CALF). The floss band was applied by two physical therapists (SM and FZ) with 5 years of experience of tissue flossing methods. In both flossing visits, a simple bandaging technique was used: the elastic band was first pulled and then wrapped in a circular motion around the limb moving proximally toward the knee in a progressive way. Each subsequent wrap overlapped the previous by approximately 50%, before fixing the last part of the band (approx. 5 cm) beneath the final wrap. In the CALF visit, the first wrap started at the middle of an imaginary line between the external malleolus and the head of the fibula, approximately 5 cm above the position of the EMG electrodes. In the ANKLE visit, the first wrap started at the middle of the metatarsal bone (distal of the talus). The calcaneus and the Achilles tendon were also wrapped with the elastic band. In both visits, the floss band covered approximately 15 cm of the

limb when fully applied. The physical therapists were instructed to apply the flossing band by pulling the band at 100% extension as they would do in regular clinical practice. Wrapping pressure was monitored during each application and the floss band was reapplied if pressure was below 150 mmHg, which happened in one case. The wrapping procedure took approximately 40 s. As soon as the last part of the band was fixed, the subject was asked to return to the H-reflex assessment position. After 120 s participants were instructed to extend their legs and the floss band was unwrapped. As soon the band was unwrapped (approximately 10 s), participants were instructed to return to the H-reflex assessment position for approximately 70 s and then to the wrapping position for the band to be reapplied. This procedure was repeated three times (3 sets of 120 s flossing followed by 80 s rest and 40 s of reapplication).

Data Processing

MVC and ROM data were processed using the RcppRoll package (Ushey, 2018) within the R language environment (R Core Team, 2020). MVC data was first processed using a rolling average filter (0.2 s). The highest peak torque across the two trials for the same assessment time point (PRE, POST, or POST10) was taken for further analysis. ROM data was first processed using a rolling average filter (0.1 s). The highest plantarflexion and dorsiflexion angles across two trials for the same assessment time point was taken for further analysis. The AROM parameter was computed by adding the plantarflexion and dorsiflexion angle data.

10 H reflexes were elicited at each assessment time point and checked for consistency. The first stimuli at each timepoint were used to adjust the stimulation intensity and were discarded during the data processing (discarded: 264). Moreover, the remaining M waves with peak to peak amplitudes differing more than ± 2 SDs (Budini et al., 2017) from the baseline of each visit were discarded (elicited: 2,376; discarded: 40 = 1.7%). The data was normalized to the maximal *M*-values. The average value of all H reflexes within a time point was used for further analysis as the HM parameter (**Figure 2**).

Statistical Analysis

Data was analyzed using the R (version 3.5.4) programming language (R Core Team, 2020). Normal distribution was verified using the Shapiro–Wilk test for small samples across all parameters. A 3 × 3 two-way repeated-measures ANOVA using the Afex package (Singmann et al., 2020) was performed to determine the effect of different treatments (CON, CALF, ANKLE) and time (PRE, POST, POST10) on MVC and AROM. A 3 × 8 two-way repeated-measures ANOVA was performed to determine the effect of different treatments (CON, CALF, ANKLE) and time (PRE, POST, POST10, F1, F2, F3R1, R2) on the H-reflex, M wave (M10) and stimulation intensity (STIMint). In addition, a 2 × 3 two-way repeated-measures ANOVA was performed to determine the effects of 2 flossing conditions (CALF, ANKLE) over the three time points where the elastic band was applied (F1, F2, F3) on NRS and pressure parameter. The assumption of sphericity was assessed using the Mauchly test. Whenever the assumption of sphericity was violated, the degrees of freedom were corrected using the Greenhouse-Geisser correction (GGe). *Post hoc* tests were performed as pairwise comparisons using Tukey's adjustment within the Emmeans package (Lenth et al., 2020) to determine

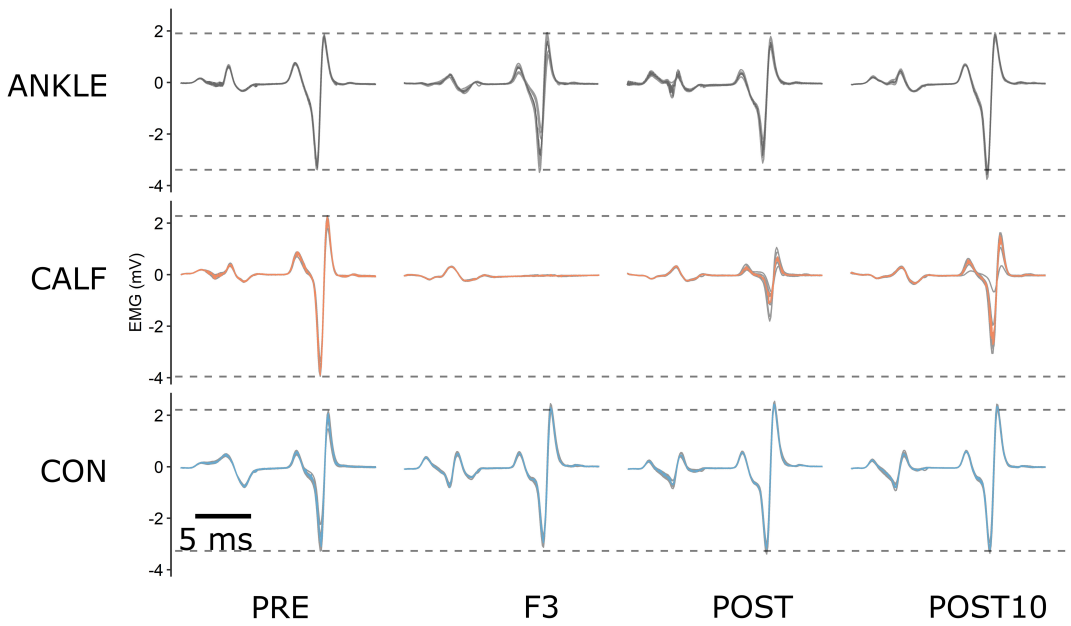

FIGURE 2 | An example of raw H reflex data for one representative participant at PRE, during F3, POST and POST10 time points. The colored lines represent the average of 9 consecutive signals at each time point. ANKLE, CALF, and CON conditions are represented by gray, orange and blue lines, respectively. Dashed lines represent baseline levels for each condition.

the differences between single treatments at different time points. Standardized changes in the mean of each measure were used to assess magnitudes of effects and were calculated using Cohen's *d* and then interpreted using thresholds of 0.2, 0.5, 0.8 for small, moderate and large effects, respectively (Batterham and Hopkins, 2006). An effect size of ± 0.2 was considered the smallest worthwhile effect, with an effect size of < 0.2 considered to be trivial. The effect was considered unclear if its 95% confidence interval overlapped the thresholds for small positive and small negative effects (Batterham and Hopkins, 2006). Statistical significance was set at $p < 0.05$ for all analyses. Correlations between H-reflex relative changes from baseline and pressure were computed using the Pearson correlation coefficient.

RESULTS

Descriptive statistics (mean and SD) for ASLR, MVC, and H-reflex data are given in **Table 1** and for NRS and pressure in **Table 2**. All observed variables were normally distributed. Cohen's *d* effect sizes for comparisons of all measures (POST, POST10) to pre-test values are given in **Table 3**.

The analysis of NRS revealed that there was not a statistically significant interaction between the effect of intervention type and time [$F_{(2,20)} = 2.17$, $P = 0.141$, $\eta_p^2 = 0.178$]. Simple main effect analysis showed that time [$F_{(2,20)} = 0.31$, $P = 0.735$, $\eta_p^2 = 0.030$] and intervention type [$F_{(2,20)} = 2.17$, $P = 0.141$, $\eta_p^2 = 0.178$] did not have a statistically significant effect on NRS.

The analysis of pressure revealed that there was not a statistically significant interaction between the effect of intervention type and time [$F_{(2,20)} = 0.26$, $P = 0.771$, $\eta_p^2 = 0.026$]. Simple main effect analysis showed that intervention type did have a statistically significant effect on pressure [$F_{(1,10)} = 21.05$, $P < 0.001$, $\eta_p^2 = 0.678$]. Simple main effect analysis showed that time did not have a statistically significant effect on pressure [$F_{(2,20)} = 1.47$, $P = 0.254$, $\eta_p^2 = 0.128$].

The analysis of AROM revealed that there was not a statistically significant interaction between the effect of intervention type and time [$F_{(4,40)} = 0.64$, $P = 0.635$, $\eta_p^2 = 0.060$]. Simple main effect analysis showed that intervention type did have a statistically significant effect on AROM [$F_{(2,20)} = 4.19$, $P = 0.030$, $\eta_p^2 = 0.295$]. Simple main effect analysis showed that time did not have a statistically significant effect on AROM [$F_{(2,20)} = 1.23$, $P = 0.312$, $\eta_p^2 = 0.110$]. *Post hoc* tests revealed no statistically significant differences.

The analysis of MVC revealed that there was not a statistically significant interaction between the effect of intervention type and time [$F_{(4,40)} = 1.56$, $P = 0.203$, $\eta_p^2 = 0.135$]. Simple main effect analysis showed that time [$F_{(2,20)} = 1.06$, $P = 0.366$, $\eta_p^2 = 0.096$] and intervention type [$F_{(2,20)} = 1.73$, $P = 0.202$, $\eta_p^2 = 0.148$] did not have a statistically significant effect on MVC.

The analysis of M10 revealed that there was not a statistically significant interaction between the effect of intervention type and time [$F_{(14,140)} = 0.89$, $P = 0.568$, $\eta_p^2 = 0.082$]. Simple main effect analysis showed that time [$F_{(7,70)} = 0.76$, $P = 0.626$, $\eta_p^2 = 0.070$] and intervention type [$F_{(2,20)} = 1.80$, $P = 0.191$, $\eta_p^2 = 0.153$] did not have a statistically significant effect on M10.

The analysis of STIMint revealed that there was not a statistically significant interaction between the effect of intervention type and time [$F_{(14,140)} = 0.29$, $P = 0.995$, $\eta_p^2 = 0.028$]. Simple main effect analysis showed that time did have a statistically significant effect on STIMint [$F_{(7,70)} = 2.74$, $P = 0.014$, $\eta_p^2 = 0.215$]. Intervention type did not have a statistically significant effect on STIMint [$F_{(2,20)} = 1.52$, $P = 0.242$, $\eta_p^2 = 0.132$].

TABLE 1 | Descriptive statistics (mean ± SD).

Variable	ANKLE	CALF	CON
AROM (°)			
PRE	66.4 ± 9.2	63.3 ± 11.6	66.3 ± 8.8
POST	67.5 ± 11.4	63.7 ± 12.2	65.5 ± 10.0
POST10	65.9 ± 10.7	63.2 ± 13.0	63.8 ± 10.5
MVC (Nm)			
PRE	115.0 ± 15.1	113.6 ± 14.3	111.2 ± 16.2
POST	117.6 ± 19.4	109.7 ± 15.5	108.7 ± 16.3
POST10	116.4 ± 17.0	113.6 ± 19.1	117.9 ± 19.8
H (%Mmax)			
PRE	49.4 ± 26.9	54.8 ± 22.0	53.2 ± 19.9
F1	30.5 ± 29.6	21.7 ± 20.6	45.0 ± 23.4
R1	44.5 ± 31.7	43.6 ± 23.1	47.8 ± 21.3
F2	31.7 ± 29.9	20.1 ± 22.3	45.2 ± 22.0
R2	45.7 ± 32.0	38.8 ± 23.1	45.1 ± 20.5
F3	34.6 ± 29.6	22.8 ± 19.6	47.7 ± 22.2
POST	46.0 ± 31.8	37.5 ± 23.6	46.2 ± 21.6
POST10	46.7 ± 33.8	48.5 ± 26.1	45.3 ± 25.9
M10 (%Mmax)			
PRE	8.0 ± 4.8	10.8 ± 6.1	11.8 ± 5.8
F1	7.5 ± 4.3	10.9 ± 6.4	10.3 ± 4.9
R1	7.6 ± 3.9	10.5 ± 5.1	10.5 ± 5.0
F2	8.0 ± 4.8	11.6 ± 7.0	10.6 ± 5.3
R2	7.6 ± 4.2	10.4 ± 5.8	11.3 ± 6.3
F3	7.7 ± 4.1	11.0 ± 6.5	10.6 ± 5.0
POST	8.3 ± 4.8	11.1 ± 6.3	10.4 ± 4.9
POST10	8.0 ± 4.4	11.0 ± 6.6	10.5 ± 5.2
STIMint (mA)			
PRE	25.0 ± 7.3	26.1 ± 9.1	30.5 ± 16.4
F1	25.6 ± 8.9	27.1 ± 8.7	31.0 ± 14.2
R1	24.4 ± 8.6	27.4 ± 9.6	30.4 ± 13.8
F2	23.4 ± 9.1	25.1 ± 7.3	29.9 ± 13.9
R2	23.7 ± 9.5	26.0 ± 9.0	29.9 ± 13.7
F3	24.0 ± 9.0	25.0 ± 7.3	29.8 ± 13.0
POST	23.0 ± 8.5	25.3 ± 8.4	29.5 ± 13.2
POST10	21.2 ± 8.1	24.2 ± 9.3	27.5 ± 13.3

ANKLE, elastic band wrapped around the ankle joint; CALF, elastic band wrapped around the calf muscles; CON, control intervention; PRE, assessment before intervention; POST, assessment after the intervention; POST10, assessment 10 min after the intervention; F1, F2, F3, assessments during first, second and third band application; R1, R2, assessment during first and second rest between band applications; ROM, ankle range of motion from maximal plantarflexion to maximal dorsiflexion; MVC, plantarflexion maximum voluntary contractions; H, soleus H reflex expressed as a percentage of maximal M wave; M10, soleus M wave expressed as a percentage of maximal M wave; STIMint, stimulation intensity.

TABLE 2 | Descriptive statistics (mean ± SD).

Variable	ANKLE	CALF
NRS		
F1	4.4 ± 1.4	4.6 ± 1.5
F2	4.1 ± 1.5	4.3 ± 1.5
F3	5.0 ± 1.4	4.1 ± 1.1
Pressure (mmHg)		
F1	290.3 ± 48.5	226.2 ± 57.6
F2	294.8 ± 51.3	238.4 ± 48.4
F3	296.7 ± 64.3	236.2 ± 51.9

ANKLE, elastic band wrapped around the ankle joint; CALF, elastic band wrapped around the calf muscles; F1, F2, F3, assessments during first, second and third band application; NRS, numerical rating scale for pain assessment during flossing; Pressure, pressure exerted by the elastic band.

TABLE 3 | Cohen' d effect size and 95% confidence intervals.

Variable	ΔANKLE – ΔCON effect size ± 95%CI	ΔCALF – ΔCON effect size ± 95%CI	ΔCALF – ΔANKLE effect size ± 95%CI
ROM (°)			
POST	0.5 ± 0.9 *unclear*	0.3 ± 0.8 *unclear*	0.2 ± 0.9 *unclear*
POST10	0.4 ± 0.8 *unclear*	0.5 ± 0.8 *unclear*	0.1 ± 0.7 *unclear*
MVC (Nm)			
POST	0.5 ± 0.7 *unclear*	−0.1 ± 1.0 *unclear*	−0.6 ± 0.8 *medium*
POST10	−0.4 ± 0.4 *small*	−0.4 ± 0.8 *unclear*	−0.1 ± 0.7 *unclear*
H (% Mmax)			
F1	−0.6 ± 0.7 *medium*	−1.4 ± 1.3 *large*	−0.7 ± 0.7 *medium*
R1	0.0 ± 0.4 *unclear*	−0.4 ± 0.9 *unclear*	−0.4 ± 0.8 *unclear*
F2	−0.6 ± 0.8 *unclear*	−1.5 ± 1.4 *large*	−0.8 ± 0.7 *large*
R2	0.3 ± 0.6 *unclear*	−0.5 ± 0.8 *unclear*	−0.7 ± 0.7 *medium*
F3	−0.6 ± 0.8 *medium*	−1.9 ± 1.3 *large*	−0.9 ± 0.5 *large*
POST	0.3 ± 0.5 *small*	−0.6 ± 1.0 *unclear*	−0.7 ± 0.9 *medium*
POST10	0.4 ± 0.5 *small*	0.1 ± 0.9 *unclear*	−0.2 ± 0.6 *unclear*

ANKLE, elastic band wrapped around the ankle joint; CALF, elastic band wrapped around the calf muscles; CON, control intervention; POST, assessment after the intervention; POST10, assessment 10 min after the intervention; F1, F2, F3, assessments during first, second and third band application; R1, R2, assessment during first and second rest between band applications; ROM, ankle range of motion from maximal plantarflexion to maximal dorsiflexion; MVC, plantarflexion maximum voluntary contractions; H, soleus H reflex expressed as a percentage of maximal M wave; 95%CI, 95% confidence interval.

The analysis of H-reflex revealed that there was a statistically significant interaction between the effect of intervention type and time [$F_{(14,140)} = 6.08$, $P < 0.001$, $\eta_p^2 = 0.378$]. Simple main effect analysis showed that time did have a statistically significant effect on H-reflex [$F_{(7,70)} = 11.68$, $P < 0.001$, $\eta_p^2 = 0.539$]. Simple main effect analysis showed that intervention type did not have a statistically significant effect on H-reflex [$F_{(2,20)} = 2.45$, $P = 0.112$, $\eta_p^2 = 0.197$]. *Post hoc* comparisons revealed significant statistical differences for CALF condition between PRE and F1, F2, R2, F3, and POST measurements. Significant differences were found for the ANKLE condition between PRE, F1, F2, F3. The average value of all H reflexes within a time point was used for further analysis as the HM parameter (**Figure 3**).

A medium, but statistically significant correlation was found between pressure and H-reflex mean relative change from baseline during F1, F2, and F3 timepoints for the CALF [$r(33) = -0.48$, $P = 0.006$] and ANKLE condition [$r(33) = -0.43$, $P = 0.013$] (**Figure 4**).

DISCUSSION

The aim of this study was to investigate the effects of tissue flossing applied on the ankle joint or on the calf muscles on the ankle ROM, plantarflexor MVC and SOL H reflex. To the best of our knowledge, this is the first study that compared the effects of the two most common tissue flossing techniques on various neuromuscular parameters.

The main findings of this study were that the H reflex was statistically significantly reduced during flossing in CALF and ANKLE conditions and immediately after flossing in the CALF condition. However, the H reflex was much more affected during the CALF condition compared to the ANKLE condition (*medium* to *large* effect size). The data shows a possible cumulative effect of tissue flossing application on spinal excitability in the CALF condition. In fact, there were statistically significant changes in H reflex at R2 (second rest between band applications) and at POST timepoint. In comparison, H reflex in ANKLE condition returned to baseline levels as soon as the floss band was unwrapped. To the best of our knowledge, this was the first study to investigate the effects of tissue flossing on H reflex; therefore, there were no studies to compare our results to. We have found only a few studies investigating the effect of local acute ischemia on H reflex: Zakutansky et al. (2005) registered a significant decline in Hmax/Mmax ratio (−12%) during and after 5 min of acute ischemia. In comparison, our study revealed a much larger decrease in H reflex during flossing (CALF: −63%; ANKLE: −38%) and after the intervention (−32%) for the CALF condition. In contrast, Mendonca et al. (2020) found no differences in H reflex amplitude and nerve conduction velocity following 60 and 80% arterial occlusion. Significant differences between our work and the aforementioned studies on inducing local acute ischemia could be related to the fact that in our study, the elastic band had been wrapped closer to the EMG electrodes; with acute ischemia being induced by femoral artery occlusion in the proximal part of the thigh. There is some evidence in the literature that changes in neuron excitability threshold is more pronounced closer to the site of ischemic compression (Bostock et al., 1991). This could also partially explain the observed difference between conditions since the CALF application was closer to the EMG electrodes compared to the ANKLE application. In addition to the effects of vascular occlusion induced by ischemia, we should take in consideration the effects of compression on muscles, skin and fascia. It was recently suggested by Young et al. (2018) that high-intensity foam rolling can affect spinal excitability, resulting in a decrease of soleus H reflex up to 58%. A similar reduction in spinal reflexes can be seen during manual massage therapy (Morelli et al., 1990; Goldberg et al., 1992; Behm et al., 2013). We can speculate that the large decrease in H reflex during tissue flossing registered in this

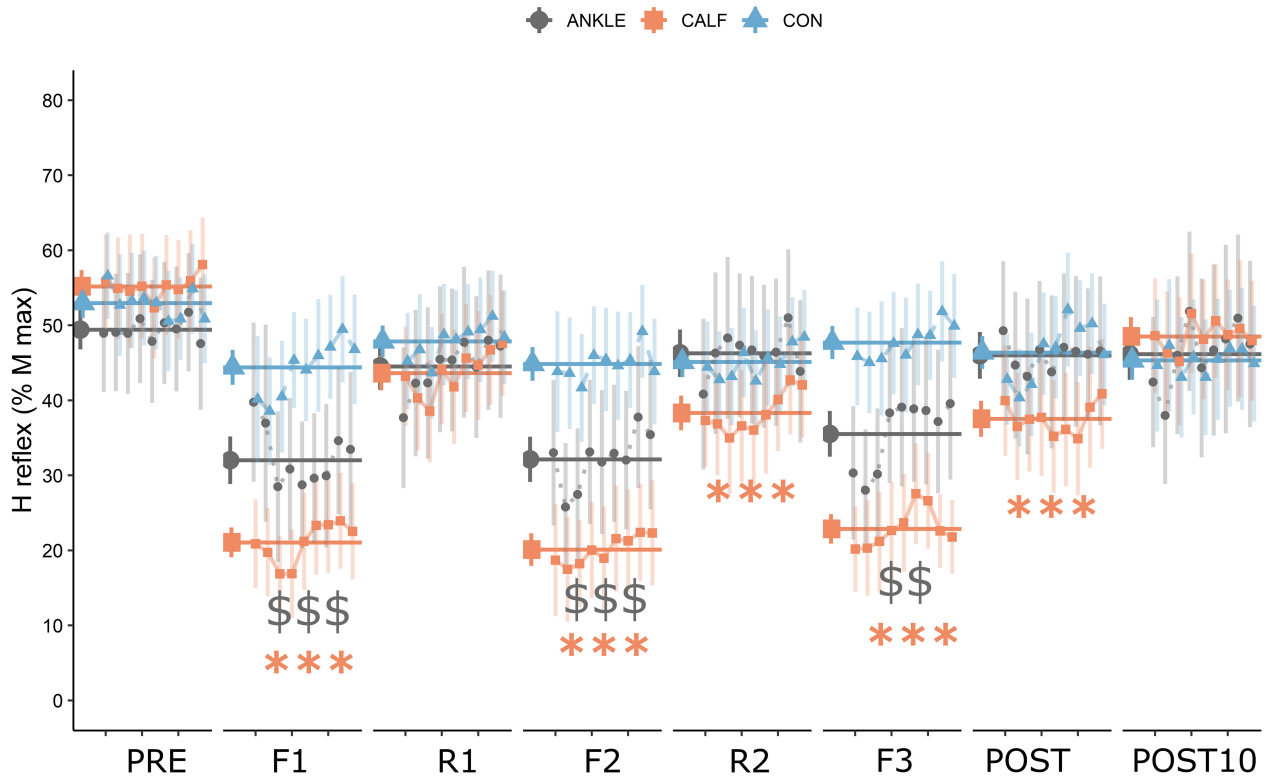

FIGURE 3 | H reflex data expressed as a percentage of Mmax. Orange squares represent data for the CALF condition, gray dots represent data for the ANKLE condition and blue triangles represent data for the CON condition. Larger points and horizontal lines represent the mean and standard error of the average of all H reflex (9 signals) amplitudes in each time point. Small points represent the mean and standard error of each measured H reflex. Statistically significant differences from baseline are represented by asterisks for the CALF condition: $^{***}P < 0.001$; and dollars for the ANKLE condition: $^{\$\$}P < 0.01$, $^{\$\$\$}P < 0.001$.

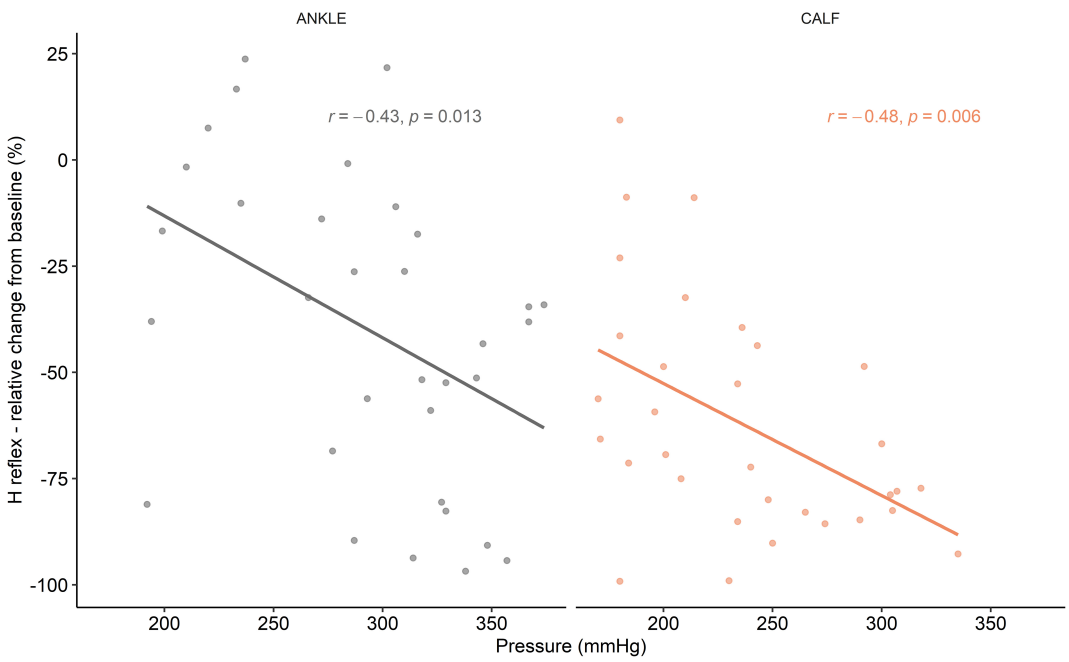

FIGURE 4 | Correlations between H reflex relative changes from baseline and flossing pressure.

study originate from mechanisms related to local ischemia and compression of mechanoreceptors present in the muscles, skin and fascia. The fast modulation of the H reflex observed during flossing and rest periods suggest that highly sensitive and rapidly adapting receptors are responsible for mediating this response.

One of the possible mechanisms explaining the reduction of the H reflex registered in this study is presynaptic inhibition. It has been well documented that this mechanism regulates the amount of neurotransmitters to be released in the Ia-motoneuron synapse regardless of the firing rate of the Ia afferents (Chalmers and Knutzen, 2002). Therefore, it is plausible that ischemia and compression of mechanoreceptors may affect the presynaptic interneurons and downregulate the effect of Ia fibers into motoneurons (Burke et al., 1984). However, even though there are several methods to measure presynaptic inhibition (Knikou, 2008), this study was not designed to do so. Therefore, the effect of tissue flossing on presynaptic inhibition needs to be examined in a future study.

A second explanation for the decrease in H reflex is the possible effect that produces a hyperpolarized motoneuron. There is emerging evidence in the literature that group III and IV afferences play an important role in spinal modulation (Burke et al., 1984). A hyperpolarized motoneuron would result in a less excitable motoneuron pool, requiring more stimulation intensity to induce the same H reflex. However, the mechanism is less probable in this study since there were no differences in stimulation intensity between time points. Group III and IV muscle afferents are also thought to be activated by nociceptive stimuli and are associated with pain perception (McCord and Kaufman, 2010), which could explain differences in the spinal excitability observed in this study. However, there were no differences in the perception of pain between CALF and ANKLE conditions.

Nonetheless, we cannot dismiss the possibility that compression induced by the elastic band could induce reversible mechanical changes in the wrapped tissue. It is unlikely that short-lasting tissue flossing could affect the viscoelastic or mechanical properties of the fascia, since it was demonstrated that forces outside the normal physiological range are required to produce significant release of the fascia (Chaudhry et al., 2008). Compression of muscle tissue, however, could have caused muscle shortening and changes in muscle pennation angle, thus affecting the sensitivity of muscle spindles and other mechanoreceptors, altering the H reflex. It has been well established that muscle lengthening and stretching can dramatically influence spinal neural pathways (Budini and Tilp, 2016) because of the activation of the muscle spindle. However, this cannot explain the depression of H reflex registered in the ANKLE condition, where the muscles were not directly compressed. A possible mechanism explaining the drop of H reflex during tissue flossing around the ankle could be the activation of Ib afferents from the Golgi tendon organ (GTO). Even though GTO is usually activated when large pulling forces are exerted to the muscle-tendon complex (i.e., during landing or at large-amplitude stretches) (Guissard and Duchateau, 2006), tissue flossing around the ankle joint could have directly compressed the muscle-tendon junction of the Achilles tendon. Thus, there is possible that some inhibition could arise from the activation of Ib afferents.

In addition, the wrapping pressures in this study were substantially higher compared to previous studies, where an ankle (Driller and Overmayer, 2017) or muscle technique (Kaneda et al., 2020; Konrad et al., 2020) were used. Differences in pressures among studies can arise from several factors such as sensor placement, pressure monitors and flossing technique. As noted by Vogrin et al. (2020a) different wrapping pressures might lead to different physiological responses. They found a statistically significant improvement in knee extensors MVC after a medium wrapping pressure (approximately 140–160 mmHg), but no differences after high wrapping pressure (>200 mmHg). Similar pressure dependency has been recently confirmed using the ankle wrapping technique (Galis and Cooper, 2020). In the present study, there was a negative correlation between wrapping pressure and H reflex change from baseline during the flossing periods (F1–F3), suggesting that the higher the pressure, the greater the inhibition of the H reflex in both ANKLE and CALF conditions. A similar effect was observed in a study, where high-intensity foam-rolling induced a higher H reflex inhibition compared to moderate-intensity and a sham condition (Young et al., 2018). The higher pressure of manual massage led to higher H reflex inhibition, suggesting that higher pressures activate deeper mechanoreceptors (Goldberg et al., 1992).

The results show that the effects of tissue flossing on the H reflex are short-lasting since there were no differences in H reflex 10 min after the intervention. However, the effects may last longer than a few minutes, which was confirmed in the study by Zakutansky et al. (2005) observing that the H reflex was not fully recovered 5 min after acute local ischemia. On the contrary, in a foam rolling study, the soleus H reflex returned to baseline immediately after the pressure was released (Young et al., 2018).

The differences observed at the spinal level did not transfer into functional changes such as higher joint ROM or higher muscle force production. This is surprising since many studies have shown a convincing increase in ROM after joint application (Driller et al., 2017; Driller and Overmayer, 2017) and muscle application (Kaneda et al., 2020); and an increase in MVC after muscle application (Vogrin et al., 2020a; Konrad et al., 2021). In addition, findings from ischemic preconditioning studies suggest that partial or total arterial occlusion leads to improvements in knee extensor voluntary contraction (Paradis-Deschênes et al., 2016b) and higher repeated force capacity in strength-trained athletes (Paradis-Deschênes et al., 2016a). However, the results of this study are well in line with the study conducted by Mills et al. (2020), who found no significant improvements in ROM, jumping and sprint performance in professional rugby union players. As such, the tissue flossing method may be less effective on highly trained individuals.

This study might have several limitations. First, there was a statistically significant difference in the applied pressure of the flossing application between CALF and ANKLE. In this regard, placement of the pressures sensor between both situations needs to be taken into consideration, which in the ANKLE condition was placed directly on a hard structure (cuneiform bones), while in the CALF condition was placed on the muscle aponeurosis

between the gastrocnemius bulks (a softer structure). Although the wrapping pressure was monitored in this study, there was no insight into the actual blood-flow occlusion created in the affected leg. To the best of our knowledge, the latter limitation applies to all studies in the field of tissue flossing published up to date. Second, there was a lack of movement while the elastic band was applied, compared to other studies where the participants performed an active ROM movement during the tissue flossing treatment. The participants in the present study were instructed to maintain a steady position in the dynamometer during the flossing intervention so as to measure the H reflex. One can speculate that additional active movement during the flossing intervention, as seen in other studies, play an important role in ROM and MVC improvement. Third, we used a relatively small number of electrical stimuli to evoke the H reflex at each time point. Electrophysiological measurements can be highly variable; thus a large number of stimuli (>20) is usually required to obtain reliable results (Burke, 2016). We were, however, limited by the flossing and rest time (120 s), where we were able to elicit only 10 reflexes at the selected stimulation rate without occurring at the risk of post-activation depression. Finally, to maintain the homogeneity of the group (young elite martial art fighters) we were able to recruit only 11 participants, which represents a limitation to the statistical power of the study.

Even though the majority of the studies investigating the effects of tissue flossing were conducted on young adults, the participants were usually older (>20 years) than the subjects recruited in this study (16 years). It is well known that joint flexibility is age, sex, joint, and movement dependent and decreases with age (Medeiros et al., 2013). However, there is some evidence that junior taekwondo athletes demonstrate lower limb flexibility (sit-and-reach test) scores than most seniors (Bridge et al., 2014). There is a lack of studies comparing the acute effects of stretching methods on adolescents. In a meta-analysis investigating the acute effects of foam rolling on joint flexibility (Skinner et al., 2020), the only study that included adolescent athletes (15 years old) lacked to find significant improvement in ankle ROM after foam rolling (Škarabot et al., 2015). In contrast, other studies, including young adults (>20 years), confirmed that there is a clear beneficial effect of foam rolling on ROM (Skinner et al., 2020). Thus, it is possible that, similarly to other ROM improvement techniques, tissue flossing could affect young athletes differently compared to their older counterparts. As a prospect, it will be interesting to investigate the effects of tissue flossing on different age groups and training statuses.

CONCLUSION

Some studies have suggested that tissue flossing could be used as a specific warm-up technique for inducing ROM and explosive strength improvement. However, the findings of this study indicate that high wrapping pressure tissue flossing has a limited influence on joint ROM and plantarflexor MVC in healthy young martial arts athletes. On the other hand, tissue flossing around the muscle has a significant but short-lasting effect on spinal reflex inhibition. The observed changes at the spinal level did not translate into a higher ankle ROM or plantarflexor MVC. Taking into consideration the results of this study, we suggest that tissue flossing is not an advisable technique to be used as a specific warm-up in young elite athletes. The inhibition of the spinal mechanism induced by tissue flossing has to be further investigated to fully take advantage of this method.

DATA AVAILABILITY STATEMENT

The raw data supporting the conclusions of this article will be made available by the authors, without undue reservation.

ETHICS STATEMENT

The studies involving human participants were reviewed and approved by the Medical Ethics Committee of the University Medical Centre Maribor, Slovenia (UKC-MB-KME-6/21). Written informed consent to participate in this study was provided by the participants' legal guardian/next of kin.

AUTHOR CONTRIBUTIONS

MK, SM, and TS contributed to the conception and design of the study. MK, SM, and FŽ carried out the experiment and data collection and organized the database and data analysis. MK performed the statistical analysis and wrote the first draft of the manuscript. SM, FŽ, MV, and TS wrote sections of the manuscript. All authors contributed to manuscript revision, read, and approved the submitted version.

FUNDING

This study was supported by the Slovenian Research Agency (Project no. J2-1731).

ACKNOWLEDGMENTS

We would like to thank all participants who volunteered to participate in this study and demonstrated great motivation and commitment. We would like to thank Mr. Tomaž Barada, who made this study possible.

REFERENCES

Batterham, A. M., and Hopkins, W. G. (2006). Making meaningful inferences about magnitudes. *Int. J. Sports Physiol. Perform.* 1, 50–57. doi: 10.1123/ijspp.1.1.50

Behm, D. G., Peach, A., Maddigan, M., Aboodarda, S. J., DiSanto, M. C., Button, D. C., et al. (2013). Massage and stretching reduce spinal reflex excitability without affecting twitch contractile properties. *J. Electromyogr. Kinesiol.* 23, 1215–1221. doi: 10.1016/j.jelekin.2013.05.002

Bostock, H., Baker, M., and Reid, G. (1991). Changes in excitability of human motor axons underlying post-ischaemic fasciculations: evidence for two stable states. *J. Physiol.* 441, 537–557. doi: 10.1113/jphysiol.1991.sp018766

Bridge, C. A., Ferreira da Silva Santos, J., Chaabène, H., Pieter, W., and Franchini, E. (2014). Physical and Physiological Profiles of Taekwondo Athletes. *Sports Med.* 44, 713–733. doi: 10.1007/s40279-014-0159-9

Brophy-Williams, N., Driller, M., Halson, S., Fell, J., and Kitic, C. (2013). Evaluating the Kikuhime pressure monitor for use with sports compression clothing. *Sports Eng.* 2013:125. doi: 10.1007/s12283-013-0125-z

Budini, F., Gallasch, E., Christova, M., Rafolt, D., Rauscher, A. B., and Tilp, M. (2017). One minute static stretch of plantar flexors transiently increases H reflex excitability and exerts no effect on corticospinal pathways. *Exp. Physiol.* 102, 901–910. doi: 10.1113/EP086374

Budini, F., and Tilp, M. (2016). Changes in H-reflex amplitude to muscle stretch and lengthening in humans. *Rev. Neurosci.* 27, 511–522. doi: 10.1515/revneuro-2016-0001

Burke, D. (2016). Clinical uses of H reflexes of upper and lower limb muscles. *Clin. Neurophysiol. Pract.* 1, 9–17. doi: 10.1016/j.cnp.2016.02.003

Burke, D., Gandevia, S. C., and McKeon, B. (1984). Monosynaptic and oligosynaptic contributions to human ankle jerk and H-reflex. *J. Neurophysiol.* 52, 435–448. doi: 10.1152/jn.1984.52.3.435

Chalmers, G. R., and Knutzen, K. M. (2002). Soleus H-Reflex Gain in Healthy Elderly and Young Adults When Lying, Standing, and Balancing. *J. Gerontol. Ser. A* 57, B321–B329. doi: 10.1093/gerona/57.8.B321

Chaudhry, H., Schleip, R., Ji, Z., Bukiet, B., Maney, M., and Findley, T. (2008). Three-Dimensional Mathematical Model for Deformation of Human Fasciae in Manual Therapy. *J. Osteopath. Med.* 108, 379–390. doi: 10.7556/jaoa.2008.108.8.379

Cherry-Allen, K. M., Gidday, J. M., Lee, J.-M., Hershey, T., and Lang, C. E. (2015). Remote limb ischemic conditioning enhances motor learning in healthy humans. *J. Neurophysiol.* 113, 3708–3719. doi: 10.1152/jn.01028.2014

Cocking, S., Wilson, M. G., Nichols, D., Cable, N. T., Green, D. J., Thijssen, D. H. J., et al. (2018). Is There an Optimal Ischemic-Preconditioning Dose to Improve Cycling Performance? *Int. J. Sports Physiol. Perform.* 13, 274–282. doi: 10.1123/ijspp.2017-0114

Delliaux, S., and Jammes, Y. (2006). Effects of hypoxia on muscle response to tendon vibration in humans. *Muscle Nerve* 34, 754–761. doi: 10.1002/mus.20633

Driller, M. W., Mackay, K., Mills, B., and Tavares, F. (2017). Tissue flossing on ankle range of motion, jump and sprint performance: A follow-up study. *Phys. Ther. Sport* 28, 29–33. doi: 10.1016/j.ptsp.2017.08.081

Driller, M. W., and Overmayer, R. G. (2017). The effects of tissue flossing on ankle range of motion and jump performance. *Phys. Ther. Sport* 25, 20–24. doi: 10.1016/j.ptsp.2016.12.004

Galis, J., and Cooper, D. J. (2020). Application of a Floss Band at Differing Pressure Levels: Effects at the Ankle Joint. *J. Strength Cond. Res.* 2020:3833. doi: 10.1519/JSC.0000000000003833

Garland, S. J., and McComas, A. J. (1990). Reflex inhibition of human soleus muscle during fatigue. *J. Physiol.* 429, 17–27. doi: 10.1113/jphysiol.1990.sp018241

Goldberg, J., Sullivan, S. J., and Seaborne, D. E. (1992). The Effect of Two Intensities of Massage on H-Reflex Amplitude. *Phys. Ther.* 72, 449–457. doi: 10.1093/ptj/72.6.449

Gorny, V., and Stöggl, T. (2018). [Tissue flossing as a recovery tool for the lower extremity after strength endurance intervals]. *Sportverletz. Sportschaden Organ Ges. Orthopadisch-Traumatol. Sportmed.* 32, 55–60. doi: 10.1055/s-0043-122782

Guissard, N., and Duchateau, J. (2006). Neural Aspects of Muscle Stretching. *Exerc. Sport Sci. Rev.* 34, 154–158. doi: 10.1249/01.jes.0000240023.30373.eb

Halley, S. L., Marshall, P., and Siegler, J. C. (2018). The effect of ischaemic preconditioning on central and peripheral fatiguing mechanisms in humans following sustained maximal isometric exercise. *Exp. Physiol.* 103, 976–984. doi: 10.1113/ep086981

Hjermstad, M. J., Fayers, P. M., Haugen, D. F., Caraceni, A., Hanks, G. W., Loge, J. H., et al. (2011). Studies Comparing Numerical Rating Scales, Verbal Rating Scales, and Visual Analogue Scales for Assessment of Pain Intensity in Adults: A Systematic Literature Review. *J. Pain Symptom Manage.* 41, 1073–1093. doi: 10.1016/j.jpainsymman.2010.08.016

Kacin, A., Rosenblatt, B., Žargi, T. G., and Biswas, A. (2015). Safety considerations with blood flow restricted resistance training. *Ann. Kinesiol.* 6, 3–26.

Kaneda, H., Takahira, N., Tsuda, K., Tozaki, K., Kudo, S., Takahashi, Y., et al. (2020). Effects of Tissue Flossing and Dynamic Stretching on Hamstring Muscles Function. *J. Sports Sci. Med.* 19, 681–689.

Kayser, B., Bökenkamp, R., and Binzoni, T. (1993). Alpha-motoneuron excitability at high altitude. *Eur. J. Appl. Physiol.* 66, 1–4. doi: 10.1007/BF00863391

Knikou, M. (2008). The H-reflex as a probe: Pathways and pitfalls. *J. Neurosci. Methods* 171, 1–12. doi: 10.1016/j.jneumeth.2008.02.012

Konrad, A., Bernsteiner, D., Budini, F., Reiner, M. M., Glashüttner, C., Berger, C., et al. (2020). Tissue flossing of the thigh increases isometric strength acutely but has no effects on flexibility or jump height. *Eur. J. Sport Sci.* 2020, 1–11. doi: 10.1080/17461391.2020.1853818

Konrad, A., Močnik, R., and Nakamura, M. (2021). Effects of Tissue Flossing on the Healthy and Impaired Musculoskeletal System: A Scoping Review. *Front. Physiol.* 12:43.

Lenth, R., Singmann, H., Love, J., Buerkner, P., and Herve, M. (2020). *emmeans: Estimated Marginal Means, aka Least-Squares Means*. Available online at: https://CRAN.R-project.org/package=emmeans (accessed December 29, 2018).

Macefield, G., Hagbarth, K. E., Gorman, R., Gandevia, S. C., and Burke, D. (1991). Decline in spindle support to alpha-motoneurones during sustained voluntary contractions. *J. Physiol.* 440, 497–512. doi: 10.1113/jphysiol.1991.sp018721

McCord, J. L., and Kaufman, M. P. (2010). "Reflex Autonomic Responses Evoked by Group III and IV Muscle Afferents," in *Translational Pain Research: From Mouse to Man* Frontiers in Neuroscience, eds L. Kruger and A. R. Light (Boca Raton, FL: CRC Press).

Medeiros, H. B., de, O., Araújo, D. S. M. S., de, Araújo, C. G. S., and de. (2013). Age-related mobility loss is joint-specific: an analysis from 6000 Flexitest results. *Age* 35, 2399–2407. doi: 10.1007/s11357-013-9525-z

Mendonca, G. V., Mouro, M., Vila-Chã, C., and Pezarat-Correia, P. (2020). Nerve conduction during acute blood-flow restriction with and without low-intensity exercise Nerve conduction and blood-flow restriction. *Sci. Rep.* 2020, 10.

Mills, B., Mayo, B., Tavares, F., and Driller, M. (2020). The Effect of Tissue Flossing on Ankle Range of Motion, Jump, and Sprint Performance in Elite Rugby Union Athletes. *J. Sport Rehabil.* 29, 282–286. doi: 10.1123/jsr.2018-0302

Morelli, M., Seaborne, D. E., and Sullivan, S. J. (1990). Changes in H-Reflex Amplitude During Massage of Triceps Surae in Healthy Subjects. *J. Orthop. Sports Phys. Ther.* 12, 55–59. doi: 10.2519/jospt.1990.12.2.55

Murry, C. E., Jennings, R. B., and Reimer, K. A. (1986). Preconditioning with ischemia: a delay of lethal cell injury in ischemic myocardium. *Circulation* 74, 1124–1136. doi: 10.1161/01.cir.74.5.1124

Neubauer, J. A., and Sunderram, J. (2004). Oxygen-sensing neurons in the central nervous system. *J. Appl. Physiol.* 1985, 367–374. doi: 10.1152/japplphysiol.00831.2003

Opplert, J., and Babault, N. (2018). Acute Effects of Dynamic Stretching on Muscle Flexibility and Performance: An Analysis of the Current Literature. *Sports Med.* 48, 299–325. doi: 10.1007/s40279-017-0797-9

Opplert, J., Genty, J.-B., and Babault, N. (2016). Do Stretch Durations Affect Muscle Mechanical and Neurophysiological Properties? *Int. J. Sports Med.* 37, 673–679. doi: 10.1055/s-0042-104934

Paradis-Deschênes, P., Joanisse, D. R., and Billaut, F. (2016b). Sex-Specific Impact of Ischemic Preconditioning on Tissue Oxygenation and Maximal Concentric Force. *Front. Physiol.* 7:674. doi: 10.3389/fphys.2016.00674

Paradis-Deschênes, P., Joanisse, D. R., and Billaut, F. (2016a). Ischemic preconditioning increases muscle perfusion, oxygen uptake, and force in strength-trained athletes. *Appl. Physiol. Nutr. Metab.* 41, 938–944. doi: 10.1139/apnm-2015-0561

Pavlů, D., Pánek, D., Kuncová, E., and Thung, J. S. (2021). Effect of Blood Circulation in the Upper Limb after Flossing Strategy. *Appl. Sci.* 11:1634. doi: 10.3390/app11041634

Power, K., Behm, D., Cahill, F., Carroll, M., and Young, W. (2004). An acute bout of static stretching: effects on force and jumping performance. *Med. Sci. Sports Exerc.* 36, 1389–1396. doi: 10.1249/01.mss.0000135775.51937.53

R Core Team (2020). *R: A Language and Environment for Statistical Computing*. Vienna: R Foundation for Statistical Computing.

Schieppati, M. (1987). The Hoffmann reflex: A means of assessing spinal reflex excitability and its descending control in man. *Prog. Neurobiol.* 28, 345–376. doi: 10.1016/0301-0082(87)90007-4

Schleip, R. (2003). Fascial plasticity – a new neurobiological explanation: Part 1. *J. Bodyw. Mov. Ther.* 7, 11–19. doi: 10.1016/S1360-8592(02)00067-0

Schleip, R., and Müller, D. G. (2013). Training principles for fascial connective tissues: scientific foundation and suggested practical applications. *J. Bodyw. Mov. Ther.* 17, 103–115. doi: 10.1016/j.jbmt.2012.06.007

Singmann, H., Bolker, B., Westfall, J., Aust, F., Højsgaard, S., Fox, J., et al. (2020). *afex: Analysis of Factorial Experiments*. Available online at: https://CRAN.R-project.org/package=afex (accessed December 29, 2018).

Škarabot, J., Beardsley, C., and Štirn, I. (2015). Comparing the effects of self-myofascial release with static stretching on ankle range-of-motion in adolescent athletes. *Int. J. Sports Phys. Ther.* 10, 203–212.

Skinner, B., Moss, R., and Hammond, L. (2020). A systematic review and meta-analysis of the effects of foam rolling on range of motion, recovery and markers of athletic performance. *J. Bodyw. Mov. Ther.* 24, 105–122. doi: 10.1016/j.jbmt.2020.01.007

Taylor, J. L. (2009). "Proprioception," in *Encyclopedia of Neuroscience*, ed. L. R. Squire (Oxford: Academic Press), 1143–1149. doi: 10.1016/B978-008045046-9.01907-0

Ushey, K. (2018). *RcppRoll: Efficient Rolling/Windowed Operations*. Available online at: https://cran.r-project.org/web/packages/RcppRoll/index.html

Verges, S., Maffiuletti, N. A., Kerherve, H., Decorte, N., Wuyam, B., and Millet, G. Y. (2009). Comparison of electrical and magnetic stimulations to assess quadriceps muscle function. *J. Appl. Physiol.* 1985, 701–710. doi: 10.1152/japplphysiol.01051.2007

Verges, S., Rupp, T., Jubeau, M., Wuyam, B., Esteve, F., Levy, P., et al. (2012). Cerebral perturbations during exercise in hypoxia. *Am. J. Physiol. Regul. Integr. Comp. Physiol.* 302, R903–R916.

Vogrin, M., Ličen, T., Greiner, N., Novak, F., Mikl, S., and Kalc, M. (2020b). Acute Effects of Tissue Flossing on Ankle Range of Motion and Tensiomyography Parameters. *J. Sport Rehabil.* 2020, 1–7.

Vogrin, M., Kalc, M., and Ličen, T. (2020a). Acute Effects of Tissue Flossing Around the Upper Thigh on Neuromuscular Performance: A Study Using Different Degrees of Wrapping Pressure. *J. Sport Rehabil.* 2020, 1–8.

Willer, J. C., Miserocchi, G., and Gautier, H. (1987). Hypoxia and monosynaptic reflexes in humans. *J. Appl. Physiol.* 63, 639–645. doi: 10.1152/jappl.1987.63.2.639

Young, J. D., Spence, A.-J., and Behm, D. G. (2018). Roller massage decreases spinal excitability to the soleus. *J. Appl. Physiol.* 124, 950–959. doi: 10.1152/japplphysiol.00732.2017

Zakutansky, D. W., Kitano, K., Wallace, J. P., and Koceja, D. M. (2005). H-reflex and motor responses to acute ischemia in apparently healthy individuals. *J. Clin. Neurophysiol. Off. Publ. Am. Electroencephalogr. Soc.* 22, 210–215.

Zehr, E. P. (2002). Considerations for use of the Hoffmann reflex in exercise studies. *Eur. J. Appl. Physiol.* 86, 455–468. doi: 10.1007/s00421-002-0577-5

Conflict of Interest: The authors declare that the research was conducted in the absence of any commercial or financial relationships that could be construed as a potential conflict of interest.

Publisher's Note: All claims expressed in this article are solely those of the authors and do not necessarily represent those of their affiliated organizations, or those of the publisher, the editors and the reviewers. Any product that may be evaluated in this article, or claim that may be made by its manufacturer, is not guaranteed or endorsed by the publisher.

frontiers in Human Neuroscience

ORIGINAL RESEARCH
published: 22 October 2021
doi: 10.3389/fnhum.2021.728405

Abnormalities of Resting-State Electroencephalographic Microstate in Rapid Eye Movement Sleep Behavior Disorder

Anjiao Peng[1†], *Ruien Wang*[2†], *Jiamin Huang*[2], *Haiyan Wu*[2*] *and Lei Chen*[1*]

[1] *Department of Neurology and Joint Research Institute of Altitude Health, West China Hospital, Sichuan University, Chengdu, China,* [2] *Centre for Cognitive and Brain Sciences and Department of Psychology, University of Macau, Macau SAR, China*

Objective: Rapid eye movement (REM) sleep behavior disorder (RBD) is a disease characterized by dream enacting behavior and is now commonly believed to be a harbinger to alpha-synucleinopathy diseases such as dementia with Lewy bodies, Parkinson's disease, and multiple system atrophy. The aim of this study was to explore the quasi-stable topological structure of the brain in RBD by analyzing resting-state electroencephalography (EEG) microstates.

Methods: We enrolled 22 participants with RBD and 46 healthy controls (HCs) with age and gender-matched. After the resting-state EEG recordings were acquired, EEG microstate features were analyzed to assess the functional networks of all participants.

Results: Significant differences in the brain topological structure and temporal characteristics of sub-second brain activity were identified between the RBD and HCs. The RBD group had a shorter average duration of microstate A and microstate D when compared with HCs, and microstate B contributed more, while microstate D contributed significantly less to the RBD group. Furthermore, the average duration and proportion of microstate D were negatively correlated with the RBD questionnaire Hong Kong (RBDQ-HK) score.

Conclusion: The result of this study indicates that the microstate dynamics is disturbed in RBD, which might jeopardize the flexibility and adaptability of the brain. Microstates are potential biomarkers to explore the early electrophysiological abnormality of alpha-synucleinopathy diseases.

Keywords: electroencephalogram, REM sleep behavior disorder, microstate, biomarker, neurodegeneration diseases

OPEN ACCESS

Edited by:
Ramona Ritzmann, Clinic Rennbahn AG, Switzerland

Reviewed by:
John Peever, University of Toronto, Canada
Yun Shen, Second Affiliated Hospital of Soochow University, China

***Correspondence:**
Haiyan Wu
haiyanwu@um.edu.mo
Lei Chen
leilei_25@126.com

[†] *These authors have contributed equally to this work*

Specialty section:
This article was submitted to Motor Neuroscience, a section of the journal Frontiers in Human Neuroscience

Received: *21 June 2021*
Accepted: *23 September 2021*
Published: *22 October 2021*

Citation:
Peng A, Wang R, Huang J, Wu H and Chen L (2021) Abnormalities of Resting-State Electroencephalographic Microstate in Rapid Eye Movement Sleep Behavior Disorder. Front. Hum. Neurosci. 15:728405. doi: 10.3389/fnhum.2021.728405

HIGHLIGHTS

- The brain topological structure and temporal characteristics of sub-second brain activity were altered in RBD.
- The average duration and proportion of microstate D were negatively correlated with the severity of the symptom.
- Microstates are potential biomarkers to explore the early electrophysiological features of neurodegenerative diseases.

INTRODUCTION

Rapid eye movement (REM) sleep behavior disorder (RBD) is a parasomnia characterized by muscle atonia during REM sleep, which is usually accompanied by vivid dream enactment (Postuma and Berg, 2019). Previous studies showed that nearly 80% of RBD individuals could develop Parkinson's disease (PD) and other alpha-synucleinopathy diseases within 10–15 years (Iranzo et al., 2014; Postuma and Berg, 2019). Therefore, RBD is now widely recognized as a prodrome of alpha-synucleinopathy diseases and is ideal for exploring early pathological changes of these diseases (Postuma et al., 2009; Perkins et al., 2021).

Electroencephalography (EEG) microstates are defined as short periods (80–120 ms) during which the EEG scalp topography remains quasi-stable, meaning that the global topography is fixed but strength might vary and polarity invert (Strik and Lehmann, 1993). These microstates have been considered as the building blocks of information processing in the human brain, disruption of which could significantly influence cognitive function (Schumacher et al., 2019). The investigation of temporal aspects of microstate sequences also provides us with essential information on the dynamic repertoire across different timescales of the brain (Van de Ville et al., 2010).

For now, four EEG microstates have been widely identified to be closely correlated with resting-state networks by using simultaneous functional MRI (fMRI) (Lehmann et al., 2005; Michel and Koenig, 2018). Microstate A is interpreted as an auditory or sensorimotor system, which is significantly correlated with the changes in negative blood-oxygen-level dependence (BOLD) activation of the temporal-parietal cortex (Britz et al., 2010; Gschwind et al., 2016). Microstate B is regarded as a visual network, which mainly correlates with the BOLD changes in striate and extrastriate cortices and the negative BOLD activation of the occipital cortex (Michel and Koenig, 2018). Microstate C is construed as the salience network, associated with positive BOLD activation in frontal, anterior cingulate cortex, and anterior insular cortices (Gschwind et al., 2016; Michel and Koenig, 2018). Microstate D is interpreted as the attention network, mainly reflecting the activation of the right inferior parietal, right middle and superior frontal gyri, and right insula (Yuan et al., 2012; Custo et al., 2017).

As an ideal way to study the momentary local states and interaction between networks of the brain, microstates have been accumulating attention in recent years (Khanna et al., 2015; Serrano et al., 2018; Chu et al., 2020). It has been widely studied in neuropsychiatric disorders such as schizophrenia (Koenig et al., 1999), depression (Murphy et al., 2020), Alzheimer's disease (Tait et al., 2020), PD (Chu et al., 2020), and Lewy body dementia (Schumacher et al., 2019). Previous studies found that individuals with PD showed many altered states of microstates such as longer duration and more occurrences of specific types of microstates, which were closely associated with motor function and recognition level (Chu et al., 2020). The duration and occurrence of microstates were also abnormal in individuals with Lewy body dementia (Schumacher et al., 2019). This study indicates that brain networks were altered in alpha-synucleinopathy diseases. As a predictor of alpha-synucleinopathy diseases, stronger functional connectivity between the left thalamus and occipital regions was also found in RBD using fMRI (Byun et al., 2020). In fact, a thorough understanding of the spatiotemporal dynamics of the large-scale neural network is helpful for identifying the abnormality of the RBD and would provide us with a novel perspective to understand the early pathogenesis of neurodegenerative diseases. However, EEG microstates have not been studied in RBD hitherto. The main goal of this study was to analyze the characteristics of resting-state EEG microstates in individuals with RBD, compared with healthy controls (HCs), and at the same time, to explore the potential validity of EEG microstate in assessing early stage alpha-synucleinopathy diseases and the potential clinical value of resting-state microstate as an early biomarker for the diagnosis of RBD.

METHODS

Study Population

With approval from the Ethics Committee of West China Hospital, Sichuan University, 22 participants with RBD and 46 HCs with age and gender-matched were enrolled with informed consents. All participants were free of diagnosis of PD, Alzheimer's disease, traumatic brain injury, stroke, depression, anxiety, schizophrenia, or any other neuropsychiatric disorder. No participant was taking any medicine. Individuals with RBD were first screened based on the Chinese RBD questionnaire Hong Kong (RBDQ-HK), which was verified to have high sensitivity (82.2–85%), specificity (81–86.9%), internal consistency, and test-retest reliability in the Chinese population (Li et al., 2010; Shen et al., 2014). The total score ranges from 0 to 100, and a score of 17 or higher was considered as candidates of RBD. When RBD was suspected, the diagnosis would be further confirmed by neurologists. Results from a previous study showed that the clinical diagnosis by clinicians could provide a good sensitivity (100%) and specificity (99.6%) in diagnosing RBD (Eisensehr et al., 2001). Thus, although the diagnoses of RBD in this study were not confirmed by polysomnography, we believed that the vast majority of participants were correctly grouped.

EEG Recording and Task Procedure

Participants were seated in a quiet room for exams. The data of a 5-min resting-state EEG were obtained from all participants using 64 Ag/AgCl electrodes (Brain Products, Munich, Germany) placed following the 10/20 system with impedance <10 kΩ. An actiCHamp amplifier (BrainVision system amplifier; Brain Products, Munich, Germany) was used to amplify and collect the EEG data at a sampling rate of 1,000 Hz. Participants were instructed to fixate their sight at the center of the screen and try to avoid body movement during the EEG recording.

EEG Data Pre-processing

EEGLAB toolbox (Delorme and Makeig, 2004) in MATLAB (R2017a, MathWorks, Natick, MA, USA) was used to process the EEG data offline. Data were first down-sampled to 250 Hz, filtered with a 1–40 Hz filter, and then filtered with a 50 Hz notch filter for removing line noise. Then, a clean raw data

plug-in of EEGLAB was used for bad channel detection and removal. Maximum flatline duration was set at 5 s for the detail parameter setting, baseline noise criterion was set at 4 SDs, and the minimum acceptable correlation with nearby channels was set at 0.8. All the removed channels were interpolated by using the spherical method, and all channels were referenced to the average reference after interpolation. As for the proportion of the bad channel rejection and interpolation, the overall average proportion of bad channel rejection is 18.88 (SD = 8.80); specifically, 19.81 (SD = 9.21) for the RBD group and 18.39 (SD = 8.73) for the HC group. To further minimize artifacts, the artifact subspace reconstruction method (Mullen et al., 2015) was used to correct the EEG data, and the maximum acceptable 0.5-s window was set at 20 SDs.

TABLE 1 | Demographic features for participants with RBD or healthy controls.

	Controls ($n = 46$)	RBD ($n = 22$)	*P*-value
Age (mean ± SD, years)	55.0 ± 4.5	56.9 ± 6.2	0.165
Gender (female, %)	35 (76.0%)	16 (72.7%)	0.772
Educational level	10.3 ± 3.2	10.6 ± 3.9	0.674
Marital status (married, %)	39 (84.8%)	20 (90.9%)	0.707
MoCA	26.26 ± 3.2	25.27 ± 5.0	0.328

MoCA, Montreal Cognitive Assessment; RBD, REM sleep behavior disorder; SD, standard deviation.

After preliminary data processing, the continuous data were segmented into epochs of 2 s for further microstate analysis. Independent component analysis (ICA) was implemented by using the runica function in EEGLAB to remove the artifact caused by ocular movement, cardio activity, and muscle movement. A semiautomatic manner (i.e., ICLabel plug-in) was used to remove the artifact, and visual inspection was used for further removal.

Microstate Analysis

Microstate analysis was performed using the microstate plug-in of EEGLAB developed by Thomas Koenig (Koenig, 2021). First, at the individual level, we calculated the global field power (GFP) across the whole channels and the microstate segmentation by using the Atomize and Agglomerate Hierarchical Clustering (AAHC) method. Polarity was ignored during the microstate analysis. After obtaining the microstate segmentation of each participant, we calculated a mean microstate segmentation of each group as templates. The original individual successive EEG series were then assigned into four classic microstate maps (i.e., A, B, C, and D classes). For each microstate, the following parameters were extracted for further analysis: the mean duration (i.e., the duration of each microstate status with a unit of milliseconds), occurrence rate per second (i.e., times a certain microstate status would occur in a second), the time proportion of a microstate status (i.e., the percentage of each microstate status in the segmentation), and the percentage of transitions between microstate status.

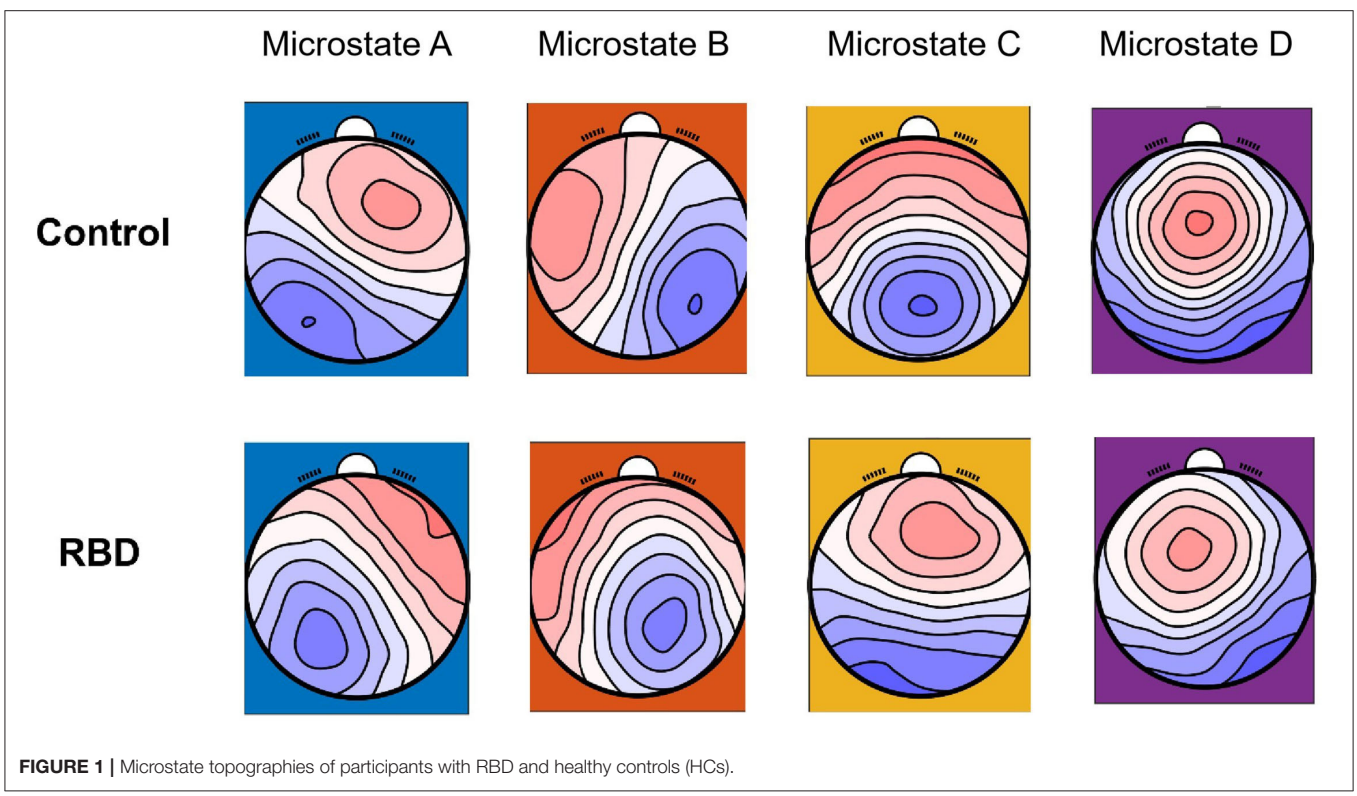

FIGURE 1 | Microstate topographies of participants with RBD and healthy controls (HCs).

Statistical Analysis

Continuous variables for clinical data were described as mean and SD and calculated using the *t*-test. Categorical variables were expressed as frequencies and percentages and calculated using the chi-square test. The mean and SE of mean were calculated for the microstate global explained variance (GEV) in two groups. Shapiro-Wilk test was used to examine the normality of the microstate parameters, and the difference of microstate parameters between two groups was compared by using the independent *t*-test if the data conform to normality. Otherwise, the Mann-Whitney *U* test was used. Pearson correlation analyses and linear regression were adopted to analyze the relationship between the microstate parameters and RBDQ-HK scores, and ANCOVA was further used to test the effects of grouping on the relationship between microstate parameters and RBDQ-HK score. Statistical analysis was performed using R language (version 4.0.5, R Core Team, Vienna, Austria) and SPSS version 25 (version 25, IBM Inc., Armonk, NY, USA).

RESULTS

Demographic Characteristics and Clinical Assessment Data

A total of 22 participants with RBD and 46 HCs were included. The mean age was 56.9 ± 6.2 years for the RBD group and 55.0 ± 4.5 years for HCs ($p = 0.165$). The mean score of the Montreal Cognitive Assessment (MoCA) was 25.27 ± 5.0 for the RBD

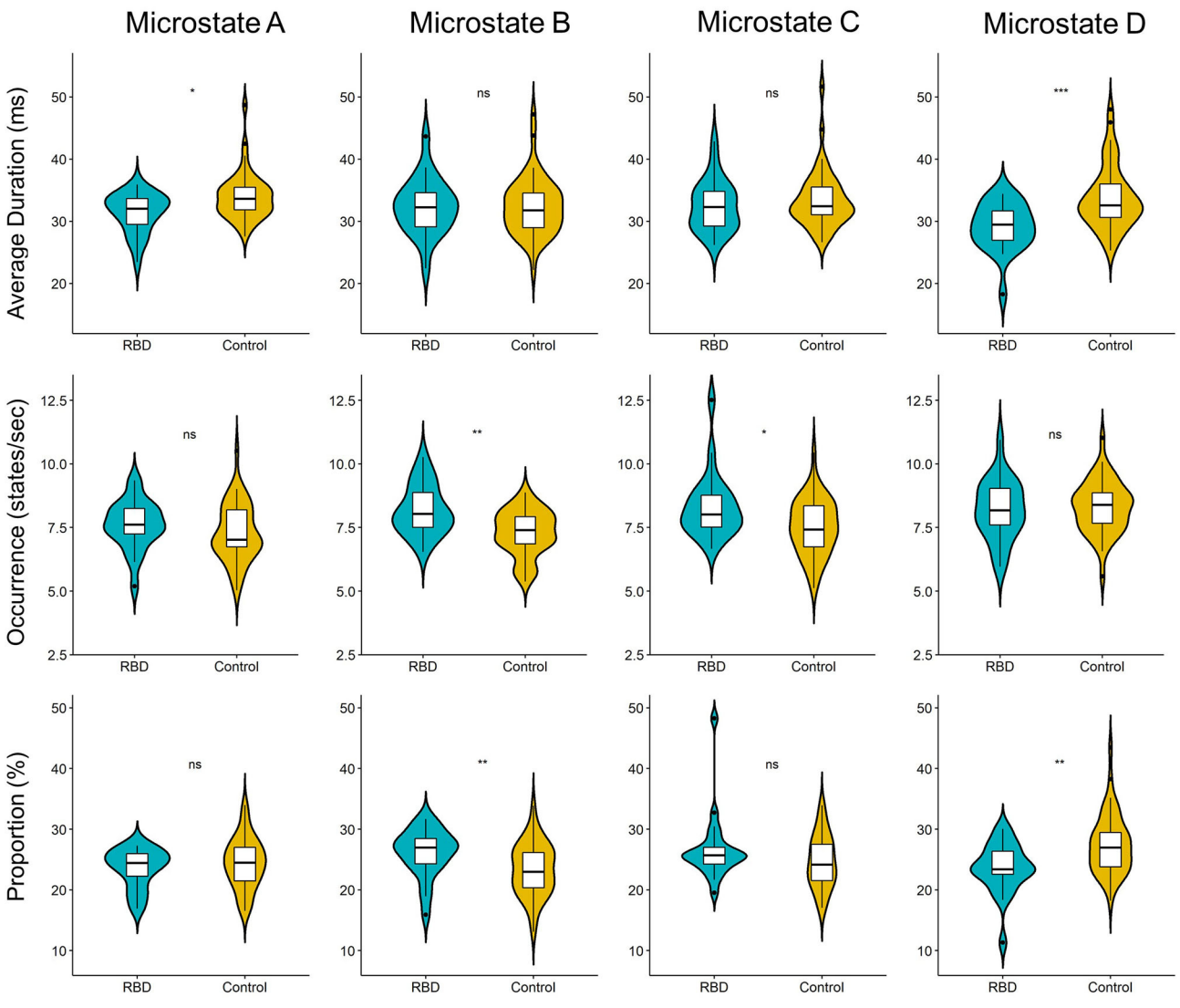

FIGURE 2 | Violin plot of the microstate parameters of each microstate between participants with RBD and HCs. The RBD group had a shorter average duration of microstate A ($p = 0.013$) and microstate D ($p < 0.001$). Regarding the occurrence, the RBD group produced more microstate B ($p = 0.002$) and microstate C ($p = 0.017$) per second than HCs. Microstate B contributed more ($p = 0.007$), while microstate D contribute significantly less ($p = 0.003$) in the RBD group when compared with HCs (ns, not significant; *$p < 0.05$, **$p < 0.01$, and ***$p < 0.001$).

group and 26.26 ± 3.2 for HCs ($p = 0.328$). Gender, educational level, and marital status were compared between the two groups (**Table 1**).

Microstate Topographies Were Altered in RBD

Four classes of mean microstate topographies were obtained from both groups (**Figure 1**). The mean microstate maps of each group were used as the template for further analysis, and the GEV of each template was consistent between the two groups with 0.725 (SE of mean, SEM = 0.004) for the RBD group and 0.716 (SEM = 0.006) for HCs. The results showed that the topographies were altered in the RBD group compared with HCs, characterized by more diffused center microstate B on the left frontal region and more focused center microstate C on the middle frontal-central region. Besides, the center of microstate D was more lateralized to the left frontal-central area in RBD.

Abnormalities of Microstate Parameters in RBD

Three parameters (i.e., average duration, occurrence, and proportion) were calculated for each EEG microstate. The results showed that compared with HCs, the RBD group had a shorter average duration of microstate A (M_{HC} 33.98 vs. M_{RBD} 31.38; $p = 0.013$) and microstate D (M_{HC} 33.75 vs. M_{RBD} 29.13; $p < 0.001$). Regarding the occurrence, the RBD group produced more microstate B (M_{HC} 7.29 vs. M_{RBD} 8.19; $p = 0.002$) and microstate C (M_{HC} 7.53 vs. M_{RBD} 8.33; $p = 0.017$) per second than HCs. Furthermore, the results showed that microstate B contributed more (M_{HC} 23.37 vs. M_{RBD} 26.11; $p = 0.007$), while microstate D contributed significantly less (M_{HC} 27.48 vs. M_{RBD} 23.58; $p = 0.003$) in the RBD group than HCs (**Figure 2**).

We further explored the relationship between the microstate parameters and the RBDQ-HK score. The correlational analysis that included all the individuals from both groups showed that the average duration, proportion of microstate D, and average duration of microstate A were negatively correlated with the RBDQ-HK score ($r = -0.49$, $p < 0.001$; $r = -0.44$, $p < 0.001$; and $r = -0.38$, $p = 0.0012$, respectively), while the occurrence of microstate B and microstate C was positively correlated with the RBDQ-HK score ($r = 0.34$, $p = 0.0051$ and $r = 0.45$, $p < 0.001$, respectively) (**Figure 3**).

Moreover, linear regression was implemented within the two groups to further test the association between the parameters and RBD severity. After testing the statistical assumptions of linear regression, the duration and proportion of microstate D and the occurrence of microstates B and C were valid, and the RBDQ-HK score was regressed on them. The results showed that the duration ($\beta = -1.58$, $p = 0.0023$) and proportion ($\beta = -1.36$, $p = 0.0048$) of microstate D were negatively associated with the RBDQ-HK score within the RBD group but not within the HC group ($p = 0.67$ and $p = 0.99$). The significant ANCOVA

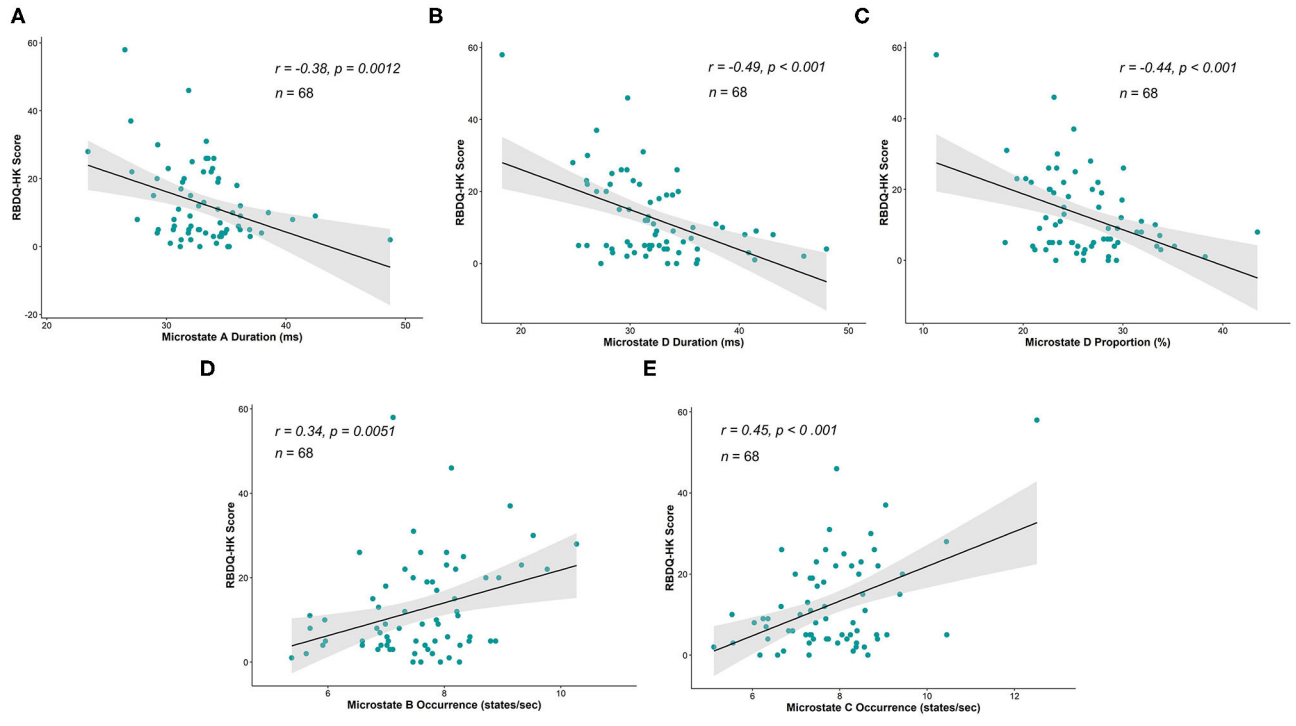

FIGURE 3 | Correlations between microstate parameters and RBDQ-HK score. The average duration of microstate A ($r = -0.38$, $p = 0.0012$), average duration of microstate D ($r = -0.49$, $p < 0.001$), and proportion of microstate D ($r = -0.44$, $p < 0.001$) were significantly negatively correlated with the RBDQ-HK score **(A–C)**, while the occurrence of microstate B ($r = 0.34$, $p = 0.0051$) and occurrence of microstate C ($r = 0.45$, $p < 0.001$) were significantly positively related to the RBDQ-HK score **(D,E)**.

test (both $p < 0.001$) further revealed the effect of grouping on the relationship between these microstate parameters and RBDQ-HK score. The occurrence of microstate C ($\beta = 4.90$, $p = 0.0014$) was positively associated with the RBDQ-HK score within the RBD group but not within the HC group ($p = 0.76$). The ANCOVA test also revealed a positive result ($p < 0.001$). The occurrence of microstate B was not associated with the RBDQ-HK score neither in the RBD group ($p = 0.83$) nor in the HC group ($p = 0.84$) (**Figure 4**).

Microstate Transitions Were Altered in the RBD Group

Finally, the percentages of transitions were compared with the expected value by using unpaired *t*-test. The result showed that the observed transition was similar to the expected value in both groups. The plot of transition with mean and SE was shown in **Figure 5**. Furthermore, we compared the observed transitions between two groups, and the result showed that the frequencies of transitions from microstates A to D and D to A were significantly decreased in the RBD group than the HCs ($t = -2.87$, $p_{adjusted} = 0.0066$, Cohen's $d = -0.77$ and $t = -2.81$, $p_{adjusted} = 0.0074$, Cohen's $d = -0.74$, respectively), while the RBD group produced increased frequencies of transitions from microstate B to C and C to B ($t = 3.52$, $p_{adjusted} = 0.0012$, Cohen's $d = 0.97$ and $t = 4.05$, $p_{adjusted} < 0.001$, Cohen's $d = 1.11$, respectively) (**Figure 5**).

DISCUSSION

In this study, we found that the topological structure of the brain and the temporal characteristics of the sub-second brain activity were significantly altered in RBD, which cast a new light on the abnormality of the electrophysiological features of RBD. Furthermore, we found that several parameters of EEG microstates were closely related to the RBDQ-HK score. These results indicated that abnormalities of resting-state EEG microstates may be endophenotypes of RBD with a great potential clinical value.

The results showed a significant alteration of the topological structure in RBD, which was characterized by the more lateralization and less contribution of microstate D. The

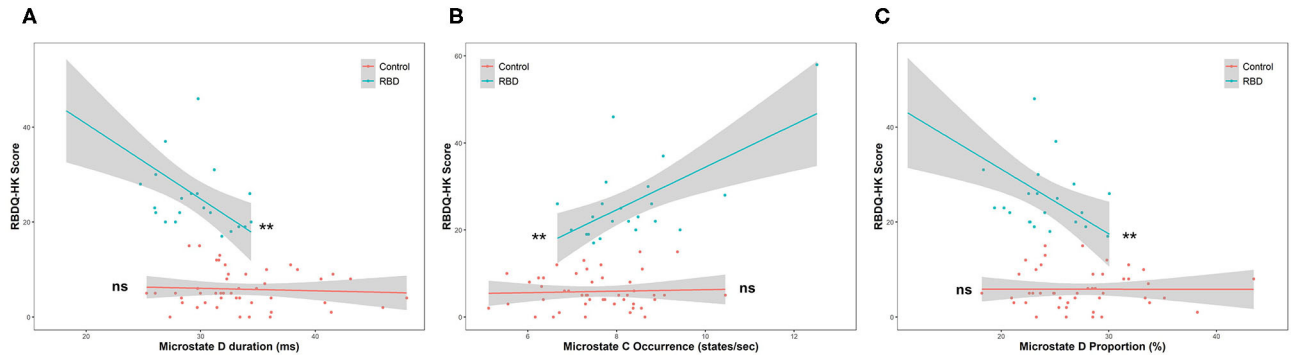

FIGURE 4 | Linear regression between microstate parameters and RBDQ-HK score. The duration ($\beta = -1.58$, $p = 0.0023$) and proportion of microstate D ($\beta = -1.36$, $p = 0.0048$) were negatively associated with the RBDQ-HK score within the RBD group but not within the HC group ($p = 0.67$ and $p = 0.99$, respectively) **(A,B)**. The occurrence of microstate C ($\beta = 4.90$, $p = 0.0014$) was positively associated with the RBDQ-HK score within the RBD group but not within the HC group ($p = 0.76$) **(C)**. ns, not significant; $^{**}p < 0.01$.

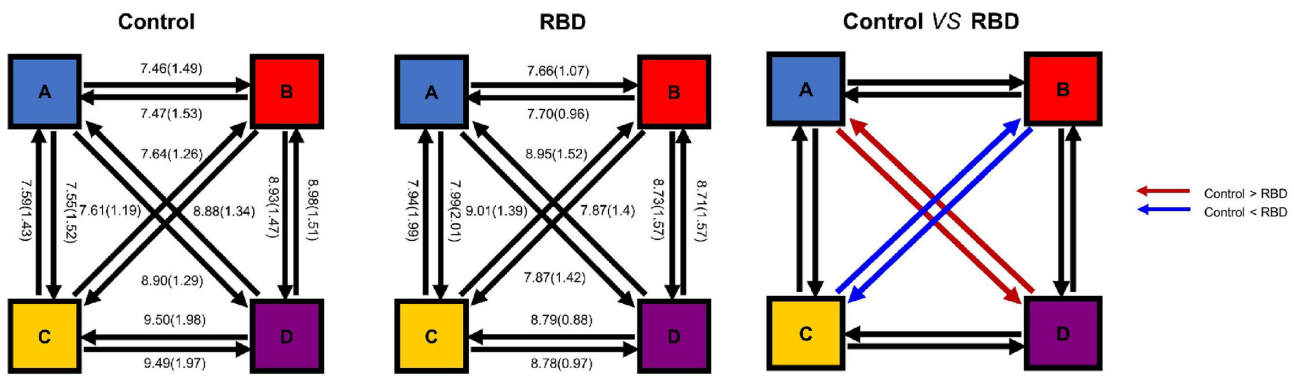

FIGURE 5 | Microstate transitions were altered in the RBD group. The mean observed percentage of transitions of HCs **(Left)** and participants with RBD **(Middle)**. The frequencies of transitions from microstate A to D and D to A were significantly decreased in the RBD group, while the RBD group produced increased frequencies of transitions between B and C **(Right)**.

alteration of spatial topography of EEG microstate D shown in RBD was also found in PD (Chu et al., 2020), which was believed to be due to the deficit of dopaminergic neurons (Van den Brink et al., 2018). The previous study also found that the frequency and duration of microstate D were significantly increased after taking levodopa, suggesting that the decreased duration of microstate D reflects abnormal dopaminergic activity (Serrano et al., 2018). Interestingly, we found that the average duration and proportion of microstate D were negatively correlated with the RBDQ-HK score, which represents the clinical RBD severity (Li et al., 2010). The results of this study, together with previous findings, demonstrated that the alteration of microstate D parameters could represent the degree of dopaminergic deficit.

Considering topography, microstate D was believed to be due to the activation of right inferior parietal, right middle and superior frontal gyri, and right insula (Custo et al., 2017). These areas were found to be vital for motor planning, executive control, and vision-guided movements (Kann et al., 2020). The alteration of the topological structure in microstate D implies the dysfunction of these areas in individuals with RBD. A similar finding was also found in patients with PD (Chen et al., 2021). What is more, the dysfunction of the functional connectivity of frontal-parietal- temporal network in individuals with RBD was also confirmed by the unusual transitions between microstates A and D. The deviated pattern may further indicate an imbalance between the resting state network and a deficit of several cognition processes. Taken together, these studies suggest that the resting-state EEG microstate D could reflect early abnormality of the frontal-parietal network, which might be critical for the pathological mechanism of neurodegenerative diseases and could be detected long before the occurrence of movement symptoms. Specifically, the decreased duration of microstate D has been reported in affective (Murphy et al., 2020) and psychotic disorders (Rieger et al., 2016). These findings may suggest that microstate D may be involved in the common pathophysiological process of many neuropsychiatric diseases.

Other disruption patterns of microstate dynamics including the increased frequency of microstate B and increased transitions between microstates B and C were also found in RBD, which could indicate the aberrant functional connectivity between the salience network and the visual cortex. Since the anterior insular receives the convergent multisensory inputs and regulates cognition (Menon and Uddin, 2010), the disturbance of microstate dynamics indicates a disturbance of these areas.

There are some limitations in this study. First, all patients with RBD were diagnosed by questionnaires and clinical evaluation. Therefore, the confirmation of these results in a group of patients with RBD diagnosed with the "gold standard"- polysomnography is warranted. Second, this study is unable to localize the corresponding neural correlate of each microstate status and the potential structural or functional connectivity abnormalities. Third, most participants belong to the aging group, which is unable to provide an indicator that tracks the development of RBD, and future longitudinal studies should be conducted to track the high-risk population and to reveal the underlying neural mechanism of the developmental trajectory of RBD.

CONCLUSION

The results of this study deepened our understanding of brain dysfunction in the early stage of alpha-synucleinopathy diseases and suggested that microstates may be potential biomarkers of RBD. These results highlighted the clinical value of microstate analysis, which could enable early detection and diagnosis of RBD and early intervention accordingly.

DATA AVAILABILITY STATEMENT

The raw data supporting the conclusions of this article will be made available by the authors, without undue reservation.

ETHICS STATEMENT

The studies involving human participants were reviewed and approved by the Ethics Committee of West China Hospital, Sichuan University. The participants provided their written informed consent to participate in this study.

AUTHOR CONTRIBUTIONS

AP: conceptualization, data curation, methodology, investigation, and writing—original draft. RW: formal analysis, investigation, methodology, and writing—original draft. JH: data curation, methodology, and writing—original draft. HW and LC: funding acquisition, resources, supervision, conceptualization, writing—review, and editing. All authors contributed to the article and approved the submitted version.

FUNDING

This study was supported by 1·3·5 project for disciplines of excellence–Clinical Research Incubation Project, West China Hospital, Sichuan University (No. 2021HXFH012), the National Clinical Research Center for Geriatrics, West China Hospital, Sichuan University West China Hospital, Sichuan University (No. Z2018B24), and Shenzhen-Hong Kong-Macau Technology Research Programme (202011033000116).

ACKNOWLEDGMENTS

The authors thank the staff of the Department of Clinical Research Management who aided in participant recruitment and all participants for supporting this study.

REFERENCES

Britz, J., Van De Ville, D., and Michel, C. M. (2010). BOLD correlates of EEG topography reveal rapid resting-state network dynamics. *Neuroimage* 52, 1162–1170. doi: 10.1016/j.neuroimage.2010.02.052

Byun, J. I., Kim, H. W., Kang, H., Cha, K. S., Sunwoo, J. S., Shin, J. W., et al. (2020). Altered resting-state thalamo-occipital functional connectivity is associated with cognition in isolated rapid eye movement sleep behavior disorder. *Sleep Med.* 69, 198–203. doi: 10.1016/j.sleep.2020.01.010

Chen, L., Bedard, P., Hallett, M., and Horovitz, S. G. (2021). Dynamics of top-down control and motor networks in Parkinson's disease. *Mov. Disord.* 36, 916–926. doi: 10.1002/mds.28461

Chu, C., Wang, X., Cai, L., Zhang, L., Wang, J., Liu, C., et al. (2020). Spatiotemporal EEG microstate analysis in drug-free patients with Parkinson's disease. *Neuroimage Clin.* 25:102132. doi: 10.1016/j.nicl.2019.102132

Custo, A., Van De Ville, D., Wells, W. M., Tomescu, M. I., Brunet, D., and Michel, C. M. (2017). Electroencephalographic resting-state networks: source localization of microstates. *Brain Connect.* 7, 671–682. doi: 10.1089/brain.2016.0476

Delorme, A., and Makeig, S. (2004). EEGLAB: an open-source toolbox for analysis of single-trial EEG dynamics including independent component analysis. *J. Neurosci. Methods* 134, 9–21. doi: 10.1016/j.jneumeth.2003.10.009

Eisensehr, I., Lindeiner, H., Jäger, M., and Noachtar, S. (2001). REM sleep behavior disorder in sleep-disordered patients with versus without Parkinson's disease: is there a need for polysomnography? *J. Neurol. Sci.* 186, 7–11. doi: 10.1016/S0022-510X(01)00480-4

Gschwind, M., Hardmeier, M., Van De Ville, D., Tomescu, M. I., Penner, I. K., Naegelin, Y., et al. (2016). Fluctuations of spontaneous EEG topographies predict disease state in relapsing-remitting multiple sclerosis. *Neuroimage Clin.* 12, 466–477. doi: 10.1016/j.nicl.2016.08.008

Iranzo, A., Fernández-Arcos, A., Tolosa, E., Serradell, M., Molinuevo, J. L., Valldeoriola, F., et al. (2014). Neurodegenerative disorder risk in idiopathic REM sleep behavior disorder: study in 174 patients. *PLoS ONE* 9:e89741. doi: 10.1371/journal.pone.0089741

Kann, S. J., Chang, C., Manza, P., and Leung, H. C. (2020). Akinetic rigid symptoms are associated with decline in a cortical motor network in Parkinson's disease. *NPJ Parkinsons Dis.* 6:19. doi: 10.1038/s41531-020-00120-3

Khanna, A., Pascual-Leone, A., Michel, C. M., and Farzan, F. (2015). Microstates in resting-state EEG: status and future directions. *Neurosci. Biobehav. Rev.* 49, 105–113. doi: 10.1016/j.neubiorev.2014.12.010

Koenig, T. (2021). *EEGLAB Microstate Plug-In*. Available online at: http://www.thomaskoenig.ch/ (accessed June 7, 2021).

Koenig, T., Lehmann, D., Merlo, M. C., Kochi, K., Hell, D., and Koukkou, M. (1999). A deviant EEG brain microstate in acute, neuroleptic-naive schizophrenics at rest. *Eur. Arch. Psychiatry Clin. Neurosci.* 249, 205–211. doi: 10.1007/s004060050088

Lehmann, D., Faber, P. L., Galderisi, S., Herrmann, W. M., Kinoshita, T., Koukkou, M., et al. (2005). EEG microstate duration and syntax in acute, medication-naive, first-episode schizophrenia: a multi-center study. *Psychiatry Res.* 138, 141–156. doi: 10.1016/j.pscychresns.2004.05.007

Li, S. X., Wing, Y. K., Lam, S. P., Zhang, J., Yu, M. W., Ho, C. K. W., et al. (2010). Validation of a new REM sleep behavior disorder questionnaire (RBDQ-HK). *Sleep Med.* 11, 43–48. doi: 10.1016/j.sleep.2009.06.008

Menon, V., and Uddin, L. Q. (2010). Saliency, switching, attention and control: a network model of insula function. *Brain Struct. Funct.* 214, 655–667. doi: 10.1007/s00429-010-0262-0

Michel, C. M., and Koenig, T. (2018). EEG microstates as a tool for studying the temporal dynamics of whole-brain neuronal networks: a review. *Neuroimage* 180, 577–593. doi: 10.1016/j.neuroimage.2017.11.062

Mullen, T. R., Kothe, C. A., Chi, Y. M., Ojeda, A., Kerth, T., Makeig, S., et al. (2015). Real-time neuroimaging and cognitive monitoring using wearable dry EEG. *IEEE Trans. Biomed. Eng.* 62, 2553–2567. doi: 10.1109/TBME.2015.2481482

Murphy, M., Whitton, A. E., Deccy, S., Ironside, M. L., Rutherford, A., Beltzer, M., et al. (2020). Abnormalities in electroencephalographic microstates are state and trait markers of major depressive disorder. *Neuropsychopharmacology* 45, 2030–2037. doi: 10.1038/s41386-020-0749-1

Perkins, J. E., Janzen, A., Bernhard, F. P., Wilhelm, K., Brien, D. C., Huang, J., et al. (2021). Saccade, pupil, and blink responses in rapid eye movement sleep behavior disorder. *Mov. Disord.* 36, 1720–1726. doi: 10.1002/mds.28585

Postuma, R. B., and Berg, D. (2019). Prodromal Parkinson's disease: the decade past, the decade to come. *Mov. Disord.* 34, 665–675. doi: 10.1002/mds.27670

Postuma, R. B., Gagnon, J. F., Vendette, M., Fantini, M. L., Massicotte-Marquez, J., and Montplaisir, J. (2009). Quantifying the risk of neurodegenerative disease in idiopathic REM sleep behavior disorder. *Neurology* 72, 1296–1300. doi: 10.1212/01.wnl.0000340980.19702.6e

Rieger, K., Diaz Hernandez, L., Baenninger, A., and Koenig, T. (2016). 15 years of microstate research in schizophrenia–where are we? A meta-analysis. *Front. Psychiatry* 7:22. doi: 10.3389/fpsyt.2016.00022

Schumacher, J., Peraza, L. R., Firbank, M., Thomas, A. J., Kaiser, M., Gallagher, P., et al. (2019). Dysfunctional brain dynamics and their origin in Lewy body dementia. *Brain* 142, 1767–1782. doi: 10.1093/brain/awz069

Serrano, J. I., Del Castillo, M. D., Cortés, V., Mendes, N., Arroyo, A., Andreo, J., et al. (2018). EEG microstates change in response to increase in dopaminergic stimulation in typical Parkinson's disease patients. *Front. Neurosci.* 12:714. doi: 10.3389/fnins.2018.00714

Shen, S. S., Shen, Y., Xiong, K. P., Chen, J., Mao, C. J., Huang, J. Y., et al. (2014). Validation study of REM sleep behavior disorder questionnaire–Hong Kong (RBDQ-HK) in east China. *Sleep Med.* 15, 952–958. doi: 10.1016/j.sleep.2014.03.020

Strik, W. K., and Lehmann, D. (1993). Data-determined window size and space-oriented segmentation of spontaneous EEG map series. *Electroencephalogr Clin. Neurophysiol.* 87, 169–174. doi: 10.1016/0013-4694(93)90016-O

Tait, L., Tamagnini, F., Stothart, G., Barvas, E., Monaldini, C., Frusciante, R., et al. (2020). EEG microstate complexity for aiding early diagnosis of Alzheimer's disease. *Sci Rep.* 10:17627. doi: 10.1038/s41598-020-74790-7

Van de Ville, D., Britz, J., and Michel, C. M. (2010). EEG microstate sequences in healthy humans at rest reveal scale-free dynamics. *Proc Natl Acad Sci U. S. A.* 107, 18179–18184. doi: 10.1073/pnas.1007841107

Van den Brink, W. J., Palic, S., Köhler, I., and de Lange, E. C. M. (2018). Access to the CNS: biomarker strategies for dopaminergic treatments. *Pharm. Res.* 35:64. doi: 10.1007/s11095-017-2333-x

Yuan, H., Zotev, V., Phillips, R., Drevets, W. C., and Bodurka, J. (2012). Spatiotemporal dynamics of the brain at rest—exploring EEG microstates as electrophysiological signatures of BOLD resting state networks. *Neuroimage.* 60, 2062–2072. doi: 10.1016/j.neuroimage.2012.02.031

Conflict of Interest: The authors declare that the research was conducted in the absence of any commercial or financial relationships that could be construed as a potential conflict of interest.

frontiers in Physiology

ORIGINAL RESEARCH
published: 08 December 2021
doi: 10.3389/fphys.2021.740728

Integrated Physiological, Biomechanical, and Subjective Responses for the Selection of Assistive Level in Pedelec Cycling

Sheng-Chieh Yang[1,2] *and Yun-Ju Lee*[2]*

[1] Cycling & Heath Tech Industry R&D Center, Taichung, Taiwan, [2] Department of Industrial Engineering and Engineering Management, National Tsing Hua University, Hsinchu, Taiwan

In recent decade, pedelec has become one of the most popular transportation modes due to its effectiveness in reducing physical effort. The effects of using pedelec as an alternative mode of exercise were explored in previous studies. However, the effects of pedelec parameters were not quantified for the self-selected gear ratio, random riding speed, and varied road slopes, which restricted its application. Hence, this study aimed to evaluate the effects of gear ratio and assistive torque and to determine the optimum riding condition regarding physiological, biomechanical, and subjective responses of the rider. The riding tests consisted of simulated slope (1.0 vs. 2.5% grade), gear ratio (light vs. heavy), and assistive levels (0.5, 1, 1.5, and 2), and the tests were conducted in a randomized order. A total of 19 non-athletes completed the riding tests to evaluate physiological [metabolic equivalent of task (MET), heart rate, and gross efficiency (GE)], biomechanical [muscle activity (expressed as reference voluntary contraction, RVC) and power output], and subjective responses [rating of perceived exertion (RPE) and sense of comfort (SC)]. The test conditions induced moderate to vigorous intensities (3.7–7.4 METs, 58.5–80.3% of maximal heart rate, 11.1–29.5% of RVC rectus femoris activity, and 9.4–14.2 RPEs). The effects of gear ratio and assistive level on the physiological responses were significant. Riding with the heavy gear ratio showed advantages in METs and GE. For the optimum assistive level selection, low GE and limited improvement in subjective responses suggested the impact of low-power output conditions. Overall, for the health pedelec commuters, riding with 0.75 W/kg power output with 50 rpm cadence is recommended to obtain the moderate intensity (4.7 METs) and the advantages in GE and subjective feelings. Moreover, the findings can be applied to exercise intensity control and save battery energy effectively in varying riding conditions.

Keywords: pedelec, simulated slope resistance, assistive power, physical intensity, muscle activity, rating of perceived exertion

OPEN ACCESS

Edited by:
Christoph Centner,
University of Freiburg, Germany

Reviewed by:
Claudio Pizzolato,
Griffith University, Australia
Chiang Liu,
University of Taipei, Taiwan
Heinz Kleinöder,
German Sport University Cologne, Germany

***Correspondence:**
Yun-Ju Lee
yunjulee@ie.nthu.edu.tw

Specialty section:
This article was submitted to Exercise Physiology, a section of the journal Frontiers in Physiology

Received: *13 July 2021*
Accepted: *09 November 2021*
Published: *08 December 2021*

Citation:
Yang S-C and Lee Y-J (2021) Integrated Physiological, Biomechanical, and Subjective Responses for the Selection of Assistive Level in Pedelec Cycling. Front. Physiol. 12:740728. doi: 10.3389/fphys.2021.740728

INTRODUCTION

Active commuting by bike induces cardiorespiratory and muscular loads, which fulfills the required intensity and volume for maintaining health (Hendriksen et al., 2000; Oja et al., 2011; Schäfer et al., 2020). However, uphill the route would affect the motivation for active commuting due to the fear of vigorous-intensity (van Bekkum et al., 2011). Addressing the need for avoiding strenuous

physical effort during commuting, pedelec, known as an electric-assisted bike, is gaining popularity for its effectiveness in providing an easier pedaling experience. The magnitude of assistive torque is provided proportionally to the pedaling torque of the rider, and an assistive level denotes the relative contribution of the motor and the rider. For example, with the assistive level of 0.5, the motor will generate 10 newton-meter (Nm) torque while the rider produces 20 Nm pedaling torque. The other measure to obtain the preferred pedaling torque and cadence is adjusting the gear ratio. Combining the manual adjustment of pedelec parameters, the pedelec riders could maintain the intensity level when the slope or speed changes. But there is still a gap in integrated evaluation of the effect of pedelec parameters, which leads to the limits in optimizing riding experience, progressing toward auto-adjusting, exercising prescription execution, and effectively managing battery energy.

The assistive torque of the pedelec helps overcome the challenges of prolonging riding, long distances, or uphill for untrained or sedentary people (Gojanovic et al., 2011; Sperlich et al., 2012). Previous studies have investigated the effects of assistive torque on physical intensity in flat and uphill route ridings and found that the intensities, as evaluated by the metabolic equivalent of task (MET), ranged from moderate (3–6 METs) to vigorous (>6 METs) levels (Simons et al., 2009; Gojanovic et al., 2011). Compared with the conventional bicycle or the pedelec without assistance, riding with the assistive torque resulted in significantly decreased oxygen consumption, energy expenditure, heart rate (Simons et al., 2009; Gojanovic et al., 2011; Louis et al., 2012; Langford et al., 2017), and muscle activity (Sperlich et al., 2012). Pedelec riding was also found to facilitate subjective feelings (Simons et al., 2009; Gojanovic et al., 2011; Louis et al., 2012; Sperlich et al., 2012; Langford et al., 2017). Previous studies reported the significantly lower rating of perceived exertion (RPE) (Simons et al., 2009; Gojanovic et al., 2011; Louis et al., 2012) with the simultaneously higher level of enjoyment (Langford et al., 2017) and sense of comfort (SC) (Simons et al., 2009). Moreover, for the moderate riding intensity, a pedelec is also thought to be a proper modality for commuting (Simons et al., 2009; Gojanovic et al., 2011) purposes. For the untrained or sedentary people, the health benefits of using pedelec transportation include improved maximal power output (De Geus et al., 2013), post-OGTT (oral glucose tolerance test), and maximum oxygen consumption (Peterman et al., 2016).

Although gear ratio adjustment was not documented explicitly in previous pedelec studies, it was evidenced by the simultaneous changes in pedaling rate and speed. In the studies that allowed the pedelec riders to choose their preferred speed with an assigned assistive level, the rider generally adopted a faster speed with a constant (Gojanovic et al., 2011) or decreased pedaling rate (Simons et al., 2009) compared with the non-assistance condition, which indicated a heavier gear ratio was selected. This might be explained by the gear-shifting behaviors of professional cyclists in racing events. Professional cyclists attempt to ride with the optimum pedal torque and pedal rate to minimize the physiological and biomechanical load (Chavarren and Calbet, 1999; Watson and Swensen, 2006; Abbiss et al., 2009) through the gear ratio adjustment. A light gear ratio that leads to the lower pedal torque is chosen to avoid the use of the less fatigue-resistance type II muscle fibers (Lucía et al., 2001). In contrast, a heavy gear ratio increases the required torque but reduces the pedal cadence for the desired speed and saves the bioenergy expenditure caused by the repetitive limb movement (Chavarren and Calbet, 1999; Louis et al., 2012). For the pedelec riders, using the heavier gear ratio under the assigned assistive level may imply the need for compensating the low resultant torque under the use of assistance. In contrast, this also indicated the motor generated excessive assistive torque and suggested the consequent battery energy wasting. From the health benefit and energy-saving points of view, the proper assistive level should be determined based on physiological, biomechanical, and subjective responses. However, there is still limited knowledge of effective pedelec parameter adjusting to maintain the preferred intensity while avoiding energy wasting.

The pedelec was a proper modality for exercise training (De Geus et al., 2013; Peterman et al., 2016) and commuting, but the non-integrated evaluations of assistive level and gear ratio under the varying slopes limit the improvement of training effectiveness or user satisfaction. A recent review reported two of the most prevalent barriers of pedelec riders, namely, less physical activity and range anxiety (Bourne et al., 2020), which imply the need for a comprehensive investigation of rider response and the required assistance. Both of the barriers are mainly associated with excessive assistive torque. Due to the random changes in slope and speed in previous studies, the data are inadequate to develop the strategy that is effectively keeping optimum physiological, biomechanical, and subjective status. Therefore, this study aimed to elicit a wide range of responses in the simulated riding conditions and investigate the responses, especially under low-power output conditions to identify the improper assistive level. The hypothesis was that the positive effect of torque assistance on rider responses is limited, particularly in the low-power output conditions. A series of indoor pedelec riding tests with simulated slope resistances were conducted to eliminate the random effects of varying inclination in outdoor riding.

MATERIALS AND METHODS

Participants

A total of 10 female and 9 male healthy (without musculoskeletal and cardiorespiratory disorders) adults were enrolled in this study. The protocol was approved by the Ethics Committee of the National Tsing Hua University (REC: 10811HE094). The participants were given an introduction to the aim and procedure of the study. After fully understanding and being willing to join, the participants signed the informed consent. Before data collection sessions, the Chinese version of the "Physical Activity Readiness Questionnaire for Everyone" (PAR-Q+) (Warburton et al., 2018) survey was used to assess the readiness of the participant in performing the indoor riding test. All participants were free from disorders listed in the questionnaire.

Personal data, such as age, body height, and body mass, were recorded. Besides, self-reported physical activity status, frequency (number of times per week), duration, and type were also

recorded *via* a questionnaire. According to the self-reported data, all the participants were non-athlete adults, and 14 participants engaged in recreational physical activities. All participants had experiences in riding conventional bikes.

Experiment Procedure

The experiment consisted of 16 indoor pedelec riding tests. On the day of the riding test, the participants were asked to intake a meal at least 2 h before the riding test. Alcohol and caffeine were restricted. The saddle height was adjusted according to the inseam length of the participants. Before the riding test, the participants were familiarized with riding at the target riding speed, 21 km·h^{-1} (Louis et al., 2012; Boele-Vos et al., 2017) when two different gear ratios were used. The real-time speed and cadence feedback were displayed on a monitor in front of the rider. All participants were able to maintain the target speed within ± 1 km·h^{-1} by controlling their cadence. The participants were then warmed up with the resistance relative to the flat road (0% slope) for 5 min.

For each riding test, the simulated slope resistance was provided, while the gear ratio and assistive level were specified. The simulated slopes were 1 and 2.5%. With the target riding speed of 21 km·h^{-1}, the heavy (H, 46:14) and light (L, 46:17) gear ratios resulted in the cadence of approximately 50 and 60 revolutions per minute (rpm) were chosen, respectively. Around 50 rpm was the cadence freely selected by the participants in previous outdoor studies (Simons et al., 2009), and 60 rpm was suggested to be the most efficient cadence (Gojanovic et al., 2011). As for the assistive levels, "0.5", "1", "1.5", and "2" were selected in the experiment, where "0.5" denotes the motor provided half of the torque of the rider under the testing conditions. The conditions were conducted in a randomized order. For each condition, the participants continuously rode on the indoor pedelec for 3 min (De Koning et al., 2012; Bini et al., 2019), and 3 min of rest were provided between the test conditions. In the rest period, the participants were asked to stand beside the pedelec. Each test started with the participant resting their feet on the pedal and ended for 3 min. Physiological and biomechanical responses were recorded for the entire 3-min period, and the subjective responses were recorded at the end of each condition.

For the riding test, a pedelec with a motor located at the bracket bottom (Fast SR E+, Giant, Taiwan) was adopted. The original pedals of the pedelec were replaced by a pair of pedal power meters (PowerTap P1, SRAM, Chicago, IL, United States) (Pallarés and Lillo-Bevia, 2018; Wright et al., 2019) to measure the power output of the rider (watt, W) and pedal cadence (revolution per minute, rpm) (**Figure 1**). The validity and reliability of PowerTap P1 had been reported as acceptable (with rho >0.98 and mean CV = 2.3% compared with the gold standard) in the previous study (Pallarés and Lillo-Bevia, 2018). The pedal power meter was zero calibrated before riding tests. Once the speed attained 21 km·h^{-1}, the power output and cadence data were utilized for analysis. For the simulated slope assistance generation, the rear wheel of the pedelec was removed and replaced by an indoor trainer (Cyclus2, RBM Elektronik-automation GmbH, Leipzig, Germany). The indoor trainer is capable of providing simulated slope resistance according to the target slope, the body mass of the rider and the front projection area (Debraux et al., 2011), the mass of the pedelec (16 kg), the riding speed, and the road surface coefficient of rolling resistance (Ba Hung et al., 2017).

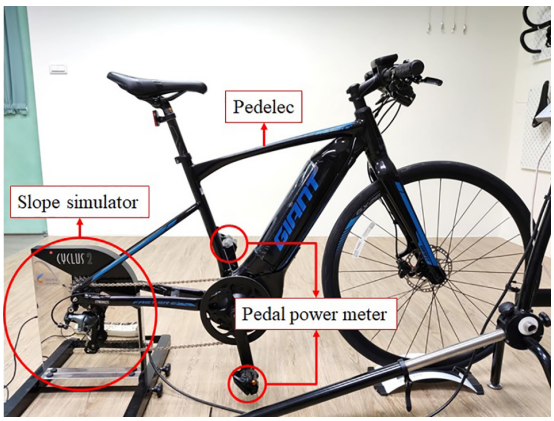

FIGURE 1 | The pedelec, pedal power meter, and the slope simulator.

Measurement of Physiological Responses

The participants wore a face mask and a chest strap heart-rate monitor during the riding test. The face mask covers the nose and mouth of the participant and collects gas samples with a sampling tube and a flowmeter. Breathing gas and heart rate data were transmitted to a gas analyzer (Quark CPET, COSMED, Italy). Before data collection, the standard gas (16% oxygen and 5% carbon dioxide) was used to calibrate the gas analyzer, and a 3-L cylinder pump was used to calibrate the flowmeter. Energy expenditure (EE) was estimated *via* oxygen and carbon dioxide data (Simons et al., 2009). Breath-by-breath oxygen consumption ($\dot{V}O_2$, ml·kg^{-1}·min^{-1}), energy expenditure (Joule·min^{-1}), and heart rate (beat per minute) data from the last 30-s period of each test were averaged for further analysis. Previous studies suggested moderate intensity (3–6 METs) as the appropriate intensity for commuters (Simons et al., 2009; Gojanovic et al., 2011; Louis et al., 2012; Berntsen et al., 2017), and the criteria can be defined accordingly in this study.

Measurement of Biomechanical Responses

Muscle activity of rectus femoris (RF), vastus lateralis (VL), and vastus medialis (VM) of the dominant leg (determined by asking the participant to kick an object with the intuitively selected leg) were measured and analyzed using wireless surface electromyography (EMG) sensors (TeleMyo DTS, Noraxon, Scottsdale, AZ, United States) and the MyoResearch software (version 3.16.32, Noraxon, Scottsdale, AZ). The parameters of the EMG sensor were as follows: baseline noise <1 μV RMS; input impedance >100 Mohm; CMR >100 dB; and overall gain = 200. Skin preparation was done before the placement of the electrodes.

The locations of the electrode were determined according to the recommendation from SENIAM (Hermens et al., 2000).

Measurement of Subjective Responses

The subjective evaluation of exertion and SC was recorded at the end of each riding test. The RPE (Borg, 1982) was subjectively evaluated using the Borg scale (from 6, easy, to 20, maximal effort). The five-point Likert scale was used to evaluate the SC, where "1" represents the most comfort level and "5" represents the lowest comfort level (Simons et al., 2009). According to Simons et al. (2009), the criteria of RPE and SC can be defined as 13.1 and 1.7, respectively, to present the lower limits of subjective responses when assistance was not provided. Namely, once the assistance is provided, the score of RPE and SC should be lower than the reference value as the assistive level increases.

Data Processing and Statistical Analysis

The MET and normalized heart rate (nHR) were obtained from the physiological data to determine the relative intensities. The MET was obtained by dividing $\dot{V}_{O_2}$ by 3.5 $ml \cdot kg^{-1} \cdot min^{-1}$ (Simons et al., 2009; Louis et al., 2012). The nHR was obtained by dividing the mean heart rate by the age-predicted maximal heart rate (220 – age) for each participant (Garber et al., 2011). The processed data of each test were then categorized into one of the intensity levels from very light to maximal according to the position stand of the American College of Sports Medicine (Garber et al., 2011). For gross efficiency (GE) estimation, power output and EE data of the participant were used in the followed equation (Louis et al., 2012).

$$\begin{aligned} &Gross\ efficiency\ (GE, \%) \\ &= \frac{Work\ (W, Joule)}{Energy\ Expenditure\ (E, Joule)} \times 100\% \end{aligned} \quad (1)$$

The EMG data were filtered by the Butterworth bandpass filter (20–500 Hz) and smoothed *via* the root mean square (RMS) technique with a 50-ms window. Averaged EMG data from the last 10 crank cycles of each test were used for further analysis. An accelerometer (Accelerometer Wireless, Noraxon, Scottsdale, AZ, United States) was attached to the right crank with its orientation aligned with the crank stem to determine the individual crank cycle. The acceleration data were synchronized with EMG data, and the peak value represented the pedal located at the top position of the whole crank cycle. For the non-athlete participants, the reference voluntary contraction (RVC) method was used to normalize the EMG data for each muscle (Candotti et al., 2009; Sinclair et al., 2015). The maximum muscle activity level was assumed to be elicited from the highest muscle force demanded condition (i.e., 2.5% slope, heavy gear ratio, and assistive level of 0.5), and the EMG data were selected as the RVC.

All data were expressed as means ± standard deviation. Analyses were performed using SPSS version 17.0 (SPSS Inc, Chicago, IL, United States). As the assistive level is defined as a specific proportion of assistive torque to the pedal torque of the rider, the absolute assistive torque would be greater in high pedal-torque demand conditions even though the same assistance level is selected, which led to the complexity in data interpreting. Hence, data from different slope conditions were divided into 1.0% slope or 2.5% slope sets and analyzed, respectively. Considering the small size and the distribution normality of samples, generalized estimating equations (GEE) analyses were conducted using the factors of gear ratio [light (46:17) and heavy (46:14)] and assistance level (0.5, 1, 1.5, and 2). The condition with light gear ratio and assistive level of 2 served as the reference for all analysis. *Post hoc* pairwise comparisons were performed using the Bonferroni method. For the statistical analysis, a value of $p < 0.05$ was accepted as the level of significance.

RESULTS

Characteristics of Participants

All participants completed the laboratory test. The mean age of the participant was 29.1 ± 6.2 years. Their body weight and body height were 65.6 ± 12.3 kg and 165.3 ± 8.0 cm, respectively. The mean physical activity frequency was 2.5 ± 2.0 times per week. Five participants did not have regular physical activity, and the other participants engaged in various habitual recreational activities.

Effects of Gear Ratio and Assistance on Physiological Responses

In the 1.0% slope conditions, the effect of gear ratio was significant on METs ($p = 0.001$) and GE ($p = 0.002$). Significant effects of assistance were shown on METs, nHR (except for the assistive level of 1.5, $p = 0.06$), and GE. Significant interaction effects of gear ratio and assistance were revealed on METs and nHR only for the heavy gear ratio and assistive level of 1.5 conditions (**Table 1**). The result of pairwise comparison showed significant differences between assistive levels (level 0.5 > 1 > 1.5 > 2, all $p < 0.01$) in METs, nHR, and GE, respectively.

In the 2.5% slope conditions, the effects of gear ratio on MET ($p = 0.004$) and GE ($p = 0.014$) were significant. The effect of assistance was significant on METs, nHR, and GE (with all $p < 0.01$), whereas the interaction effects of gear ratio and assistance were not significant (**Table 2**). Likewise, the results of pairwise comparison showed significant differences between assistive levels in METs, nHR, and GE (level 0.5 > 1 > 1.5 > 2, all $p < 0.01$). **Tables 1**, **2** present the coefficients (β), standard errors, and p values of physiological responses in 1.0 and 2.5% slope conditions, respectively. **Figures 2A–C** depicts the mean MET, nHR, and GE of each riding condition. According to ACSM, the mean METs corresponded with moderate to vigorous levels, respectively, the mean nHRs corresponded with light to vigorous levels.

Effects of Gear Ratio and Assistance on Biomechanical Responses

In the 1.0% slope conditions, the effect of gear ratio was not significant on RF, VL, and VM activities. The effects of

TABLE 1 | Coefficients (β), standard errors (S.E.) and p values of physiological responses in 1.0% slope conditions.

	METs			nHR			GE		
	β	S.E.	*p*	β	S.E.	*p*	β	S.E.	*p*
Intercept	4.87	(0.13)	<0.001	63.95	(2.04)	<0.001	13.72	(0.37)	<0.001
G									
Heavy	−0.15	(0.05)	0.001	−0.15	(0.71)	0.267	0.52	(0.21)	0.002
A									
0.5	2.51	(0.11)	<0.001	16.39	(1.50)	<0.001	4.82	(0.26)	<0.001
1	1.37	(0.10)	<0.001	9.46	(1.24)	<0.001	3.31	(0.22)	<0.001
1.5	0.57	(0.08)	<0.001	4.20	(1.07)	<0.001	1.63	(0.29)	<0.001
G × A									
H × 0.5	0.18	(0.10)	0.082	−0.42	(1.05)	0.685	−0.51	(0.32)	0.115
H × 1	0.01	(0.08)	0.877	−0.74	(0.92)	0.419	−0.30	(0.30)	0.318
H × 1.5	0.06	(0.10)	0.520	0.08	(0.80)	0.921	−0.31	(0.33)	0.345

The condition with light gear ratio (G) and assistive level (A) of 2 served as reference.

TABLE 2 | Coefficients (β), standard errors (S.E.) and p values of physiological responses in 2.5% slope conditions.

	METs			nHR			GE		
	β	S.E.	*p*	β	S.E.	*p*	β	S.E.	*p*
Intercept	3.88	(0.11)	<0.001	59.08	(1.83)	<0.001	9.99	(0.30)	<0.001
G									
Heavy	−0.20	(0.06)	0.001	−0.61	(0.55)	0.267	0.66	(0.22)	0.002
A									
0.5	1.89	(0.07)	<0.001	11.64	(1.18)	<0.001	5.22	(0.32)	<0.001
1	0.88	(0.09)	<0.001	5.54	(0.95)	<0.001	3.51	(0.33)	<0.001
1.5	0.30	(0.08)	<0.001	1.41	(0.75)	0.059	1.53	(0.30)	<0.001
G × A									
H × 0.5	−0.06	(0.11)	0.617	−1.26	(0.67)	0.061	−0.22	(0.38)	0.557
H × 1	0.13	(0.11)	0.236	0.02	(0.79)	0.979	−0.53	(0.37)	0.152
H × 1.5	0.17	(0.08)	0.035	1.41	(0.7)	0.044	−0.21	(0.25)	0.399

The condition with light gear ratio (G) and assistive level (A) of 2 served as reference. METs: metabolic equivalent of task. nHR: normalized heart rate, %. GE: gross efficiency, %.

assistance were significant on RF (except for assistive level of 1.5, $p = 0.12$), VL (except for assistive level of 1.5, $p = 0.31$), and VM (except for assistive level of 1.5, $p = 0.07$). There was no interaction effect found on the muscles. The results of pairwise comparison revealed significant activity differences between the assistive levels (assistive level of $0.5 > 1 > 1.5 > 2$, all $p < 0.01$) in each muscle.

In the 2.5% slope conditions, the effect of gear ratio was not significant on RF, VL, and VM activities, whereas the effects of assistance were significant on RF, VL, and VM (all $p < 0.01$). No significant interaction effect was found in each muscle. The results of pairwise comparison revealed significant activity differences between the assistive levels (level of $0.5 > 1 > 1.5 > 2$, all $p < 0.01$) in each muscle. **Tables 3**, **4** present the coefficients (β), standard errors, and *p* values of biomechanical responses in 1.0 and 2.5% slope conditions, respectively. **Figure 3** depicts the muscle activity of each riding condition.

In both 1.0 and 2.5% slope conditions, the effects of gear ratio on power output were not significant ($p = 0.85$ and 0.91), while the effect of assistance was significant (both $p < 0.01$). The results of pairwise comparison indicated significant differences between assistive levels (**Figure 4**) (level of $0.5 > 1 > 1.5 > 2$, all $p < 0.01$). The non-significant effect of gear ratio on power output ($p = 0.88$) indicated that in the same slope and assistance conditions, the participants could maintain the same power output with the heavy and light gear ratio settings, i.e., the pedal cadence and pedal torque may account for the differences in the measured responses.

Effects of Gear Ratio and Assistance on Subjective Responses

In the 1.0% slope conditions, the effect of gear ratio was not significant on RPE ($p = 0.85$) and SC ($p = 0.56$). The effect of assistance on RPE was significant only with the assistive level of 0.5 ($p = 0.016$) but not significant on SC. Significant pairwise RPE differences were found between the assistive level of 0.5 and the other levels, respectively, whereas no significant pairwise difference was found between assistive levels of 1, 1.5, and 2 (level $0.5 < 1 = 1.5 = 2$). As for SC, the only pairwise difference was

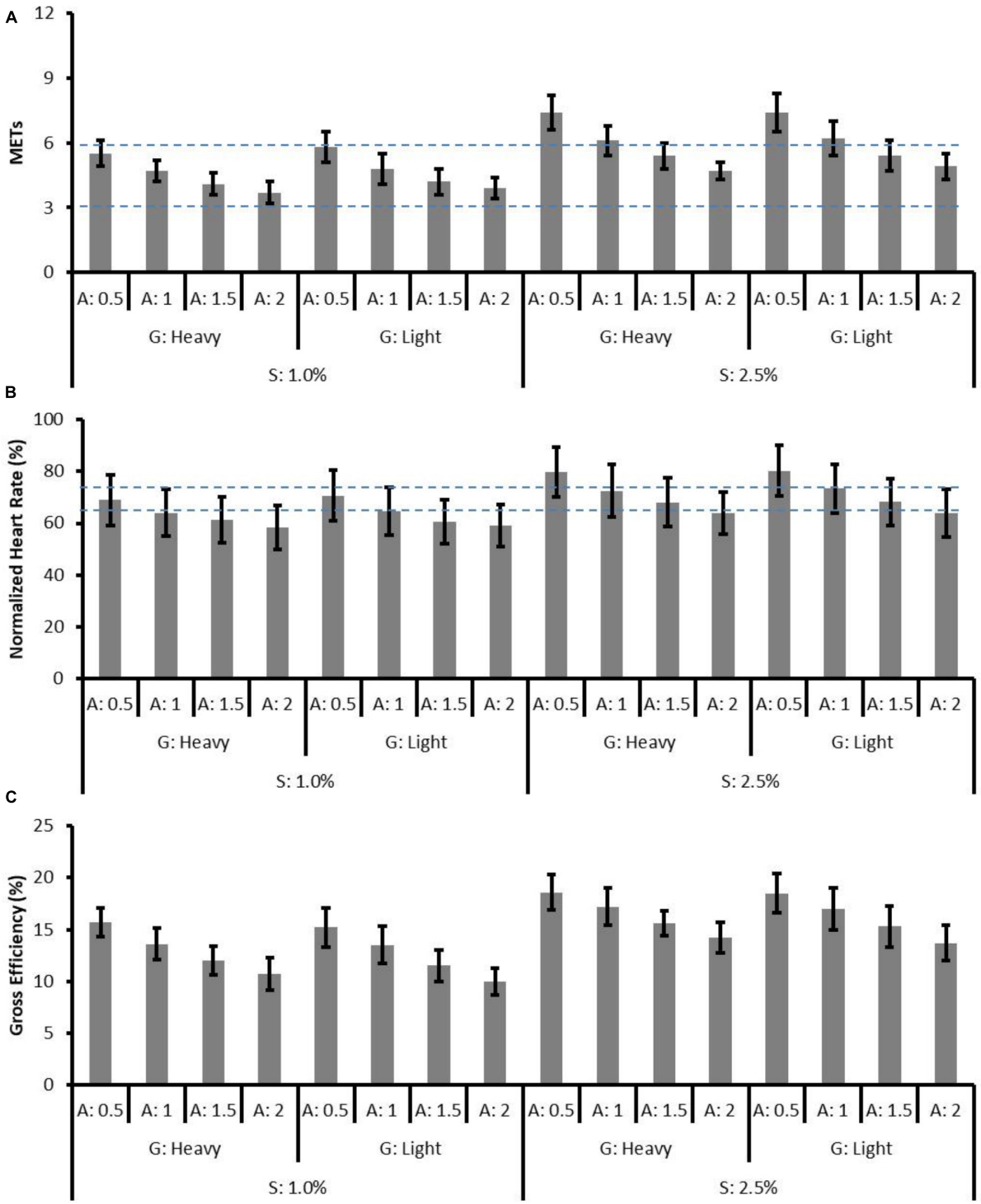

FIGURE 2 | The means and standard deviations of **(A)** MET, **(B)** normalized heart rate (%), and **(C)** gross efficiency (%) in all conditions. S, slope; G, gear ratio; A, assistive level. The horizontal dashed lines represent the upper and lower bound of moderate level defined by ACSM.

found between the assistive level of 1.5 and 2 (1.66 ± 0.14 vs. 2.05 ± 0.20, $p = 0.017$).

Tables 5, **6** present the coefficients (β), standard errors, and p values of subjective responses in 1.0 and 2.5% slope conditions, respectively. **Figures 5A,B** depicts the results of RPE and SC. In the 2.5% slope conditions, the effect of gear ratio was not significant on RPE ($p = 0.40$) and SC ($p = 0.36$). The effect of assistance was significant on RPE and SC (except for assistive

TABLE 3 | Coefficients (β), standard errors (SE), and *p*-values of biomechanics responses in 1.0% slope conditions.

	RF			VL			VM		
	β	SE	*p*	β	SE	*p*	β	SE	*p*
Intercept	11.14	(0.75)	<0.001	8.7	(0.73)	<0.001	8.83	(0.76)	<0.001
G									
Heavy	0.61	(0.69)	0.374	−1.13	(0.63)	0.074	−0.98	(0.58)	0.093
A									
0.5	7.39	(0.59)	<0.001	7.55	(0.49)	<0.001	8.37	(0.51)	<0.001
1	4.35	(0.7)	<0.001	4.01	(0.75)	<0.001	4.24	(0.73)	<0.001
1.5	0.93	(0.59)	0.116	0.51	(0.51)	0.313	1.06	(0.58)	0.067
G × A									
H × 0.5	0.43	(0.71)	0.543	0.58	(0.79)	0.464	0.16	(0.73)	0.825
H × 1	0.42	(0.7)	0.549	0.8	(0.67)	0.234	1.11	(0.73)	0.128
H × 1.5	0.56	(0.73)	0.442	1.07	(0.85)	0.207	0.52	(0.8)	0.516

The condition with light gear ratio (G) and assistive level (A) of 2 served as reference. RF, muscle activity of rectus femoris, %RVC; VL, muscle activity of vastus lateralis, %RVC; VM, muscle activity of vastus medialis, %RVC.

TABLE 4 | Coefficients (β), standard errors (SE), and *p*-values of biomechanics responses in 2.5% slope conditions.

	RF			VL			VM		
	β	SE	*p*	β	SE	*p*	β	SE	*p*
Intercept	14.69	(0.78)	<0.001	12.51	(0.85)	<0.001	13.17	(0.85)	<0.001
G									
Heavy	0.9	(0.87)	0.374	−0.94	(0.86)	0.074	0.32	(1.76)	0.093
A									
0.5	13.43	(1.68)	<0.001	12.85	(0.63)	<0.001	13.19	(0.65)	<0.001
1	6.96	(1.27)	<0.001	6.49	(0.58)	<0.001	6.57	(0.66)	<0.001
1.5	2.83	(0.71)	<0.001	2.78	(0.58)	<0.001	3.19	(0.61)	<0.001
G × A									
H × 0.5	0.46	(1.36)	0.732	0.32	(0.8)	0.69	−1.28	(1.69)	0.448
H × 1	0.04	(1.03)	0.969	0.75	(1)	0.456	−0.43	(1.74)	0.806
H × 1.5	1.14	(1.03)	0.272	1.37	(1.03)	0.184	−0.07	(1.77)	0.969

The condition with light gear ratio (G) and assistive level (A) of 2 served as reference.

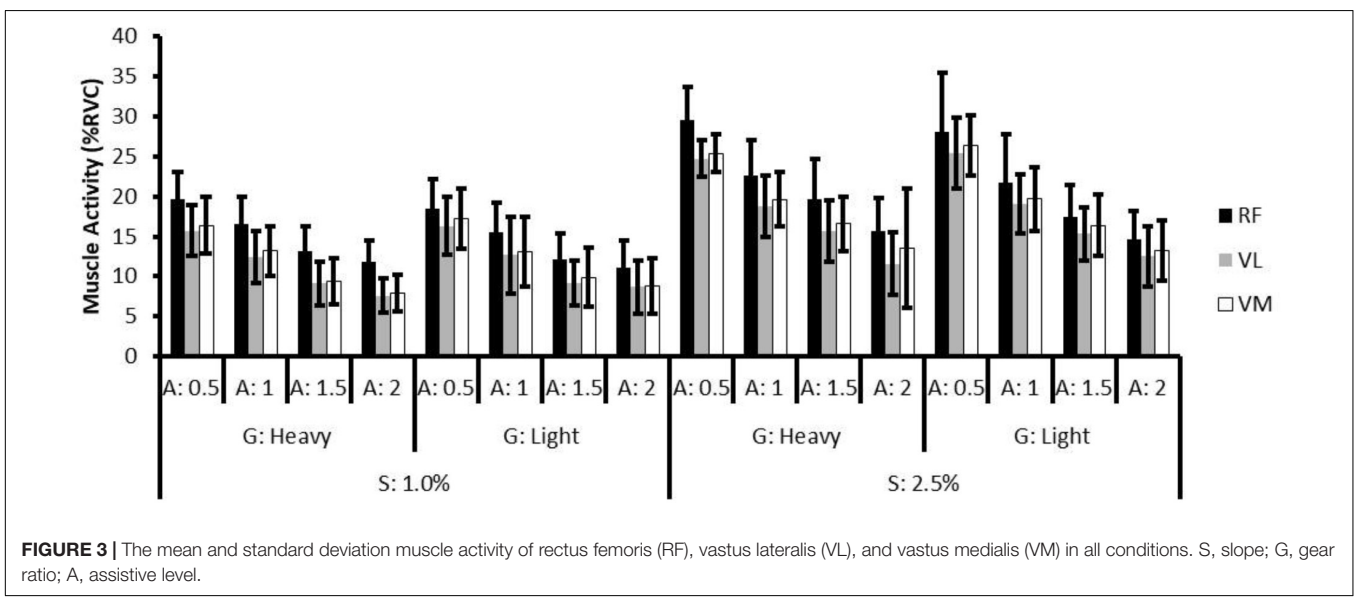

FIGURE 3 | The mean and standard deviation muscle activity of rectus femoris (RF), vastus lateralis (VL), and vastus medialis (VM) in all conditions. S, slope; G, gear ratio; A, assistive level.

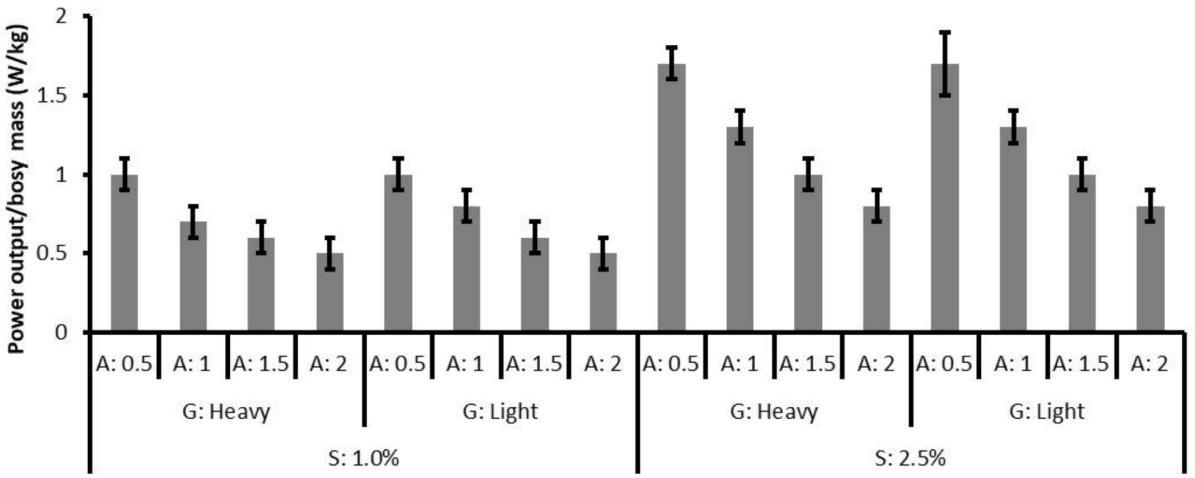

FIGURE 4 | The mean and standard deviation of normalized power output (W/kg) in all conditions.

level of 1.5). Significant pairwise RPE differences were found between each assistive levels (level $0.5 > 1 > 1.5 > 2$, all $p < 0.01$), while pairwise SC differences were found between each assistive level, except for levels 1.5 and 2 (level $0.5 > 1 > 1.5 = 2$).

DISCUSSION

This study investigated the effect of simulated slope resistance, gear ratio, and quantified assistive level on physiological, biomechanical, and subjective responses. In both slope conditions, the significant effects of gear ratio and assistance on physiological, biomechanical, and subjective responses were explored. The heavy gear ratio was associated with slight but significant lower METs and higher GE whereas did not influence the biomechanics and subjective responses. Increased assistive levels alleviated the METs, nHR, muscle activities and improved subjective responses but decreased GE. Furthermore, pairwise comparison between assistive levels of 1.5 and 2 in 1.0% slope conditions revealed that although there was a significant decrease in physiological load and muscle activity, limited improvement in subjective response might indicate the redundancy of assistive torque (**Figures 6A–E**).

Pedelec Parameters and the Integrated Responses

The pedelec parameters resulted in moderate to vigorous intensity levels (3.7 to 7.4 MET) within the simulated slope conditions in this study. Although comparison among previous studies was difficult due to the differences in pedelec model and route, Gojanovic and colleagues (Gojanovic et al., 2011) reported 7.3 METs on a hilly route (with an average grade of 3.4%) with the "standard" assistance mode, and Simons and colleagues

TABLE 5 | Coefficients (β), standard errors (SE), and *p*-values of subjective responses in 1.0% slope conditions.

	RPE			SC		
	β	SE	*p*	β	SE	*p*
Intercept	9.42	(0.51)	<0.001	2	(0.2)	<0.001
G						
Heavy	0.05	(0.28)	0.853	0.11	(0.18)	0.56
A						
0.5	1.11	(0.46)	0.016	0	(0.24)	1
1	0.16	(0.49)	0.747	−0.42	(0.25)	0.093
1.5	−0.21	(0.25)	0.406	−0.21	(0.16)	0.186
G × A						
H × 0.5	0.11	(0.46)	0.821	−0.16	(0.2)	0.431
H × 1	−0.16	(0.41)	0.7	0.05	(0.32)	0.869
H × 1.5	−0.42	(0.25)	0.093	−0.37	(0.33)	0.259

The condition with light gear ratio (G) and assistive level (A) of 2 served as reference. RPE: rating of perceived exertion.

TABLE 6 | Coefficients (β), standard errors (SE), and *p*-values of subjective responses in 2.5% slope conditions.

	RPE			SC		
	β	SE	*p*	β	SE	*p*
Intercept	9.47	(0.37)	<0.001	1.84	(0.13)	<0.001
G						
Heavy	0.26	(0.31)	0.853	−0.16	(0.17)	0.56
A						
0.5	4.32	(0.41)	<0.001	1.16	(0.28)	<0.001
1	2.16	(0.37)	<0.001	0.37	(0.19)	0.093
1.5	0.89	(0.36)	0.406	0	(0.2)	0.186
G × A						
H × 0.5	0.16	(0.39)	0.685	0.68	(0.21)	0.001
H × 1	0.16	(0.58)	0.786	0.58	(0.25)	0.021
H × 1.5	0.32	(0.56)	0.571	0.26	(0.27)	0.324

The condition with light gear ratio (G) and assistive level (A) of 2 served as reference.

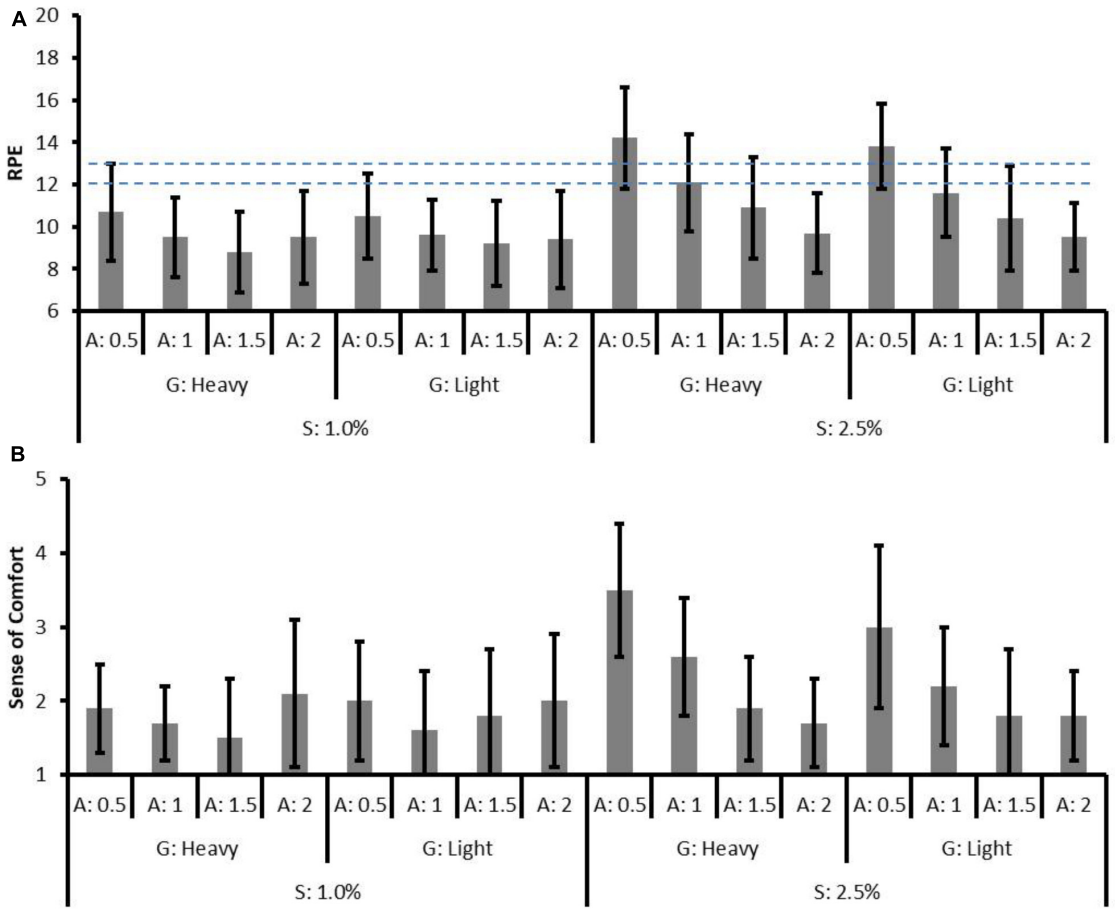

FIGURE 5 | The mean and standard deviation of **(A)** rate of perceived exertion (RPE) and **(B)** sense of comfort (SC) in all conditions. The horizontal dashed lines represent the upper and lower bound of moderate level defined by ACSM.

(Simons et al., 2009) reported 5.2 to 5.7 METs with "POW" and "ECO" mode on a flat route. The similar ranges of intensity would suggest the feasibility of slope simulation in this study. Likewise, despite the assistive power and the power output of the rider being rarely reported in the literature (Bulthuis et al., 2020), the assistive levels resulted in the averaged intensities of moderate and vigorous levels while no light level was shown, which also agreed with previous studies. This may further support the feasibility of the simulated pedelec riding as a standard test to evaluate the influences of a pedelec.

In **Figure 6**, the outcome measures are plotted against the normalized power output and the linear trends are presented in 2.5% slope conditions (black scatters). The power output changes due to assistive levels might explain the changes in physiological responses, muscle activity, and subjective responses. In 2.5% slope conditions, the lack of SC difference between assistive levels of 1.5 and 2 (**Figure 5A**) might be explained by few differences in power output. Taking a 70 kg adult as an example, the power output differences were only 14 W (the absolute power output with the assistive level of 1.5 is 70 kg × 0.99 W/kg = 69.3 W and with the assistive level of 2 is 70 kg × 0.79 W/kg = 55.3 W, respectively). Indeed, the15 W difference, as reported by Louis et al. (2012), was associated with no significant RPE difference in untrained participants. Similar results can be found in 1.0% slope conditions while assistive level of 0.5 (that resulted in 70 kg × 1.02 W/kg = 71.4 W power output) and assistive level of 1 (70 kg × 0.75 W/kg = 52.5 W) were used. Furthermore, despite the significant decreases in METs, nHR, and muscle activities were presented as the assistive level increased, RPE and SC showed a non-linear trend in 1.0% slope conditions. In the low-power output conditions (e.g., 1.0% slope, assistive levels of 1, 1.5, and 2), a non-significant decrease in RPE indicated that the assistive torque no longer generates subjective benefits. Moreover, the significantly worsen SC [increase in scores from 1.66 ± 0.14 (assistive level of 1.5) to 2.05 ± 0.2 (level 2), pairwise $p = 0.017$, **Figure 6**] might reflect the negative impact of high assistance in the low pedal-torque demand conditions. The limited subjective improvement in this study could be partly explained by the simultaneous decreases in GE (**Figure 6**). In this study, the GE increased with the power output and a positive relationship can be observed as found in professional cyclists (Chavarren and Calbet, 1999). In reverse, a systematic GE decreased (from 17.8 to 12.0%) with the decreased power output under different levels of assistance. The lower GE in

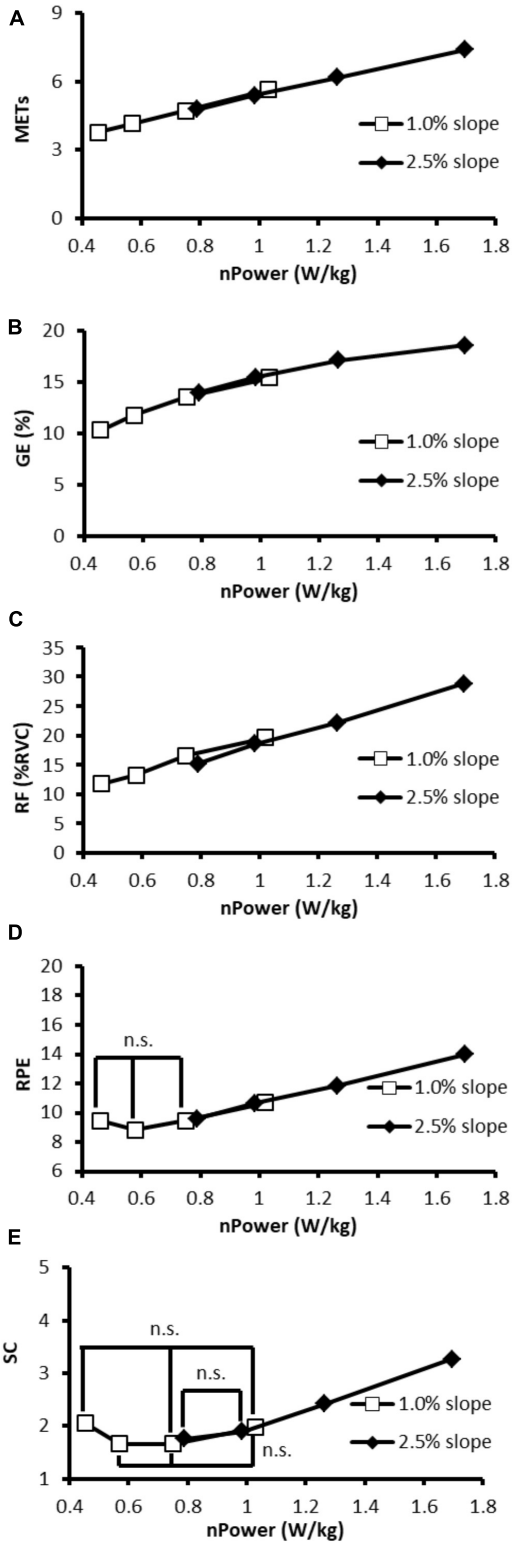

FIGURE 6 | The relationship between **(A)** MET, **(B)** GE, **(C)** RF, **(D)** RPE, **(E)** SC, and the normalized power output. Data from heavy and light gear ratios are averaged. Pairwise differences existed between assistive levels except for the non-significant (n.s.) marked conditions. nHR, VL, and VM were omitted due to the similar patterns were presented.

the low-power output demand conditions might suggest that bioenergy was still consumed elsewhere (e.g., moving limbs) rather than generating power. Indeed, some of the participants verbally reported that excessive assistance caused difficulties in keeping the specific riding speed, and this might support the corresponding non-significant changes in the subjective response between assistive levels of 1, 1.5, and 2.

Using the heavy gear ratio induced a slight but statistically significant decrease in METs and an increase in GE. This finding might explain the adoption of the heavier gear ratio in previous studies (Simons et al., 2009; Gojanovic et al., 2011). Theoretically, using the light gear ratio decreased the required pedal-torque whereas it increased the required pedal cadence to maintain the same speed (10 more revolutions per minute). Although the muscle activity was not significantly affected by the differences in the required pedal-torque, the increased need for cadence might be the cause of the slight but significant increases in MET and decreases in GE. This might indicate that only a small portion of bioenergy was saved due to the decreased torque, but a relatively larger portion of bioenergy was still consumed in performing the additional limb movements. Meanwhile, muscular co-activation, frictions/viscous resistance of the joint cartilage, the ligaments, and the tendons may account for the slightly higher MET (Chavarren and Calbet, 1999; Louis et al., 2012).

Pedelec Parameter Selection and Riding Intensity Control

Previous studies have recognized the health benefits of pedelec riding, and moderate exercise intensity has been suggested to ensure the benefits. The lowest intensity (3.7 METs) as found in the condition of 1.0% slope and assistive level of 2, fulfills the requirement of moderate-intensity (3 METs), and it is predictable that greater assistive levels would further decrease physiological and biomechanical intensity according to the linear relationship in **Figure 6**. However, the larger battery capacity and the greater electric assistance would annihilate the health-improving characteristics of pedelec riding (Gojanovic et al., 2011). Moreover, the limited effect and the negative effect of assistance in RPE and SC are foreseeable according to the findings from 1.0% slope conditions. Overall, moderate intensity can be achieved *via* pedelec parameter adjustments on different slopes. Simons et al. (2009) recommended that commuters use adequate assistance to prevents sweating on their way to work whereas use less assistance on the way home to gain training benefits. From the present findings, a more detailed suggestion can be made based on the integrated evaluation: choosing the pedelec parameters that result in about 50 rpm cadence and at least 0.75 W/kg power output to obtain physiological advantages and the acceptable subjective feeling while preventing battery energy wasting.

These findings can be applied to various fields without the constraints of specific pedelec models or test conditions. The exercise intensity could be controlled by changing the gear ratio and assistive level for the riders (Bulthuis et al., 2020). Based on **Figure 6**, the concept of intensity control can be supported by the overlapped portion of the two linear relationships of 1.0 and

2.5% slopes in which similar physiological, biomechanical, and subjective responses can be observed. It suggested the possibility of automatic assistance adjustment and exercise intensity control *via* a real-time algorithm to simplify pedelec operating and to achieve the fitness goals effectively. Future studies could address the assistance demand for the unfit, elderly, or disordered populations, whose demands may differ from the commuters. Moreover, establishing a personalized assistance control strategy that best meets the demands of an individual in various situations would be beneficial to the field.

Limitations

Although the full-factorial experiment design is ideal for assessing the effects of all related factors thoroughly, several factors were not involved due to a considerable amount of tests that would be combined in testing limitations. For example, the effect of pedelec weight was not evaluated due to relatively less influence in slope resistance and rolling resistance, and a representative value, 16 kg, was adopted. Furthermore, the riding speed was not manipulated in this study, but the riding speed of 21 $km{\cdot}h^{-1}$ was specified to make our result comparable to the previous studies (Louis et al., 2012; Boele-Vos et al., 2017). The other limitation is the possible effect of fatigue in the high-power output demand conditions. Although the EMG data from the last 10 cycles enabled the comparison among the test conditions, the evaluation of fatigue within each test was not available. The changes in muscle activity in each condition might also provide important information that is related to the optimization of user experience.

CONCLUSION

We proposed an integrated evaluation method that enables the analysis of the responses under various riding conditions. The effects of simulated slope, gear ratio, and numeric assistive level affected power output and the consequent physiological, biomechanical, and subjective responses. The pedelec parameters and the simulated slope resistance resulted in moderate to vigorous METs. In the low power, output demand conditions, increased assistive levels significantly decreased the MET, nHR, and muscle activities without improving the subjective feelings. For the pedelec commuters, riding with at least 0.75 W/kg resultant power output with about 50 rpm cadence is recommended to obtain the moderate intensity and the optimum subjective feelings. It is worth mentioning that preventing battery energy-wasting and releasing range anxiety might be the additional benefits of the recommended parameters.

DATA AVAILABILITY STATEMENT

The raw data supporting the conclusions of this article will be made available by the authors, without undue reservation.

ETHICS STATEMENT

The studies involving human participants were reviewed and approved by the Ethics Committee of the National Tsing Hua University (REC: 10811HE094). The patients/participants provided their written informed consent to participate in this study.

AUTHOR CONTRIBUTIONS

S-CY and Y-JL conceived of the presented idea. S-CY carried out the experiment. S-CY wrote the manuscript with support from Y-JL. Y-JL supervised the findings of this work and edited the final manuscript. The authors discussed the results and contributed to the final manuscript. All authors contributed to the article and approved the submitted version.

REFERENCES

Abbiss, C. R., Peiffer, J. J., and Laursen, P. B. (2009). Optimal cadence selection during cycling: review article. *Int. SportMed J.* 10, 1–15.

Ba Hung, N., Jaewon, S., and Lim, O. (2017). A study of the effects of input parameters on the dynamics and required power of an electric bicycle. *Appl. Energy* 204, 1347–1362. doi: 10.1016/j.apenergy.2017.03.025

Berntsen, S., Malnes, L., Langaker, A., and Bere, E. (2017). Physical activity when riding an electric assisted bicycle. *Int. J. Behav. Nutr. Phys. Act.* 14:55.

Bini, R., Wundersitz, D., and Kingsley, M. (2019). Biomechanical and physiological responses to electrically assisted cycling during simulated mail delivery. *Appl. Ergon.* 75, 243–249. doi: 10.1016/j.apergo.2018.11.004

Boele-Vos, M. J., Commandeur, J. J. F., and Twisk, D. A. M. (2017). Effect of physical effort on mental workload of cyclists in real traffic in relation to age and use of pedelecs. *Accid. Anal. Prev.* 105, 84–94. doi: 10.1016/j.aap.2016.11.025

Borg, G. A. (1982). Psychophysical bases of perceived exertion. *Med. Sci. Sports Exerc.* 14, 377–381.

Bourne, J. E., Cooper, A. R., Kelly, P., Kinnear, F. J., England, C., Leary, S., et al. (2020). The impact of e-cycling on travel behaviour: a scoping review. *J. Transp. Health* 19:100910. doi: 10.1016/j.jth.2020.100910

Bulthuis, R., Tabak, M., Schaake, L., and Hermens, H. (2020). Outdoor E-trike cycling: a low intensity physical activity. *Assist. Technol.* 1–8. [Epub ahead of print] doi: 10.1080/10400435.2020.1858995

Candotti, C. T., Loss, J. F., Bagatini, D., Soares, D. P., Da Rocha, E. K., De Oliveira, A. R., et al. (2009). Cocontraction and economy of triathletes and cyclists at different cadences during cycling motion. *J. Electromyogr. Kinesiol.* 19, 915–921. doi: 10.1016/j.jelekin.2008.04.008

Chavarren, J., and Calbet, J. A. (1999). Cycling efficiency and pedalling frequency in road cyclists. *Eur. J. Appl. Physiol. Occup. Physiol.* 80, 555–563.

De Geus, B., Kempenaers, F., Lataire, P., and Meeusen, R. (2013). Influence of electrically assisted cycling on physiological parameters in untrained subjects. *Eur. J. Sport Sci.* 13, 290–294. doi: 10.1080/17461391.2011.606845

De Koning, J. J., Noordhof, D. A., Lucia, A., and Foster, C. (2012). Factors affecting gross efficiency in cycling. *Int. J. Sports Med.* 33, 880–885. doi: 10.1055/s-0032-1306285

Debraux, P., Grappe, F., Manolova, A. V., and Bertucci, W. (2011). Aerodynamic drag in cycling: methods of assessment. *Sports Biomech.* 10, 197–218.

Garber, C. E., Blissmer, B., Deschenes, M. R., Franklin, B. A., Lamonte, M. J., Lee, I.-M., et al. (2011). Quantity and quality of exercise for developing and maintaining cardiorespiratory, musculoskeletal, and neuromotor fitness in apparently healthy adults: guidance for prescribing exercise. *Med. Sci. Sports and Exerc.* 43, 1334–1359. doi: 10.1249/MSS.0b013e318213fefb

Gojanovic, B., Welker, J., Iglesias, K., Daucourt, C., and Gremion, G. (2011). Electric bicycles as a new active transportation modality to promote health. *Med. Sci. Sports Exerc.* 43, 2204–2210. doi: 10.1249/MSS.0b013e31821cbdc8

Hendriksen, I. J., Zuiderveld, B., Kemper, H. C., and Bezemer, P. D. (2000). Effect of commuter cycling on physical performance of male and female employees. *Med. Sci. Sports Exerc.* 32, 504–510. doi: 10.1097/00005768-200002000-00037

Hermens, H. J., Freriks, B., Disselhorst-Klug, C., and Rau, G., (2000). Development of recommendations for SEMG sensors and sensor placement procedures. *J. Electromyog. Kinesiol.* 10, 361–374

Langford, B. C., Cherry, C. R., Bassett, D. R., Fitzhugh, E. C., and Dhakal, N. (2017). Comparing physical activity of pedal-assist electric bikes with walking and conventional bicycles. *J. Transp. Health* 6, 463–473. doi: 10.1016/j.jth.2017.06.002

Louis, J., Brisswalter, J., Morio, C., Barla, C., and Temprado, J. J. (2012). The electrically assisted bicycle: an alternative way to promote physical activity. *Am. J. Phys. Med. Rehabil.* 91, 931–940. doi: 10.1097/PHM.0b013e318269d9bb

Lucía, A., Hoyos, J., and Chicharro, J. L. (2001). Preferred pedalling cadence in professional cycling. *Med. Sci. Sports Exerc.* 33, 1361–1366. doi: 10.1097/00005768-200108000-00018

Oja, P., Titze, S., Bauman, A., De Geus, B., Krenn, P., Reger-Nash, B., et al. (2011). Health benefits of cycling: a systematic review. *Scand. J. Med. Sci. Sports* 21, 496–509. doi: 10.1111/j.1600-0838.2011.01299.x

Pallarés, J. G., and Lillo-Bevia, J. R. (2018). Validity and reliability of the PowerTap P1 pedals power meter. *J. Sports Sci. Med.* 17, 305–311.

Peterman, J. E., Morris, K. L., Kram, R., and Byrnes, W. C. (2016). Pedelecs as a physically active transportation mode. *Eur. J. Appl. Physiol.* 116, 1565–1573. doi: 10.1007/s00421-016-3408-9

Schäfer, C., Mayr, B., Fernandez La Puente De Battre, M. D., Reich, B., Schmied, C., Loidl, M., et al. (2020). Health effects of active commuting to work: the available evidence before GISMO. *Scand. J. Med. Sci. Sports* 30 Suppl 1, 8–14. doi: 10.1111/sms.13685

Simons, M., Van Es, E., and Hendriksen, I. (2009). Electrically assisted cycling: a new mode for meeting physical activity guidelines? *Med. Sci. Sports Exerc.* 41, 2097–2102. doi: 10.1249/MSS.0b013e3181a6aaa4

Sinclair, J., Taylor, P. J., Hebron, J., Brooks, D., Hurst, H. T., and Atkins, S. (2015). The reliability of electromyographic normalization methods for cycling analyses. *J. Hum. Kinet.* 46, 19–27. doi: 10.1515/hukin-2015-0030

Sperlich, B., Zinner, C., Hebert-Losier, K., Born, D. P., and Holmberg, H. C. (2012). Biomechanical, cardiorespiratory, metabolic and perceived responses to electrically assisted cycling. *Eur. J. Appl. Physiol.* 112, 4015–4025. doi: 10.1007/s00421-012-2382-0

van Bekkum, J. E., Williams, J. M., and Graham Morris, P. (2011). Cycle commuting and perceptions of barriers: stages of change, gender and occupation. *Health Educ.* 111, 476–497. doi: 10.1108/09654281111180472

Warburton, D. E. R., Jamnik, V., Bredin, S. S. D., Shephard, R. J., and Gledhill, N. (2018). The 2019 physical activity readiness questionnaire for everyone (PAR-Q+) and electronic physical activity readiness medical examination (ePARmed-X+): 2019 PAR-Q+. *Health Fit. J. Canada* 11, 80–83.

Watson, G., and Swensen, T. (2006). Effects of altering pedal cadence on cycling time-trial performance. *Int. J. Sports Med.* 27, 296–300. doi: 10.1055/s-2005-865654

Wright, J., Walker, T., Burnet, S., and Jobson, S. A. (2019). The reliability and validity of the PowerTap P1 power pedals before and after 100 hours of use. *Int. J. Sports Physiol. Perform.* 14, 855–858. doi: 10.1123/ijspp.2018-0563

Conflict of Interest: The authors declare that no financial and personal relationships with other people or organizations have inappropriately influenced the content of the work reported in this manuscript.

Publisher's Note: All claims expressed in this article are solely those of the authors and do not necessarily represent those of their affiliated organizations, or those of the publisher, the editors and the reviewers. Any product that may be evaluated in this article, or claim that may be made by its manufacturer, is not guaranteed or endorsed by the publisher.

frontiers in Human Neuroscience

ORIGINAL RESEARCH
published: 16 December 2021
doi: 10.3389/fnhum.2021.809544

Symptom Locus and Symptom Origin Incongruity in Runner's Dystonia – Case Study of an Elite Female Runner

Issei Ogasawara[1], Noriaki Hattori[2], Gajanan S. Revankar[1,3], Shoji Konda[1], Yuki Uno[1], Tomohito Nakano[4], Yuta Kajiyama[4,5], Hideki Mochizuki[4]* and Ken Nakata[1]**

[1] Department of Health and Sport Sciences, Graduate School of Medicine, Osaka University, Osaka, Japan, [2] Department of Rehabilitation, Faculty of Medicine, Academic Assembly, University of Toyama, Toyama, Japan, [3] Institute for Transdisciplinary Graduate Degree Programs, Osaka University, Osaka, Japan, [4] Department of Neurology, Graduate School of Medicine, Osaka University, Osaka, Japan, [5] Department of Neurology, Sakai City Medical Center, Osaka, Japan

OPEN ACCESS

Edited by:
Ramona Ritzmann, Clinic Rennbahn AG, Switzerland

Reviewed by:
Carlos Henrique Ferreira Camargo, Federal University of Paraná, Brazil
Shiro Horisawa, Tokyo Women's Medical University, Japan

***Correspondence:**
Issei Ogasawara
ogasawaraissei@hss.osaka-u.ac.jp
Hideki Mochizuki
hmochizuki@neurol.med.osaka-u.ac.jp
Ken Nakata
ken.nakata@hss.osaka-u.ac.jp

Specialty section:
This article was submitted to Motor Neuroscience, a section of the journal Frontiers in Human Neuroscience

Received: *05 November 2021*
Accepted: *24 November 2021*
Published: *16 December 2021*

Citation:
Ogasawara I, Hattori N, Revankar GS, Konda S, Uno Y, Nakano T, Kajiyama Y, Mochizuki H and Nakata K (2021) Symptom Locus and Symptom Origin Incongruity in Runner's Dystonia – Case Study of an Elite Female Runner. Front. Hum. Neurosci. 15:809544. doi: 10.3389/fnhum.2021.809544

Objectives: Runner's dystonia is a task-specific dystonia that occurs in the lower limbs and trunk, with diverse symptomatology. We aimed to identify the origin of a dystonic movement abnormality using combined three-dimensional kinematic analysis and electromyographic (EMG) assessment during treadmill running.

Participant: A 20-year-old female runner who complained of right-foot collision with the left-leg during right-leg swing-phase, which mimicked right-ankle focal dystonia.

Results: Kinematic and EMG assessment of her running motion was performed, which showed a significant drop of the left pelvis during right-leg stance-phase, and a simultaneous increase of right hip adductor muscle activity. This resulted in a pronounced adduction of the entire right lower limb with respect to the pelvis segment. Trajectories of right foot were seen to encroach upon left-leg area.

Discussion: These findings suggested that the symptom of this runner was most likely a form of segmental dystonia originating from an impaired control of hip and pelvis, rather than a distal focal ankle dystonia.

Conclusion: We conclude that, for individualized symptom assessment, deconstructing the symptom origin from its secondary compensatory movement is crucial for characterizing dystonia. Kinematic and EMG evaluation will therefore be a prerequisite to distinguish symptom origin from secondary compensatory movement.

Keywords: movement disorder, task-specific focal dystonia, involuntary movement, motion capture system, electromyography, female athlete, yips, running

INTRODUCTION

Focal task-specific dystonia (FTSD) is a type of movement disorder that results in an abnormal involuntary muscle contraction of a focal body part during a specific well-learned task (Stahl and Frucht, 2017). FTSD has been frequently observed as writer's cramps or musician's dystonia in literature (Frucht, 2004; Goldman, 2015). One little-known phenomenon is runner's dystonia

(RD), symptoms characterized by an involuntary lower limb movement during running such as toe clawing/extension, ankle supination/inversion/eversion, and knee hyperextension (Leveille and Clement, 2008; Martino et al., 2009; Cutsforth-Gregory et al., 2016; Ahmad et al., 2018). When severe, the symptom also occurs during walking (Wu and Jankovic, 2006; McClinton and Heiderscheit, 2012; Cutsforth-Gregory et al., 2016). Foot and the lower limb muscles are commonly affected (Leveille and Clement, 2008), which may spread to the pelvis and trunk (Suzuki et al., 2011; Cutsforth-Gregory et al., 2016; Ahmad et al., 2018). Runners older than 40 years of age or those trained for a long time tend to suffer from this symptom (Schneider et al., 2006; Wu and Jankovic, 2006; Ramdhani and Frucht, 2013; Ahmad et al., 2018).

Routinely, surface electromyography (EMG) and X-ray/magnetic resonance imaging (MRI) of the lower limb are performed to identify abnormalities in the musculature or to explore a secondary basis including musculoskeletal problems (Schneider et al., 2006; McClinton and Heiderscheit, 2012; Ahmad et al., 2018). Most cases of RD are not associated with family history of movement disorders wherein genetic testing is performed to rule out DYT-1 phenotype dystonia (Schneider et al., 2006; Cutsforth-Gregory et al., 2016; Ahmad et al., 2018). Imaging of brain and spinal cord using MRI is frequently normal in most cases (Wu and Jankovic, 2006; McClinton and Heiderscheit, 2012). Visual inspections or offline video observation are often performed to investigate abnormal movement patterns (Schneider et al., 2006; McClinton and Heiderscheit, 2012). Very few studies have applied detailed motion capture assessment to quantify the joint kinematics associated with the RD symptoms (McClinton and Heiderscheit, 2012; Ahmad et al., 2018). Since RD is a rare pathology relative to the upper limb's dystonia (Wu and Jankovic, 2006; Leveille and Clement, 2008; Martino et al., 2009) and the kinematic or muscle activity patterns are known to vary widely even among the small number of reported cases (Wu and Jankovic, 2006; Cutsforth-Gregory et al., 2016; Ahmad et al., 2018), the localization of symptomatic origin is therefore a diagnostic challenge.

Recently, a 20-year-old female elite runner presented to us with an abnormal, involuntary, right-ankle movement, consistently occurring during shoed running. Following examination by a general physician, she was diagnosed with RD of the right ankle and advised exercise-based physiotherapy for the right ankle. However, this physiotherapy intervention was unsuccessful. Since her problems persisted without relief, she was then referred to our department at Osaka University for a detailed evaluation of the problem.

To address and manage the athlete's condition, we at Osaka University performed a dynamic evaluation of her running movement pattern using joint kinematics and surface EMG. Previous descriptive case studies have outlined movement pattern estimation mainly by visual inspection or by offline video observation (Schneider et al., 2006; Stan et al., 2020; Lee et al., 2021). However, subjective visual judgment of lower limb kinematics results in an inaccurate estimation of joint angles (Krosshaug et al., 2007), given that the resolution of visual observation is imprecise to identify the targeted motion of RD athletes. Therefore, a high-resolution objective measure such as the motion capture system combined with the dynamic surface EMG assessment was speculated to be ideal for an accurate quantification of the athlete's spatiotemporal running patterns (Karp and Alter, 2017; Ahmad et al., 2018).

With respect to motion analysis, it is crucial to justify what an "abnormal" running pattern is. Given that movement patterns of RD patients are highly individualistic and stereotyped, we performed detailed, athlete-specific motion capture evaluation characterizing involved-uninvolved limb asymmetry that would define abnormal limb control. To that end, the aim of our study was to report the case of an athlete with lower limb task-specific dystonia to clarify spatiotemporal joint kinematics and dynamic surface EMG patterns of lower limb muscles to pinpoint symptom origin and explore whether the side-to-side limb asymmetry was localized only at the ankles. To define these changes within this athlete, we employed a sensitive statistical technique known as one-dimensional statistical parametric mapping (SPM) (Pataky et al., 2013) to explore the spatiotemporal asymmetries of truncal and lower limb kinematics and their associated EMG patterns during cyclic walking and running conditions. We hypothesized that the SPM comparison between affected and unaffected lower limbs as well as pelvic movement in running would reveal abnormal kinematic and EMG patterns to characterize the dystonic features in this runner.

METHOD

Ethical Considerations

This study was approved by the ethics review board of Osaka University Hospital (14250). Written informed consent was obtained from the athlete before data collection. Consent for publication was also obtained from this athlete.

Patient Description

The patient was a 20-year-old female elite long-distance runner. Her first symptom appeared when she was around 18 years old. She gave a history that only during forward running, the medial side of her right forefoot collided with the medial aspect of the left calf during the right-leg swing-phase (see **Supplementary Video**). She was able to walk forward, backward, and sideways normally. Brain, spinal cord, and lower-limb MRI were characteristically normal. The cerebrospinal fluid examination also showed no findings to suggest any phenotypes of genetic dystonia. She had a normal motor development in her childhood. No family histories were identified for any movement disorders.

Preparation for Motion Analysis

The motion-capture analysis for the athlete was performed at Osaka University 2 years and 4 months after the first diagnosis of RD in ankle elsewhere. The athlete wore a black-colored spandex shirt and pants with her own running shoes (Tarther Japan Black 1013A007, ASICS, Japan). Forty reflective markers were attached to the body landmarks (**Table 1**) and four marker-cluster

TABLE 1 | Maker name and position.

Marker Name	Side	Position	Remove
TOE	Both	Anterior tip of shoe sole, 1 cm above from shoe sole surface.	
MMP	Both	Aiming at the head of first metatarsal bone on the shoe.	*
LMP	Both	Aiming at the head of fifth metatarsal bone on the shoe.	
FBC	Both	Aiming at base of third metatarsal bone on the shoe.	
CAL	Both	Most posterior edge of shoe heel wedge, 1 cm above shoe sole surface.	
MAKL	Both	Most prominent point of medial malleolus.	*
LAKL	Both	Most prominent point of lateral malleolus.	
MKNEE	Both	Most prominent point of medial femoral epicondyle.	*
LKNEE	Both	Most prominent point of lateral femoral epicondyle.	
TTB	Both	On the mid of tibial tuberosity.	
ATH	Both	Anterior aspect of thigh segment, approximately mid-way of hip and knee joint.	
GT	Both	Most laterally prominent point of great trochanter.	
ASIS	Both	Most prominent point of anterior superior iliac spine.	
PSIS	Both	Most prominent point of posterior superior iliac spine.	
SCRM	Center	On the mid of sacrum.	
STRN	Center	On the top edge of sternum.	
C7	Center	Most prominent point of seventh cervical spinous process.	
SHD	Both	Most prominent point of acromion process.	
ELB	Both	Most prominent point of the lateral humeral epicondyle.	
WRIST	Both	Most prominent point of the ulnar styloid process.	
HND	Both	On the head of third metacarpal bone.	
HEAD	Center	Tip of head.	

*Remove * – Markers were removed after static calibration trial since those markers were potentially problematic due to foot collision symptom. The position of the removed marker was reconstructed by information of marker clusters or other markers on the same segment.*

plates with three reflective makers on each were placed on both side thigh and shank segments for the optical motion analysis. After skin preparation, the wireless surface EMG sensors (Trigno Avanti system, Delsys, Inc., United States) were fixed to vastus medialis (VM), semitendinosus (ST), gluteus medius (GM), hip adductor longus (HAL), tibialis anterior (TA), and lateral head of gastrocnemius (GC) of both legs. The sensors were firmly covered with the elastic tape to minimize movement artifacts. To protect the damage of foot collision, the posterior aspect of left calf was covered with the elastic tape. The athlete wore safety harness to prevent falling. We ascertained that the harness did not impede her locomotion. The static posture trial was captured with full maker set calibration, and then some markers (see **Table 1**) were removed before treadmill trials.

Treadmill Walking and Running Trial

The athlete was asked to perform a walking to running task on the electric treadmill (MYRUN model: DCKN1B, Technogym S.p.A, Italy). A total of six trials were performed. Each trial lasted approx 2.5 min long. The athlete initially took a static pose on the treadmill, then gradually increased the speed of the treadmill to 6.0 km/h by herself, and performed fast walking for about 50 steps. When cued by the experimenter, the athlete started to run at the same speed and performed another 60 running steps. The running speed of 6.0 km/h was the lowest speed to induce her symptom. To measure the athlete's natural performance, no specific instructions were given on how to walk and run. The athlete was allowed to stop running at any time she felt sustained running would be injurious.

Data Collection

The 3D positions of the body markers were captured with the 12 optical cameras (OptiTrack Prime 17W, Software: Motive version 1.9, NaturalPoint, Inc., United States) with a sampling frequency of 360 Hz. The EMG signals from the selected muscles were sampled at 2,000 Hz with the Delsys Trigno Avanti sensors and measured using LabChart version 8.0.9 (ADInstruments, United States). A clock device (eSync2, NaturalPoint, Inc., United States) was used to synchronize the OptiTrack and LabChart. For offline visual inspection, video recordings from the rear and on the right side of the athlete were taped (HDR-PJ800, 30 fps, SONY, Japan). The EMG signal during the maximum voluntary contraction (MVC) test (two repetitions of 2 s MVC for each muscle with intensive verbal encouragement) was collected for offline signal normalization.

Data Analysis and Assessment Variables

Offline data analysis was performed with custom scripts written in Scilab 6.01 (ESI Group, France). The motion capture data were smoothed with the second-order Butterworth digital filter (low-pass, zero-lag, cutoff-frequency of 10 Hz). Since the athlete was a typical heel-first contact runner, the timing of heel contact (HC) was identified as the local minimums observed in the vertical component of the heel marker "CAL." The timing of toe-off (TO) was judged when the first increase of vertical component of the toe-marker "TOE" appeared after HC. One gait cycle was defined as the period from the previous HC to the next HC for each leg. Data for one gait cycle was normalized to 101 data points (0–100%). One gait cycle was consisted of the stance-phase (HC to TO) followed by the swing-phase (TO to the next HC).

The seven-link kinematic model, consisting of both feet, shanks, thighs, and one pelvis segment, was constructed using the time-normalized marker data. The local coordinate system was defined for each segment. For the kinematic assessment of athlete movement, hip adduction(+)/abduction(−), hip flexion(+)/extension(−), hip internal(+)/external(−) rotation, knee flexion(+)/extension(−), ankle adduction(+)/abduction(−), and ankle dorsi(+)/planter(−) flexion were calculated as time-series kinematic variables. To evaluate the contralateral pelvis-drop at the stance-phase, we calculated the local minimum of the vertical component of both-side ASIS markers during one gait cycle (the lowest value occurred in one gait cycle) was determined and was offset with the static trial. To visualize the three-dimensional (3D) foot trajectory relative to the pelvis segment,

the position vector going from the center of pelvis segment (midpoint of two ASIS and two PSIS markers) to the center of foot segment (FBC marker) was calculated and expressed with the pelvis coordinate system. To quantify the severity of right-foot collision to the left calf, the distance from the right-foot's FBC marker and the left shank segment (e.g., foot-calf distance) was calculated based on the measured marker data. The simulated foot-calf distance was also calculated assuming that the right-ankle position was maintained appropriately with respect to the left-ankle position (assuming that there was no side-to-side difference in the ankle position).

Electromyographic signals during trials were high-pass filtered (5 Hz), full-wave rectified, and low-pass filtered (10 Hz) with a second-order zero-lag Butterworth digital filter to obtain enveloped signals. The same procedure was applied to the MVC trials, and the peak MVC value was detected for each muscle. EMG signals during trials were normalized to the peak MVC values (%MVC). Single gait/running cycle EMG data were also time normalized to 101 data points synchronizing with motion capture data.

Statistical Analysis

To assess the side-to-side difference of the stance-phase and one gait cycle durations, paired *t*-test was conducted ($p < 0.01$). For the time-series kinematic and EMG data, 40 cycles for walking and 50 cycles for running sequences were used to condense the movement features for each leg. The ensemble averages and standard deviations (SD) of 40-cycle walking and 50-cycle running data were input into one-dimensional paired statistical parametric mapping (1D SPM) technique (Pataky et al., 2013) to test the temporal side-to-side differences. This ensemble procedure provided enough statistical power to detect any side-to-side difference during cyclic movement. The alpha level for SPM analysis was adjusted to 0.0017 (=0.01/6) for six component comparisons (Robinson et al., 2014). When the SPM test detected significant side-to-side difference in a certain duration within one

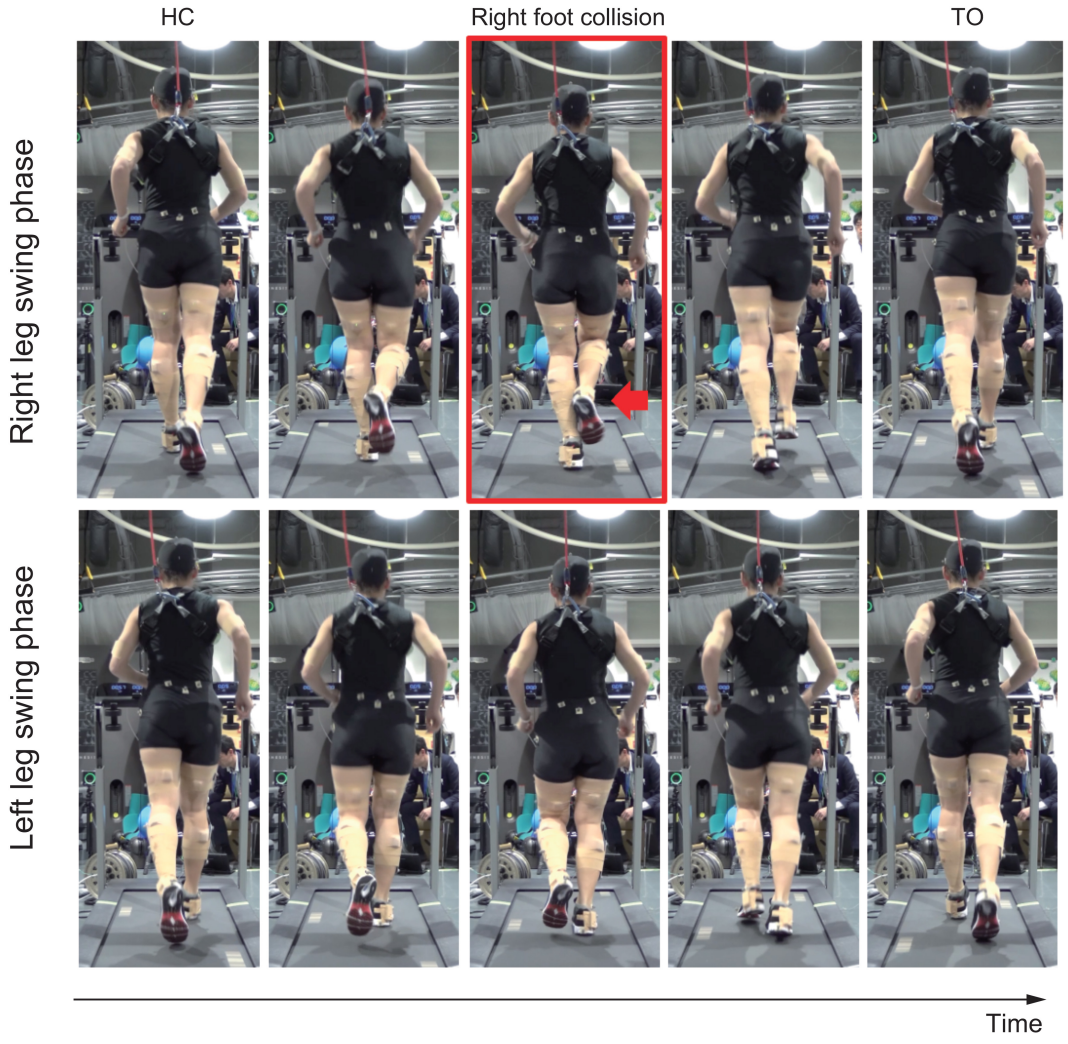

FIGURE 1 | Rear view of the running movement. Upper row shows right leg swing-phase, and lower row shows left leg swing-phase. Red arrow in the red squared panel shows right foot collision with the left calf.

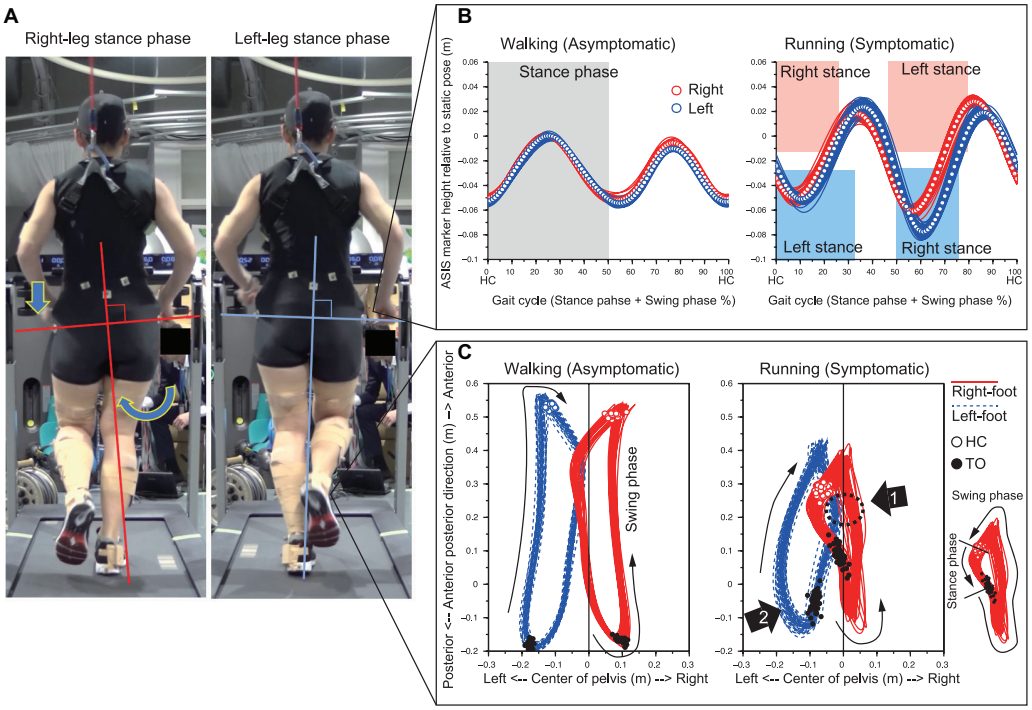

FIGURE 2 | Prominent left pelvis-drop observed during right-leg stance-phase **(A)**. The temporal change of the ASIS markers height illustrated that left pelvis-drop only occurred during right-leg stance-phase of running **(B)**. The top view of 3D trajectory of foot segment with respect to the pelvis coordinate system showed that right-foot trajectory medially shifted and impinged with left-leg area (Arrow 1). The left leg in turn circumducted to escape from right foot interference (Arrow 2) **(C)**.

gait cycle, the effect size (Cohen's *d*) averaged over the significant duration was calculated. All SPM analyses were implemented using the open-source spm1d code[1] in Python 3.6.3.

RESULTS

Since all trials (= 6) showed consistent features, the results of an illustrative third trial are described below.

Characteristics of Symptom From Video Observation

The medial side of the right foot collided with the calf of the left leg during the right-leg swing-phase in running (**Figure 1** and see **Supplementary Video**). The foot collision consistently occurred during running (53 times collisions in 60 steps), and this phenomenon was seen in only the right foot. The left pelvis-drop in the right-leg stance-phase was significantly greater than that of right pelvis-drop in the left-leg stance-phase (−0.06 (0.003) vs. −0.08 (0.00) m, $p < 0.05$). The large left pelvis-drop induced a medial shift of overall right lower limb segments with respect to the center of pelvis segment (**Figures 2A,B**). The top view of foot segment's trajectory with respect to the center line of the pelvis segment illustrated that despite symmetrical foot movement patterns seen during walking, significant side-to-side difference was observed while running. Overall, right foot trajectory was medially shifted and partially impinged with the left foot trajectory at mid-to-late swing-phase (**Figure 2C**, arrow 1). In contrast, the left foot trajectory was generally shifted laterally, and a prominent circumduction was found in the early swing-phase (**Figure 2C**, arrow 2).

Gait Cycle Temporal Asymmetry

In walking, the time required for one gait cycle was 0.88s (SD 0.01) for right and 0.88s (SD 0.01) for left leg of which the stance-phase was 0.51s (0.00) for right and 0.52s (0.01) for left leg, showing no statistical significance (**Figure 3**). In running, although the time taken for one gait cycle did not differ between limbs (0.71s [SD 0.01] vs. 0.71s [SD 0.01], $p > 0.05$), the stance-phase of right leg was significantly shorter than that of left leg (0.18s [SD 0.02] vs. 0.24s [SD 0.02], $p < 0.05$, **Figure 3**). Due to this phasic difference between limbs, note that both the stance-to-swing transition time and the foot collision time differed between limbs for 100% cycle representation.

Kinematic Characteristics

The side-to-side difference in the time-series kinematic data increased when the athlete started to run (**Figure 4**). For running data, as the stance-phase for right leg was shorter than that of left leg, the sagittal plane kinematics (knee extension/flexion, ankle plantar/dorsi flexion, and hip extension/flexion) showed phasic differences between limbs, i.e., an early initiation of knee flexion,

[1]www.spm1d.org

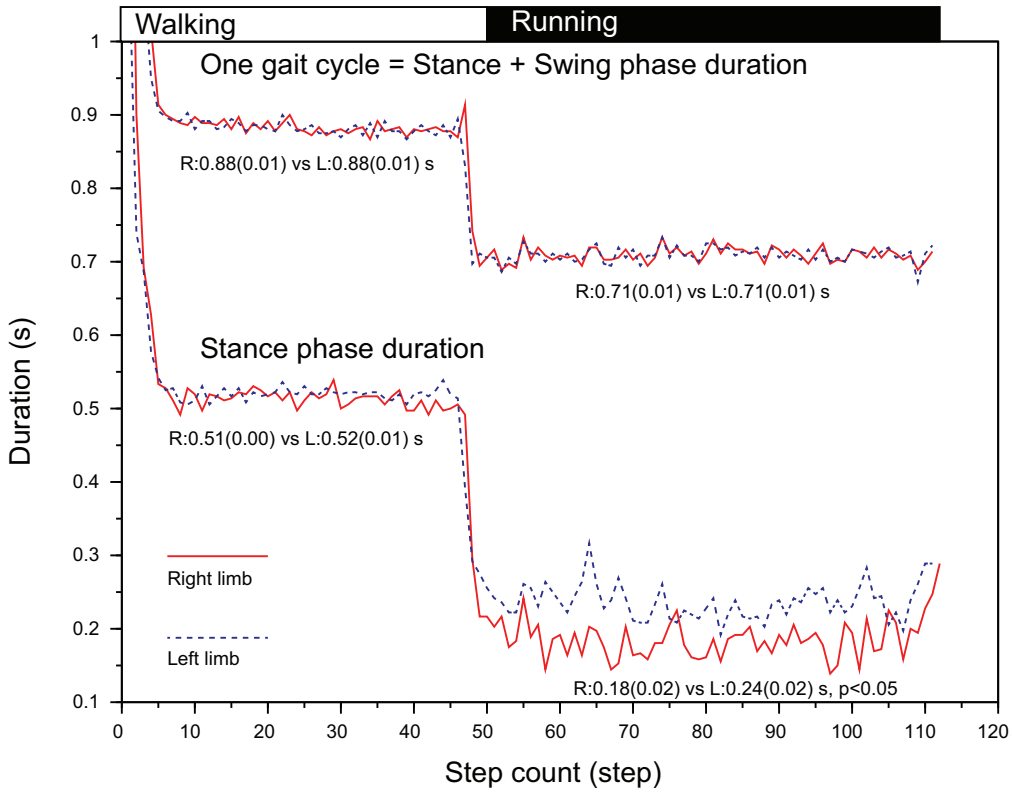

FIGURE 3 | Duration of one gait cycle (HC to HC interval) and stance-phase (HC to TO interval) from an illustrative trial. The stance-phase duration for **right** leg during running was significantly shorter than that of **left** leg. HC, heel contact; TO, toe off.

ankle dorsiflexion, and hip flexion for the right-leg from stance-to-swing transition (30% of gait cycle, **Figures 4G–I**). The right ankle was additionally abducted by approx. 7° and dorsiflexed by 10° at around the foot-collision phase as compared to the left ankle (**Figures 4H,J**).

The right hip was further adducted as compared to the left hip during stance-phase (0–30% of gait cycle, **Figure 4K**). Although the left hip showed a significantly greater abduction around 50–80% of gait cycle (around the time when the foot collided), the right hip did not show a prominent hip abduction (**Figure 4K**). The cycle-to-cycle variability for hip adduction/abduction angle was relatively small (**Figure 4K**). The hip rotation angle for right hip was more internally shifted throughout the cycle as compared to the left hip (**Figure 4L**). The left hip showed a rapid external rotation during 60–70% of gait cycle; however, the right hip did not show such an angular change (**Figure 4L**).

Results of simulation analysis of foot–calf distance, assuming the absence of 7° abduction and 10° dorsiflexion seen in the right ankle at foot collision phase (**Figures 4H,J**), indicated that right forefoot would have been about 2.5 cm closer to the left calf (**Figure 5**).

Electromyographic Characteristics

Consistent with the sagittal plane kinematic data, three muscles [vastus medialis (VM), semitendinosus (ST), and gastrocnemius (GC)] contributing to the sagittal plane kinematics showed slight advanced phasic shifts for right leg as compared to the left leg (**Figures 6G–I**) in running.

For running data, right VM showed a significantly greater activity from 40 to 100% gait cycle with the earlier occurrence pre-activation for subsequent HC at 100% (**Figure 6G**). Both STs showed a prominent activity at late swing-phase. Left ST showed a significantly greater activity than that of left leg from 80 to 95% of gait cycle (**Figure 6H**). GC activity initiated slightly before the heel contact (100%) and decreased as the stance-phase finished. Right GC activity was significantly smaller than that of left GC especially at the later part (push-off timing) of stance-phase (**Figure 6I**).

The right TA showed a significantly greater activity from 30 to 50% of gait cycle as compared to the left TA (**Figure 6J**). This time duration corresponded to the duration where the less planer-flexed right ankle was observed (**Figure 4H**).

A prominent increase of hip adductor muscle was observed at the stance-to-swing transition phase (around 20–40% of gait cycle) for both limbs, but the activity for the right hip adductor muscle was significantly greater than that of the left hip. The right hip adductor activation again increased around 65–85% with a significant difference relative to left hip adductor (**Figure 6K**). Gluteus Medius (GM) activity exhibited a prominent increase toward the heel contact for both limbs. Although right GM activity was significantly greater than that of left GM, right hip showed a significantly greater

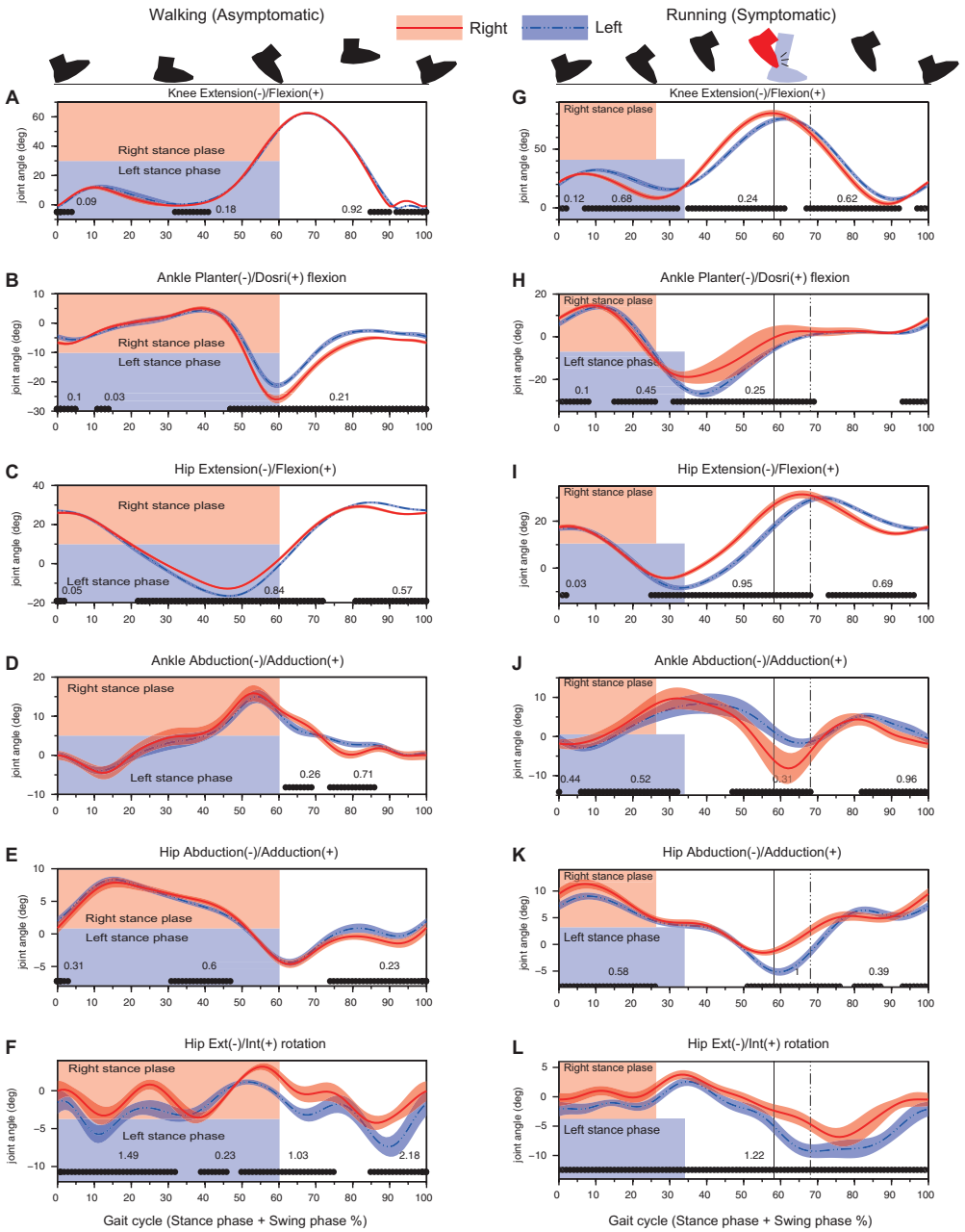

FIGURE 4 | Results of kinematic analysis during walking (left column) and running (right column) assessed by 1D SPM. Black lines with the Cohen's *d*-value at the horizontal axis of each panel showed significant difference between the right and left legs. Vertical lines denote the timing of foot collision for right leg (solid line) and for left leg (dashed line). Note that the percentage of the stance-phase and the foot collision time was different between the right and left legs in 100% gait cycle representation since the absolute stance-phase duration was significantly different between limbs (as shown in **Figure 3**).

hip adduction than that of left hip around the HC phase (**Figures 6L**, **2A,B**).

DISCUSSION

This is the first detailed attempt to quantify the spatiotemporal characteristics of an elite athlete with RD via advanced time-series analysis using motion capture and EMG data. This athlete presented with right-foot collision with the left calf during right-leg swing-phase. However, side-to-side differences were not limited only to the ankle, but was observed throughout the leg. Her lower limb kinematics revealed that there was an asymmetric left pelvic-drop synchronized with an increased right-hip adductor burst, resulting in a medially shifted right-leg trajectory enough to interfere the contralateral left-leg space (**Figures 1–4**). These findings allowed us to contemplate that the right-foot collision was

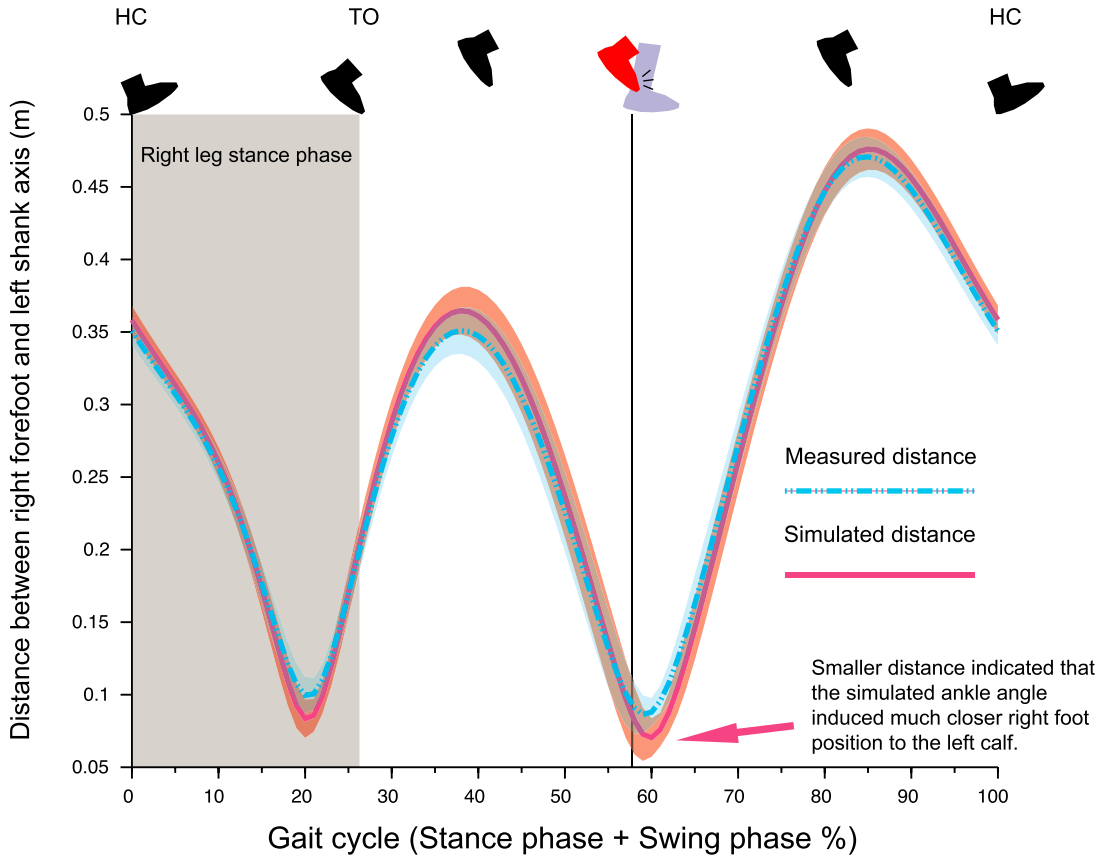

FIGURE 5 | Temporal pattern of the distance between right forefoot (marker FBC) to the left shank segment. If the right ankle was adducted by 7° and plantarflexed by 10° from the observed ankle position as that of left ankle, the distance between right foot and left shank was much closer (Arrow), suggesting the right ankle position observed in this trial was a collision-avoiding strategy.

a secondary phenomenon to abnormal pelvis and hip motor control.

One likely explanation of the foot collision being a secondary phenomenon to the abnormal pelvis and hip control was that the right ankle position (abducted and dorsiflexed than left ankle) prior to the foot collision was a voluntary avoidance strategy rather than an involuntary abnormal movement. Our findings were supported by the results of kinematic simulation analysis which illustrated that the abducted and dorsiflexed right-foot position contributed significantly to widening the distance between the right foot and left leg (**Figure 5**).

The isolated right TA activity increasing systematically prior to foot collision (30–50% of cycle) without remarkable GC co-activity was suggestive of a non-dystonic type of movement (**Figure 6**). Prior reports of focal ankle dystonia have shown involuntary co-contraction of agonist–antagonist muscle pair (Ahmad et al., 2018), but in this case, since no such involuntary co-contraction of ankle muscles was observed (**Figure 6**). The increased right TA activity appearing before foot collision may be an anticipatory muscle activity to configure the dorsiflexed ankle position and widen the distance between the right foot and left calf. Therefore, we believe that the right TA-GC contraction pattern found around foot collision phase also clarifies that the ankle collision was possibly a secondary phenomenon.

Acute, involuntary presentation of symptoms, occurring only during running, and its absence during walking normally, or walking sideways or backward, clinically fit to those with distal ankle dystonia. However, with our current interpretation, we believe this attribute to be a type of segmental dystonia in the truncal and proximal lower limb. In this case, though the symptoms shared several similarities with FTSD at the ankle, the measured kinematic and EMG patterns were quite specific to this athlete. A similar case was reported by Ahmad et al. (2018) in a 56-year-old elite male runner with a 4-year history of involuntary movement in his left limb during running. Some commonalities observed with our case were: (1) an early shift of gait cycle associated with a shorter stance duration in the affected limb and (2) left forefoot scraping the medial aspect of the right ankle. The authors suspected the ankle inversion was due to left foot collision with the right ankle, although motion capture assessment revealed that an excessive hip adduction induced the collision between the distal segments. However, the tonic co-contraction observed between TA and GC by these authors was notably absent within our athlete. Ahmad et al. (2018) also reported a truncal

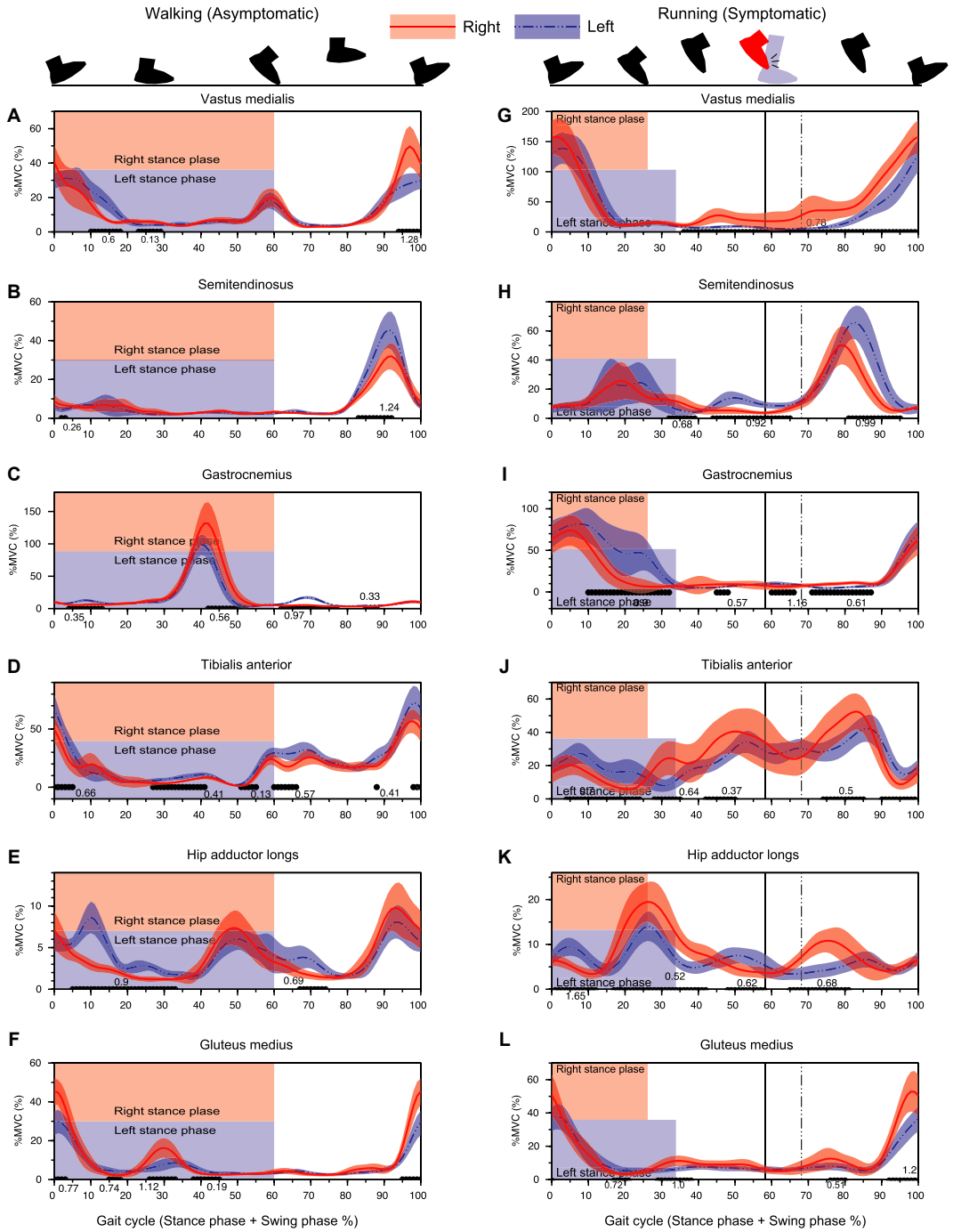

FIGURE 6 | Results of EMG analysis during walking (left column) and running (right column) assessed by 1D-SPM. The black lines with the Cohen's *d*-value at the horizontal axis of each panel showed significant differences between the right and left legs. Vertical lines denote the timing of foot collision for right leg (solid line) and for left leg (dashed line). Note that the percentage of the stance-phase and the foot collision time was different between the right and left legs in 100% gait cycle representation since the absolute stance-phase duration was significantly different between limbs (**Figure 3**).

dystonia—a 58-year-old man with 10-year history of long-distance running who exhibited the bilateral posterior pelvic tilt and upward obliquity on the right pelvis, resulting in an abnormal forward and rightward flexion of the trunk (Ahmad et al., 2018). Whereas these cases were comparable to some extent with respect to abnormal truncal or pelvis control, their posture abnormalities were tonic which were considerably different wherein our athlete demonstrated phasic asymmetrical pelvic drop during the right-leg stance-phase. We believe our findings are a worthwhile addition of an

uncommon variant of RD symptoms to the knowledge base of task-specific dystonia.

Considering the nature of task-specific dystonia, synchronized visualization of muscle-input (EMG data) and the corresponding movement outcome (3D motion capture data) were vital to elucidate symptom origins in this patient. Additionally, we performed time-series analysis using 1d-spm, aiming to describe slight differences in complex running movement involving cycle-by-cycle movement variation. The ensemble average of 50 running-cycle data input into 1d-spm enabled us to condense the movement features of both affected and unaffected sides, resulting in the identification of statistically meaningful inter-limb difference. Sole visual inspection by experts may not sufficiently quantify the subtle discrepancy between affected and unaffected limbs over whole gait cycle, nor be able to assess muscle activation adequately. Our quantification with motion capture systems with dynamic EMG time-series visualization is therefore beneficial for an accurate understanding of patients' 3D motion. This will in turn assist expert evaluators to help localize the dystonic origin in the clinical scenarios.

Limitation

As per literature, the diagnosis of RD should be based on a synthesis of detailed history taking and comprehensive neurological tests, often supported by laboratory data and medical imaging. This study demonstrated the usefulness of additional kinematic and electromyographic assessment. Despite its impact, motion capture system combined with EMG is not necessarily a convenient tool in daily clinical practice because of its significant cost burden in terms of equipment and data analysis. In addition, the measurement method itself is not for diagnosis but merely for biomechanical inference of cause-effect relationships between different muscle elements within the whole-body kinematic chain. Therefore, every effort should be made to increase the practical convenience of such systems.

CONCLUSION

This study assessed the kinematic and electromyographic characteristics of a unique RD case. Although the main complaint was that of right foot's collision with the left leg during the right-leg swing-phase, motion capture assessment suggested that this foot collision may not have originated from the ankle but due to an impaired control mechanism of the right hip and pelvis segment. The multimodal evaluation procedure enabled us to precisely characterize the symptomatology and is therefore a crucial modality for a deeper understanding of the pathogenesis and characteristics of RD.

DATA AVAILABILITY STATEMENT

The raw data supporting the conclusions of this article will be made available by the authors, without undue reservation.

ETHICS STATEMENT

The studies involving human participants were reviewed and approved by the Osaka University Clinical Research Review Committee. The patients/participants provided their written informed consent to participate in this study.

AUTHOR CONTRIBUTIONS

IO, NH, and GR conceptualized and designed the study and wrote the manuscript. NH, HM, and KN provided medical consultations. IO, NH, YU, and TN organized the experiments. IO, NH, YU, YK, and TN performed the experiments and data collection. IO, NH, SK, and GR analyzed the data and performed the statistical analysis. IO, NH, GR, SK, YU, TN, YK, HM, and KN reviewed the manuscript, suggested corrections, and approved its final version. All authors contributed to the article and approved the submitted version.

FUNDING

This work was supported by the Sports Research Innovation Project (SRIP) grant, sponsored by the Japan Sports Agency.

ACKNOWLEDGMENTS

We express our sincere gratitude to the runner who participated in this study. We would like to thank Shohei Beppu and Shin Nabatame for their assistance in diagnose process. We would also like to thank Chen Shuo for a great assistance in data collection.

SUPPLEMENTARY MATERIAL

The Supplementary Material for this article can be found online at: https://www.frontiersin.org/articles/10.3389/fnhum.2021.809544/full#supplementary-material

REFERENCES

Ahmad, O. F., Ghosh, P., Stanley, C., Karp, B., Hallett, M., Lungu, C., et al. (2018). Electromyographic and joint kinematic patterns in runner's dystonia. *Toxins* 10:166. doi: 10.3390/toxins10040166

Cutsforth-Gregory, J. K., Ahlskog, J. E., McKeon, A., Burnett, M. S., Matsumoto, J. Y., Hassan, A., et al. (2016). Repetitive exercise dystonia: a difficult to treat hazard of runner and non-runner athletes. *Park. Relat. Disord.* 27, 74–80. doi: 10.1016/j.parkreldis.2016.03.013

Frucht, S. J. (2004). Focal task-specific dystonia in musicians. *Adv. Neurol.* 94, 225–230.

Goldman, J. G. (2015). Writer's cramp. *Toxicon* 107, 98–104.

Karp, B. I., and Alter, K. (2017). Muscle selection for focal limb dystonia. *Toxins* 10:20. doi: 10.3390/toxins10010020

Krosshaug, T., Nakamae, A., Boden, B., Engebretsen, L., Smith, G., Slauterbeck, J., et al. (2007). Estimating 3D joint kinematics from video sequences of running and cutting maneuvers—assessing the accuracy of simple visual inspection. *Gait Posture* 26, 378–385. doi: 10.1016/j.gaitpost.2006.10.010

Lee, J. H., Kim, H. J., Park, D. G., and Yoon, J. H. (2021). A novel task-specific dystonia: running-induced cervical dystonia in a triathlete. *Neurol. Sci.* 42, 3051–3052. doi: 10.1007/s10072-021-05224-z

Leveille, L. A., and Clement, D. B. (2008). Case Report: action-induced focal dystonia in long distance runners. *Clin. J. Sport Med.* 18, 467–468. doi: 10.1097/JSM.0b013e3181845f35

Martino, D., Macerollo, A., Abbruzzese, G., Bentivoglio, A. R., Berardelli, A., Esposito, M., et al. (2009). Lower limb involvement in adult-onset primary dystonia: frequency and clinical features: adult-onset primary lower limb dystonia. *Eur. J. Neurol.* 17, 242–246.

McClinton, S., and Heiderscheit, B. (2012). Diagnosis of primary task-specific lower extremity dystonia in a runner. *J. Orthop. Sports Phys. Ther.* 42, 688–697. doi: 10.2519/jospt.2012.3892

Pataky, T. C., Robinson, M. A., and Vanrenterghem, J. (2013). Vector field statistical analysis of kinematic and force trajectories. *J. Biomech.* 46, 2394–2401. doi: 10.1016/j.jbiomech.2013.07.031

Ramdhani, R. A., and Frucht, S. J. (2013). Adult-onset idiopathic focal lower extremity dystonia: a rare task-specific dystonia. *Tremor Other Hyperkinet. Mov.* 3:tre-03-142-2990-1.

Robinson, M. A., Donnelly, C. J., Tsao, J., and Vanrenterghem, J. (2014). Impact of knee modeling approach on indicators and classification of anterior cruciate ligament injury risk. *Med. Sci. Sports Exerc.* 46, 1269–1276. doi: 10.1249/MSS.0000000000000236

Schneider, S. A., Edwards, M. J., Grill, S. E., Goldstein, S., Kanchana, S., Quinn, N. P., et al. (2006). Adult—onset primary lower limb dystonia. *Mov. Disord.* 21, 767–771.

Stahl, C. M., and Frucht, S. J. (2017). Focal task specific dystonia: a review and update. *J. Neurol.* 264, 1536–1541.

Stan, A., Gherghel, N., and Muresanu, D. F. (2020). Adult-onset idiopathic lower-extremity dystonia: a rare task-specific dystonia. *Clin. Neurol. Neurosurg.* 198:106106.

Suzuki, K., Izawa, N., Aiba, S., Hashimoto, K., Hirata, K., Nakamura, T., et al. (2011). Interoceptive sensory trick for runner's dystonia. *Mov. Disord.* 26, 758–760. doi: 10.1002/mds.23440

Wu, L. J. C., and Jankovic, J. (2006). Runner s dystonia. *J. Neurol. Sci.* 251, 73–76.

Conflict of Interest: The authors declare that the research was conducted in the absence of any commercial or financial relationships that could be construed as a potential conflict of interest.

Publisher's Note: All claims expressed in this article are solely those of the authors and do not necessarily represent those of their affiliated organizations, or those of the publisher, the editors and the reviewers. Any product that may be evaluated in this article, or claim that may be made by its manufacturer, is not guaranteed or endorsed by the publisher.

frontiers in Bioengineering and Biotechnology

ORIGINAL RESEARCH
published: 17 December 2021
doi: 10.3389/fbioe.2021.761766

Proactive Modulation in the Spatiotemporal Structure of Muscle Synergies Minimizes Reactive Responses in Perturbed Landings

Victor Munoz-Martel[1,2], *Alessandro Santuz*[1,2], *Sebastian Bohm*[1,2] *and Adamantios Arampatzis*[1,2]*

[1]*Department of Training and Movement Sciences, Humboldt-Universität zu Berlin, Berlin, Germany,* [2]*Berlin School of Movement Science, Humboldt-Universität zu Berlin, Berlin, Germany*

Stability training in the presence of perturbations is an effective means of increasing muscle strength, improving reactive balance performance, and reducing fall risk. We investigated the effects of perturbations induced by an unstable surface during single-leg landings on the mechanical loading and modular organization of the leg muscles. We hypothesized a modulation of neuromotor control when landing on the unstable surface, resulting in an increase of leg muscle loading. Fourteen healthy adults performed 50 single-leg landings from a 30 cm height onto two ground configurations: stable solid ground (SG) and unstable foam pads (UG). Ground reaction force, joint kinematics, and electromyographic activity of 13 muscles of the landing leg were measured. Resultant joint moments were calculated using inverse dynamics and muscle synergies with their time-dependent (motor primitives) and time-independent (motor modules) components were extracted via non-negative matrix factorization. Three synergies related to the touchdown, weight acceptance, and stabilization phase of landing were found for both SG and UG. When compared with SG, the motor primitive of the touchdown synergy was wider in UG ($p < 0.001$). Furthermore, in UG the contribution of gluteus medius increased ($p = 0.015$) and of gastrocnemius lateralis decreased ($p < 0.001$) in the touchdown synergy. Weight acceptance and stabilization did not show any statistically significant differences between the two landing conditions. The maximum ankle and hip joint moment as well as the rate of ankle, knee, and hip joint moment development were significantly lower ($p < 0.05$) in the UG condition. The spatiotemporal modifications of the touchdown synergy in the UG condition highlight proactive adjustments in the neuromotor control of landings, which preserve reactive adjustments during the weight acceptance and stabilization synergies. Furthermore, the performed proactive control in combination with the viscoelastic properties of the soft surface resulted in a reduction of the mechanical loading in the lower leg muscles. We conclude that the use of unstable surfaces does not necessarily challenge reactive motor control nor increase muscle loading per se. Thus, the characteristics of the unstable surface and the dynamics of the target task must be considered when designing perturbation-based interventions.

Keywords: balance control, modular organization, muscle loading, perturbation-based balance training, motor control, unstable surface training

OPEN ACCESS

Edited by:
Alessandro Del Vecchio, University of Erlangen Nuremberg, Germany

Reviewed by:
Claudio Pizzolato, Griffith University, Australia
Sai Wei Yang, National YangMing ChiaoTung University, Taiwan

***Correspondence:**
Adamantios Arampatzis
a.arampatzis@hu-berlin.de

Specialty section:
This article was submitted to Biomechanics, a section of the journal Frontiers in Bioengineering and Biotechnology

Received: *20 August 2021*
Accepted: *16 November 2021*
Published: *17 December 2021*

Citation:
Munoz-Martel V, Santuz A, Bohm S and Arampatzis A (2021) Proactive Modulation in the Spatiotemporal Structure of Muscle Synergies Minimizes Reactive Responses in Perturbed Landings. Front. Bioeng. Biotechnol. 9:761766. doi: 10.3389/fbioe.2021.761766

INTRODUCTION

Perturbation-based training interventions are an effective way to improve reactive balance performance and increase muscle strength (Arampatzis et al., 2011; Hamed et al., 2018b; Bohm et al., 2020). Moreover, the effectiveness of perturbation-based interventions for successfully reducing fall risk in different populations has been previously reported (Jöbges et al., 2004; Okubo et al., 2017; Sherrington et al., 2017; Hamed et al., 2018a; Mansfield et al., 2018). Using compliant or unstable surfaces as well as specific treadmill-slips to challenge balance control by introducing external mechanical perturbations (i.e., an alteration of the function of a biological system induced by external mechanism) have been widely used in clinical and training settings (Mansfield et al., 2015; Kurz et al., 2016; Hamed et al., 2018b; Wang et al., 2019). Recently, it was found that exercising mechanisms of dynamic stability control (i.e., increasing the base of support and counter-rotating body segments around the center of mass) in the presence of perturbations improved reactive balance recovery performance and muscle strength already after 3 weeks of exercise in older participants (Bohm et al., 2020). It was proposed that exercising specific balance tasks in the presence of perturbations could increase the demand for the neuromotor system to perceive sensory signals and to generate appropriate motor commands, thus facilitating the sensory-motor integration (Hamed et al., 2018a; Bohm et al., 2020).

External mechanical perturbations increase movement instability (Santuz et al., 2018; Munoz-Martel et al., 2019; Mademli et al., 2021) and challenge the neuromotor system during motion execution. In response, the neuromotor system modifies its strategies to increase control's robustness (i.e., the ability to cope with perturbations) (Santuz et al., 2018; Munoz-Martel et al., 2019). In earlier studies adopting the muscle synergies approach, we found specific modulations (i.e., wider, less unstable and less complex basic activation patterns of muscle groups) of the temporal structure of muscle synergies in the presence of perturbations (Santuz et al., 2018, 2020; Munoz-Martel et al., 2021). Such regulations of motor function in the presence of perturbations might be related to the efficacy of perturbation-based exercise interventions and its potential to enhance the ability of the motor system to respond and adapt to challenging conditions related to environmental changes during the daily life. Landing-related tasks on unstable surfaces have been widely used in perturbation-based training interventions to induce variable and partly unpredictable disturbances that promotes balance improvement and adaptation (Arampatzis et al., 2011; Hamed et al., 2018a; Bohm et al., 2020). Compliant surfaces have the potential to modify foot kinematics and forefoot stability during landings (Arampatzis et al., 2002, 2005), thus challenging the neuromotor control.

Fundamental basic building blocks defined as motor primitives are compositional elements for movement construction and have been established as kinematic, kinetic, and neural drive entities, which reflect an organizational principle of movement formation (Bizzi et al., 1991; Kargo and Giszter, 2000; Hart and Giszter, 2010; Hogan and Sternad, 2012). It is assumed that a complex movement task can be generated by rearranging and combining motor primitives and therefore motor primitives may provide an insight into underlying neurophysiological mechanisms for motor control (Giszter, 2015). The idea that the neuromotor system faces the redundancy of available degrees of freedom by activating functionally related muscle groups rather than individual muscles is well accepted (Bernstein, 1967; Bizzi et al., 1991). The resultant coordinated patterns of muscle activity are commonly known as muscle synergies and are flexibly combined to produce robust locomotor drive (Mussa-Ivaldi et al., 1994; d'Avella et al., 2003; Bizzi et al., 2008). Synergies—as low dimensional units—produce a complex electromyographic (EMG) pattern in muscles, involving a time-dependent basic activation pattern (temporal structure of the synergy or motor primitives) with variable time-independent weights of activity distribution to different muscles (spatial structure of the synergy or motor modules) (Dominici et al., 2011; Bizzi and Cheung, 2013; Santuz et al., 2017).

Recently, investigating forward and backward lunges on stable and unstable surfaces and using the muscle synergies approach, we found alterations in the spatiotemporal structure of muscle synergies during the stance phase (i.e., weight acceptance and stabilization synergy), resulting in an increased overlap between chronologically adjacent synergies in the unstable condition (Munoz-Martel et al., 2021). However, studies investigating the EMG activity in the lower leg muscles during landings on stable and unstable grounds reported marginal effects of landing surface on the EMG activity (Prieske et al., 2013; Hollville et al., 2020). The biomechanical differences between lunges (movement of the center of mass in both horizontal and vertical direction) and landings (mainly a vertical motion of the center of mass) may affect the effectiveness of proactive neuromuscular adjustments (i.e., before touchdown), resulting in distinct modifications in the spatial and temporal components of the muscle synergies after touchdown in the two tasks. To the best of our knowledge, no study investigated the spatiotemporal activation structure of muscle synergies during landings on unstable surfaces yet. Investigating the spatiotemporal structure of muscle synergies might present an opportunity to better understand the neuromotor control of landings in the presence of perturbations and thus promoting the design of effective exercise programs.

Therefore, the purpose of the current study was to investigate the effects of perturbations induced by an unstable surface on the mechanical loading (i.e., each muscle's group mechanical demands) and modular organization of neuromotor control during single-leg drop landings. We hypothesized that landing on unstable surfaces would result in a modulation of motor control, reflected in the spatiotemporal components of muscle synergies and in an increase of muscle loading reflected by an increased muscle activity and/or resultant joint moments, in response to the increased challenges in balance control.

MATERIALS AND METHODS

Experimental Protocol

We performed an *a priori* power analysis using the findings from our earlier study investigating forward and backward lunges in stable and unstable surfaces (Munoz-Martel et al., 2021). We

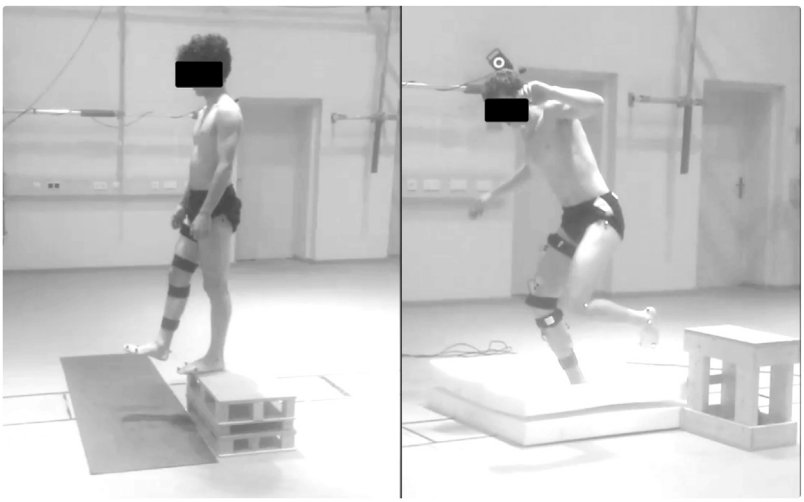

FIGURE 1 | Visual description of the performed task. Participants performed a single-leg landing by dropping onto two ground configurations: stable solid ground **(A)** and two foam pads used as unstable ground **(B)**. Fifty repetitions were performed onto each ground condition and the height of the platform was adjusted to keep a 30 cm distance to the surface.

found an effect size of 1.17 for the differences in the temporal structure of muscle synergies (i.e., width of the motor primitives) between stable and unstable condition, and assuming type I and type II errors of 0.05, we calculated that seven participants were sufficient for the designed study. Fourteen healthy adults volunteered for the study (10 males, 4 females, height 1.75 ± 0.10 m, body mass 67 ± 11 kg, age 28 ± 5 years). None of the participants had a history of acute lower limb injury or back pain in the 6 months preceding the recordings, nor did they suffer from any chronic neuromuscular or musculoskeletal impairments. In accordance with the Declaration of Helsinki, all participants provided written informed consent for the experimental procedure, which was reviewed and approved by the Ethics Committee of the Humboldt-Universität zu Berlin (HU-KSBF-EK_2018_0013).

Participants were instructed to step off a platform, dropping into a single-leg landing (right leg) and maintain the achieved single-leg stance after the touchdown with a strategy of their choice until they felt completely stable (**Figure 1**). The height of the platform was adjusted to keep a drop height of 30 cm over two possible ground configurations: hard uniform stable ground or unstable ground built out of two 100 × 100 × 10 cm foam pads (one cold foam pad with density = 50 kg/m^3 and compressive strength = 6.0 kPa; one polyurethane foam pad with density = 40 kg/m^3 and compressive strength = 7.0 kPa). Landings happened over a force plate (40 × 60 cm, AMTI BP400600-200; Advanced Mechanical Technology, Inc. Watertown, MA, USA) sampling the ground reaction force (GRF) at 1 kHz. A minimum of five landings in each condition were used as familiarization and warm-up, after which the participants performed a series of 52 valid landings per condition at a self-managed pace. If the participant was not able to maintain the single-leg stance (e.g., touched the floor with any other part of the body or changed the position of the foot on the ground), the attempt was considered failed and repeated. The order of the series was randomized and a self-managed rest period (minimum 3 min, seating allowed) was given in-between series to avoid fatigue.

A ten-infrared-camera motion capture system (Vicon Motion Systems, Oxford, UK) operating at 250 Hz was used to collect kinematic data from 20 spherical reflective markers (14 mm diameter) placed over the following anatomical landmarks: spinal process of the second, seventh, and 10th thoracic along with the second lumbar vertebrae, and bilaterally over the greater trochanter, lateral and medial epicondyle of the femur, Achilles tendon insertion on the calcaneus, lateral malleolus, tip of the first toe, and the dorsal margin of the first and fifth metatarsal heads. We also assessed the EMG activity of the following 13 right-leg muscles: gluteus medius, gluteus maximus, tensor fasciae latae, rectus femoris, vastus medialis, vastus lateralis, semitendinosus, biceps femoris (long head), tibialis anterior, peroneus longus, gastrocnemius medialis, gastrocnemius lateralis, and soleus using a 16-channel wireless EMG system (Myon m320; Myon AG, Schwarzenberg, Switzerland), with a sampling frequency of 1 kHz. The electrodes were not replaced between series. EMG and force plate analog data streams were collected together with the kinematics and then converted to digital information within the same A/D converter (Vicon MX Giganet).

Kinetic Analysis

Touchdown of each landing was defined as the first data point of the vertical GRF crossing a 20 N threshold (Malfait et al., 2016). An interval of interest was defined for each landing as the time window between 300 ms prior to the touchdown (flight phase) and until the first point crossing a threshold of body weight ±2.5% following a minimum in the vertical GRF after the touchdown (stance phase). Marker trajectories were filtered using a fourth-order Butterworth low-pass filter with a cut-off frequency of

18 Hz (Malfait et al., 2016). Sagittal kinematics of the ankle, knee, and hip joints from the landing-leg and the resultant internal joint moments for the aforementioned joints were calculated using a custom Matlab (v. R2012a, The MathWorks, Natick, MA, USA) inverse dynamics procedure (Hof, 1992) with segmental masses and inertial parameters derived from literature (Winter 2005). Kinematics and resultant joint moments were time-normalized to 300 points with 100 points assigned to the flight and 200 points to the stance phase, pasted one after another (i.e., concatenated) and kept for further analysis. We calculated the Euclidean norm of the GRF and time-normalized it in the same way as the kinematic and resultant joint moments data. The 2D center of pressure (CoP) data was used to analyze the effect of the ground (SG vs. UG) on the postural sway during the stance phase of each landing. The CoP's 95% confidence ellipse area (CoP area), representing the area of the smallest ellipse able to contain 95% of all the measured CoP points, was calculated using a custom Matlab script.

Muscle Synergies

EMG signals were filtered with a fourth-order IIR Butterworth zero-phase high-pass filter with a cut-off frequency of 50 Hz full-wave rectified and low-pass filtered with a cut-off frequency of 20 Hz (Santuz et al., 2017). The amplitude of the EMG signal was then normalized to the maximum activity of each muscle in the SG series of each participant. Lastly, all intervals of interest were time-normalized in the aforementioned manner. Thus, all variables were time-normalized in a similar manner. The rationale for this normalization (i.e., 100 and 200 points to the flight and stance phase, respectively) was to respect the time structure of each landing (i.e., roughly a 1:2 ratio for the flight and the stance) and provide a common time reference for all landings (i.e., the touchdown) while allowing any time-dependent modulation that could have occurred independently of the absolute duration of the events. All EMG off-line processing and further analysis on all variables were performed in R (R v4.0.3, R Core Team, 2020; R Foundation for Statistical Computing, Vienna, Austria).

Muscle synergies were extracted from the filtered and normalized EMG signals and classified using the open source script musclesyneRgies v0.7.1-alpha (Santuz, 2021) based on the classical Gaussian non-negative matrix factorization (NMF) algorithm (Lee and Seung, 1999; Santuz et al., 2017). It is to be mentioned that several other factorization methods have been used in the literature to extract muscle synergies as principal component analysis, independent component analysis, or factor analysis (Tresch et al., 2006; Lambert-Shirzad and Van der Loos, 2017). Nonetheless, NMF has been reported to provide a more intuitive physiological representation of synergies compared with other factorization methods (Lambert-Shirzad and Van der Loos, 2017) and as the best factorization method for identifying muscle synergies in dynamic tasks with different levels of muscle contraction (Rabbi et al., 2020). The concatenated EMG data vectors were grouped in a m × n matrix V, where m = 13 (number of muscles) and n = number of points (300). This matrix was factorized such that $V \approx V_R = MP^T$, where V_R represents a new reconstructed matrix that approximates the original matrix V, while M and P describe the synergies necessary to accomplish a movement. M represents the m × p motor modules matrix (Gizzi et al., 2011; Santuz et al., 2017), containing the time-invariant muscle weightings. P represents the p × n time-dependent coefficients (motor primitives) matrix (Dominici et al., 2011; Santuz et al., 2017), where p represents the number of synergies necessary to reconstruct the signal and n the number of data points. The number of synergies p was defined as the amount of synergies that did not improve the reconstruction of the signals with the addition of an extra module and it was calculated using the R^2 between V and VR. When the mean squared error of a linear regression model fitting the curve of R^2 values versus synergies for all the synergies fell below 10^{-5}, we assumed that the addition of an extra synergy did not improve the quality of the reconstruction (Santuz et al., 2017, 2018).

To compare the extracted synergies and give them a functionally meaningful interpretation, we classified them using an unsupervised method based on k-means clustering, with the aim to reduce possible operator-dependent bias in the classification. The algorithm initially clusters the average motor primitives (i.e., one primitive of 300 points per series, average of all the 52 obtained for that series) for each condition separately. This is done for a number of clusters going from one until the number of muscles, with 20 random start sets and using the Hartigan and Wong algorithm (Hartigan and Wong, 1979). Then, a curve "number of clusters vs. within-cluster sum of squares" is built and normalized between zero and one. The minimum number of clusters (or their centroids) is then selected as the number of muscles minus the number of points on the curve that can be linearly interpolated with a mean squared error lower than 10^{-3}. Motor modules are then clustered by imposing the number of centroids thus obtained with the analysis on motor primitives. The average full width at half maximum (FWHM) and center of activity (CoA) of the motor primitives are then summed and normalized by the number of points (i.e., 300), and this value is used as a score to compare the k-means classification of modules and primitives. The FWHM was calculated as the number of points exceeding each cycle's half maximum, after subtracting the cycle's minimum (Martino et al., 2014), and the CoA is defined as the angle of the vector (in polar coordinates) that points to the center of mass of that circular distribution and its calculation method has been previously described. Common classifiers identify fundamental synergies, while discording classifiers return combined (i.e., spurious) synergies. If no matching is found, only primitive-based classification is retained. Motor primitives between SG and UG condition were compared across condition by means of the FWHM. Furthermore, we calculated the overlapping intervals of the motor primitives for each synergy per every landing trial and then averaged for each participant and surface condition. An overlap is happened when at least two motor primitives were exceeding half maximum at the same time.

To compare motor modules across conditions, we assessed the distribution of muscle contributions for each synergy separately. We defined the ratio of flexor and extensor muscle contribution to each joint in a specific motor module as the coactivation index (CaI). For its calculation, we considered the tensor fasciae latae

and rectus femoris as hip flexors and the gluteus medius and gluteus maximus as hip extensors. For the knee, the flexors were the semitendinosus and biceps femoris and the extensors the rectus femoris, vastus medialis, and vastus lateralis. For the ankle, only the tibialis anterior was considered as flexor (i.e., foot dorsiflexor) and the peroneus longus, gastrocnemius medialis, gastrocnemius lateralis, and soleus as extensors (i.e., foot plantar flexors). For each joint, the mean of the flexor contributions Flex and the mean of the extensor contributions Ext were forced to sum to 1:

$$CaI = \frac{\overline{Flex}}{\left(\overline{Flex} + \overline{Ext}\right)}$$

Hence, the CaI is equal to a) zero when only extensors are contributing to the considered joint, b) one when only flexors are giving their contribution, and c) 0.5 if flexors and extensors are equally contributing (i.e., full coactivation of flexors and extensors).

Statistical Analysis

After removing the first and last landings, the remaining 50 landings were used to create a representative dataset for each participant on each ground condition of the following variables: FWHM, maximum range of joint angles (defined as the difference between minimum of the joint angle and angle at touchdown), maximum of joint moments and GRF, rate of joint moment development (defined as the ratio between joint moment maxima and the time interval between touchdown and time to maxima), joint moments' lever arm, and CoP area. Then the mean of the 50 repetitions of each participant was used as the participant's data for the statistical test. We tested the homogeneity of variances on the residuals of each aforementioned variable using Levene's test. If the variables were normally distributed, we used a parametric test to investigate the effect of ground condition on variable. Hence, we performed a one-way ANOVA for repeated measures on each of the following variables: GRF maxima, CoP area, and FWHM of the synergies. Correspondingly, we used a two-way ANOVA for repeated measures on the joint kinematics, resultant moments, joint moment's lever arm, and joint moment's rate using ground (SG–UG) and variable (i.e., ankle, knee hip joint angle or moment) as within-subjects variables. The same two-way ANOVA for repeated measures was used for each synergy using ground (SG–UG) and muscle or CaI, for the motor modules as within-subjects variables. When normality conditions on the residuals were not met (i.e., joint range of motion, resultant joint moment maxima, and FWHM of the touchdown synergy), we used a rank-based robust ANOVA from the R package "Rfit" (v 0.24.2, function "raov") (Kloke and McKean, 2012). If an interaction of main effects was observed, we performed a Tukey *post hoc* analysis with false discovery rate α-value adjustment. All the significance levels were set at 0.05.

Moreover, we adopted a similar approach using the statistical parametric mapping (SPM) on all the aforementioned continuous variables (i.e., time-normalized vectors). Correspondingly, the individual time-normalized joint kinematics, resultant joint moments, GRF, EMG, and overlaps curve for each landing were averaged to create a representative dataset of each participant on each ground condition. We tested for normality using a D'Agostino–Pearson test corrected for arbitrary one-dimensional domains using random field theory (Pataky, 2012). If non-parametric tests were needed, the corresponding two-way ANOVA for repeated measures permutation test (Nichols and Holmes, 2002) was used. SPM allows us to analyze the entire time series by using random field theory (Naouma and Pataky, 2019). Based on the temporal smoothness of the data (i.e., each time-normalized dataset) residuals trajectory, a critical threshold f* was calculated. Then a test statistics SPM{F} was evaluated at each point of the time series. In the case that SPM{F} exceeded f*, a significant difference was detected. Similar to the previously described analyses, significance level was set at 0.05. In case of finding an interaction of main effects, we conducted a SPM two-tailed paired *t*-test with significance t* level Bonferroni corrected for multiple comparisons (n = number of levels in the variable) between each relevant pair of variables as a *post hoc* analysis. All SPM calculations were performed using the open-source package spm1d (v 0.4.3).

RESULTS

Participants needed a longer time to reach their body weight threshold (i.e., stabilization) when landing on UG. This led to a significantly longer stance phase after landing onto the unstable ground compared with the stable condition (SG: 0.491 ± 0.062 s, UG: 0.629 ± 0.085 s, $t(1,13) = -5.611$, $p < 0.001$). Two participants were excluded from the kinematic analysis due to poor reconstruction of the markers' trajectories. The SPM analysis revealed a significant main effect of the ground type on joint kinematics during the flight ($F^* = 9.877$, $p = 0.012$) and the first half of the stance phase ($F^* = 9.877$, $p = 0.034$). An interaction of ground by joint was found shortly before touchdown and during the entire stance phase ($F^* = 5.724$, $p < 0.001$). The *post hoc* analysis revealed no differences in the flight phase in a specific joint but showed that landing on UG led the participants to reach a less dorsiflexed position at the ankle joint after the touchdown (35–55% of the task duration, $t^* = 3.618$, $p = 0.010$) and in the middle of the stance phase (59–78% of the task duration, $t^* = 3.618$, $p = 0.007$, **Figure 2**). Landing on UG also had a significant main effect on the joint range of motion ($F(1,11) = 5.48$, $p = 0.023$) and a significant interaction of ground by joint ($F(2, 22) = 9.81$, $p < 0.001$). The *post hoc* analysis showed that landing on UG resulted in a less range of dorsiflexion at the ankle joint during the stance phase (UG: 37.19 ± 12.76°, SG: 52.03 ± 6.45°, $p < 0.001$).

There was a significant ground effect on the internal resultant joint moments shortly after the touchdown ($F^* = 17.500$, $p = 0.003$) and an interaction of ground by joint in the swing phase (~20–25% of the task duration, $F^* = 8.572$, $p = 0.025$), around touchdown ($F^* = 8.572$, $p = 0.012$), and during three periods of the stance phase: between 36 and 40% ($F^* = 8.572$, $p = 0.023$), 45–75% ($F^* = 8.572$, $p < 0.001$), and between 60 and 76% of the task duration ($F^* = 8.572$, $p < 0.001$). The *post hoc* analysis

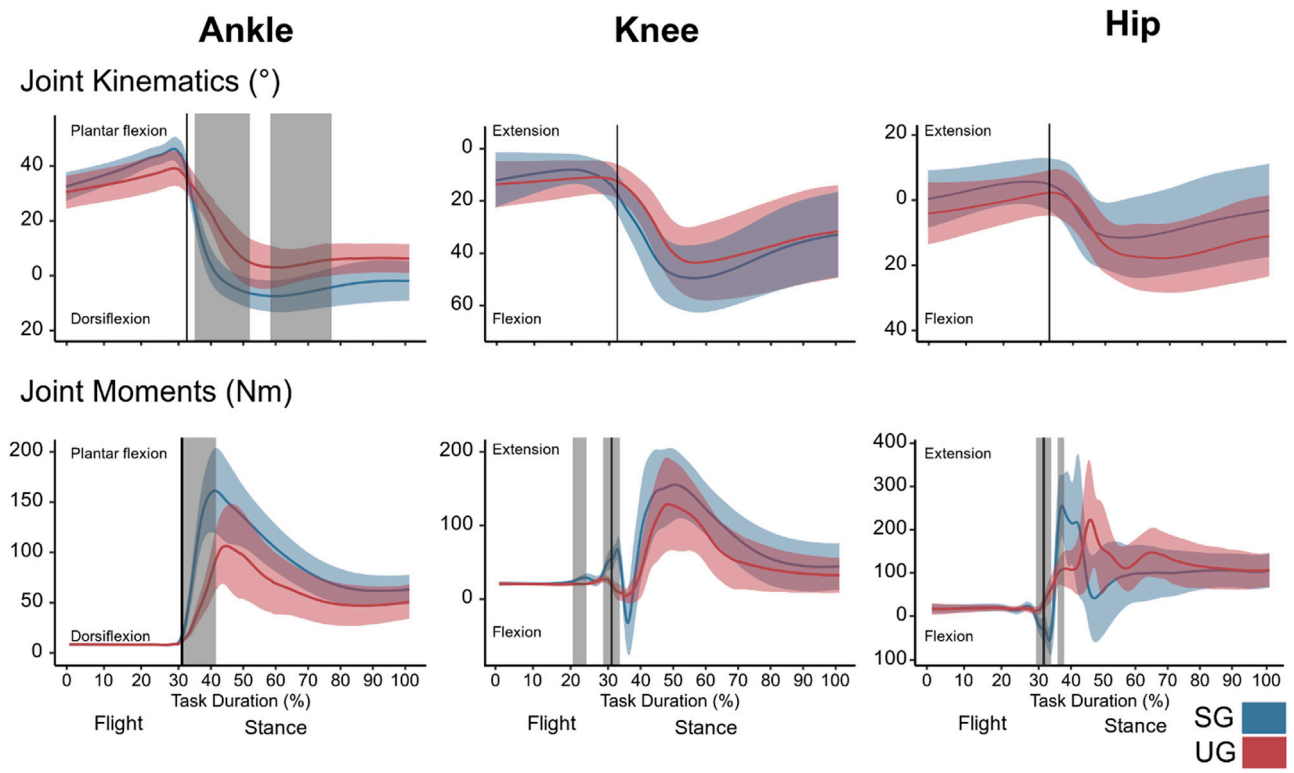

FIGURE 2 | Lower limb kinematics and internal resultant joint moments of the single-leg drop landing (from 300 ms previous to the touchdown until the first point crossing a threshold of body weight ±2.5% following a minimum in the vertical ground reaction force after the touchdown). Each panel shows the mean values and SD bands for the ankle, knee, and hip joint angles and moments for the stable (SG—blue) and unstable (UG—red) ground condition. Panels are presented in a time-normalized base; vertical lines represent the touchdown. Gray vertical bands highlight time periods of significant differences assessed by statistical parametric mapping.

TABLE 1 | Maxima of the resultant joint moment, lever arm at moment maxima, and rate of moment development for the ankle, knee, and hip joint during a single-leg drop landing on stable (SG) and unstable ground (UG). Values are presented as mean ± SD. Asterisks denote statistically significant ($p < 0.05$) difference between the two ground conditions.

Joint	Parameter	SG	UG
Ankle	Moment max (Nm)*	183.7 ± 46.5	142.4 ± 41.4
	Lever arm (m)*	0.102 ± 0.02	0.079 ± 0.02
	Rate of moment (Nm/s)*	2,665 ± 487	1,094 ± 275
	Time to peak torque (ms)	56 ± 14	60 ± 21
Knee	Moment max (Nm)	136.6 ± 41.1	118.5 ± 53.2
	Lever arm (m)	0.093 ± 0.02	0.077 ± 0.03
	Rate of moment (Nm/s)*	1,593 ± 554	788 ± 260
	Time to peak torque (ms)	73 ± 11	86 ± 22
Hip	Moment max (Nm)*	261.6 ± 78.1	207.5 ± 92.1
	Lever arm (m)	0.104 ± 0.02	0.090 ± 0.01
	Rate of moment (Nm/s)*	4,514 ± 1923	1,610 ± 806
	Time to peak torque (ms)	77 ± 13	78 ± 23

showed a lower plantar flexion moment at the ankle joint (~30–40% of the task duration, $t^* = 4.097$, $p = 0.002$) in UG compared with SG (**Figure 2**). At the knee joint, the extension moment was also lower in UG during the flight phase (20–25% of the task duration, $t^* = 4.118$, $p = 0.017$) and around the touchdown (28–34% of the task duration, $p = 0.010$, **Figure 2**). A lower hip flexion moment in UG condition around the touchdown (~30% on the task duration, $t^* = 4.166$, $p = 0.008$) was found (**Figure 2**). Furthermore, the maximum resultant ankle ($p = 0.002$) and hip ($p = 0.004$) joint moment and the rate of moment development in all joints ($p = 0.029$ at the knee and $p < 0.001$ for the ankle and hip) were significantly lower in UG compared with SG (**Table 1**). The lever arm of ankle joint center to GRF vector at moment maximum was also lower in the UG condition (**Table 1**). The SPM analysis identified a significantly lower GRF after touchdown in UG ($t^* = 3.305$, $p = 0.013$, **Figure 3**); however, the maximum of the GRF did not differ ($F(1,13) = 2.025$, $p = 0.178$, **Figure 3**) between the two ground conditions. CoP area during the landing was smaller in UG ($F(1,14) = 7.527$, $p = 0.020$) compared with SG (**Figure 3**).

The ground condition affected the EMG activity during the second half of the swing ($F^* = 14.364$, $p < 0.001$), and in three brief periods of the stance phase ($p = 0.049$, 0.014, and 0.029). There was also a significant interaction between ground and muscle in both the flight ($F^* = 2.718$, $p < 0.001$) and stance ($F^* = 2.718$, $p = 0.001$) phase. The *post hoc* analysis revealed lower EMG activity before touchdown in the gastrocnemius medialis

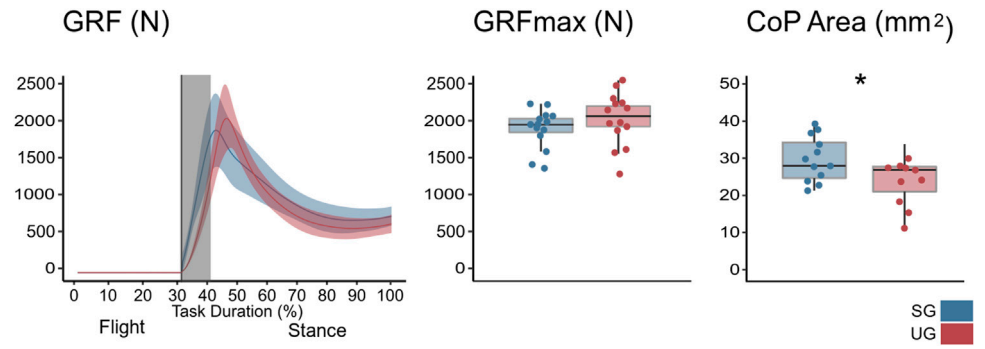

FIGURE 3 | Right panel presents the mean Euclidean norm and SD bands of the ground reaction force (GRF) during a single-leg drop landing for the stable (SG) and unstable ground conditions (UG). Vertical lines represent touchdown; gray vertical bands highlight time periods of significant differences assessed by statistical parametric mapping. Central panel represent the maximum of the GRF with points denoting single trials. Left panel shows the CoP 95% confidence area for the stance phase with points denote single trials. Asterisks denote statistically significant ($p < 0.05$) differences between the two conditions.

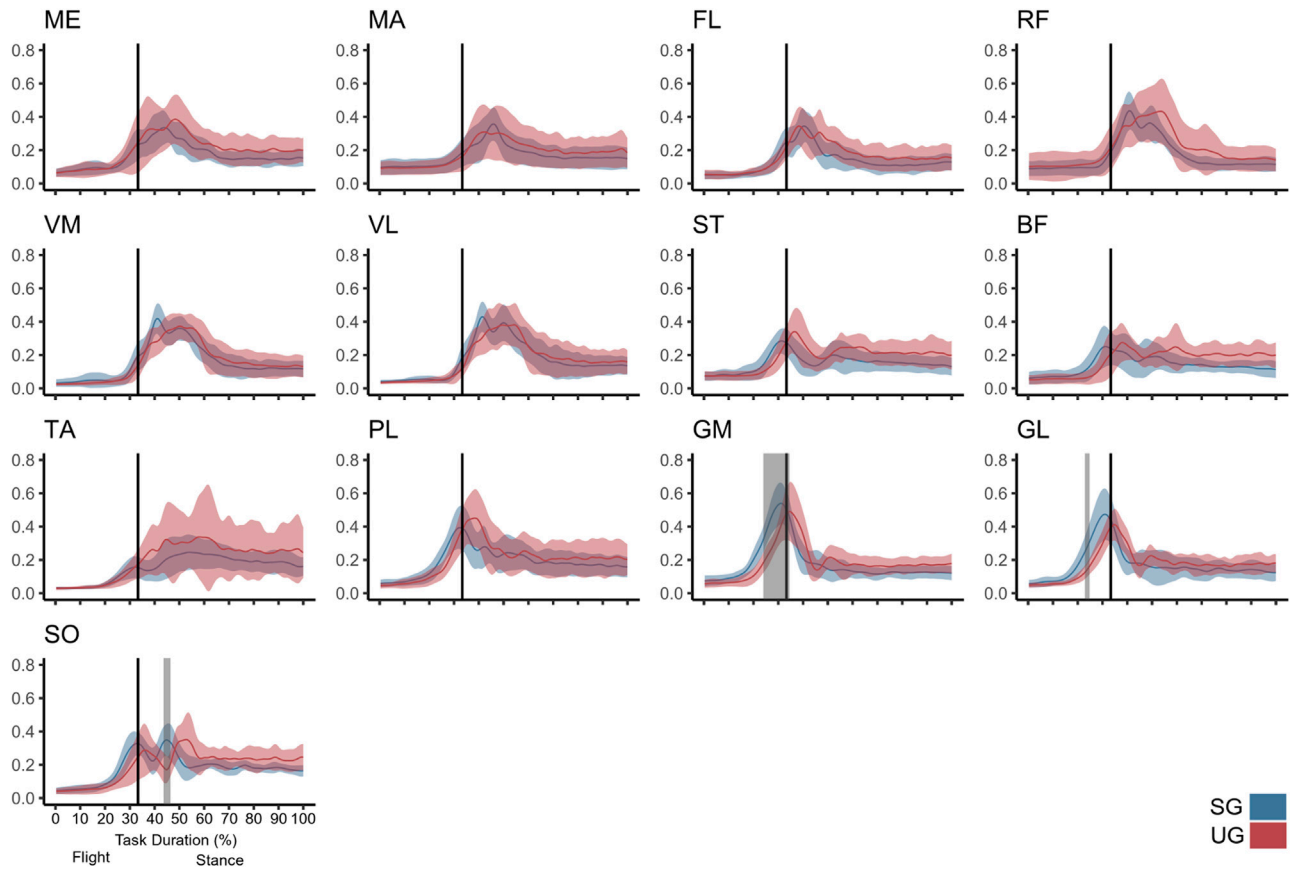

FIGURE 4 | Mean values and SD bands for the EMG activities for a single-leg drop landing on stable (SG, blue) and unstable ground condition (UG, red) normalized to the maximum activity of each muscle on the SG condition. Vertical lines represent touchdown. Gray bands denote time periods of significant difference found by the statistical parametric mapping analysis. ME, gluteus medius; MA, gluteus maximus; FL, tensor fascia latae; RF, rectus femoris; VM, vastus medialis; VL, vastus lateralis; ST, semitendinosus; BF, biceps femoris (long head); TA, tibialis anterior; PL, peroneus longus; GM, gastrocnemius medialis; GL, gastrocnemius lateralis; SO, soleus.

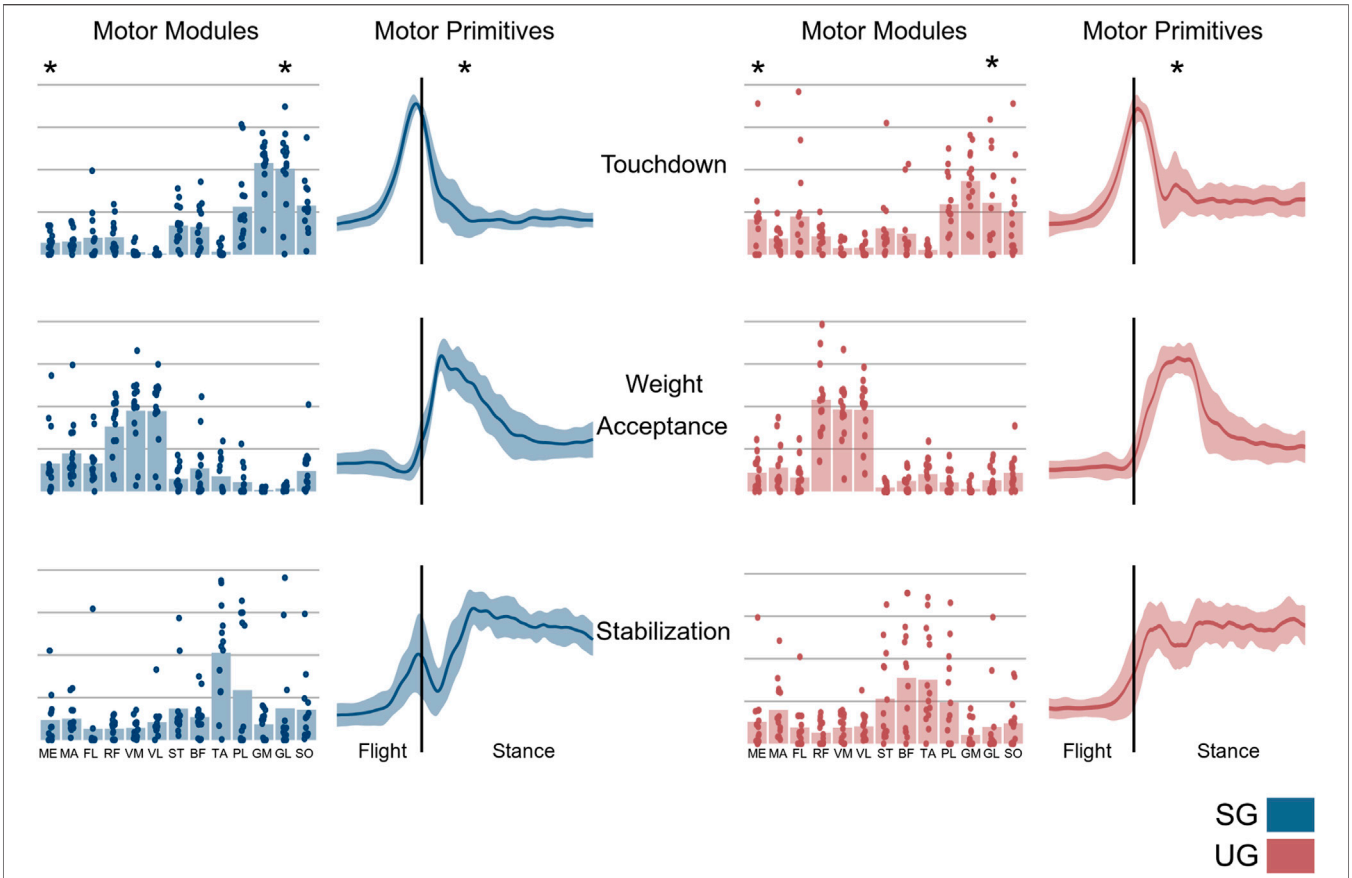

FIGURE 5 | Average and individual motor module values and average with their SD bands motor primitives of the fundamental synergies classified from a single-leg drop landing on stable (SG, blue) and unstable (UG, red) ground. The vertical lines in the primitive panels indicate the touchdown. ME, gluteus medius; MA, gluteus maximus; FL, tensor fascia latae; RF, rectus femoris; VM, vastus medialis; VL, vastus lateralis; ST, semitendinosus; BF, biceps femoris (long head); TA, tibialis anterior; PL, peroneus longus; GM, gastrocnemius medialis; GL, gastrocnemius lateralis; SO, soleus. Asterisks denote *post hoc* ($p < 0.05$) differences in the motor modules and width on the motor primitives between stable (SG) and unstable (UG) condition.

(~25–33% of the task duration, $t^* = 4.544$, $p < 0.001$) and gastrocnemius lateralis (~25% of the task duration, $t^* = 4.447$, $p = 0.004$) and after the touchdown in the soleus (~45% of the task duration, $t^* = 4.709$, $p = 0.020$, **Figure 4**) in the UG condition.

The number of extracted synergies that sufficiently reconstructed the original EMG signals did not differ between the two ground conditions (SG = 4.64 ± 0.49, UG = 4.85 ± 0.53, $p = 0.282$). We identified three fundamental synergies on both SG and UG (**Figure 5**). The first synergy was functionally related to the preparation of touchdown and showed a major contribution of plantar flexors. The second synergy presented its main activity shortly after the touchdown, thus it was functionally related to the weight acceptance and showed a main contribution of knee extensors. The third synergy represented the stabilization phase after landing and was characterized, in SG, by a major contribution of the muscles acting around the ankle joint, while in UG we observed a main contribution of hamstrings, tibialis anterior, and peroneus longus. A significant interaction of ground by muscle was observed in the motor module of the touchdown synergy ($F(12, 144) = 2.594$, $p = 0.004$). The *post hoc* analysis showed a higher contribution of gluteus medius ($p = 0.015$) and a lower contribution of gastrocnemius lateralis ($p < 0.001$) when landing on UG compared with SG (**Figure 5**). An interaction of ground by joint ($F(2, 24) = 6.347$, $p = 0.006$) was observed in the CaI of muscles in the touchdown synergy. The *post hoc* analysis showed that landing on UG significantly increased coactivation around the knee joint compared with SG ($p = 0.001$, **Figure 6**). The FWHM of the touchdown primitive was in UG on average 61 ± 17 points and was significantly greater ($F(1,13) = 11.27$, $p = 0.005$) than in SG (48 ± 7 points). The overlaps of the motor primitives showed a statistically significant difference ($t^* = 4.752$, $p < 0.049$) only at about 90% of the task duration (**Figure 7**).

DISCUSSION

We investigated the effects of perturbations induced by unstable surfaces on the mechanical loading and modular organization of leg muscles during single-leg landings. We hypothesized a modulation of the neuromotor control when landing on UG resulting in an increase of leg muscle loading. When landing on UG, the participants

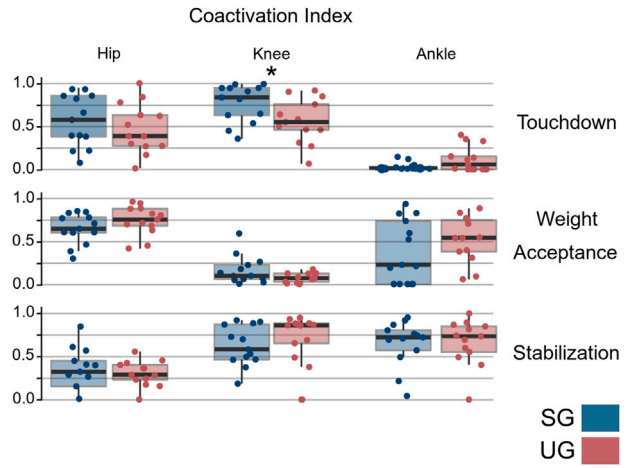

FIGURE 6 | Coactivation index (Cal) for the motor modules for the recognized synergies. The Cal may vary from 0 (exclusive contribution of extensors) to 1 (exclusive contribution of flexors). A Cal of 0.5 indicates equal contribution of flexors and extensors for that motor module. Points denote single trials and asterisks denote statistically significant ($p < 0.05$) differences between stable (SG) and unstable (UG) conditions.

modulated the spatiotemporal structure of muscle synergies mainly in the touchdown phase, indicating a proactive adjustment to the unstable surface and confirming our first hypothesis. The experience-based proactive control in combination with the deformation characteristic of the soft surface resulted in a lower maximum resultant ankle and hip joint moment, lower rate of joint moment development, and no increase in muscle EMG activity observed during the landing phase. Thus, the hypothesis of an increased muscle loading was rejected. Our results show that the participants managed to use their experience and awareness of the unstable ground characteristics to proactively deal with the predicted perturbation before touchdown, minimizing the consequences of the perturbation.

The modulation of the spatiotemporal structure of the touchdown synergy (i.e., widening of the motor primitive and modified contribution of gluteus medius and gastrocnemius medialis muscles) indicates proactive adjustments in the neuromotor control of landing on UG. Proactive control strategies have been shown to be very effective to support stability in the presence of perturbations and to prevent a fall (Patla, 2003; Bierbaum et al., 2010; Bohm et al., 2012). Moreover, proactive adjustments have been proposed to successfully compensate proprioceptive impairments (Gordon et al., 2020) and enhance passive stabilizing mechanisms (Moritz and Farley, 2004; Morey-Klapsing et al., 2007). In our experiment, the landings were performed with open eyes and participants had previously acquired knowledge about the ground and task characteristics during the familiarization trials. Therefore, it is likely that the spatiotemporal modifications found in the touchdown synergy reflect a proactive strategy driving the preparation to the predictable perturbation. Widening of motor primitives is a phenomenon commonly associated with the presence of perturbations which has been proposed to reflect a mechanism that increases the robustness of neuromotor control (Martino et al., 2015; Santuz et al., 2018; Munoz-Martel et al., 2019; Janshen et al., 2020). The reduced CoP area when landing on UG indicates that the proactive control successfully predicted most of the challenges induced by the compliant surface, facilitating landing stability (Morey-Klapsing et al., 2007).

It is to mention that motor control can be quickly improved and the experience of just one or two trials in a predicted perturbation modifies significantly proactive strategies (Bierbaum et al., 2010; Bohm et al., 2012). In our statistical analysis, we used 50 landing trials in each condition and therefore the repeated experience on the unstable ground might introduce an acute, trial-dependent modification of the temporal structure of muscle synergies, potentially biasing the findings. To check for possible acute adaptations in the neuromotor control due to the repeated execution of the landings, we tested the FWHM of the motor primitives during

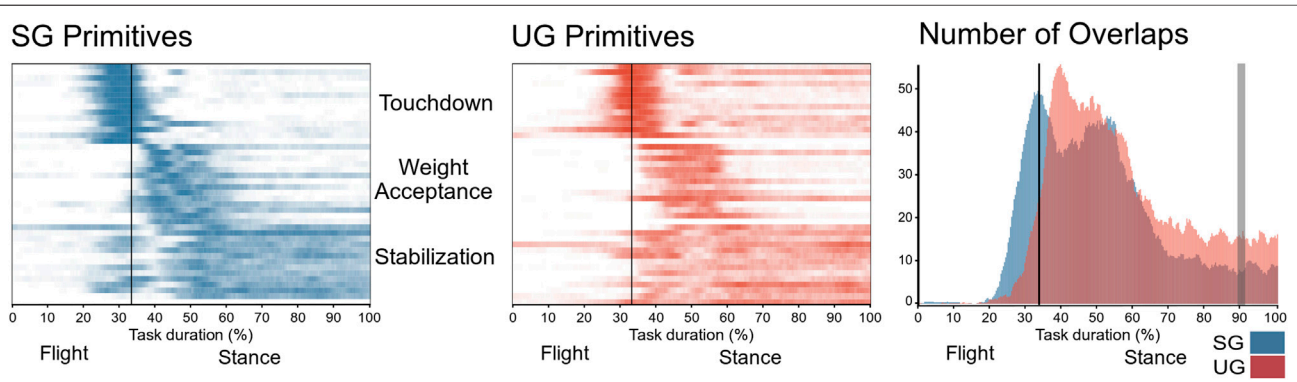

FIGURE 7 | Overlapping time intervals of motor primitives for the single-leg drop landings on stable (SG, right panel blue) and unstable ground (UG, middle panel red). Each row of the heat maps represents a single motor primitive. A colored time point indicates the primitive is exceeding half maximum. Darker colors indicate higher number of occurrences across all cycles per participant. At the right panel, the average number of overlaps across all trials and all participants per ground condition with gray bands denoting time period of significant difference found by the statistical parametric mapping. For all graphs, the *x*-axis full scale represents one trial time-normalized to 300 points. The vertical line indicates the touchdown.

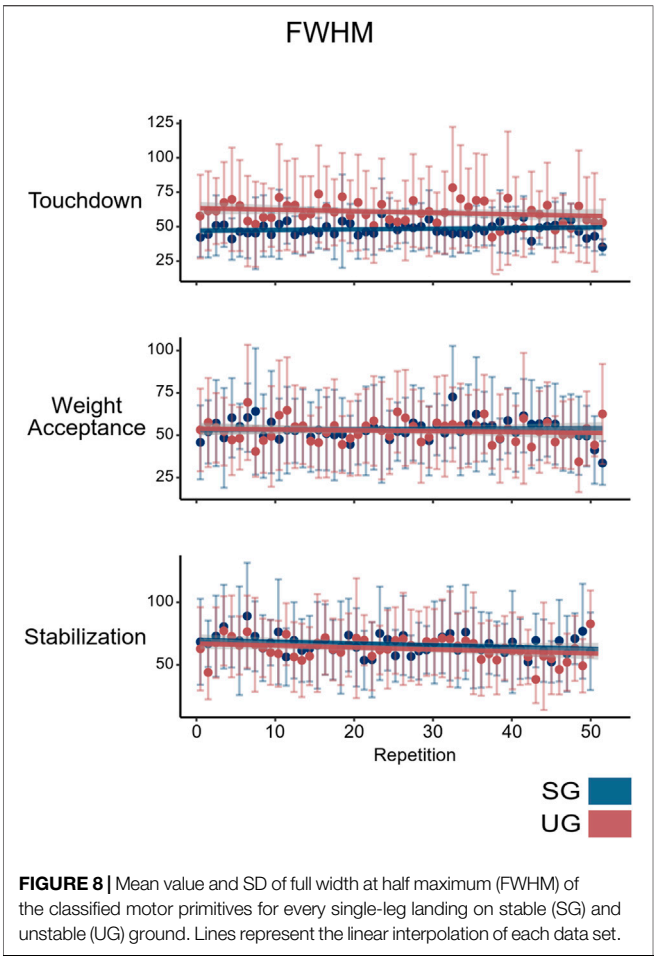

FIGURE 8 | Mean value and SD of full width at half maximum (FWHM) of the classified motor primitives for every single-leg landing on stable (SG) and unstable (UG) ground. Lines represent the linear interpolation of each data set.

the 50 repetitions using a linear mixed model. We did not find any effect of repetition on the FWHM of any of the three synergies: an indication that the basic activation patterns were not influenced by the landing repetitions (**Figure 8**). The participants performed some familiarization trials that were not included in this analysis. These initial repetitions might also have played a role in reinforcing previous knowledge of the landing characteristics initiating possible acute modifications in the modular organization and providing an adapted neuromotor control of the task.

When landing on UG, we observed a decreased CaI at the knee joint in the touchdown synergy indicating a higher contribution of the knee extensors compared with SG. Looking at the motor modules of the touchdown synergy, it is however visible that both knee flexors and extensors showed an almost negligible contribution to this synergy. Thus, the decreased CaI can be interpreted as functionally irrelevant. The knee joint plays a critical role during the landing phase to absorb the kinetic energy of the body (McNitt-Gray et al., 1993; Zhang et al., 2000; Hollville et al., 2020). The contribution of knee extensor muscles to the weight acceptance synergy is very high and the knee extension moment achieved its maximum in this phase, evidencing the importance of the knee joint for the kinetic energy dissipation during landings.

The weight acceptance and stabilization synergies were not modified in the UG condition and the overlapping of the motor primitives showed a short and small difference indicating a negligible influence of the unstable surface on the neuromotor control of the stance phase. Hence, it seems that predictive adjustment made by the participants during the single-leg landings were sufficient to cope with the UG and the unstable ground did not trigger reactive modulations of the neuromotor control which might be elicited if the difficulty of the task is increased. The result of our present setup is somewhat in disagreement with our previous findings during forward and backward lunging onto a foam beam—with similar mechanical characteristics to the current UG surface—where we found a modulation of the touchdown as well as the weight acceptance and stabilization synergies leading to a higher frequency of overlaps in the unstable condition (Munoz-Martel et al., 2021). From a biomechanical point of view, a basic difference between single-leg landings and lunges is the dynamic state of the body mass at touchdown. Landings were characterized by a vertical movement of the body center of mass with negligible components in the horizontal direction. On the other hand, the body mass moved in both horizontal and vertical direction during the forward and backward lunges. It seems that the two-dimensional body motion during the lunges was challenging to a greater degree the neuromotor control of the task in the presence of perturbations. This shows that the consequences of perturbations present a task specificity that should be accounted for when designing perturbation-based balance interventions. Sufficient reactive balance control after unpredicted perturbations is very important to maintain or even regain balance and avoid a fall. One of the main purposes of perturbation-based interventions is to improve balance reactive control, especially in older adults (Hamed et al., 2018a, 2018b; Mansfield et al., 2018; Gerards et al., 2021). Our results show that the unstable ground used for single-leg landings did not trigger reactive modulations of the neuromotor control and that predictive adjustment were sufficient to cope with the UG. Thus, we can argue that the use of unstable surfaces does not necessarily challenge reactive control. Challenging dynamic tasks (i.e., including anteroposterior and mediolateral body motion) or including a large catalogue of unstable conditions to increase the unpredictability of perturbations (Bohm et al., 2020) are key points in the design of perturbation-based interventions.

We expected an increase in the muscle activity and resultant joint moments as indicators of increased muscle loading in the UG condition. However, the ankle and hip maximum resultant joint moment and rate of moment development for all three joints were higher in SG. The damping behavior of the foam pads due to its viscoelastic properties might explain the significantly lower development of the GRF after touchdown and the reduced rate of joint moment development; the shorter lever arm of the GRF at the ankle joint, however, indicates an additional mechanism that explains the lower maximum ankle joint moment in UG. We found similar results (i.e., scarce differences in the EMG activity and a tendency toward lower resultant joint moments in the lower extremities) during forward and backward lunges on stable and unstable surfaces (Munoz-Martel et al., 2021). Therefore, we can

conclude that using unstable surfaces does not necessarily increase muscle loading per se. We should remark that estimating resultant joint moments and the electromyographic activity of a muscle are indirect estimators of the mechanical demands for a muscle group. Nonetheless, both methods are valid and highly reliable and therefore provide an accurate estimation of the training stimuli. We should also remark that the foam pads used in the UG condition were bigger than the force plate and this might have transmitted a small portion of the landing forces to the ground. The size choice was dictated by the fact that pads as small as the force plate would show different mechanical properties and would lift their perimeter so strongly after landing that the foot would be completely enveloped and the effect of the foam strongly affected. Yet, our main focus was on the modular organization, thus we decided to use a bigger foam pad size, despite the potential bias in the measured GRF. In any case, we observed from the data that the vertical GRF at steady state was similar between SG and UG (i.e., body weight), indicating that the force dissipation due to the extra size might be negligible despite the acknowledged limitation.

In conclusion, our results provide evidence that the neuromotor system relied on a proactive control to modulate the spatiotemporal structure of muscle synergies during perturbed landing, particularly in the touchdown synergy. These modulations allowed the participants to deal with the predictable perturbation before touchdown and minimize the mechanical consequences of the perturbation. Moreover, our results show that the use of unstable surfaces did not challenge reactive motor control nor increase muscle loading per se. Since perturbation-based interventions aim to improve reactive balance, the task characteristics and the intensity of the challenge imposed by the unstable surface should be carefully designed when planning this kind of intervention programs.

DATA AVAILABILITY STATEMENT

The raw data supporting the conclusion of this article will be made available by the authors, without undue reservation.

ETHICS STATEMENT

The studies involving human participants were reviewed and approved by the Ethics Committee of the Humboldt-Universität zu Berlin (HU-KSBF-EK_2018_0013). The patients/participants provided their written informed consent to participate in this study.

AUTHOR CONTRIBUTIONS

VM-M and AA designed the experiment. VM-M conducted the experiment and analyzed the data. AS and AA substantially contributed to data analysis. VM-M, AS, and AA interpreted the data and drafted the article. SB made important intellectual contributions during revision. All authors approved the final version of the article and agree to be accountable for the content of the work.

ACKNOWLEDGMENTS

VM-M is a scholarship holder of the German Academic Exchange Service (D.A.A.D.). The authors acknowledge support by the German Research Foundation (DFG) and the Open Access Publication Fund of Humboldt-Universität zu Berlin.

REFERENCES

Arampatzis, A., Brüggemann, G. P., and Morey Klapsing, G. (2002). A Three-Dimensional Shank-Foot Model to Determine the Foot Motion during Landings. *Med. Sci. Sports Exerc.* 34, 130–138. doi:10.1097/00005768-200201000-00020

Arampatzis, A., Morey-Klapsing, G., and Brüggemann, G.-P. (2005). Orthotic Effect of a Stabilising Mechanism in the Surface of Gymnastic Mats on Foot Motion during Landings. *J. Electromyogr. Kinesiol.* 15, 507–515. doi:10.1016/j.jelekin.2004.12.002

Arampatzis, A., Peper, A., and Bierbaum, S. (2011). Exercise of Mechanisms for Dynamic Stability Control Increases Stability Performance in the Elderly. *J. Biomech.* 44, 52–58. doi:10.1016/j.jbiomech.2010.08.023

Bernstein, N. A. (1967). in *Coordination and Regulation of Movements*. Editor (Oxford, New York: Pergamon Press.

Bierbaum, S., Peper, A., Karamanidis, K., and Arampatzis, A. (2010). Adaptational Responses in Dynamic Stability during Disturbed Walking in the Elderly. *J. Biomech.* 43, 2362–2368. doi:10.1016/j.jbiomech.2010.04.025

Bizzi, E., Cheung, V. C. K., d'Avella, A., Saltiel, P., and Tresch, M. (2008). Combining Modules for Movement. *Brain Res. Rev.* 57, 125–133. doi:10.1016/j.brainresrev.2007.08.004

Bizzi, E., and Cheung, V. C. K. (2013). The Neural Origin of Muscle Synergies. *Front. Comput. Neurosci.* 7, 51. doi:10.3389/fncom.2013.00051

Bizzi, E., Mussa-Ivaldi, F. A., and Giszter, S. (1991). Computations Underlying the Execution of Movement: a Biological Perspective. *Science* 253, 287–291. doi:10.1126/science.1857964

Bohm, S., Mandla-Liebsch, M., Mersmann, F., and Arampatzis, A. (2020). Exercise of Dynamic Stability in the Presence of Perturbations Elicit Fast Improvements of Simulated Fall Recovery and Strength in Older Adults: A Randomized Controlled Trial. *Front. Sport Act. Living* 2, 52. doi:10.3389/fspor.2020.00052

Bohm, S., Mersmann, F., Bierbaum, S., Dietrich, R., and Arampatzis, A. (2012). Cognitive Demand and Predictive Adaptational Responses in Dynamic Stability Control. *J. Biomech.* 45, 2330–2336. doi:10.1016/j.jbiomech.2012.07.009

d'Avella, A., Saltiel, P., and Bizzi, E. (2003). Combinations of Muscle Synergies in the Construction of a Natural Motor Behavior. *Nat. Neurosci.* 6, 300–308. doi:10.1038/nn1010

Dominici, N., Ivanenko, Y. P., Cappellini, G., d'Avella, A., Mondì, V., Cicchese, M., et al. (2011). Locomotor Primitives in Newborn Babies and Their Development. *Science* 334, 997–999. doi:10.1126/science.1210617

Gerards, M. H. G., Marcellis, R. G. J., Poeze, M., Lenssen, A. F., Meijer, K., and de Bie, R. A. (2021). Perturbation-based Balance Training to Improve Balance Control and Reduce Falls in Older Adults - Study Protocol for a Randomized Controlled Trial. *BMC Geriatr.* 21, 9. doi:10.1186/s12877-020-01944-7

Giszter, S. F. (2015). Motor Primitives-New Data and Future Questions. *Curr. Opin. Neurobiol.* 33, 156–165. doi:10.1016/j.conb.2015.04.004

Gizzi, L., Nielsen, J. F., Felici, F., Ivanenko, Y. P., and Farina, D. (2011). Impulses of Activation but Not Motor Modules Are Preserved in the Locomotion of Subacute Stroke Patients. *J. Neurophysiol.* 106, 202–210. doi:10.1152/jn.00727.2010

Gordon, J. C., Holt, N. C., Biewener, A., and Daley, M. A. (2020). Tuning of Feedforward Control Enables Stable Muscle Force-Length Dynamics after Loss of Autogenic Proprioceptive Feedback. *Elife* 9. doi:10.7554/eLife.53908

Hamed, A., Bohm, S., Mersmann, F., and Arampatzis, A. (2018a). Exercises of Dynamic Stability under Unstable Conditions Increase Muscle Strength and Balance Ability in the Elderly. *Scand. J. Med. Sci. Sports* 28, 961–971. doi:10.1111/sms.13019

Hamed, A., Bohm, S., Mersmann, F., and Arampatzis, A. (2018b). Follow-up Efficacy of Physical Exercise Interventions on Fall Incidence and Fall Risk in Healthy Older Adults: a Systematic Review and Meta-Analysis. *Sports Med. - Open* 4, 56. doi:10.1186/s40798-018-0170-z

Hart, C. B., and Giszter, S. F. (2010). A Neural Basis for Motor Primitives in the Spinal Cord. *J. Neurosci.* 30, 1322–1336. doi:10.1523/JNEUROSCI.5894-08.2010

Hartigan, J. A., and Wong, M. A. (1979). Algorithm AS 136: A K-Means Clustering Algorithm. *Appl. Stat.* 28, 100. doi:10.2307/2346830

Hof, A. L. (1992). An Explicit Expression for the Moment in Multibody Systems. *J. Biomech.* 25, 1209–1211. doi:10.1016/0021-9290(92)90076-D

Hogan, N., and Sternad, D. (2012). Dynamic Primitives of Motor Behavior. *Biol. Cybern.* 106, 727–739. doi:10.1007/s00422-012-0527-1

Hollville, E., Nordez, A., Guilhem, G., Lecompte, J., and Rabita, G. (2020). Surface Properties Affect the Interplay between Fascicles and Tendinous Tissues during landing. *Eur. J. Appl. Physiol.* 120, 203–217. doi:10.1007/s00421-019-04265-9

Janshen, L., Santuz, A., Ekizos, A., and Arampatzis, A. (2020). Fuzziness of Muscle Synergies in Patients With Multiple Sclerosis Indicates Increased Robustness of Motor Control During Walking. *Sci. Rep.* 10, 7249. doi:10.1038/s41598-020-63788-w

Jöbges, M., Heuschkel, G., Pretzel, C., Illhardt, C., Renner, C., and Hummelsheim, H. (2004). Repetitive Training of Compensatory Steps: a Therapeutic Approach for Postural Instability in Parkinson's Disease. *J. Neurol. Neurosurg. Psychiatry* 75, 1682–1687. doi:10.1136/jnnp.2003.016550

Kargo, W. J., and Giszter, S. F. (2000). Rapid Correction of Aimed Movements by Summation of Force-Field Primitives. *J. Neurosci.* 20, 409–426. doi:10.1523/jneurosci.20-01-00409.2000

Kloke, J. D., and McKean, J. W. (2012). Rfit: Rank-Based Estimation for Linear Models. *R. J.* 4, 57–64. doi:10.32614/rj-2012-014

Kurz, I., Gimmon, Y., Shapiro, A., Debi, R., Snir, Y., and Melzer, I. (2016). Unexpected Perturbations Training Improves Balance Control and Voluntary Stepping Times in Older Adults - a Double Blind Randomized Control Trial. *BMC Geriatr.* 16, 58. doi:10.1186/s12877-016-0223-4

Lambert-Shirzad, N., and Van der Loos, H. F. M. (2017). On Identifying Kinematic and Muscle Synergies: a Comparison of Matrix Factorization Methods Using Experimental Data from the Healthy Population. *J. Neurophysiol.* 117, 290–302. doi:10.1152/jn.00435.2016

Lee, D. D., and Seung, H. S. (1999). Learning the Parts of Objects by Non-negative Matrix Factorization. *Nature* 401, 788–791. doi:10.1038/44565

Mademli, L., Mavridi, D., Bohm, S., Patikas, D. A., Santuz, A., and Arampatzis, A. (2021). Standing on Unstable Surface Challenges Postural Control of Tracking Tasks and Modulates Neuromuscular Adjustments Specific to Task Complexity. *Sci. Rep.* 11, 6122. doi:10.1038/s41598-021-84899-y

Malfait, B., Dingenen, B., Smeets, A., Staes, F., Pataky, T., Robinson, M. A., et al. (2016). Knee and Hip Joint Kinematics Predict Quadriceps and Hamstrings Neuromuscular Activation Patterns in Drop Jump Landings. *PLoS One* 11, e0153737. doi:10.1371/journal.pone.0153737

Mansfield, A., Aqui, A., Danells, C. J., Knorr, S., Centen, A., DePaul, V. G., et al. (2018). Does Perturbation-Based Balance Training Prevent Falls Among Individuals with Chronic Stroke? A Randomised Controlled Trial. *BMJ Open* 8, e021510. doi:10.1136/bmjopen-2018-021510

Mansfield, A., Wong, J. S., Bryce, J., Knorr, S., and Patterson, K. K. (2015). Does Perturbation-Based Balance Training Prevent Falls? Systematic Review and Meta-Analysis of Preliminary Randomized Controlled Trials. *Phys. Ther.* 95, 700–709. doi:10.2522/ptj.20140090

Martino, G., Ivanenko, Y. P., d'Avella, A., Serrao, M., Ranavolo, A., Draicchio, F., et al. (2015). Neuromuscular Adjustments of Gait Associated with Unstable Conditions. *J. Neurophysiol.* 114, 2867–2882. doi:10.1152/jn.00029.2015

Martino, G., Ivanenko, Y. P., Serrao, M., Ranavolo, A., d'Avella, A., Draicchio, F., et al. (2014). Locomotor Patterns in Cerebellar Ataxia. *J. Neurophysiol.* 112, 2810–2821. doi:10.1152/jn.00275.2014

McNitt-Gray, J. L., Yokoi, T., and Millward, C. (1993). Landing Strategy Adjustments Made by Female Gymnasts in Response to Drop Height and Mat Composition. *J. Appl. Biomech.* 9, 173–190. doi:10.1123/jab.9.3.173

Morey-Klapsing, G., Arampatzis, A., and Brüggemann, G.-P. (2007). Evidence of Proactive Forefoot Control during Landings on Inclined Surfaces. *J. Mot. Behav.* 39, 89–102. doi:10.3200/JMBR.39.2.89-102

Moritz, C. T., and Farley, C. T. (2004). Passive Dynamics Change Leg Mechanics for an Unexpected Surface during Human Hopping. *J. Appl. Physiol.* 97, 1313–1322. doi:10.1152/japplphysiol.00393.2004

Munoz-Martel, V., Santuz, A., Bohm, S., and Arampatzis, A. (2021). Neuromechanics of Dynamic Balance Tasks in the Presence of Perturbations. *Front. Hum. Neurosci.* 14, 560630. doi:10.3389/fnhum.2020.560630

Munoz-Martel, V., Santuz, A., Ekizos, A., and Arampatzis, A. (2019). Neuromuscular Organisation and Robustness of Postural Control in the Presence of Perturbations. *Sci. Rep.* 9, 12273. doi:10.1038/s41598-019-47613-7

Mussa-Ivaldi, F. A., Giszter, S. F., and Bizzi, E. (1994). Linear Combinations of Primitives in Vertebrate Motor Control. *Proc. Natl. Acad. Sci.* 91, 7534–7538. doi:10.1073/pnas.91.16.7534

Naouma, H., and Pataky, T. C. (20192019). A Comparison of Random-Field-Theory and False-Discovery-Rate Inference Results in the Analysis of Registered One-Dimensional Biomechanical Datasets. *PeerJ* 7, e8189–20. doi:10.7717/peerj.8189

Nichols, T. E., and Holmes, A. P. (2002). Nonparametric Permutation Tests for Functional Neuroimaging: A Primer with Examples. *Hum. Brain Mapp.* 15, 1–25. doi:10.1002/hbm.1058

Okubo, Y., Schoene, D., and Lord, S. R. (2017). Step Training Improves Reaction Time, Gait and Balance and Reduces Falls in Older People: A Systematic Review and Meta-Analysis. *Br. J. Sports Med.* 51, 586–593. doi:10.1136/bjsports-2015-095452

Pataky, T. C. (2012). One-dimensional Statistical Parametric Mapping in Python. *Computer Methods Biomech. Biomed. Eng.* 15, 295–301. doi:10.1080/10255842.2010.527837

Patla, A. E. (2003). Strategies for Dynamic Stability during Adaptive Human Locomotion. *IEEE Eng. Med. Biol. Mag.* 22, 48–52. doi:10.1109/MEMB.2003.1195695

Prieske, O., Muehlbauer, T., Mueller, S., Krueger, T., Kibele, A., Behm, D. G., et al. (2013). Effects of Surface Instability on Neuromuscular Performance during Drop Jumps and Landings. *Eur. J. Appl. Physiol.* 113, 2943–2951. doi:10.1007/s00421-013-2724-6

Rabbi, M. F., Pizzolato, C., Lloyd, D. G., Carty, C. P., Devaprakash, D., and Diamond, L. E. (2020). Non-negative Matrix Factorisation Is the Most Appropriate Method for Extraction of Muscle Synergies in Walking and Running. *Sci. Rep.* 10, 8266. doi:10.1038/s41598-020-65257-w

Santuz, A., Brüll, L., Ekizos, A., Schroll, A., Eckardt, N., Kibele, A., et al. (2020). Neuromotor Dynamics of Human Locomotion in Challenging Settings. *iScience* 23, 100796. doi:10.1016/j.isci.2019.100796

Santuz, A., Ekizos, A., Eckardt, N., Kibele, A., and Arampatzis, A. (2018). Challenging Human Locomotion: Stability and Modular Organisation in Unsteady Conditions. *Sci. Rep.* 8, 2740. doi:10.1038/s41598-018-21018-4

Santuz, A., Ekizos, A., Janshen, L., Baltzopoulos, V., and Arampatzis, A. (2017). On the Methodological Implications of Extracting Muscle Synergies from Human Locomotion. *Int. J. Neur. Syst.* 27, 1750007. doi:10.1142/S0129065717500071

Santuz, A. (2021). musclesyneRgies v0.7.1-alpha. Available at: https://github.com/alesantuz/musclesyneRgies/releases/tag/v0.7.1-alpha.

Sherrington, C., Michaleff, Z. A., Fairhall, N., Paul, S. S., Tiedemann, A., Whitney, J., et al. (2017). Exercise to Prevent Falls in Older Adults: an Updated Systematic Review and Meta-Analysis. *Br. J. Sports Med.* 51, 1750–1758. doi:10.1136/bjsports-2016-096547

Tresch, M. C., Cheung, V. C. K., and d'Avella, A. (2006). Matrix Factorization Algorithms for the Identification of Muscle Synergies: Evaluation on Simulated and Experimental Data Sets. *J. Neurophysiol.* 95, 2199–2212. doi:10.1152/jn.00222.2005

Wang, Y., Bhatt, T., Liu, X., Wang, S., Lee, A., Wang, E., et al. (2019). Can Treadmill-Slip Perturbation Training Reduce Immediate Risk of Over-ground-slip Induced Fall Among Community-Dwelling Older Adults? *J. Biomech.* 84, 58–66. doi:10.1016/j.jbiomech.2018.12.017

Winter, D. A. (2005). *Biomechanics and Motor Control of Human Movement*. 3rd ed. Hoboken, New Jersey, United States: Wiley Online Library.

Zhang, S.-N., Bates, B. T., and Dufek, J. S. (2000). Contributions of Lower Extremity Joints to Energy Dissipation during Landings. *Med. Sci. Sports Exerc.* 32, 812–819. doi:10.1097/00005768-200004000-00014

Conflict of Interest: The authors declare that the research was conducted in the absence of any commercial or financial relationships that could be construed as a potential conflict of interest.

Publisher's Note: All claims expressed in this article are solely those of the authors and do not necessarily represent those of their affiliated organizations, or those of the publisher, the editors, and the reviewers. Any product that may be evaluated in this article, or claim that may be made by its manufacturer, is not guaranteed or endorsed by the publisher.

frontiers in Physiology

ORIGINAL RESEARCH
published: 23 December 2021
doi: 10.3389/fphys.2021.786625

Influence of Axial Load and a 45-Degree Flexion Head Position on Cervical Spinal Stiffness in Healthy Young Adults

Léonie Hofstetter[1,2], Melanie Häusler[1,2], Petra Schweinhardt[1,2], Ursula Heggli[3], Denis Bron[3†] and Jaap Swanenburg[1,2†]*

[1] Integrative Spinal Research ISR, Department of Chiropractic Medicine, Balgrist University Hospital, Zurich, Switzerland, [2] Faculty of Medicine, University of Zurich, Zurich, Switzerland, [3] AeMC, Aeromedical Center, Swiss Air Forces, Dubendorf, Switzerland

Background: Neck pain is a major cause of disability worldwide. Poor neck posture such as using a smartphone or work-related additional cervical axial load, such headgear of aviators, can cause neck pain. This study aimed at investigating the role of head posture or additional axial load on spinal stiffness, a proxy measure to assess cervical motor control.

Methods: The posterior-to-anterior cervical spinal stiffness of 49 young healthy male military employees [mean (SD) age 20 ± 1 years] was measured in two head positions: neutral and 45-degree flexed head position and two loading conditions: with and without additional 3 kg axial load. Each test condition comprised three trials. Measurements were taken at three cervical locations, i.e., spinous processes C2 and C7 and mid-cervical (MC).

Results: Cervical spinal stiffness measurements showed good reliability in all test conditions. There was a significant three-way interaction between location × head position × load [$F(2, 576) = 9.305$, $p < 0.001$]. Significant two-way interactions were found between measurement locations × loading [$F(2, 576) = 15.688$, $p < 0.001$] and measurement locations × head position [$F(2, 576) = 9.263$, $p < 0.001$]. There was no significant interaction between loading × head position [$F(1, 576) = 0.692$, $p = 0.406$]. *Post hoc* analysis showed reduction of stiffness in all three measurement locations in flexion position. There was a decrease in stiffness in C2 with loading, increase in stiffness in C7 and no change in MC.

Discussion: A flexed head posture leading to decreased stiffness of the cervical spine might contribute to neck pain, especially if the posture is prolonged and static, such as is the case with smartphone users. Regarding the additional load, stiffness decreased high cervical and increased low cervical. There was no change mid cervical. The lower spinal stiffness at the high cervical spine might be caused by capsular ligament laxity due to the buckling effect. At the lower cervical spine, the buckling effect seems to be less dominant, because the proximity to the ribs and sternum provide additional stiffness.

Keywords: cervical spine, flexion, axial load, stiffness, posture

Abbreviations: CI, Confidence intervals; EMG, Electromyography; FRP, Flexion relaxation phenomenon; ICC, Intraclass correlation coefficient; NDI, Neck Disability Index; SEM, Standard error of measurement.

OPEN ACCESS

Edited by:
Ramona Ritzmann, Clinic Rennbahn AG, Switzerland

Reviewed by:
Riza Bayoglu, NuVasive, United States
Leila Rahnama, Kennesaw State University, United States

***Correspondence:**
Jaap Swanenburg
jaap.swanenburg@balgrist.ch

† These authors share last authorship

Specialty section:
This article was submitted to Exercise Physiology, a section of the journal Frontiers in Physiology

Received: *30 September 2021*
Accepted: *03 December 2021*
Published: *23 December 2021*

Citation:
Hofstetter L, Häusler M, Schweinhardt P, Heggli U, Bron D and Swanenburg J (2021) Influence of Axial Load and a 45-Degree Flexion Head Position on Cervical Spinal Stiffness in Healthy Young Adults. Front. Physiol. 12:786625. doi: 10.3389/fphys.2021.786625

INTRODUCTION

Neck pain is a common problem and one of the highest contributors to disability worldwide (James et al., 2018). An awkward head position is the most commonly reported physical risk factor for a first episode of neck pain (Kim et al., 2018), and working with the neck flexed at more than 20° has been suggested to increase this risk (Ariens et al., 2001). Awkward posture is exacerbated when using a smartphone (Lee et al., 2015), which is associated with strain of cervical extensor muscles, altered postural control and pain (Eitivipart et al., 2018). In addition to awkward head position, cervical axial load can contribute to neck pain. For example, neck pain can occur in people who endure increased cervical axial load, such as aviators wearing headgear and individuals carrying loads with their heads (Echarri and Forriol, 2002; Geere et al., 2010; Posch et al., 2019). In sports such as gymnastics, ice hockey, American football, and rugby, which have a high incidence of neck injury, axial loading of the cervical spine is considered the primary mechanism of injury (Torg et al., 2002; Barile et al., 2007; Trewartha et al., 2015).

To protect the neck from pain and injury due to flexion position and/or axial load, a functional cervical motor control system is needed (Posch et al., 2019). Motor control, which consists of active, passive and neurological subsystems (Panjabi, 1992), can be accessed via different proxy measures. Most commonly, muscle activity, i.e., the active subsystem, is measured (Stokes and Gardner-Morse, 2003; Honkanen et al., 2017). The passive subsystem has also been studied, mainly *in vitro* using human spines or porcine models, typically reduced to bones and ligaments (Gardner-Morse and Stokes, 2003; Stokes and Gardner-Morse, 2003; Zhang et al., 2020). The assessment of spinal stiffness *in vivo* is considered a proxy measure of the active and passive subsystems combined (Swanenburg et al., 2018, 2020; Hausler et al., 2020).

It has been observed recently that lumbar and thoracic spinal stiffness is dependent on body position and axial load (Hausler et al., 2020; Swanenburg et al., 2020). Thoracic and lumbar spinal stiffness was found to increase while standing, compared with a prone position (Hausler et al., 2020). With increased axial load, either added via adding an additional axial load larger than 45% of the body weight with the help of a long weight bar or during hypergravity induced by parabolic flight, spinal stiffness decreased (Swanenburg et al., 2018, 2020; Hausler et al., 2020; Glaus et al., 2021).

The relationships between axial load, head flexion position and cervical spinal stiffness are yet to be determined, despite increasing evidence showing a relationship between neck pain and cervical flexion. Therefore, this study aimed to investigate the effects of cervical flexion position, with or without additional cervical axial load, on cervical spinal stiffness.

MATERIALS AND METHODS

A total of 49 healthy young adult male participants were recruited, aged 18–23 years and employees of the Swiss military. Swiss military personnel were selected because they are used to wearing a helmet. Written informed consent was obtained from all participants. The exclusion criteria were: any current or chronic neck pain, age younger than 18 years and a Neck Disability Index (NDI) score of more than 15 points. The NDI is a self-report questionnaire with 10 items assessing: pain intensity, personal care, lifting, work, headaches, concentration, sleeping, driving, reading and recreation. Each item is scored on a 0–5 scale. Zero means no disability, 5 complete disability. The scores are summed, resulting in a total score between 0 and 50. The NDI German Version has demonstrated good reliability (Swanenburg et al., 2014). The study was approved by the Ethics Committee of the Canton of Zurich (Reference: BASEC 2019–00830) (ClinicalTrials.gov Identifier: NCT04434235).

Data Collection Procedures

First, demographic data, such as sex, age, weight, and height of each participant were collected. After completing the NDI questionnaire, participants were asked to sit with a straight back on a workout bench. Two of the three measurement locations [the spinous processes of C2 (high-cervical) and C7 (low-cervical)] were manually identified by two experienced manual therapists, with the spinous process of C2 being the most cranial one that can clearly be palpated and using the flexion-extension test to locate C7 (Povoa et al., 2018). C2 and C7 were marked with ink to label the location for spinal stiffness assessment and the marking was verified by both therapists to increase accuracy. For the third mid-cervical (MC) assessment location, half of the distance between the spinous process of C2 and C7 was taken.

Head Position

The first spinal stiffness measurements were conducted sitting straight with their hands placed relaxed on their thighs and with a neutral head position, with the forehead lightly touching against a horizontal bar, to guarantee position. The common head flexion angle while using a smartphone is 45 degrees from vertical (Lee et al., 2015; Guan et al., 2016). Therefore, the flexion condition was performed with 45-degree flexion, by asking the participant to put a size-adjustable foam pad between the sternum and the chin to guarantee constant head position (**Figure 1**). The size of the foam pad was defined before the measurements. First, the 45° flexion head position was determined using an electronic goniometer (EasyAngle®, Meloq AB, Stockholm, Sweden). Then, a size-adjustable foam pad was placed between the sternum and the chin to keep the angle. Pre-testing showed no effect of the foam pad on the stiffness results.

Load

After the neutral and flexion measurements, the participants were asked to put on an ice hockey helmet (size M) (CCM, Saint Laurent, QC, Canada) to recreate the real world-working situation. Additional load was fixed to the helmet, on the sagittal balance axis, resulting in a total helmet weight of 3 kg (**Figure 2**). This weight was chosen because helmets of helicopter pilots weigh up to 2.5 kg (Lange et al., 2013). Then, measurements in both head positions were repeated with additional axial load.

FIGURE 1 | Experimental set-up in cervical flexion position. Arrow 1: Size-adjustable foam pad. Arrow 2: Stiffness device.

FIGURE 2 | Experimental set-up in neutral position with additional axial load (red). Arrow 1: Foam pad. Arrow 2: Stiffness device.

For each test situation, the measurements were repeated three times. The participants were asked to inform the examiner if they experienced any pain during measurement.

Cervical Spinal Stiffness Assessments

A computer-assisted device (PulStarFRAS, Sense Technology Inc., Pittsburgh, PA) was used to measure posterior-to-anterior spinal stiffness (Leach et al., 2003). This device possesses good test–retest reliability, with intraclass correlation coefficient (ICC) values greater than 0.83 (Hausler et al., 2020). Spinal stiffness is defined as the impulse response to the deformation of the spine system; a linear, time-invariant response to a very short (<1 ms) impulse. This time invariance allows the impulse response to be measure in Newton, rather than Newton seconds (as in classical measurements) (Girod et al., 2003). A preload of 18 N was applied to trigger the assessment and overcome possible confounders caused by soft tissue components. After reaching the preload of 18 Newton, the device automatically applied an impulse with a single contact probe—a force of 27 N in a 90° angle relative to the surface of the back.

Statistical Analysis

Baseline characteristics of study participants were summarized using descriptive statistics. Mean cervical spinal stiffness and 95% confidence intervals (CI) of each measurement location in all testing situations were plotted graphically.

Reliability

ICC with 95% CI was calculated to assess test–retest reliability. To determine absolute reliability and standard error of measurement (SEM) were calculated. Cronbach's alpha was calculated to evaluate internal consistency.

Influence of Measurement Locations, Head Position, and Axial Load

A three-way ANOVA was used to determine if there are interaction effects between the three independent variables head position (neutral and flexion), loading (unloaded and loaded), and measurement locations (C2, MC, and C7) regarding the dependent variable cervical stiffness. An alpha level of 0.05 was used to determine statistical significance. *Post hoc* tests were calculated to investigate the factors head position, loading. All statistical analyses were performed using SPSS 23 (IBM, Chicago, IL).

RESULTS

Participants

Forty-nine male participants were recruited [mean age: 19.9 ± (SD) 1.1 years; mean height: 179.8 ± 11.4 cm; mean weight: 74.4 ± 11.4 kg]. None were excluded and none reported pain during the assessments. **Figures 3–5** represents mean spinal stiffness with 95% CI for all three measurement locations, in both head positions and loading conditions.

Reliability

Spinal stiffness measurements showed good reliability in both head position and measurement locations with ICCs > 0.799 and

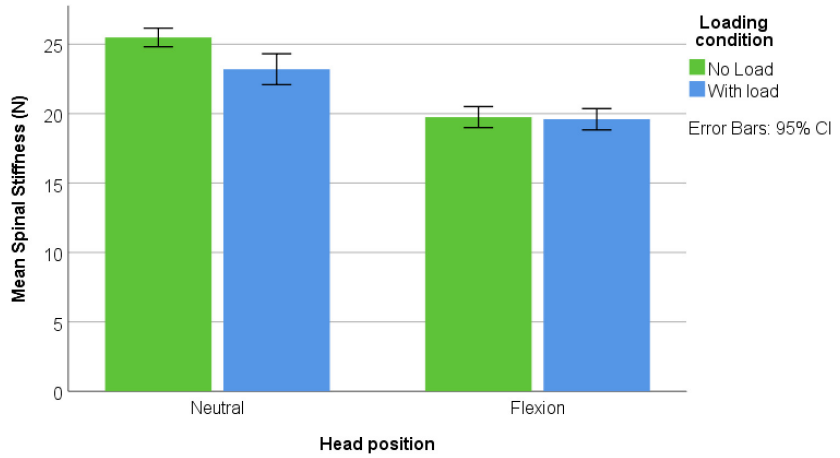

FIGURE 3 | C2 location; spinal stiffness mean values in both head positions and both loading conditions.

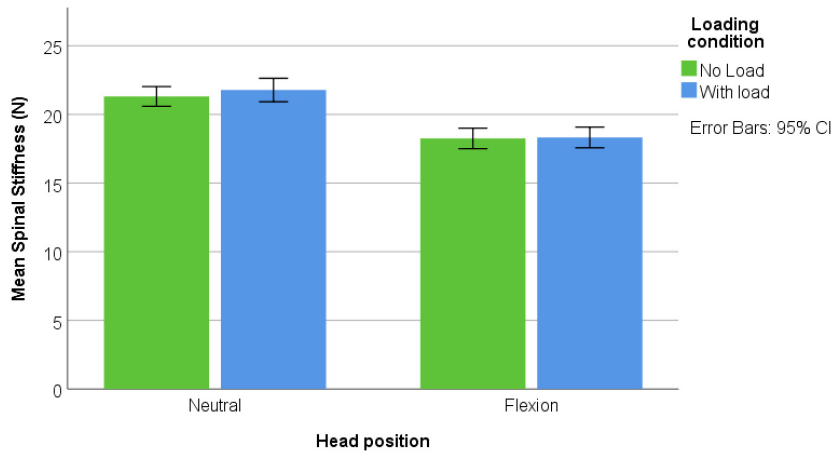

FIGURE 4 | MC location; spinal stiffness mean values in both head positions and both loading conditions.

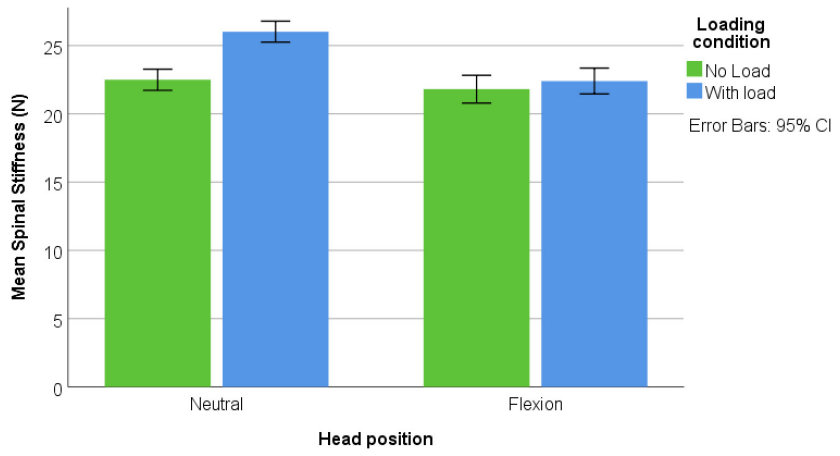

FIGURE 5 | C7 location; spinal stiffness mean values in both head positions and both loading conditions.

TABLE 1 | Reliability of the three stiffness measurements in all four test situations at al all three locations.

	C2			MC			C7		
	ICC (95% CI)	A	SEM (N)	ICC (95% CI)	A	SEM (N)	ICC (95% CI)	A	SEM (N)
Neutral	0.875 (0.799–0.925)	0.874	1.016	0.799(0.677–0.880)	0.883	1.534	0.810(0.695–0.887)	0.808	1.537
Flexion	0.873(0.796–0.924)	0.878	1.226	0.868(0.811–0.930)	0.866	0.931	0.883(0.813–0.930)	0.883	1.267
Neutral + loaded	0.872(0.795–0.924)	0.872	1.056	0.818(0.708–0.892)	0.815	1.401	0.844(0.749–0.907)	0.843	1.528
Flexion + loaded	0.891(0.824–0.935)	0.889	0.870	0.948(0.946–0.969)	0.948	0.430	0.916(0.866–0.950)	0.916	0.840

ICC, intraclass correlation coefficient; CI, confidence interval; A, Cronbach's alpha; N, Newton; SEM, standard error of measurement; Neutral + loaded, neutral head position with additional axial load; Flexion + loaded, flexed head position with additional axial load; MC, mid-cervical: C2 and C7, cervical vertebra 2 and 7.

Cronbach's alpha 0.808—0.948. All reliability values of both head position, two loading conditions, and measurement locations are shown in **Table 1**. All cervical stiffness values split in measurement locations are shown in **Figures 3–5**.

Influence of Measurement Locations, Head Position, and Axial Load

Levene's test showed that the assumption of homogeneity of variance was satisfied. A three-way ANOVA was performed to examine the interaction effects of head position, loading, and measurement location regarding cervical spinal stiffness. There was a significant three-way interaction [$F(2, 576) = 9.305$, $p < 0.001$]. Significant two-way interactions were found between loading x measurement location [$F(2, 576) = 15.688$, $p < 0.001$] and head position $\times$ measurement location [$F(2, 576) = 9.263$, $p < 0.001$]. There was no significant interaction between loading $\times$ head position [$F(1, 576) = 0.692$, $p = 0.406$]. *Post hoc* analysis showed reduction of stiffness in all three measurement locations in flexion position. There was a decrease in stiffness in C2 with loading, increase in stiffness in C7 and no change in MC. The *post hoc* results are shown in **Table 2** and **Supplementary Figures 1–3** show the respective interactions.

TABLE 2 | *Post hoc* results for head position and loading conditions in all measurement locations.

	Cervical spinal stiffness (Newton)		
Measurement location	**Neutral mean (SD)**	**Flexion mean (SD)**	***p***
C2	24.35 (3.84)	19.67 (2.64)	<0.001*
MC	21.54 (2.45)	18.29 (2.60)	<0.001*
C7	24.26 (3.20)	22.10 (3.42)	<0.001*
	Unloaded mean (SD)	**Loaded mean (SD)**	***P***
C2	22.62 (3.80)	21.40 (3.77)	0.025*
MC	19.78 (2.97)	20.05 (3.29)	0.546
C7	22.15 (3.14)	24.21 (3.50)	<0.001*

*$p < 0.05$.
MC, mid-cervical: C2 and C7, cervical vertebra 2 and 7.

DISCUSSION

In this study, cervical spinal stiffness was examined in two different head positions, with and without additional axial load, at three cervical measurement locations. The measurements of spinal stiffness in asymptomatic individuals were found to be reliable. Our results show a reduction of cervical spinal stiffness in the 45-degree flexion position compared to the neutral position in all measurement locations.

An earlier study measured the effect of different head positions on cervical spinal stiffness in a prone body posture, not reporting any significant change between neutral and flexed position (Snodgrass and Rhodes, 2012). In contrast to our study, the stiffness (insignificantly) increased from neutral to flexion position. This contrasting result might be explained by prone body posture in which the head is fully supported, possibly leading to an increase in the measured stiffness. Further, neck stiffness was found to be significantly decreased after 10 min static neck flexion, after returning into neutral position (Mousavi-Khatir et al., 2018). This suggests that the decrease in stiffness that was found in the present study during flexion might remain, even if the head has returned to a neutral position.

Head Position

The decrease in spinal stiffness in the flexion head position could be due to the flexion relaxation phenomenon (FRP) of the cervical spine, which describes a myoelectric "silence" of the neck extensor muscles during cervical flexion (Simon et al., 2006). This can be explained by a transfer of the extension moment from the active to the passive structures of the spine with further flexion (Pialasse et al., 2009). The FRP has been observed only for the cervical erector spinae muscle, whereas the upper trapezius muscle showed no FRP response (Colloca and Hinrichs, 2005; Maroufi et al., 2013). Furthermore, cervical flexor muscles, as antagonists, are likely to be less activated in the flexion position (Maroufi et al., 2013). At the low-cervical spine, a smaller decrease in stiffness was found in the 45-degree flexion position compared to the neutral head position. More likely, the low-cervical spine is at the end of motion given that the cervicothoracic junction experiences less flexion than other segments of the cervical spine (Nightingale et al., 2007). Therefore, this could

have caused a smaller decrease in spinal stiffness. Overall, it can be hypothesized that less support by a less active muscular subsystem led to decreased cervical stiffness in the flexion head position.

Another explanation for the decrease in cervical spinal stiffness could be the pressure on the cervical intervertebral discs during flexion. During the movement of the neck in the different directions, the loads on the cervical intervertebral discs increases resulting in an increase in cervical intervertebral disc pressure (Bayoglu et al., 2019). Another study reported a twofold increase in pressure in the cervical discs with flexion and a fourfold increase of the shear forces (Barrett et al., 2020). This additional load, generated by flexion, leads to capsular ligament laxity of the facet joints (Steilen et al., 2014), the so-called buckling effect (Nightingale et al., 1996). By reducing the passive stability, the buckling effect might have decreased the spinal stiffness in the present study.

Additional Load

The interaction effect between loading and measurement location showed that loading had some effect. A decrease in stiffness in the high cervical region and an increase in the low-cervical spine was observed. The change in stiffness in the high cervical spine due to the additional load might be explained by capsular ligament laxity due to the buckling effect (Nightingale et al., 1996). Thus, the reduced tension on the passive structures might have led to a play between the structures that resulted in a reduction in spinal stiffness. The unchanged spinal stiffness in the mid-cervical vertebrae might be the results of opposite effects that cancel each other out, namely muscle activity and buckling. In contrast to the high-cervical spine, more low cervical muscle activity is needed to stabilize not only the head and the additional load, but also the high-cervical spine (Bergmark, 1989; Swanenburg et al., 2020; Glaus et al., 2021). This increased muscle activation would be expected to lead to an increase in spinal stiffness (Swanenburg et al., 2020). Thus, the unchanged stiffness of the mid-cervical spine might be the net effect of buckling effects and increased muscle activity. The stiffness at the low-cervical spine increased with additional load. This increase in spinal stiffness can be explained by an increase in muscle activity to stabilize not only the head and extra load, but also the decreased stiffness of the high-cervical spine. Moreover, mobility is maximal at the low-cervical spine (Penning, 1978). Compression of the cervical spine due to the additional load and the consequent relaxation of the stabilizing ligaments appears to be less dominant in the low-cervical spine. More muscle activity is needed to stabilize the cervical spine because of the lesser passive stability (Izzo et al., 2013). Additionally, the low-cervical spine is closer to structures that provide additional stability, such as the ribs and the sternum. It could be argued that the more mobile low-cervical spine needs more muscle activation to stabilize the cervical spine with the additional load, which led to increased stiffness at the low-cervical spine.

Clinical Implication

There is relationship between a flexion neck posture and neck pain symptoms (Barrett et al., 2020), especially if this flexed posture is sustained for a long period of time, as in the case of excessive use of mobile devices (Ariens et al., 2001; Bayoglu et al., 2019). Avoiding prolonged static postures and a flexed head position greater than 30 degrees might help to prevent neck pain.

Limitations

The generalizability of the present study's results is unknown because only asymptomatic young male subjects were included. Additionally, other factors that might influence cervical spinal stiffness were not measured. For example, muscle activity was not directly assessed by electromyography (EMG). The activity of the deep neck flexors, such as the longus capitis and longus colli, cannot be measured with superficial EMG; this would require the use of a nasopharyngeal catheter, the application of which would have been invasive and impractical in the study environment (Robinson et al., 2009). Individual differences in muscle dimensions that stabilize the cervical spine were not considered. The individuals' cervical range of motion in flexion direction was not assessed. Nevertheless, all participants were able to assume the 45-degree flexion position without any difficulty.

CONCLUSION

A flexed head posture leads to a decrease in the stiffness of the cervical spine. The decreased stiffness might be due to increased pressure and shear forces on the cervical intervertebral discs during a 45-degree flexion. It is expected that such effects would be pronounced when the posture is prolonged and static, such as is the case with smartphone users. Regarding the additional load, stiffness decreased high cervical and increased low cervical. There was and no change in mid cervical. The lower spinal stiffness at the high cervical spine might be caused by capsular ligament laxity due to the buckling effect. At the lower cervical spine, the buckling effect seems to be less dominant, because the proximity to the ribs and sternum provide additional stiffness.

DATA AVAILABILITY STATEMENT

The raw data supporting the conclusions of this article will be made available by the authors, without undue reservation.

ETHICS STATEMENT

The studies involving human participants were reviewed and approved by the Ethics Committee of the Canton of Zurich (Reference: BASEC 2019–00830). The patients/participants provided their written informed consent to participate in this study.

AUTHOR CONTRIBUTIONS

JS developed the research question and the design. LH, MH, and UH conducted the data acquisition. LH, MH, and JS carried out analysis and interpretation of the results. LH produced an early version of the manuscript. JS, DB, LH, MH, UH, and PS revised the manuscript to bring it to its current version. All authors contributed to the article and approved the submitted version.

ACKNOWLEDGMENTS

We like to thank Anita Meinke for the drawings.

SUPPLEMENTARY MATERIAL

The Supplementary Material for this article can be found online at: https://www.frontiersin.org/articles/10.3389/fphys.2021.786625/full#supplementary-material

REFERENCES

Ariens, G. A., Bongers, P. M., Douwes, M., Miedema, M. C., Hoogendoorn, W. E., van der Wal, G., et al. (2001). Are neck flexion, neck rotation, and sitting at work risk factors for neck pain? Results of a prospective cohort study. *Occup. Environ. Med.* 58, 200–207. doi: 10.1136/oem.58.3.200

Barile, A., Limbucci, N., Splendiani, A., Gallucci, M., and Masciocchi, C. (2007). Spinal injury in sport. *Eur. J. Radiol.* 62, 68–78. doi: 10.1016/j.ejrad.2007.01.017

Barrett, J. M., McKinnon, C., and Callaghan, J. P. (2020). Cervical spine joint loading with neck flexion. *Ergonomics* 63, 101–108. doi: 10.1080/00140139.2019.1677944

Bayoglu, R., Galibarov, P. E., Verdonschot, N., Koopman, B., and Homminga, J. (2019). Twente spine model: a thorough investigation of the spinal loads in a complete and coherent musculoskeletal model of the human spine. *Med. Eng. Phys.* 68, 35–45. doi: 10.1016/j.medengphy.2019.03.015

Bergmark, A. (1989). Stability of the lumbar spine. A study in mechanical engineering. *Acta Orthop. Scand. Suppl.* 230, 1–54. doi: 10.3109/17453678909154177

Colloca, C. J., and Hinrichs, R. N. (2005). The biomechanical and clinical significance of the lumbar erector spinae flexion-relaxation phenomenon: a review of literature. *J. Manipulative Physiol. Ther.* 28, 623–631. doi: 10.1016/j.jmpt.2005.08.005

Echarri, J. J., and Forriol, F. (2002). Effect of axial load on the cervical spine: a study of Congolese woodbearers. *Int. Orthop.* 26, 141–144. doi: 10.1007/s00264-002-0336-6

Eitivipart, A. C., Viriyarojanakul, S., and Redhead, L. (2018). Musculoskeletal disorder and pain associated with smartphone use: a systematic review of biomechanical evidence. *Hong Kong Physiother. J.* 38, 77–90. doi: 10.1142/S1013702518300010

Gardner-Morse, M. G., and Stokes, I. A. (2003). Physiological axial compressive preloads increase motion segment stiffness, linearity and hysteresis in all six degrees of freedom for small displacements about the neutral posture. *J. Orthop. Res.* 21, 547–552. doi: 10.1016/S0736-0266(02)00199-7

Geere, J. A. L., Hunter, P. R., and Jagals, P. (2010). Domestic water carrying and its implications for health: a review and mixed methods pilot study in Limpopo Province, South Africa. *Environ. Health* 9:52. doi: 10.1186/1476-069x-9-52

Girod, B., Rabenstein, R., and Stenger, A. (2003). *Einführung in die Systemtheorie*. Wiesbaden: Vieweg+Teubner Verlag.

Glaus, L. S., Hofstetter, L., Guekos, A., Schweinhardt, P., and Swanenburg, J. (2021). In vivo measurements of spinal stiffness according to a stepwise increase of axial load. *Eur. J. Appl. Physiol.* 121, 2277–2283. doi: 10.1007/s00421-021-04705-5

Guan, X. F., Fan, G. X., Chen, Z. Q., Zeng, Y., Zhang, H. L., Hu, A. A., et al. (2016). Gender difference in mobile phone use and the impact of digital device exposure on neck posture. *Ergonomics* 59, 1453–1461. doi: 10.1080/00140139.2016.1227537

Hausler, M., Hofstetter, L., Schweinhardt, P., and Swanenburg, J. (2020). Influence of body position and axial load on spinal stiffness in healthy young adults. *Eur. Spine J.* 29, 455–461. doi: 10.1007/s00586-019-06254-0

Honkanen, T., Oksa, J., Mantysaari, M. J., Kyrolainen, H., and Avela, J. (2017). Neck and shoulder muscle activation among experienced and inexperienced pilots in +G(z) exposure. *Aerosp. Med. Hum. Perform.* 88, 90–95. doi: 10.3357/Amhp.4659.2017

Izzo, R., Guarnieri, G., Guglielmi, G., and Muto, M. (2013). Biomechanics of the spine. Part I: spinal stability. *Eur. J. Radiol.* 82, 118–126. doi: 10.1016/j.ejrad.2012.07.024

James, S. L., Abate, D., Abate, K. H., Abay, S. M., Abbafati, C., Abbasi, N., et al. (2018). Global, regional, and national incidence, prevalence, and years lived with disability for 354 diseases and injuries for 195 countries and territories, 1990-2017: a systematic analysis for the global burden of disease study 2017. *Lancet* 392, 1789–1858. doi: 10.1016/S0140-6736(18)32279-7

Kim, R., Wiest, C., Clark, K., Cook, C., and Horn, M. (2018). Identifying risk factors for first-episode neck pain: a systematic review. *Musculoskelet. Sci. Pract.* 33, 77–83. doi: 10.1016/j.msksp.2017.11.007

Lange, B., Nielsen, R. T., Skejo, P. B., and Toft, P. (2013). Centrifuge-induced neck and back pain in F-16 pilots: a report of four cases. *Aviat. Space Environ. Med.* 84, 734–738. doi: 10.3357/asem.3434.2013

Leach, R. A., Parker, P. L., and Veal, P. S. (2003). PulStar differential compliance spinal instrument: a randomized interexaminer and intraexaminer reliability study. *J. Manipulative Physiol. Ther.* 26, 493–501. doi: 10.1016/S0161-4754(03)00106-4

Lee, S., Kang, H., and Shin, G. (2015). Head flexion angle while using a smartphone. *Ergonomics* 58, 220–226. doi: 10.1080/00140139.2014.967311

Maroufi, N., Ahmadi, A., and Khatir, S. R. M. (2013). A comparative investigation of flexion relaxation phenomenon in healthy and chronic neck pain subjects. *Eur. Spine J.* 22, 162–168. doi: 10.1007/s00586-012-2517-3

Mousavi-Khatir, R., Talebian, S., Toosizadeh, N., Olyaei, G. R., and Maroufi, N. (2018). The effect of static neck flexion on mechanical and neuromuscular behaviors of the cervical spine. *J. Biomech.* 72, 152–158. doi: 10.1016/j.jbiomech.2018.03.004

Nightingale, R. W., Carol Chancey, V., Ottaviano, D., Luck, J. F., Tran, L., Prange, M., et al. (2007). Flexion and extension structural properties and strengths for male cervical spine segments. *J. Biomech.* 40, 535–542. doi: 10.1016/j.jbiomech.2006.02.015

Nightingale, R. W., McElhaney, J. H., Richardson, W. J., Best, T. M., and Myers, B. S. (1996). Experimental impact injury to the cervical spine: relating motion of the head and the mechanism of injury. *J. Bone Joint Surg. Am.* 78, 412–421. doi: 10.2106/00004623-199603000-00013

Panjabi, M. M. (1992). The stabilizing system of the spine. Part II. Neutral zone and instability hypothesis. *J. Spinal Disord.* 5, 390–396; discussion 397. doi: 10.1097/00002517-199212000-00002

Penning, L. (1978). Normal movements of the cervical spine. *AJR Am. J. Roentgenol.* 130, 317–326. doi: 10.2214/ajr.130.2.317

Pialasse, J. P., Dubois, J. D., Choquette, M. H., Lafond, D., and Descarreaux, M. (2009). Kinematic and electromyographic parameters of the cervical flexion-relaxation phenomenon: the effect of trunk positioning. *Ann. Phys. Rehabil. Med.* 52, 49–58. doi: 10.1016/j.rehab.2008.10.002

Posch, M., Schranz, A., Lener, M., Senn, W., Ang, B. O., Burtscher, M., et al. (2019). Prevalence and potential risk factors of flight-related neck, shoulder and low back pain among helicopter pilots and crewmembers: a questionnaire-based study. *BMC Musculoskelet. Disord.* 20:4. doi: 10.1186/s12891-019-2421-7

Povoa, L. C., Ferreira, A. P. A., Zanier, J. F. C., and Silva, J. G. (2018). Accuracy of motion palpation flexion-extension test in identifying the seventh cervical spinal process. *J. Chiropr. Med.* 17, 22–29. doi: 10.1016/j.jcm.2017.11.005

Robinson, R., Robinson, H. S., Bjorke, G., and Kvale, A. (2009). Reliability and validity of a palpation technique for identifying the spinous processes of C7 and L5. *Man. Ther.* 14, 409–414. doi: 10.1016/j.math.2008.06.002

Simon, S., Davis, M., Odhner, D., Udupa, J., and Winkelstein, B. (2006). CT imaging techniques for describing motions of the cervicothoracic junction and cervical spine during flexion, extension, and cervical traction. *Spine (Phila Pa 1976)* 31, 44–50. doi: 10.1097/01.brs.0000192679.25878.f9

Snodgrass, S. J., and Rhodes, H. R. (2012). Cervical spine posteroanterior stiffness differs with neck position. *J. Electromyogr. Kinesiol.* 22, 829–834. doi: 10.1016/j.jelekin.2012.04.014

Steilen, D., Hauser, R., Woldin, B., and Sawyer, S. (2014). Chronic neck pain: making the connection between capsular ligament laxity and cervical instability. *Open Orthop. J.* 8, 326–345. doi: 10.2174/1874325001408010326

Stokes, I. A., and Gardner-Morse, M. (2003). Spinal stiffness increases with axial load: another stabilizing consequence of muscle action. *J. Electromyogr. Kinesiol.* 13, 397–402. doi: 10.1016/s1050-6411(03)00046-4

Swanenburg, J., Humphreys, K., Langenfeld, A., Brunner, F., and Wirth, B. (2014). Validity and reliability of a German version of the neck disability index (NDI-G). *Man. Ther.* 19, 52–58. doi: 10.1016/j.math.2013.07.004

Swanenburg, J., Langenfeld, A., Easthope, C. A., Meier, M. L., Ullrich, O., and Schweinhardt, P. (2020). Microgravity and hypergravity induced by parabolic flight differently affect lumbar spinal stiffness. *Front. Physiol.* 11:562557. doi: 10.3389/fphys.2020.562557

Swanenburg, J., Meier, M. L., Langenfeld, A., Schweinhardt, P., and Humphreys, B. K. (2018). Spinal stiffness in prone and upright postures during 0-1.8 g induced by parabolic flight. *Aerosp. Med. Hum. Perform.* 89, 563–567. doi: 10.3357/AMHP.5031.2018

Torg, J. S., Guille, J. T., and Jaffe, S. (2002). Injuries to the cervical spine in American football players. *J. Bone Joint Surg. Am.* 84a, 112–122. doi: 10.2106/00004623-200201000-00017

Trewartha, G., Preatoni, E., England, M. E., and Stokes, K. A. (2015). Injury and biomechanical perspectives on the rugby scrum: a review of the literature. *Br. J. Sports Med.* 49, 425–U425. doi: 10.1136/bjsports-2013-092972

Zhang, C. F., Mannen, E. M., Sis, H. L., Cadel, E. S., Wong, B. M., Wang, W. J., et al. (2020). Moment-rotation behavior of intervertebral joints in flexion-extension, lateral bending, and axial rotation at all levels of the human spine: a structured review and meta-regression analysis. *J. Biomech.* 100:109579. doi: 10.1016/j.jbiomech.2019.109579

Conflict of Interest: The authors declare that the research was conducted in the absence of any commercial or financial relationships that could be construed as a potential conflict of interest.

Publisher's Note: All claims expressed in this article are solely those of the authors and do not necessarily represent those of their affiliated organizations, or those of the publisher, the editors and the reviewers. Any product that may be evaluated in this article, or claim that may be made by its manufacturer, is not guaranteed or endorsed by the publisher.

frontiers in Bioengineering and Biotechnology

HYPOTHESIS AND THEORY
published: 17 January 2022
doi: 10.3389/fbioe.2021.783501

A Vexing Question in Motor Control: The Degrees of Freedom Problem

Pietro Morasso *

Istituto Italiano di Tecnologia, Center for Human Technologies, RBCS Department (Robotics, Brain, and Cognitive Sciences), Genoa, Italy

The human "marionette" is extremely complex and multi-articulated: anatomical redundancy (in terms of Degrees of Freedom: DoFs), kinematic redundancy (movements can have different trajectories, velocities, and accelerations and yet achieve the same goal, according to the principle of Motor Equivalence), and neurophysiological redundancy (many more muscles than DoFs and multiple motor units for each muscle). Although it is quite obvious that such abundance is not noxious at all because, in contrast, it is instrumental for motor learning, allowing the nervous system to "explore" the space of feasible actions before settling on an elegant and possibly optimal solution, the crucial question then boils down to figure out how the nervous system "chooses/selects/recruits/modulates" task-dependent subsets of countless assemblies of DoFs as functional motor synergies. Despite this daunting conceptual riddle, human purposive behavior in daily life activities is a proof of concept that solutions can be found easily and quickly by the embodied brain of the human cognitive agent. The point of view suggested in this essay is to frame the question above in the old-fashioned but still seminal observation by Marr and Poggio that cognitive agents should be regarded as *Generalized Information Processing Systems* (GIPS) and should be investigated according to three nearly independent but complementary levels of analysis: 1) the *computational level*, 2) the *algorithmic level*, and 3) the *implementation level.* In this framework, we attempt to discriminate as well as aggregate the different hypotheses and solutions proposed so far: the optimal control hypothesis, the muscle synergy hypothesis, the equilibrium point hypothesis, or the uncontrolled manifold hypothesis, to mention the most popular ones. The proposed GIPS follows the strategy of factoring out shaping and timing by adopting a force-field based approach (the Passive Motion Paradigm) that is inspired by the Equilibrium Point Hypothesis, extended in such a way to represent covert as well overt actions. In particular, it is shown how this approach can explain spatio-temporal invariances and, at the same time, solve the Degrees of Freedom Problem.

Keywords: redundancy, motor equivalence, embodied cognition, central pattern generators, passive motion paradigm, two/thirds power law, unconstrained manifold concept, equilibrium point hypothesis

OPEN ACCESS

Edited by:
Alessandro Del Vecchio, University of Erlangen Nuremberg, Germany

Reviewed by:
Ioannis Delis, University of Leeds, United Kingdom
Vincent C. K. Cheung, The Chinese University of Hong Kong, China

***Correspondence:**
Pietro Morasso
Pietro.morasso@iit.it

Specialty section:
This article was submitted to Biomechanics, a section of the journal Frontiers in Bioengineering and Biotechnology

Received: *29 September 2021*
Accepted: *30 December 2021*
Published: *17 January 2022*

Citation:
Morasso P (2022) A Vexing Question in Motor Control: The Degrees of Freedom Problem. Front. Bioeng. Biotechnol. 9:783501. doi: 10.3389/fbioe.2021.783501

INTRODUCTION

The degrees of freedom problem in motor control states that there are multiple ways for humans or animals to perform a movement to achieve the same goal, leaving the question of how the brain chooses a course of action among infinite ones. The question was explicitly formulated many years ago by (Bernstein, 1967): "It is clear that the basic difficulties for co-ordination consist precisely in the extreme *abundance* of degrees of freedom (DoFs), with which the [nervous] centre is not at first in a position to deal." Specifically,

the human body is characterized by redundancy in many forms: *anatomical redundancy* (in terms of DoFs, muscles and joints), *kinematic redundancy* (movements can have different trajectories, velocities, and accelerations), and *neurophysiological redundancy* (multiple motor units recruited for each muscle); yet such redundancy is not an obstacle to achieve a common goal, according to the principle of Motor Equivalence (Lashley, 1933). In other words, despite such complexity it is quite obvious that the abundance is not noxious at all: in contrast, it is instrumental for motor adaptation and learning, allowing the nervous system the possibility to "explore" the space of feasible actions before settling on an elegant and possibly optimal solution. Ultimately, the crucial question boils down to figure out how the nervous system "chooses/selects/recruits/modulates/stores/recollects" task-dependent subsets of the countless motor variables as functional motor synergies. In any case, human purposive behavior in daily life activities is a proof of concept that solutions can be found easily and quickly by the embodied brain of the "human cognitive agent", despite this daunting conceptual riddle, A reference point suggested in this essay is to take advantage of the old-fashioned but still seminal observation by (Marr and Poggio, 1976) that cognitive agents should be regarded as *Generalized Information Processing Systems* (GIPS) and should be investigated according to three nearly independent but complementary levels of analysis: 1) the *computational level* that is supposed to clarify what needs to be computed and why; 2) the *algorithmic level*, focused on how the computation is organized, in terms of the used representations and the processes employed to build and manipulate the representations; 3) the *implementational/physical level*, related to the selection and activation of the specific neural hardware used to carry out the computation. On the other hand, the view that cognitive agents should be considered as GIPS is in contrast with radically different formulations like the "Smart Vehicles" of (Braitenberg, 1984), the claim of "Intelligence without Representation" by (Brooks, 1991) or the "Radical Embodied Cognitive Science" by (Chemero, 2009). Although intriguing, such a radical approach cannot account, in our opinion, for the large body of knowledge, derived from the field of motor imagery and embodied cognition, supporting the fact that motor cognition cannot be reduced to reactive mechanisms but is a fluid field that holds together real and mental actions in such a way to enable goal-directed actions guided by prospection. In other words, we support the concept that (motor) intelligence is fundamentally dependent on representation.

Thus, we suggest that the age-old degrees of freedom problem should be addressed as a GIPS, employing the three levels mentioned above to discriminate as well as aggregate a number of different hypotheses and solutions investigated in the literature, such as the optimal control hypothesis, the muscle synergy hypothesis, the equilibrium point hypothesis, and the uncontrolled manifold hypothesis, to mention the most popular ones. The analysis also focuses as well on the companion vexing question about the inner structure of *biological motion* revealed by Fitt's law (Fitt, 1954), the preference of straight trajectories in reaching movements, and the so-called two-thirds power law revealed by general gestures.

This essay focuses initially on the spatio-temporal invariances of multi-joint motor control that stand as a kind of background of the DoF problem and analyzes in some details the main alternative explanations of such invariances developed over the years. Then it focuses on a specific computational model, namely the Passive Motion Paradigm (PMP: Mussa-Ivaldi et al., 1988; Mussa-Ivaldi et al., 1989) that is inspired by the Equilibrium Point Hypothesis (EPH: Feldman, 1966; Feldman, 1986; Bizzi et al., 1992): more specifically, PMP is an extension of the EPH from the "real" elastic force fields, determined by the mechanical properties of skeletal muscles and applied to the "real human body," to the "virtual" force fields, that express motor intentions/goals/constraints and are applied to an internal model or "body schema." More generally, this extension implies a view of motor control fully integrated with embodied motor cognition (Mohan and Morasso, 2011; Mohan et al., 2019). The plausibility of this extension is supported by the rather recent consolidation of experimental evidence from motor imagery and the associated revitalization of the ideomotor theory of action, dating back to James' Principles of Psychology (1890). In particular, it is elucidated how and why the PMP model explains the spatio-temporal invariances and the alternative computational models mentioned above, thus providing a biologically plausible roadmap to solve the DoF Problem. Finally, it is shown how and in which sense the computational framework provided by the PMP model is consistent with the GIPS approach.

SPATIO-TEMPORAL INVARIANCES OF MULTI-JOINT MOTOR CONTROL

Until the 70s motor control studies were mostly focused on single-joint control paradigms, within a "reductionist" framework that ignored the "holistic view" implied by the Degrees of Freedom Problem or the Motor Equivalence Principle. The first step towards a more general multi-joint paradigm was the discovery of spatio-temporal invariants, that characterize 2D gestures, such as the following ones (see also **Figure 1**):

- The bell-shaped speed profile and isochrony of planar reaching movements (Morasso, 1981; Abend et al., 1982). It was found indeed that these movements are approximately straight, with an invariant bell-shape of the hand speed. In contrast, the timing and sync of joint rotation patterns are strongly dependent on the starting position and movement direction. Moreover, for self-paced movements, without specific accuracy requirements, the duration is approximately constant and, thus, peak speed is linearly correlated with target distance.
- The anti-correlation of speed and curvature profiles of movements with multiple *via* points, such as cursive handwriting or drawing gestures (Morasso and Mussa Ivaldi, 1982). When subjects produce continuous hand scribbles, the dynamics and the shape of the movements are not independent, in the sense that the time course of the hand speed and of the scribble curvature are strictly linked: both are characterized by a sequence of peaks and dips that are systematically anticorrelated, in the sense that speed peaks are synchronized with curvature dips and curvature peaks sync with speed dips.

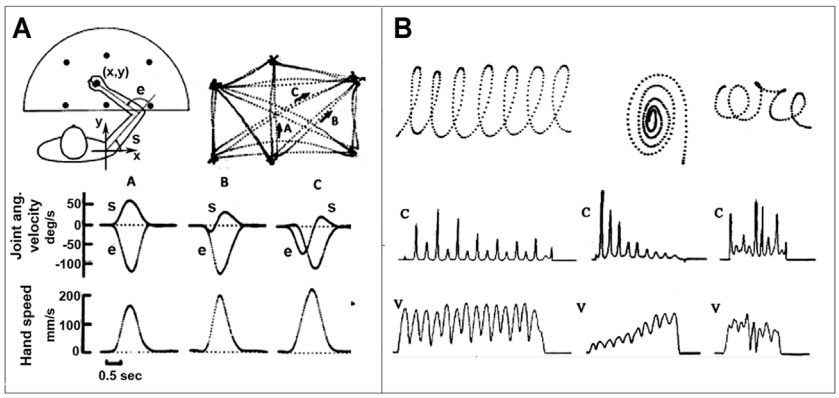

FIGURE 1 | Spatio-temporal invariants in trajectory formation. Panel **(A)**: Planar reaching movements between six target points; A, B, and C correspond to three movement examples, characterized by the joint rotation patterns and the corresponding speed profiles of the joints and the hand; note the invariant bell-shaped speed profiles. Panel **(B)**: Three examples of continuous hand scribbles displayed as digitized trajectories, including the profiles of the velocity (V) and curvature (C); note the anti-correlation of the two profiles.

Similar invariants were also found in 3D gestures (Morasso, 1983). In particular, also for 3D hand scribbles the dynamics and the shape of the movements are not independent. The shape of the 3D scribble is characterized by the time course of two parameters: the curvature and the torsion (in 2D scribbles the torsion is null). The peaks of torsion detect when the performing subject changes the virtual plane upon which he/she is producing a given fragment of scribble. The analysis of the movements (Morasso, 1983) showed in particular that the speed/curvature link is preserved and the generated gestures are approximately piecewise planar.

Alternative Explanations of the Spatio-Temporal Invariances

Discovering that planar hand gestures are characterized by spatio-temporal invariances that mutually constrain shape and kinematics prompted a whole research line, aimed at answering the following questions: Where do such spatio-temporal invariants come from? How can we explain them? How can we simulate their action in a biologically plausible framework? Among the number of different explanations that were proposed we may consider the following ones, listed in chronological order:

- *The 2/3 power law* (Lacquaniti et al., 1983). It addresses the previously mentioned anticorrelation of curvature and speed. In particular, it is shown that in repetitive elliptical scribbles the linkage between the velocity profile $\boldsymbol{v} = \boldsymbol{v}(\boldsymbol{t})$ and the curvature profile $\boldsymbol{c} = \boldsymbol{c}(\boldsymbol{t})$ can be captured by following function[1]: $\boldsymbol{v} \propto \boldsymbol{c}^{-1/3}$. The underlying hypothesis is that such dynamic constraint may be embodied in some specific neural structure that can be recruited, modulating the gain parameter, in order to control the degree of curvedness of the sequence of movements.
- *The minimum jerk model* (Flash and Hogan, 1985). The main point of this theory is that the spatio-temporal invariants of reaching movements can be fully explained by an optimization process that, given the initial and final points of the trajectory and the desired duration, computes the time course of the movement coordinates with the constraint that the hand jerk (the time derivative of the acceleration profile) must achieve a minimum value. The implicit assumption is that the internal neural mechanism that implements this model is a minimization process, operating on the internal representation of the trajectory of the end-effector. The model is limited to 2D motion of the end-effector and does not address the crucial element of the degrees of freedom problem, namely how to distribute the action to the redundant DoFs.
- *The VITE model* (Vector-Integration-To-Endpoint: Bullock and Grossberg, 1988). According to this model, the synergy formation process integrates over time a difference vector (DV), computed from the Target Position and the Present Position of the end-effector, multiplied by a GO-signal that determines the speed profile of the movement aimed to the target. The GO-signal corresponds to a non-linear gating action of the internal representation of the positional error. Also in this case the model is limited to 2D motion.
- *The PMP Model* (Passive Motion Paradigm: Mussa Ivaldi et al., 1988; Mussa Ivaldi et al., 1989). The model provides a force-field-based simulation approach, capable to coordinate implicitly the motion of the end-effector and the corresponding, redundant DoFs. The basic rationale of the model of trajectory formation is the same as the models of motor control based on a force-field approach, namely the idea that multi-joint motor coordination is the consequence of force fields applied to an internal representation of the body, force fields that express goals, intentions, environmental constraints, etc. This idea can be

[1]An equivalent formulation of this function is as follows: $\boldsymbol{\omega} \propto \boldsymbol{c}^{2/3}$, where $\boldsymbol{\omega}$ is the instantaneous angular velocity of the hand. This clarifies where the "2/3" element comes from.

traced back, on one hand, to the EPH (Equilibrium Point Hypothesis: Feldman, 1986; Bizzi et al., 1984; Bizzi et al., 1992) and, on another hand, to the impedance-control schemes proposed in robotics (Hogan, 1985). The whole body is viewed as a network of spring-like elements that individually store elastic potential energy, contributing to a global net potential energy. Considering that energy functions are additive, the global field recapitulates, in a smooth, analogic manner, the complex set of bodily interactions: the result is a "landscape," with hills and valleys, and thus the overall model will "passively" navigate in the landscape, attracted by the nearest equilibrium configuration, namely a point of minimum potential energy. The minimization of potential energy is a "global" property arising from local interactions, a general concept that has been employed for the design and analysis of large networks (Hopfield, 1982). The PMP applies the concept of "passive motion" to active synergy formation by updating the control input of each element so as to cancel the "stress" induced by a simulated external perturbation, e.g., the attractive force field to a designated target. A recent extension of the PMP model (Mohan and Morasso, 2011) incorporates a gating mechanism, derived from the concept of terminal attractor dynamics (Zak, 1988; Barhen et al., 1989) and analogous to the GO-signal of the VITE model.

- *The Uncontrolled Manifold concept* (Scholz and Schöner, 1999). This approach to solve the degrees of freedom problem generalizes the idea that, for each task, the CNS may select a minimal subset of DoFs that need to be accurately "controlled," for achieving a given goal, without any specific active control of the remaining DoFs. The idea is that for any task it is possible to subdivide the global configuration space, spanned by the whole set of DoFs, into two orthogonal subspaces: one subspace includes all the joint configurations that lead to the set of values consistent with the successful evolution of the task. This subspace is the Uncontrolled Manifold: motion within this subspace leaves the controlled variables unaffected and thus the control of joint combinations within this manifold is unnecessary. The motion orthogonal to the UCM subspace does affect the controlled variables and thus action planning should only focus on it, with the crucial consequence of reducing the dimensionality of the control problem.
- *Muscle Synergies* (Tresch et al., 1999; Saltiel et al., 2001; D'Avella et al., 2003). The underlying concept of this model of synergy formation is that an efficient solution for addressing the redundancy of the motor control problem might be achieved by representing all useful muscle patterns as combinations of a small number of generators or motion primitives, spanning the muscle activation subspace. This would reduce the dimensionality of the problem and allow sharing neural aggregates across many tasks, allowing the CNS to simplify the control problem by combining discrete elements. Such neural mechanism was investigated first in spinalized or decerebrated animals (Mussa-Ivaldi et al., 1994; Tresch et al., 1999), focusing on the activity of the spinal cord, and then in purposive motor activities of humans (D'Avella et al., 2003), aiming at the detection of correlated patterns of electromyographic activity, specific for each task.
- *Optimal Feedback Control* (Todorov and Jordan, 2002; Scott, 2004; Liu and Todorov, 2007). The Optimal Feedback Control approach (OFC) expands the line of thought initiated by the minimum jerk model. As a matter of fact, OFC is a powerful engineering technique in process control applications, with non-trivial implementation complexity: the theory is fully developed in the case of linear systems, particularly if the cost to be optimized is a quadratic function (of the state and control variables) and a reliable estimate of the state is available. In this case, the optimal control is a linear state feedback law where the control gains are obtained by solving an equation (the Riccati equation), for which robust and efficient algorithms are available. However, if the system to be controlled is characterized by nonlinear dynamics, no unique approach is available and only approximated methods can be devised, to be adapted to the specific task (Beeler et al., 2000). In the application of this design methodology to biological motor control it is necessary to guess the cost function that the brain intends to minimize and implement numerical optimization techniques that are difficult to explain in neural terms. The rationale of the approach is that the best way to engineer a complex control system is to specify a high-level performance criterion and leave the details to "numerical optimization" but while the approach is excellent for accurately fitting the experimental data (Liu and Todorov, 2007) it is of little use to figure out the biological organization of the suggested numerical optimization.
- *The Active Inference perspective* (Friston et al., 2011; Friston and Parr, 2019). This concept rests upon the idea that the brain uses an internal generative model (Jeannerod, 2001) to predict incoming sensory data. Remarkably, this force-based mechanism solves the "Degrees of Freedom problem" in an implicit manner, without explicit kinematic inversion, and it naturally allows to combine multiple goals by superimposing the corresponding force fields. It is worth pointing at the analogy between PMP and Active Inference: in both cases, there is no need to have distinct sensory and motor representations, because the "proprioceptive predictions" of the intended action, generated by the simulation process, are sufficient to allow the motor controller to produce the basic motor synergies. Such predictions encode beliefs about the state of the world, including both proprioceptive and exteroceptive components. The standard causality between sensory and motor representations is somehow inverted: motor commands are not necessarily intended to cause desired movements but desired movements (in the form of the predicted consequences of movement) May cause motor commands.

As better explained in the following, it can be shown that the PMP model explains all the other models listed above and provides a solid computational framework for both human

motor neuroscience and humanoid robot cognition (Morasso, 2021). A key point of the paper is that it is impossible to clearly separate motor control from motor cognition. The vast, recent literature on motor imagery allowed to revitalize the traditional Ideomotor Theory, proposed by William James in the 19th century and recently revisited (Shin et al., 2010), namely the concept that the "idea" of an action, i.e., the predicted/desired sensory consequences of covert action, applies as well to goal-directed overt actions and is the internal mechanism that ultimately generates it through the simulation of an internal model (Jeannerod, 2001).

The crucial point is that most theories formulated to account for spatiotemporal invariances in the motor system are "descriptive" of different aspects of the invariances of real actions, by fitting the data with a various degree of accuracy. In this sense, they are all "true" and there is no point in ranking them according to the degree of accuracy or figuring out specific modifications that may increase the accuracy of the predictions. The main goal of the paper, in the GIPS framework, is to outline a plausible approach to characterize a "generative" model that applies equally well to overt and covert actions, in agreement with the simulation theory of action formulated by Marc Jeannerod (2001). As shown in the rest of the paper, PMP appears to match this requirement in a simple "economic" manner, providing a uniform computational mechanism for both covert and overt actions that is complex but not too complex. The OFC and the muscle synergy models may also be considered "generative" but fail the requirements above in two crucial aspects: 1) they are unable to apply to overt and covert actions in a uniform way; 2) computationally, OFC is too complex to be biologically plausible and the muscle synergies model is too simple, because is a kind of table-lookup mechanism, based on a linear combination of pre-recorded high-dimensional patterns).

Before proceeding in the analysis of the PMP model, it is worth to clarify what is the specific meaning of the word Synergy in the context of this paper. As a matter of fact, the DoF Problem and the Synergy Concept are the two faces of the same coin: the human body has too many DoFs and too many muscles to allow the brain to control all of them independently. In any case, the real function of the brain is not the control of movements per se but the organization of purposive actions, identified by a small number of control variables (thus reducing dimensionality) and structured according to the principle of compositionality: this means that humans simplify the generation of various motor behaviors through the re-use of a limited number of basic motor primitives to be combined in an additive manner, rather than developing entirely new modules for each behavior/task. If we consider the etymology of "synergy" (the word derives from two ancient Greek words: συν+εργός, Sun + ergòs, i.e., "working together") it is not surprising that anybody working in motor neuroscience agrees on its fundamental role in the organization of purposive actions, although it is equally evident that in the literature there is a large variety of synergies (or "zoo of synergies" to quote Mark Latash, 2008): kinematic synergies (Freitas et al., 2006; Huang et al., 2021), kinetic synergies (Slomka et al., 2015), muscle synergies (Cheung and Seki 2021), to name a few. They all clarify the concept that the DoFs are not independent but are recruited by combining a limited number of adaptable primitives. The muscle-less synergies advocated in this manuscript may also be considered "ideomotor synergies" and their rationale is based on the equivalence between overt actions (that imply the generation of muscle patterns) and covert actions (that are muscleless by definition). The working hypothesis that muscleless synergies are "primitives on the top of the computational chain" does not contradict the evidence that low-level coordinative structures, possibly encoded by spinal premotor interneurons, exist and are recruited during overt actions. The frequently invoked need of a verified neural basis of muscle synergies is descriptive of the correlation among different neural processes but does not imply a causal relationship: in our opinion, it is not a plausible computational process capable to generate the observed correlations in overt actions and, at the same time, available to the brain for prospection in covert actions. The underlying issue is that, in an embodied cognitive framework, motor cognition and motor control of purposive actions are indeed different neural processes but they must share a common representation of action. A further point to be clarified is related to the specific meaning of "motor primitives" and the nature of the compositional process that allows them to be combined. This point will be clarified in the section related to GIPS.

HOW THE PMP MODEL EXPLAINS SPATIO-TEMPORAL INVARIANCES

Let us consider the basic form of the PMP model, which is focused on planar reaching movements but promptly generalizes to 3D movements, from a starting point P_0 to a target point P_T. The movements are driven by an attractive, virtual force field F, centered in the target position P_T and applied to the moving end-effector $p(t)$:

$$F(t) = K\left(P_T - p(t)\right) \tag{1}$$

If the matrix K is proportional to the unitary matrix, the force field is isotropic and, by applying it to the end-effector, the hand will follow a straight path terminating in the target point. However, since the field intensity vanishes as the end-effector approaches the target, the time to target is virtually infinite and the velocity profile is far from bell-shaped. An indirect control of the timing, used by the PMP model, is obtained by a non-linear gating mechanism, namely the Γ-function of **Figure 2**: this function is null before the initial time instant t_0 and grows smoothly but very quickly until the designated final time $t_f = t_0 + T$, where it diverges to infinity before collapsing to 0. The purpose of the Γ-function is to set a hard deadline to the gradient descent process seeking an equilibrium state, after the initial disequilibrium induced by the instantiation of a target, whatever the dimensionality of the underlying system and the distance of the target from the initial state. Among the different forms that can be used for this gating mechanism, the one adopted by the PMP model is defined as follows:

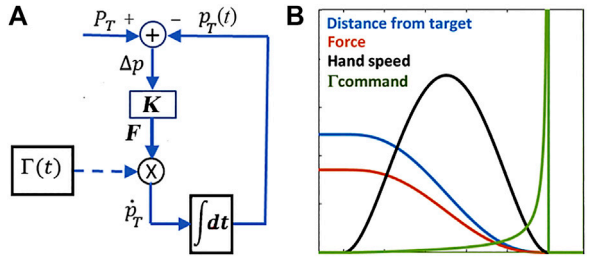

FIGURE 2 | (A): PMP model for the generation of a $\boldsymbol{p_T}(\boldsymbol{t})$ moving target aimed to the final target $\boldsymbol{P_T}$. The virtual force field $\boldsymbol{F}$ is gated by the Γ-function that indirectly control the speed profile $\dot{\boldsymbol{p}}_{\boldsymbol{T}}(t)$. **(B)** shows that the spiky Γ-command induces a bell-shaped speed profile with the corresponding smooth reduction of the distance from the target.

$$\begin{cases} \Gamma = \dfrac{\dot{\xi}}{1-\xi} & \text{for } 0 < t - t_0 < T \\ \Gamma = 0 & \text{for } t - t_0 \le 0 \text{ and } t - t_0 \ge T \end{cases} \tag{2}$$

where $\xi = 6\,\gamma^5 - 15\,\gamma^4 + 10\,\gamma^3$ is a smooth 0→1 transition and γ is the normalized time: $\gamma = \frac{t-t_0}{T}$.

The Γ-function does not impose the speed profile but forces the gradient descent driven by the force field to achieve equilibrium in finite time. **Figure 2** shows an example of reaching movement generated by **Eq. 1** and **Eq. 2**, according to the block diagram in the left panel of the figure; the right panel shows the time course of the Γ-function and demonstrates that the PMP model can indeed induce a smooth acquisition of the target (the distance monotonically decreases to zero) with a symmetric bell-shaped speed profile, without the explicit optimization suggested by the minimum jerk model. Moreover, the PMP model described above is not limited to straight trajectories: curved trajectories can be generated by the same block diagram of **Figure 2** if the gain matrix K includes a rotational component, without affecting the terminal attractor properties of the model. The model can be used iteratively in such a way to generate a sequence of PTP (Point to Point) movements: the final point of each movement becomes the initial point of the next one, provided that the Γ-functions of consecutive commands are not overlapped in time, namely the initial instant of each command occurs later than the final instant of the previous one.

The model can also be extended to any VP trajectory, i.e., trajectory with multiple *Via* Points, as in cursive handwriting or hand drawing, in a very simple and natural way. The reason is that the PMP model is based on elastic force fields and we should consider that the corresponding energy functions are additive. Thus, a generic trajectory with multiple VPs ca be generated by chaining a sequence of PTP movements with time overlap between consecutive Γ-functions. **Figure 3** shows an example, characterized by 13 targets and 12 VPs: the targets are alternated back and forth on the horizontal axis, with approximately equal distance (a small random displacement is added for improving the graphical rendering); the force field of each PTP movements is equally curved; the Γ-functions of successive commands have a 50% time overlap. The result is a sequence of elliptical shapes, except for the first and the last curved movement (top panel of **Figure 3**), and the remarkable feature of the generated trajectory with multiple VPs is clarified by the bottom panel of **Figure 3**, that plots the speed and curvature profiles, together with the sequence of Γ-functions: speed and curvature are clearly anti-correlated. The VPs are the points of peak curvature but these points are not explicitly expressed: they are implicitly generated by the systematic overlapping strategy of the chaining procedure. Moreover, by plotting speed vs. curvature in a logarithmic scale it is possible to demonstrate that the PMP model applied to a sequence of overlapped VPs matches the 2/3 power law mentioned above without an explicit implementation of the law in a neural controller of the synergy formation mechanism. Rather, the correlation of shape and kinematics implied by the law is simply the computational consequence of the repetitive application of the simple PMP mechanism with an overlap between two consecutive motor commands. In summary, the simulation of the basic form of the PMP model is capable to reproduce, at the same time, the minimum jerk hypothesis, without any optimization mechanism, and the 2/3 power law, without any explicit figural-timing constraint.

HOW THE PMP MODEL SOLVES THE DEGREES OF FREEDOM PROBLEM

In the previous section, it was shown how the PMP model can reproduce the spatio-temporal invariances of multi-joint motor control, focusing on the kinematics of the end-effector. This formulation neglected how the described neural model might be integrated with the recruitment of the redundant DoFs of the human body, namely the key point of the degrees of freedom point. Mapping the planned trajectories of the end-effector onto the redundant, articulated joint network is usually called inverse kinematics, a typically ill-posed transformation due to the kinematic redundancy of the human body. This means, in particular, that the inverse transformation can have infinite solutions or no solution at all. The rationale of the PMP approach is to avoid this critical problem by focusing on force rather than on motion, thus dealing only with a network of well-posed transformations.

For example, if we wish to induce a small displacement of the end-effector $\Delta\boldsymbol{p}_{\boldsymbol{ee}}$ from a given equilibrium point and attempt computing the incremental joint rotation $\Delta\boldsymbol{q}$ that allows the desired displacement to occur, we run into the trouble of inverse kinematics, i.e., an ill-posed transformation. However, it is possible to avoid such problem by using the force field-based approach described in the previous section: instead of forcing the system to carry out the desired incremental motion $\Delta\boldsymbol{p}_{\boldsymbol{ee}}$, we may "disturb" the current equilibrium with a force field attracting the end-effector in the same direction: $\Delta\boldsymbol{F}_{\boldsymbol{ee}} = \boldsymbol{K}_{\boldsymbol{ee}}\,\Delta\boldsymbol{p}_{\boldsymbol{ee}}$. This disturbance $\Delta\boldsymbol{F}_{\boldsymbol{ee}}$ can always be mapped from the end-effector space to all the DoFs of the joint space, giving a unique solution $\Delta\boldsymbol{\tau} = \boldsymbol{J}^T\Delta\boldsymbol{F}_{\boldsymbol{ee}}$, where $\boldsymbol{J}$ is the Jacobian matrix of the non-linear, redundant kinematic transformation $\boldsymbol{p} = \boldsymbol{f}(\boldsymbol{q})$. In other words,

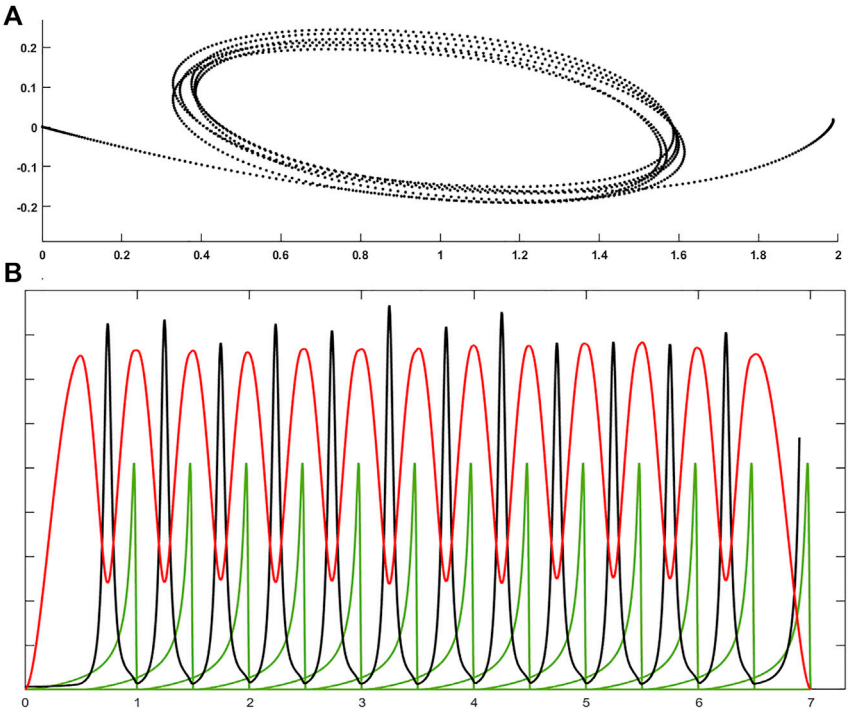

FIGURE 3 | (A): Example of a generic trajectory with multiple VPs generated by the PMP model by chaining a sequence of PTP movements with time overlap between consecutive Γ-functions; the trajectory is characterized by 13 targets and 12 VPs; the Γ-functions of successive commands have a 50% time overlap. **(B)**: time course of speed (red), curvature (black) profiles, and the 13 Γ-functions (green). Each Γ-function has a duration of 1 s, with a 50% overlap between successive functions.

while the transformation in terms of incremental motion ($\Delta \boldsymbol{p}_{ee} \rightarrow \Delta \boldsymbol{q}$) is generally ill-posed, the corresponding transformation in terms of forces ($\Delta \boldsymbol{F}_{ee} \rightarrow \Delta \boldsymbol{\tau}$) is well-posed and admits a unique solution as a consequence of the principle of virtual works.

The crucial step, at the heart of the PMP approach, is then to apply the concept of "passive motion", that consists in updating the state of each joint so as to cancel the "stress" induced by the simulated external perturbation: $\Delta \boldsymbol{q} = \boldsymbol{C}\, \Delta \boldsymbol{\tau}$, where $\boldsymbol{C}$ is a square matrix that distributes the "passive motion" induced by the virtual disturbance to all the joints. This incremental motion in the joint space can then be mapped uniquely to the end-effector space, using again the Jacobian matrix: $\Delta \hat{\boldsymbol{p}}_{ee} = \boldsymbol{J}\, \Delta \boldsymbol{q}$. Summing up, the PMP model avoids the ill-posed inverse kinematic transformation $\boldsymbol{q} = \boldsymbol{f}^{-1}(\boldsymbol{p})$ by the following chain of transformations that are all well-posed from the end-effector space to the joint space and then back to the end-effector space:

$$\Delta \boldsymbol{p}_{ee} \rightarrow \Delta \boldsymbol{F}_{ee} \rightarrow \Delta \boldsymbol{\tau} \rightarrow \Delta \boldsymbol{q} \rightarrow \Delta \hat{\boldsymbol{p}}_{ee} \tag{3}$$

Ideally, $\Delta \hat{\boldsymbol{p}}_{ee}$ should be equal to $\Delta \boldsymbol{p}_{ee}$ but this is not the case in general because the stiffness matrix of the end-effector is anisotropic: the natural solution is to close the loop of the chain of transformations indicated above by redirecting the force field to the designated target at each time instant, as shown in **Figure 4** (top panel). The figure clarifies the fact that the Passive Motion Paradigm is split into two modules: a module (A) that generates a moving target $\boldsymbol{p}_T(t)$, terminating in the final target $\boldsymbol{P}_T$, and a module (B) that moves all the DoFs in such a way to keep the end-effector $\boldsymbol{p}_{ee}(t)$ as close as possible to the moving target. Both modules are driven by force-fields and thus in the PMP model there is a concurrent "double pulling force": from the moving target to the final target ($\boldsymbol{F}_T$) and from the moving target to the moving end-effector ($\boldsymbol{F}_{ee}$). This aspect of the PMP model is supported by experimental evidence linking the maintenance of posture in a multijoint system to that of generating a movement: it was found indeed that the CNS does not apply a final position control mechanism but programs a reaching movement by shifting the equilibrium position of the hand toward the target in a continuous manner (Bizzi et al., 1984; Shadmehr et al., 1993). In the PMP model, the action of the two force fields is synchronized by gating both of them with the same Γ-function: the bottom panel of **Figure 4** shows that both the moving target point $\boldsymbol{p}_T(t)$ and the end-effector $\boldsymbol{p}_{ee}(t)$ reach the final target point $\boldsymbol{P}_T$ at the same time, dictated by the Γ-function. Moreover, the figure illustrates how the PMP model solves the DoF problem, distributing smoothly the action among all the DoFs in an implicit way.

The biological plausibility of the model described above is also supported by experiments on the coordination mechanisms underlying bimanual reaching. Apart from the spatio-temporal invariance of multi-joint reaching movements, exemplified by the bell-shaped velocity profile, independent of starting posture, movement direction and target distance, we should also consider the speed-accuracy trade-off, elucidated by the Fitt's

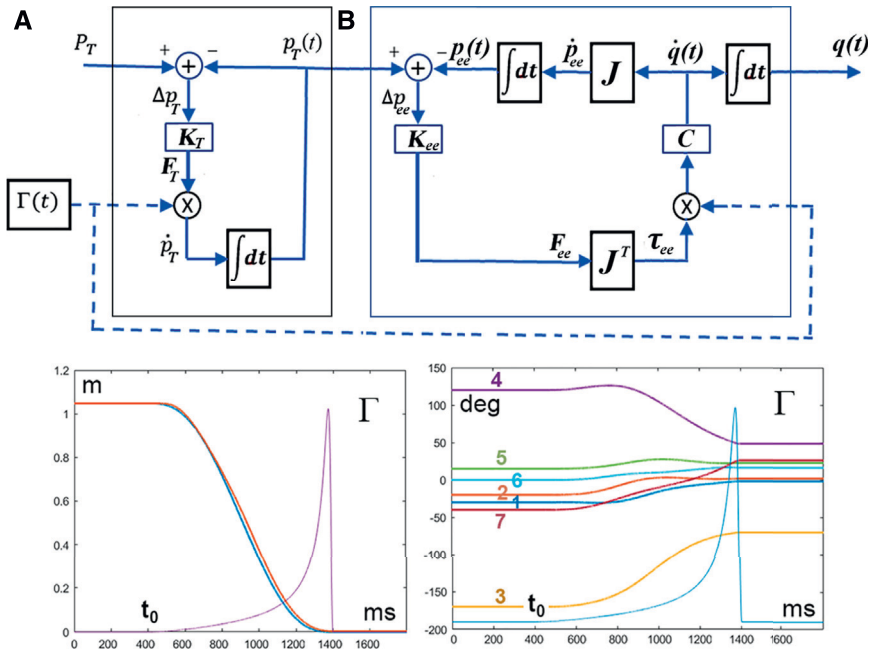

FIGURE 4 | (A): Extended PMP model for solving the Degree of Freedom problem; the module A generates the moving target $\ddot{p}_T(t)$, attracted to the final target point by the force field F_T; the module **(B)** generates the trajectory of the end-effector ($p_{ee}(t)$) and distributes the action to all the DoFs ($q(t)$) by using the force field F_{ee}. In the lower part of the figure the left graph shows the time course of the distance from the final target point of the moving target (red curve) and of the end-effector (blue curve); the right graph shows the time course of the 7 DoFs (yaw-pitch-roll of the wrist, pitch of the elbow, and yaw-pitch-roll of the wrist); both graphs also include the common Γ-command.

law (Fitts, 1954): the duration of reaching movement grows with the required index of difficulty, namely the ratio between target distance and target size. In the PMP model this means that the CNS should choose the duration of the Γ-function in accordance with the expected difficulty index. But what about bimanual reaching? Unless the two targets have the same difficulty, the Fitt's law would predict different reaching times. However, this is not what happens: the experiments by (Kelso et al., 1979) clearly show that bimanual motions reach the targets simultaneously and the common duration is dictated by the motion with the higher difficulty index. The picture that emerges from such studies of interlimb coordination is that the role of central control patterns is not to prescribe the full details of the intended action but rather to organize functional groups of DoFs, also known as coordinative structures (Turvey, 1977) or motor synergies. An extension of the PMP model for covering bimanual coordination is quite straightforward: it is sufficient to instantiate two copies of the model of **Figure 4** for the two arms (A_{left}, B_{left}, A_{right}, B_{right}) and synchronize the four modules with the same Γ-command. Other studies investigated bimanual coordination, for example manipulating a nonholonomic car (Tsuji et al., 2002) and it was found that the timing of the coordinated movements is compatible with a non-linear gating model based on a TBG (Time Based Generator) quite similar to the Γ-command.

As regards the motor synergies investigated by (D'Avella et al., 2003), they clearly fit the quest, initiated by Bernstein, for computational mechanisms capable to reduce the complexity of motor control. However, demonstrating the low dimensionality of patterns of electromyographic activities embedded in actions of daily life is not sufficient to conclude that the small number of high-dimensional muscle activation patterns "are" the sought "motor primitives" to be combined for synergy formation in general. This hypothesis is in contrast with the large body of research on motor imagery that supports the fundamental equivalence of mental and real motor actions, including the timing aspects: Decety and Jeannerod (1995) showed that imagined discrete movements obey Fitts's law and their durations are well correlated with those of actual movements; Karklinsky and Flash (2015) demonstrated that imagination of continuous scribbles is consistent with the two-thirds power law of real scribbles. Thus, in our opinion a more appropriate approach to synergy formation is not based on "muscle synergies" but on "muscle-less synergies" or "ideomotor synergies" (Mohan et al., 2019) represented and generated by the PMP model. In this framework, the muscle synergies are not the motor primitives on the top of the computational chain but the results of the force-field driven internal simulation carried out by the PMP model. The motor primitives are thus the recruited force fields and the muscle synergies, evoked only in overt actions, are the visible consequences: the dynamic effects of the interaction between a muscle-less mental synergy and the control modules recruited for a specific task, as a combination of feedforward and feedback control mechanisms, in conjunction with coactivation patterns of muscle activity for modulation of joint stiffness.

For the UCM concept, we may observe that it is incorporated intrinsically in two crucial elements of the PMP model illustrated

in **Figure 4**. First of all, the mapping of the virtual disturbance from the end-effector space (i.e., the task space) to the joint space (or DoF space) is indirectly and intrinsically ranking the whole set of DoFs according to the relevance of each DoF for the planned action: $\Delta\boldsymbol{\tau} = \boldsymbol{J}^T\Delta\boldsymbol{F}$**.** The rank of each DoF dynamically changes during the movement and we may estimate the relative weight of each DoF ($w_i(t)$), at each time instant, with the following indicator: $w_i(t) = \Delta\tau_i(t)/|\Delta\boldsymbol{\tau}|$. In particular, the DoF with the highest ranking will be the one that yields the most to the virtual disturbance. The second elements of the PMP model that may be associated to the UCM concept is the compliance matrix $\boldsymbol{C}$ that maps the disturbing torque absorbed by each DoF into the corresponding incremental displacement: $\Delta\boldsymbol{q} = \boldsymbol{C}\,\Delta\boldsymbol{\tau}$**.** This may increase or decrease the ranking of each DoF and thus influence the clustering of the whole set of DoFs in the controlled and uncontrolled manifolds. Therefore, in the PMP framework there is no need to explicitly specify the two alternative manifolds: the border between the two clusters is rather fuzzy and time varying, due to the complexity of the body kinematics and the task-dependent requirements.

A further issue that is related to the UCM concept, on one side, and to the additivity of force fields acting on complex kinematic networks, on another side, is the possibility to integrate in the dynamics of PMP models additional force fields that may express additional constraints or task requirements. An example is the "regularization" of the synergy formation process aimed at satisfying the limited range of motion of each joint. This is a constraint that would be very difficult to formulate in an exact treatment of the inverse kinematic problem. In the PMP framework it is sufficient to introduce an additional force field, in the joint space, with a non-linear repulsive action from the joint limits of each DoF. This force field may be added to the attractive force field, defined in the end-effector space for expressing the target reaching intention, and possibly to other force fields for expressing additional constraints or requirements. It is important to note that all such force fields may be defined in different spaces with different reference frames and thus the PMP model can be designated as a *multi-referential system of synergy formation*. However, the effects of the different force fields converge ultimately to the joint reference system, coordinating the motion of the whole set of DoFs, using a complex network of well-posed transformations. The crucial point of synchronizing the effects of all the different components is implemented, as shown in **Figure 4**, by gating the different perturbing sources with the same Γ-function. This also clarifies the fact that the abundance of DoFs is functionally essential for achieving at the same time the multiple sub-goals of a given task: for example, reaching a target at a given time, while keeping each joint inside its range of motion and avoiding to hit dangerous obstacles in the environment. A possible neural implementation of the Γ-function is suggested by studies that document the gating action of the basal ganglia on the activation of the motor cortex. For example (Horak and Anderson, 1984), found that two nuclei of the basal ganglia (the Substantia Nigra pars reticulata and part of the Globus Pallidus) carry out a gating and velocity scaling action of the commands sent to the motor thalamus and precentral cortex.

In summary, the PMP model integrates in the same computational framework the spatio-temporal invariants, described by the minimum-jerk model, VITE model, and two-thirds power law, as well as the coordination requirements of redundant DoFs, expressed by the UCM model and the muscle synergies.

THE GENERALIZED INFORMATION PROCESSING SYSTEMS APPROACH

The Computational Level

A computational theory for addressing the Degrees of Freedom Problem should stem from the fact that a cognitive agent is continually involved in prospectively guided, goal-directed actions that involve the whole body and thus is faced by the challenge of choosing an action course that recruits the degrees of freedom on the basis of the desirable and predictable outcome. Thus, the core of the theory, namely the definition of "what needs to be computed and why," is a mechanism that allows the brain to integrate in the same process the capability to shape the motor system in anticipation to execution as well as the awareness of the feasibility of potential actions without execution. Moreover, this internal model should incorporate a knowledge about the causal relationship between the task spaces (related to the designated "end-effectors") and the joint space (the DoF space): more specifically, it should be able to predict the incremental displacements in the task space determined by arbitrary variations in the joint space as well to compute the joint efforts capable to equilibrate virtual perturbations applied to one of the end-effectors of the body in the task space. Mathematically, such computations are equivalent to the Jacobian matrices that link the joint space and the task spaces. The computation of such Jacobian matrices is a key element for solving the DoF problem because they allow to rank in a direct and implicit way all the DoFs of the body for a given task, expressed as a set of virtual force fields applied to the end-effector.

Another requirement of the computational theory is that the theory must not be purely descriptive but provide robust generative capabilities with cognitively penetrable features: this means that the details of the simulation process that generates ideomotor synergies should be relevant to cognitive processes related to prospection, learning and decision making.

The other key element of the theory is that it must capture the spatio-temporal invariants that characterize human actions, independent of the number of involved end-effectors and DoFs. The crucial function of the invariants is to allow the process of coordination of the redundant DoFs to evolve in a smooth and coherent manner, by relying on the composition of complex gestures in terms of simpler sub-actions or motion primitives. The solution to this is to integrate in the network of Jacobian matrices, that represents the internal model of the whole body, a non-linear gating mechanism applied to the virtual force fields in such a way to dynamically synchronize all the elements of the network, in analogy with the recall of information in large associative networks, without any need of a universal clock or metronome.

The theory covers the motor cognitive aspects of synergy formation with a mechanism of recruitment of the redundant DoFs and of synchronization of motor primitives that allows smooth composition. Thus, the theory fully represents the organization of covert or mental actions but it does not and must not cover specific control aspects in action execution that are determined by the physical interaction of the body with the environment: action execution, in addition to a well-structured ideomotor synergy, will also require a combination of different control mechanisms (feedforward, feedback, and stiffness control) which are outside the scope of the computational theory.

The PMP model is intended to answer the above requirements of the computational level formulation of the DoF problem, although alternative formulations cannot be excluded. However, the different models analyzed before for explaining the spatio-temporal invariants do not fit the computational requirements except for the Active Inference model, as previously observed, and the VITE model but only for the non-linear gating mechanism. The minimum jerk model and the 2/3 power law are more descriptive than generative and, in any case, do not address the redundancy issue of the DoF problem. The UCM model is mainly descriptive, leaving open the question of dynamically sorting the set of DoFs in relevant and non-relevant subsets for a given task. The muscle synergy model, as well as the OFC model, only apply to the control part of overt actions and, in any case, they are far from being cognitively penetrable. For a computational theory of this kind, the classical planning-acting-sensing loop is not appropriate because it is impossible to separate logically in a clear manner the three components and sequence them in time.

The Algorithmic Level

In agreement with the computational theory defined above, we suggest that the algorithmic level of analysis of the DoF problem should be based on the simulation theories (Jeannerod, 2001; O'Shea and Moran, 2017) and emulation theories (Grush, 2004; Ptak et al., 2017) for the representation of prospectively guided, goal-directed actions. This point of view is strongly supported by following statement by (Marc Jeannerod, 2001): "The possibility to experimentally access to cognitive or mental states characterized by absence of overt behavior represents a new avenue for neuroscience." From this derived the hypothesis that the motor system is part of a simulation network that is activated under a variety of conditions in relation to action, either self-intended or observed from other individuals. This is indeed the starting point for the introduction of the PMP model which addresses the DoF problem by factoring it out in two main components of synergy formation: 1) giving shape to the synergy, by superimposing multiple virtual force-fields, and 2) giving rhythm to the synergy with a suitable gating and velocity modulation. The PMP model relies on a network of Jacobian matrices that correspond to the different kinematic chains of the human body, including a mechanism of serial/parallel connections. The basic algorithmic function is the simulation of the network. The algorithmic level of analysis for addressing the DoF problem is also appropriate for clarifying the concept of motor primitive, as the basic cellular element to be combined in order to generate general actions. In contrast with the common wisdom, typical for example of popular methods of movement notation, such as Labanotation (Laban, 1956), Therblig notation (Aft, 2000) or the Human Action Language (Guerra-Filho and Aloimonos, 2007), that identify motor primitives with elementary movements, we think that it is more appropriate to assume that motor primitives are force fields. The basic (algorithmic reason) for this assumption is that in a complex mechanical network, like the human body, force fields are additive while elementary movements are not.

The Implementation/Physical Level

The algorithmic hypothesis, that the same internal model is involved in the generation of overt and covert actions, can lead to different implementation strategies for transforming a selected covert action into the corresponding overt counterpart. The underlying hardware that is supposed to allow the neurobiological implementation of an internal mechanism similar to the PMP model must count onto two main modules: 1) a module for representing the Jacobian matrices and 2) a module for the control of timing and synchronization.

A biomimetic approach for defining and implementing the former module is the process of *sensorimotor babbling*. This is an idea that was originally proposed by (Piaget, 1952) for the study of sensorimotor development in children. He described a "primary circular-reaction hypothesis" supported by the fact that newborn infants repeatedly perform exploratory movements which are "centered on themselves" rather than driven by external stimuli. Such empirical observations prompted lines of research, both in developmental psychology (von Hofsten, 1982) and computational neural modeling (Kuperstein, 1988), that viewed "motor babbling" inherent to primary circular-reactions (e.g., the performance of random hand movements in front of the eyes) as a crucial mechanism for enhancing the formation of associations between efferent motor patterns and re-afferent perceptive/proprioceptive patterns. More recently, motor babbling was applied to robotics in order to promote learning the internal representation of the body: Hersch et al. (2008) proposed an algorithm enabling an embodied robot to visually learn its body schema, by visually observing its end-effectors when moving them; Sturm et al. (2009) developed a model based on Bayesian networks that allows a robot to simultaneously identify its kinematic structure and learn the geometrical relationships between its body parts as a function of the joint angles. Moreover, the babbling-based approach was also extended for the internal representation of the use of tools (Bhat et al., 2017), considering the underlying neurophysiology about the adaptation of the receptive fields of skilled users (Maravita and Iriki, 2004).

As regards the module for the control of timing and synchronization of multiple sensorimotor processes, the previously defined Γ-function or GO-signals are specific examples. A more detailed analysis of the Γ-function is provided by the TBG (Time base Generator) model (Tsuji et al., 2002) that allows a parametrization of the function, in order to describe small modifications of the symmetry of the bell-shaped velocity profile that are consistently associated with any individual (Kittaka et al., 2020). This method of analysis is also applicable in the clinical field by using it for the quantitative evaluation of the Trail Making test (Sakai et al., 2021): this is a neuropsychological test which is widely used to assess the

cognitive function of patients with motor-cognitive impairments, as in the case of stroke.

In general, we suggest that the Γ-function may be considered as a member of the large family of CPGs (Central Pattern Generators), although this kind of neural mechanisms have been investigated mainly for explaining the neural drive of rhythmic and stereotyped motor behaviors like walking, swimming, breathing, chewing, swallowing. Although it is generally assumed that CPGs, typically located in the spinal cord and brain stem, are characterized by the ability to operate with a minimal intervention of higher brain areas, still they require modulatory inputs in order to perform in a flexible way. The role of CPGs in less stereotyped motor behaviors, characterized by a clear cognitive interaction, has been clarified in the field of speech motor control (Barlow et al., 2010; Rusaw, 2013) or sign language (Tkachman et al., 2021). Reaching movements seem to be far away from the area of motor control related to rhythmicity related to CPGs. However, cursive handwriting, scribbles or hand gestures in dance strongly support the view that the observed motor patterns may be the result of the superposition of motor primitives similar to PTP movements, with a clear rhythmical and prosodic structure that may imply a pattern generator, in charge of timing. Such CPG clearly cannot be localized downstream the neuroaxis as in the case of locomotion and there is diffused evidence, summarized by (Bullock et al., 1999), that it may involve thalamo-cortical loops with the purpose of gating and velocity scaling. In any case, we suggest that the widespread use of CPGs for coordinating more or less rhythmic behaviors of the highly redundant motor system is one of the main techniques adopted by the CNS to tame the degrees of freedom problem. This consideration is also consistent with the evolutionary analysis of CPGs reported by (Katz, 2016).

CONCLUSION

In conclusion, we wish to emphasize our complete agreement with the view by (Latash, 2012) that there is no "problem" of motor redundancy; rather there is the bliss of motor abundance that allows humans as well as members of other species to exhibit adaptive behaviors across a variety of conditions, in a changing and challenging environment. This is at the heart of what (Latash, 2012) denotes as "good variance" of human behavior, in contrast with the "invariance" (and consequent inflexibility) of exact algorithmic models. We only observe that such good variance and the bliss of motor abundance are made possible by the strategy of factoring out shaping and timing, described in this essay.

DATA AVAILABILITY STATEMENT

The raw data supporting the conclusion of this article will be made available by the author, without undue reservation.

AUTHOR CONTRIBUTIONS

The author confirms being the sole contributor of this work and has approved it for publication.

FUNDING

This research was supported by internal funds of the RBCS (Robotics, Brain, and Cognitive Sciences) research unit of the Italian Institute of Technology, Genoa, Italy in the framework of the iCog initiative.

ACKNOWLEDGMENTS

The author is happy to acknowledge the fruitful discussions over the years with close colleagues and friends, in particular Giulio Sandini, Sandro Mussa Ivaldi, and Wishwanathan Mohan, on the general topics of this essay.

REFERENCES

Abend, W., Bizzi, E., and Morasso, P. (1982). Human Arm Trajectory Formation. *Brain* 105, 331–348. doi:10.1093/brain/105.2.331

Aft, L. (2000). "Therblig Analysis," in *Work Measurement and Methods Improvement* (New York: John Wiley & Sons).

Barhen, J., Gulati, S., and Zak, M. M. (1989). Neutral Learning of Constrained Nonlinear Transformations. *Computer* 22, 67–76. doi:10.1109/2.30722

Barlow, S. M., Radder, J. P. L., Radder, M. E., and Radder, A. K. (2010). Central Pattern Generators for Orofacial Movements and Speech. *Handbook Behav. Neurosci.* 19, 351–369. doi:10.1016/b978-0-12-374593-4.00033-4

Beeler, S. C., Tran, H. T., and Banks, H. T. (2000). Feedback Control Methodologies for Nonlinear Systems. *J. Optimization Theor. Appl.* 107, 1–33. doi:10.1023/a:1004607114958

Bernstein, N. (1967). *The Co-ordination and Regulation of Movements*. Oxford, UK: Pergamon Press.

Bhat, A. A., Akkaladevi, S. C., Mohan, V., Eitzinger, C., and Morasso, P. (2017). Towards a Learnt Neural Body Schema for Dexterous Coordination of Action in Humanoid and Industrial Robots. *Auton. Robot* 41, 945–966. doi:10.1007/s10514-016-9563-3

Bizzi, E., Hogan, N., Mussa-Ivaldi, F. A., and Giszter, S. (1992). Does the Nervous System Use Equilibrium-point Control to Guide Single and Multiple Joint Movements. *Behav. Brain Sci.* 15 (4), 603–613. doi:10.1017/S0140525X00072538

Bizzi, E., Accornero, N., Chapple, W., and Hogan, N. (1984). Posture Control and Trajectory Formation during Arm Movement. *J. Neurosci.* 4, 2738–2744. doi:10.1523/jneurosci.04-11-02738.1984

Braitenberg, V. (1984). *Vehicles: Experiments in Synthetic Psychology*. Cambridge MA: MIT Press.

Brooks, R. A. (1991). Intelligence without Representation. *Artif. Intelligence* 47, 139–159. doi:10.1016/0004-3702(91)90053-m

Bullock, D., Bongers, R. M., Lankhorst, M., and Beek, P. J. (1999). A Vector-Integration-To-Endpoint Model for Performance of Viapoint Movements. *Neural Networks* 12, 1–29. doi:10.1016/s0893-6080(98)00109-9

Bullock, D., and Grossberg, S. (1988). Neural Dynamics of Planned Arm Movements: Emergent Invariants and Speed-Accuracy Properties during Trajectory Formation. *Psychol. Rev.* 95 (1), 49–90. doi:10.1037/0033-295x.95.1.49

Chemero, A. P. (2009). *Radical Embodied Cognitive Science*. Cambridge MA: MIT Press.

Cheung, V. C. K., and Seki, K. (2021). Approaches to Revealing the Neural Basis of Muscle Synergies: a Review and a Critique. *J. Neurophysiol.* 125 (5), 1580–1597. doi:10.1152/jn.00625.2019

D'Avella, A., Saltiel, P., and Bizzi, E. (2003). Combinations of Muscle Synergies in the Construction of a Natural Motor Behavior. *Nat. Neurosci* 6 (3), 300–308. doi:10.1038/nn1010

Decety, J., and Jeannerod, M. (1995). Mentally Simulated Movements in Virtual Reality: Does Fitts's Law Hold in Motor Imagery. *Behav. Brain Res.* 72 (1–2), 127–134. doi:10.1016/0166-4328(96)00141-6

Feldman, A. G. (1966). Functional Tuning of the Nervous System with Control of Movement or Maintenance of a Steady Posture: II Controllable Parameters of the Muscle. *Biophysics* 11, 565–578.

Feldman, A. G. (1986). Once More on the Equilibrium-Point Hypothesis (λ Model) for Motor Control. *J. Mot. Behav.* 18, 17–54. doi:10.1080/00222895.1986.10735369

Fitts, P. M. (1954). The Information Capacity of the Human Motor System in Controlling the Amplitude of Movement. *J. Exp. Psychol.* 47 (6), 381–391. doi:10.1037/h0055392

Flash, T., and Hogan, N. (1985). The Coordination of Arm Movements: an Experimentally Confirmed Mathematical Model. *J. Neurosci.* 5 (7), 1688–1703. doi:10.1523/jneurosci.05-07-01688.1985

Freitas, S. M. S. F., Duarte, M., and Latash, M. L. (2006). Two Kinematic Synergies in Voluntary Whole-Body Movements during Standing. *J. Neurophysiol.* 95, 636–645. doi:10.1152/jn.00482.2005

Friston, K. J., and Parr, T. (2019). Passive Motion and Active Inference. *Phys. Life Rev.* 30, 112–115. doi:10.1016/j.plrev.2019.01.004

Friston, K., Mattout, J., and Kilner, J. (2011). Action Understanding and Active Inference. *Biol. Cybern.* 104, 137–160. doi:10.1007/s00422-011-0424-z

Grush, R. (2004). The Emulation Theory of Representation: Motor Control, Imagery, and Perception. *Behav. Brain Sci.* 27, 377–396. doi:10.1017/s0140525x04000093

Guerra-Filho, G., and Aloimonos, Y. (2007). A Language for Human Action. *Computer* 40 (5), 42–51. doi:10.1109/mc.2007.154

Hersch, M., Sauser, E., and Billard, A. (2008). On Line Learning of the Body Schema. *Int. J. Humanoid Robot* 5 (2), 161–181. doi:10.1142/s0219843608001376

Hogan, N. (1985). Impedance Control: An Approach to Manipulation: Part I-Theory. *ASME J. Dynamic Syst. Meas. Control.* 107, 1–7. doi:10.1115/1.3140702

Hopfield, J. J. (1982). Neural Networks and Physical Systems with Emergent Collective Computational Abilities. *Proc. Natl. Acad. Sci.* 79, 2554–2558. doi:10.1073/pnas.79.8.2554

Horak, F. B., and Anderson, M. E. (1984). Influence of Globus Pallidus on Arm Movements in Monkeys. I. Effects of Kainic Acid-Induced Lesions. *J. Neurophysiol.* 52, 290–304. doi:10.1152/jn.1984.52.2.290

Huang, B., Xiong, C., Chen, W., Liang, J., Sun, B. Y., and Gong, X. (2021). Common Kinematic Synergies of Various Human Locomotor Behaviours. *R. Soc. Open Sci.* 8, 210161. doi:10.1098/rsos.210161

James, W. (1890). *The Principles of Psychology*. New York: Henry Holt and Company.

Jeannerod, M. (2001). Neural Simulation of Action: a Unifying Mechanism for Motor Cognition. *Neuroimage* 14 (1), S103–S109. doi:10.1006/nimg.2001.0832

Karklinsky, M., and Flash, T. (2015). Timing of Continuous Motor Imagery: the Two-Thirds Power Law Originates in Trajectory Planning. *J. Neurophysiol.* 113, 2490–2499. doi:10.1152/jn.00421.2014

Katz, P. S. (2016). Evolution of central Pattern Generators and Rhythmic Behaviours. *Phil. Trans. R. Soc. B* 371, 20150057. doi:10.1098/rstb.2015.0057

Kelso, J. S., Southard, D. L., and Goodman, D. (1979). On the Coordination of Two-Handed Movements. *J. Exp. Psychol. Hum. Perception Perform.* 5, 229–238. doi:10.1037/0096-1523.5.2.229

Kittaka, M., Furui, A., Sakai, H., Morasso, P., and Tsuji, T. (2020). Spatiotemporal Parameterization of Human Reaching Movements Based on Time Base Generator. *IEEE Access* 8, 104944–104955. doi:10.1109/access.2020.3000273

Kuperstein, M. (1988). Neural Model of Adaptive Hand-Eye Coordination for Single Postures. *Science* 239 (4845), 1308–1311. doi:10.1126/science.3344437

Laban, R. (1956). *Laban's Principles of Dance and Movement Notation*. London: MacDonald and Evans.

Lacquaniti, F., Terzuolo, C., and Viviani, P. (1983). The Law Relating the Kinematic and Figural Aspects of Drawing Movements. *Acta Psychologica* 54, 115–130. doi:10.1016/0001-6918(83)90027-6

Lashley, K. S. (1933). Integrative Functions of the Cerebral Cortex. *Physiol. Rev.* 13 (1), 1–42. doi:10.1152/physrev.1933.13.1.1

Latash, M. L. (2008). *Synergy*. New York: Oxford University Press.

Latash, M. L. (2012). The bliss (Not the Problem) of Motor Abundance (Not Redundancy). *Exp. Brain Res.* 217, 1–5. doi:10.1007/s00221-012-3000-4

Liu, D., and Todorov, E. (2007). Evidence for the Flexible Sensorimotor Strategies Predicted by Optimal Feedback Control. *J. Neurosci.* 27 (35), 9354–9368. doi:10.1523/jneurosci.1110-06.2007

Maravita, A., and Iriki, A. (2004). Tools for the Body (Schema). *Trends Cogn. Sci.* 8, 79–86. doi:10.1016/j.tics.2003.12.008

Marr, D., and Poggio, T. (1976). *From Understanding Computation to Understanding Neural Circuitry*. MIT Libraries, 1–21. AIM-357.

Mohan, V., and Morasso, P. (2011). Passive Motion Paradigm: an Alternative to Optimal Control. *Front. Neurorobot* 5 (4), 4–28. doi:10.3389/fnbot.2011.00004

Mohan, V., Bhat, A., and Morasso, P. (2019). Muscleless Motor Synergies and Actions without Movements: from Motor Neuroscience to Cognitive Robotics. *Phys. Life Rev.* 30, 89–111. doi:10.1016/j.plrev.2018.04.005

Morasso, P. (1981). Spatial Control of Arm Movements. *Exp. Brain Res.* 42, 223–227. doi:10.1007/BF00236911

Morasso, P. (2021). Gesture Formation: A Crucial Building Block for Cognitive-Based Human-Robot Partnership. *Cogn. Robotics* 1, 92–110. doi:10.1016/j.cogr.2021.06.004

Morasso, P., and Mussa Ivaldi, F. A. (1982). Trajectory Formation and Handwriting: a Computational Model. *Biol. Cybern.* 45, 131–142. doi:10.1007/bf00335240

Morasso, P. (1983). Three Dimensional Arm Trajectories. *Biol. Cybern.* 48, 187–194. doi:10.1007/bf00318086

Mussa Ivaldi, F. A., Morasso, P., and Zaccaria, R. (1988). Kinematic Networks. A Distributed Model for Representing and Regularizing Motor Redundancy. *Biol. Cybern.* 60, 1–16. doi:10.1007/BF00205967

Mussa Ivaldi, F. A., Morasso, P., Hogan, N., and Bizzi, E. (1989). "Network Models of Motor Systems with many Degrees of freedom," in *Advances in Control Networks and Large Scale Parallel Distributed Processing Models*. Editor M. D. Fraser (Norwood, NJ: Ablex Publ. Corp.

Mussa-Ivaldi, F. A., Giszter, S. F., and Bizzi, E. (1994). Linear Combinations of Primitives in Vertebrate Motor Control. *Proc. Natl. Acad. Sci.* 91, 7534–7538. doi:10.1073/pnas.91.16.7534

O'Shea, H., and Moran, A. (2017). Does Motor Simulation Theory Explain the Cognitive Mechanisms Underlying Motor Imagery? A Critical Review. *Front. Hum. Neurosci* 11, 72. doi:10.3389/fnhum.2017.00072

Piaget, J. (1952). *The Origins of Intelligence in Children*. New York, NY USA: M. Cook, Trans., W. W. Norton & Co.

Ptak, R., Schnider, A., and Fellrath, J. (2017). The Dorsal Frontoparietal Network: a Core System for Emulated Action. *Trends Cogn. Sci.* 7 (21), 589–599. doi:10.1016/j.tics.2017.05.002

Rusaw, E. (2013). An Artificial Neural Network Model for Serial Speech Production and Speech Error Simulation. *The J. Acoust. Soc. America* 134 (5), 4166. doi:10.1121/1.4831272

Sakai, H., Furui, A., Hama, S., Yanagawa, A., Kubo, K., Morisako, Y., et al. (2021). Pen-point Trajectory Analysis during Trail Making Test Based on a Time Base Generator Model. *Proceed 43rd Annu. Int. Conf. IEEE Eng. Med. Biol. Soc. (Embc)* 2021, 6215–6219. doi:10.1109/embc46164.2021.9629991

Saltiel, P., Wyler-Duda, K., D'Avella, A., Tresch, M. C., and Bizzi, E. (2001). Muscle Synergies Encoded within the Spinal Cord: Evidence from Focal Intraspinal NMDA Iontophoresis in the Frog. *J. Neurophysiol.* 85 (2), 605–619. doi:10.1152/jn.2001.85.2.605

Scholz, J. P., and Schöner, G. (1999). The Uncontrolled Manifold Concept: Identifying Control Variables for a Functional Task. *Exp. Brain Res.* 126, 289–306. doi:10.1007/s002210050738

Scott, S. H. (2004). Optimal Feedback Control and the Neural Basis of Volitional Motor Control. *Nat. Rev. Neurosci.* 5, 532–546. doi:10.1038/nrn1427

Shadmehr, R., Mussa-Ivaldi, F., and Bizzi, E. (1993). Postural Force fields of the Human Arm and Their Role in Generating Multijoint Movements. *J. Neurosci.* 13 (1), 45–62. doi:10.1523/jneurosci.13-01-00045.1993

Shin, Y. K., Proctor, R. W., and Capaldi, E. J. (2010). A Review of Contemporary Ideomotor Theory. *Psychol. Bull.* 136 (6), 943–974. doi:10.1037/a0020541

Slomka, K., Juras, G., Sobota, G., Furmanek, M., Rzepko, M., and Latash, M. L. (2015). Intra-personal and Inter-personal Kinetic Synergies during Jumping. *J. Hum. Kinetics* 49, 75–88. doi:10.1515/hukin-2015-0110

Sturm, J., Plagemann, C., and Burgard, W. (2009). Body Schema Learning for Robotic Manipulators from Visual Self-Perception. *J. Physiol. Paris* 103 (3–5), 220–231. doi:10.1016/j.jphysparis.2009.08.005

Tkachman, O., Purnomo, G., and Gick, B. (2021). Repetition Preferences in Two-Handed Balanced Signs: Vestigial Locomotor central Pattern Generators Shape Sign Language Phonetics and Phonology. *Front. Commun.* 5, 147. doi:10.3389/fcomm.2020.612973

Todorov, E., and Jordan, M. I. (2002). Optimal Feedback Control as a Theory of Motor Coordination. *Nat. Neurosci.* 5, 1226–1235. doi:10.1038/nn963

Tresch, M. C., Saltiel, P., and Bizzi, E. (1999). The Construction of Movement by the Spinal Cord. *Nat. Neurosci.* 2, 162–167. doi:10.1038/5721

Tsuji, T., Tanaka, Y., Morasso, P. G., Sanguineti, V., and Kaneko, M. (2002). Bio-mimetic Trajectory Generation of Robots via Artificial Potential Field with Time Base Generator. *IEEE Trans. Syst. Man. Cybern. C* 32 (4), 426–439. doi:10.1109/tsmcc.2002.807273

Turvey, M. T. (1977). "Preliminaries to a Theory of Action with Reference to Vision," in *Perceiving, Acting, and Knowing*. Editors R. Shaw and J. Bransford (Hillsdale, NJ: Erlbaum), 211–266.

von Hofsten, C. (1982). Eye-hand Coordination in the Newborn. *Develop. Psychol.* 18, 450–461. doi:10.1037/0012-1649.18.3.450

Zak, M. (1988). Terminal Attractors for Addressable Memory in Neural Networks. *Phys. Lett.* 133, 218–222. doi:10.1016/0375-9601(88)90728-1

Conflict of Interest: The author declares that the research was conducted in the absence of any commercial or financial relationships that could be construed as a potential conflict of interest.

frontiers in Physiology

ORIGINAL RESEARCH
published: 28 January 2022
doi: 10.3389/fphys.2021.809243

Inter-Person Differences in Isometric Coactivations of Triceps Surae and Tibialis Anterior Decrease in Young, but Not in Older Adults After 14 Days of Bed Rest

*Matjaž Divjak[1], Gašper Sedej[1], Nina Murks[1], Mitja Gerževič[2,3], Uros Marusic[2,3], Rado Pišot[2], Boštjan Šimunič[2] and Aleš Holobar[1]**

[1] System Software Laboratory, Institute of Computer Science, Faculty of Electrical Engineering and Computer Science, University of Maribor, Maribor, Slovenia, [2] Science and Research Centre Koper, Institute for Kinesiology Research, Koper, Slovenia, [3] Department of Health Sciences, Alma Mater Europaea – ECM, Maribor, Slovenia

OPEN ACCESS

Edited by:
Nicolas Place, University of Lausanne, Switzerland

Reviewed by:
Taian Martins Vieira, Politecnico di Torino, Italy
Ryota Akagi, Shibaura Institute of Technology, Japan

***Correspondence:**
Aleš Holobar
ales.holobar@um.si

Specialty section:
This article was submitted to Exercise Physiology, a section of the journal Frontiers in Physiology

Received: *04 November 2021*
Accepted: *24 December 2021*
Published: *28 January 2022*

Citation:
Divjak M, Sedej G, Murks N, Gerževič M, Marusic U, Pišot R, Šimunič B and Holobar A (2022) Inter-Person Differences in Isometric Coactivations of Triceps Surae and Tibialis Anterior Decrease in Young, but Not in Older Adults After 14 Days of Bed Rest. Front. Physiol. 12:809243. doi: 10.3389/fphys.2021.809243

We examined activation patterns of the gastrocnemius medialis (GM), gastrocnemius lateralis (GL), soleus (SO), and tibialis anterior (TA) muscles in eight older (58.4 ± 3.3 years) and seven young (23.1 ± 2.9 years) participants, before and after 14 days of horizontal bed rest. Visual feedback on the exerted muscle torque was provided to the participants. The discharge patterns of individual motor units (MUs) were studied in three repetitions of isometric plantar flexion at 30 and 60% of Maximum Voluntary Contraction (MVC), before, and 1 day after the 14-day bed rest, respectively. In the GL and GM muscles, the older participants demonstrated higher MU discharge rates than the young, regardless of the contraction level, both before and after the bed rest. In the TA and SO muscles, the differences between the older and young participants were less consistent. Detailed analysis revealed person-specific changes in the MU discharge rates after the bed rest. To quantify the coactivation patterns we calculated the correlation coefficients between the cumulative spike trains of identified MUs from each muscle, and measured the root mean square difference of the correlation coefficients between the trials of the same session (intra-session variability) and between different sessions (inter-session variability) in each participant (intra-person comparison) and across participants (inter-person comparison). In the intra-person comparison, the inter-session variability was higher than the intra-session variability, either before or after the bed rest. At 60% MVC torque, the young demonstrated higher inter-person variability of coactivation than the older participants, but this variability decreased significantly after the bed rest. In older participants, inter-person variability was consistently lower at 60% than at 30% MVC torque. In young participants, inter-person variability became lower at 60% than at 30% MVC torque only after the bed rest. Precaution is required when analyzing the MU discharge and coactivation patterns, as individual persons demonstrate individual adaptations to aging or bed rest.

Keywords: high density electromyography, muscle disuse, motor units, discharge rate, aging

INTRODUCTION

Several studies demonstrated the decrease of motor unit (MU) discharge rates with age in individual muscles such as first dorsal interosseous (Erim et al., 1999; Vaillancourt et al., 2003), tibialis anterior (TA) (Connelly et al., 1999), soleus (SO) (Kallio et al., 2012), and vastus lateralis (Watanabe et al., 2016), suggesting that age-related loss of muscle strength is related to MU discharge properties. However, a recent study on the TA muscle during isometric contraction at 20% of the maximal voluntary effort (Castronovo et al., 2018) demonstrated that neither the MU discharge rate, nor the coefficient of variation for the interspike interval were associated with age.

One of possible explanations for these discrepancies could be inter-personal differences in muscle coactivation patterns, especially when the investigated movements are controlled by several agonistic and antagonistic muscles. Indeed, the inter-person diversity of muscle coactivation strategies was documented extensively in various conditions (Cutting and Kozlowski, 1977; de Rugy et al., 2012; Horst et al., 2017). In the past few years, person- and condition-specific coactivation patterns of triceps surae muscle were studied extensively (Hug et al., 2019; Aeles et al., 2021), demonstrating that the gastrocnemius medialis (GM), gastrocnemius lateralis (GL), SO and TA muscles exhibit person-specific coactivation patterns, and support person discrimination across measuring sessions. These findings led to the establishment of the concept of person-specific muscle coactivation signatures (Hug et al., 2019).

However, interactions among skeletal muscles are still not understood fully. Most of the previous studies investigated muscle coactivation patterns using amplitude envelopes of the bipolar electromyographic (EMG) signal. This methodology has several limitations. First, it is sensitive to electrode positioning (Vinti et al., 2018; Holobar and Farina, 2021; Vieira and Botter, 2021). Second, amplitude envelopes of EMG reflect not only muscle activation levels, but also the shapes of the motor unit action potentials (MUAPs) and therefore the localization of MU fibers in the MU territory (Vieira et al., 2011, 2016). The uniqueness and inter-person diversity of muscle coactivation strategies as assessed from EMG amplitude envelopes could, therefore, at least partially, originate from person-specific MU fiber localizations in the muscle tissue. Third, EMG amplitude envelopes (in bipolar or multichannel recordings) do not discriminate between the contributions of different MUs, and do not address the separation of contributions from different muscles when significant muscle crosstalk is present (for example, when recording activity of wrist extensors). Fourth, EMG amplitude envelopes are sensitive to changes of MUAPs that are caused either by contraction levels (Vieira et al., 2015), or by muscle shortening and muscle fatigue (Šavc and Holobar, 2021). At least at higher contraction levels, the fatigue may cause significant MUAP changes, decreasing the accuracy of muscle activation estimation (Holobar and Farina, 2021; Šavc and Holobar, 2021). Like MU territories and fibers' localizations, the fatiguing profiles and changes of MUAP shapes can be person specific.

Muscle activation patterns were also studied intensively by Non-negative Matrix Factorization (NMF) of the EMG amplitude envelopes (d'Avella et al., 2003, 2015; Tresch et al., 2006). However, it was shown recently that NMF does not remove the MUAP shapes, and is, thus, sensitive to MU fiber localizations, changes of MUAP shapes due to muscle shortening or muscle fatigue (Šavc and Holobar, 2021), and to muscle crosstalk (Šavc et al., 2018). Therefore, also in the case of NMF-based analysis, the inter-person diversity of assessed muscle coactivation patterns could originate from person-specific MU properties.

On the other hand, identification of MU discharges from non-invasively recorded high-density EMG (hdEMG) signals offers a detailed insight into the behavior of relatively large number of MUs (Holobar and Zazula, 2007; Negro et al., 2009; Tanzarella et al., 2021). These EMG decomposition techniques identify the MU discharge times and fully remove the effects of MUAPs from the recorded EMG signals (Holobar and Farina, 2021). They can be adapted to dynamic muscle contractions in which MUAP shapes change significantly (Glaser and Holobar, 2018; Kramberger and Holobar, 2021) and, thus, discriminate between the changes in MUAP shapes and in muscle activation levels. They also offer efficient control of MU identification accuracy (Holobar et al., 2014) and, therefore, control of the quality of the muscle activation estimation. Different approaches to muscle activation estimation from MU discharge patterns were also developed, including Principal Component Analysis of smoothed MU discharge rates (Negro et al., 2009), NMF of smoothed MU discharge rates (Tanzarella et al., 2021) and Cumulative Spike Train (CST) of identified MUs (Farina et al., 2014). Indeed, studies of simultaneous MU behavior in different muscles are increasing (Héroux et al., 2014; de Souza et al., 2018; Kranjec and Holobar, 2019; Davis et al., 2020; Potočnik et al., 2020; Cohen et al., 2021; Tanzarella et al., 2021). However, to the best of our knowledge, comparisons of MU behavior in a group of simultaneously recorded skeletal muscles of older and young persons are still largely lacking.

In this study, we propose a robust approach to estimation of the differences in activation of skeletal muscles. This approach builds on the identification of individual MU discharge patterns and on cross-correlation analysis of CSTs, and is, thus, not sensitive to the person-specific MU fiber localizations. Moreover, it supports quantification of both individual MU properties, as well as interactions between the activation patterns of different skeletal muscles. To demonstrate the efficiency of this approach we examined and mutually compared the person-specific changes of MU behavior in GL, GM, SO, and TA muscles during isometric plantar flexions in older and young participants undergoing a 14-day horizontal bed rest.

Experimental bed rest is a gold standard ground-based model for studying the effects of microgravity, as well as interaction between aging and disuse (Di Girolamo et al., 2021). Post bed rest decreases of muscle mass and strength (Koren, 2015;

Abbreviations: CST, Cumulative Spike Train; EMG, Electromyography; GM, Gastrocnemius medialis; GL, Gastrocnemius lateralis; hdEMG, High-density Electromyography; MU, Motor Unit; MUAP, Motor Unit Action Potential; MVC, Maximum Voluntary Contraction; NMF, Non-negative Matrix Factorization; PNR, Pulse-to-Noise Ratio; RMS, Root-Mean-Square difference; SDR, Smoothed motor unit discharge rate; SO, Soleus; TA, Tibialis anterior.

Pišot et al., 2016; Rejc et al., 2018; Marusic et al., 2021), as well as performance and neural drive (Duchateau, 1995) were reported in the past, along with the damaged neuromuscular junctions and muscle denervation (Monti et al., 2021). Changes in muscle architecture were also reported (Narici and Cerretelli, 1998), although, in a recent study by Koren (2015), the thickness and pennation angle of GM and TA did not change after the bed rest in either young or older persons. However, the studies of muscle activation patterns before and after the bed rest are relatively limited. In some previous bed rest studies (Duchateau, 1995) and immobilization studies (Gondin et al., 2004), amplitude envelopes of bipolar EMG were compared to a supramaximal M wave. Also, Mulder et al. (2009) studied bed rest-induced changes in neural activation properties of the vastus lateralis muscle by using amplitude envelopes of hdEMG. To the best of our knowledge, the individual MU behavior in GL, GM, SO, and TA muscles before and after the bed rest was not studied systematically, even though these muscles were frequently used to study the effect of aging on MU behavior.

In this study, we hypothesize that the previously reported interpersonal variability of muscle coactivations is also demonstrated on the level of MU discharge patterns, and is preserved throughout the aging and bed rest. Therefore, this variability influences the comparison of MU behavior between older and young persons and needs to be considered when analyzing the changes in individual skeletal muscles.

MATERIALS AND METHODS

Experimental Protocol

Fifteen healthy male adults participated in the study: Seven young (aged from 19 to 28 years with mean age of 23.1 ± 2.9 years, height 177.1 ± 5.9 cm, body mass 73.4 ± 7.5 kg) and eight older (aged from 53 to 64 years with mean age of 58.4 ± 3.3 years, height 172.7 ± 4.6 cm, body mass 77.0 ± 11.8 kg). Prior to bed rest all participants underwent medical examination and blood/urine analysis. Exclusion criteria were: Smoking, regular alcohol consumption, ferromagnetic implants, history of deep vein thrombosis, acute or chronic skeletal, neuromuscular, metabolic, and cardiovascular disease conditions, or pulmonary embolism. Participants were well informed of the purpose, procedures and risks involved before signing the informed consent. The study was performed in accordance with the Helsinki Declaration, and approved by the Republic of Slovenia National Medical Ethics Committee (KME 103/04/12).

A 14-day bed rest protocol was conducted in hospital facilities under strict medical supervision, with constant video surveillance and 24-h medical care. A detailed protocol description can be found in a previously published paper (Pišot et al., 2016). The protocol consisted of four main phases:

- 3 days of accommodation to the environment and baseline data collection;
- 14 days of horizontal bed rest with no deviations from the supine position and no active exercises or muscle contraction tests allowed, with a eucalorically controlled diet;
- 2 days of post bed rest ambulatory care;
- 28 days of supervised recovery period (not covered in this study).

Data Acquisition

Two data acquisition sessions were performed, before (BEFORE), and 1 day after the bed rest (AFTER). Each session consisted of hdEMG and plantar flexion torque measurements during controlled dominant foot isometric plantar flexions with a trapezoidal torque profile. The foot dominance was determined by an experienced physician (as the foot that kicks the ball; all the participants were right-dominant). Each participant's dominant foot was fixed in a mechanical brace (Wise Technologies, Ljubljana, Slovenia) at 90-degree knee flexion. The exerted muscle torque was measured by an electronic force sensor (HBM, Darmstadt, Germany) at 1,024 Hz. The MVC level was measured after familiarization with the experimental protocol and type of performed contractions. Afterward, each participant performed three repetitions of the plantar flexion at 30 and 60% of MVC torque, with 90-s-long pauses between them. In each repetition the participant performed a 5 s long ramp-up, followed by a 15 s long hold phase and 5 s long ramp-down. The 30 and 60% MVC torque levels were selected to analyze the potential differences between moderate and high contraction levels in both age groups (Watanabe et al., 2016).

During the plantar flexions we recorded the hdEMG of the TA, GL, GM, and SO muscles in the dominant foot. For each muscle we used a flexible grid of 13 × 5 electrodes with 8 mm interelectrode distance (LISiN–OT Bioelettronica, Torino, Italy), resulting in 64 data channels per muscle. The skin was abraded lightly using abrasive paste, and the electrode grids were filled with conductive gel (Meditec–Every, Parma, Italy). A reference electrode was put at the ankle malleolus of the dominant foot. The hdEMG was band-pass filtered (3 dB bandwidth, 10–750 Hz) and recorded in monopolar mode at 2,048 Hz and 12-bit A/D resolution (EMG-USB2 amplifier, OT Bioelettronica, Torino, Italy).

Data Processing

The torque signal was resampled to the same sampling rate as the hdEMG signals (2,048 Hz), and then both data sets were synchronized with the help of a dedicated trigger signal. The acquired monopolar hdEMG signals were decomposed offline by the Convolution Kernel Compensation (CKC) method (Holobar and Zazula, 2007), yielding binary spike trains of individual MUs. The decomposition results were inspected manually and edited by an experienced human operator, and all the MUs with irregular discharge pattern or with Pulse-to-Noise Ratio (PNR) < 28 dB were discarded (Holobar et al., 2014). This resulted in high accuracy of MU discharge identification.

Smoothed MU discharge rates (SDRs) were calculated by resampling the instantaneous MU discharge rates to the constant sampling frequency of 100 Hz, and low-pass filtering them by a zero-phase fourth order Butterworth filter with cut-off frequency set to 2 Hz. CST was calculated by summing

up the binarized spike trains of individual MUs, and low-pass filtering the result by a 400 ms long Hann window (De Luca, 1985; Negro et al., 2009). Finally, the cross-correlation coefficients between CSTs of simultaneously active TA, GL, GM, and SO muscles were calculated pair-wise to quantify the coactivation patterns of the studied muscles. The Root Mean Square (RMS) difference of CST's cross-correlation coefficients, calculated between all possible muscle pairs and for all trial combinations, was used to estimate the inter-person, intra-person, inter-session and intra-session variability of muscle coactivation patterns in each individual participant. Autocorrelations of the CSTs were excluded from the RMS difference calculations. Examples of estimated CSTs and their cross-correlation coefficients in a representative older participant are depicted in **Figure 1** (BEFORE) and **Figure 2** (AFTER).

Statistical Analysis

Statistical analysis was performed in Matlab version R2021a and JASP software version 0.15. In each sub-analysis we first used the Shapiro-Wilk test to check for normality of the data distribution. For paired comparison we performed the Repeated Measures ANOVA test with Holm-Bonferroni *post hoc* comparisons (in the case of normally distributed data), or Friedman's Repeated Measures test with Conover's *post hoc* comparisons and Holm-Bonferroni correction (for non-normally distributed data). The number of factors and their interactions tested are clarified in the Results sections. For unpaired comparison between older and young participants we used the Kruskal-Wallis test whenever the Shapiro-Wilk test indicated that the data were not normally distributed. When normal distribution was not rejected, we used one-way ANOVA. In both cases Bonferroni correction was applied when significant differences were detected.

In all the analyses the Mauchly's test was used to check the assumption of sphericity, while the Levene's test was used to check the assumption of homogeneity of variance. When required, we used Greenhouse-Geisser correction for data sphericity. The Omega squared (ω^2) method was used to estimate the effect size in Repeated Measures ANOVA, with $\omega^2 = 0.14$ indicating a large effect, $\omega^2 = 0.06$ indicating a medium effect, and $\omega^2 = 0.01$ indicating a small effect. For all statistical comparisons the level of significance was set at $p < 0.05$. To evaluate the impact of the limited number of participants included into this study, we used the ANOVA_Power software package (Lakens and Caldwell, 2019) to calculate *post hoc* statistical powers.

RESULTS

Number of Identified Motor Units

Because the distribution of the number of identified MUs violated the assumptions of normality, sphericity, and homogeneity, we performed the Friedman's Repeated Measures test (factors: Session, muscle combination, contraction level). The test didn't show any differences for the factors session or contraction level. The only difference for the factor muscle was found between TA and GM ($p = 0.011$), with TA having less identified MUs.

To compare young and older participants we performed an unpaired Kruskal-Wallis test. Before the bed rest the number of identified MUs was higher in older than in young participants for the SO muscle at 30% MVC torque, and for the TA and SO muscles at 60% MVC torque. After the bed rest, the number of identified MUs was higher in older than in young participants for the GL muscle at 60% MVC torque, and for the SO muscle at 30% MVC torque (**Table 1**).

Cross-Correlation of Cumulative Spike Trains

Representative examples of single differential hdEMG signals and the resulting smoothed MU discharge rates at 30% MVC torque at BEFORE and AFTER are depicted in **Figures 3**, **4**, respectively. In each depicted trial and muscle, different MUs are coded with different colors. Note that the identified MUs were activated in different time intervals, demonstrating temporal dynamics of muscle activation. To cope with this dispersion of MU activation intervals, the CSTs were calculated for each muscle, summing up the binary spike trains of all the MUs per muscle. Examples of the estimated CSTs in representative older participant are depicted in **Figure 1** (BEFORE) and in **Figure 2** (AFTER). The cross-correlation coefficients of CSTs are depicted in the right panels of **Figures 1**, **2**. Note the relatively consistent muscle coactivation pattern in both BEFORE and AFTER sessions in the depicted participant. However, this was not the case for all the tested participants, as depicted in **Figure 5**. In some participants, the muscle coactivation patterns were relatively preserved across the measuring sessions, whereas, in others, a higher diversity of muscle coactivations was evident, even within the same measuring session. This demonstrates the existence of several degrees of freedom in muscle control strategies during isometric plantar flexion.

In both older and young participants and in both measuring sessions, the cross-correlation of CSTs increased significantly with the contraction level. Since the Shapiro-Wilk test showed that cross-correlation values were not normally distributed, we performed a Friedman's Repeated Measures comparison (factors: Session, muscle combination, contraction level). This comparison showed that contraction level and muscle combinations have significant effects: For contraction level $\chi^2(1) = 20.578$, $p < 0.001$; for muscle combinations $\chi^2(5) = 55.457$, $p < 0.001$. Conover's *post hoc* comparisons with Holm-Bonferroni correction showed differences between 30 and 60% MVC torque, $T(321) = 2.123$, $p = 0.034$. For muscle combinations all the Holm-Bonferroni corrected p-values were not significant, likely also due to the relatively high differences observed in coactivation strategies among the participants (**Figure 5**). Additional analysis of the simple main effects for the contraction level factor showed higher cross-correlation at 60% than at 30% MVC torque for both BEFORE ($p = 0.005$) and AFTER ($p = 0.021$) in older participants, but only for AFTER in young participants ($p = 0.003$).

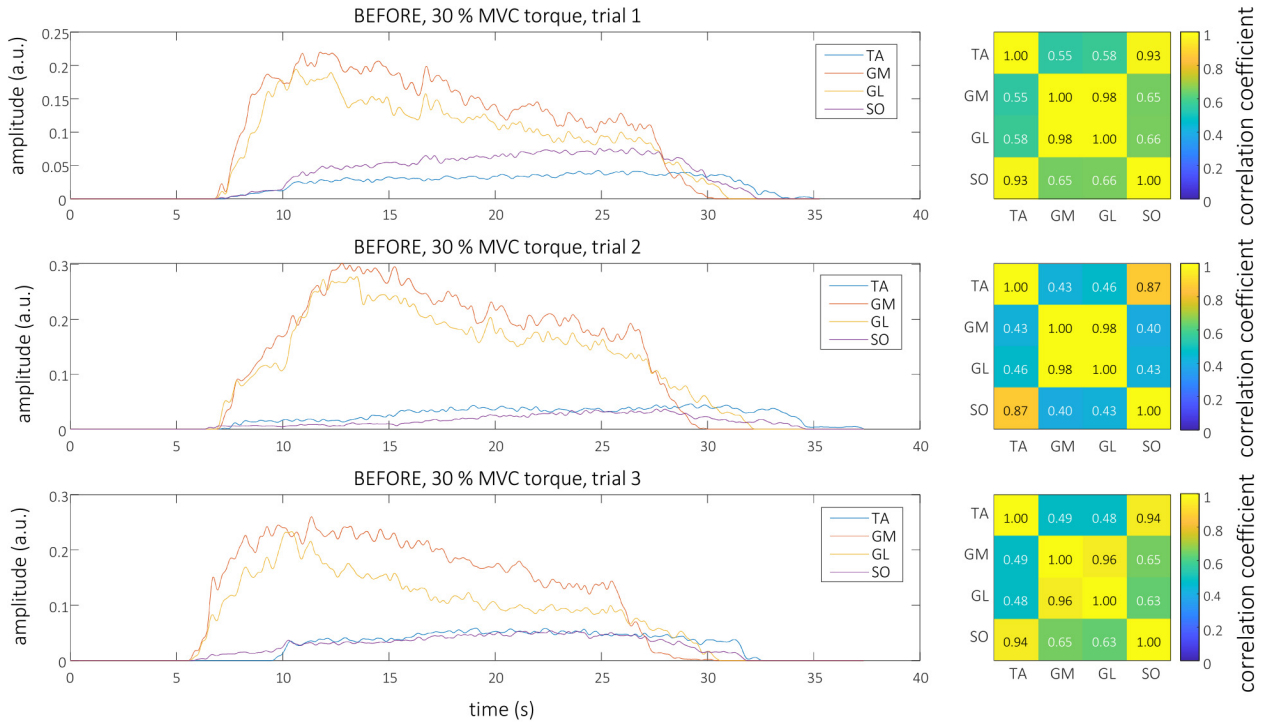

FIGURE 1 | Left, CSTs as calculated from the tibialis anterior (TA), gastrocnemius medialis (GM), gastrocnemius lateralis (GL), and soleus (SO) muscles of older participant (O1) during the three trials at 30% MVC torque before the bed rest. Right, The muscle coactivation as revealed by the cross-correlation analysis of CSTs of different muscles.

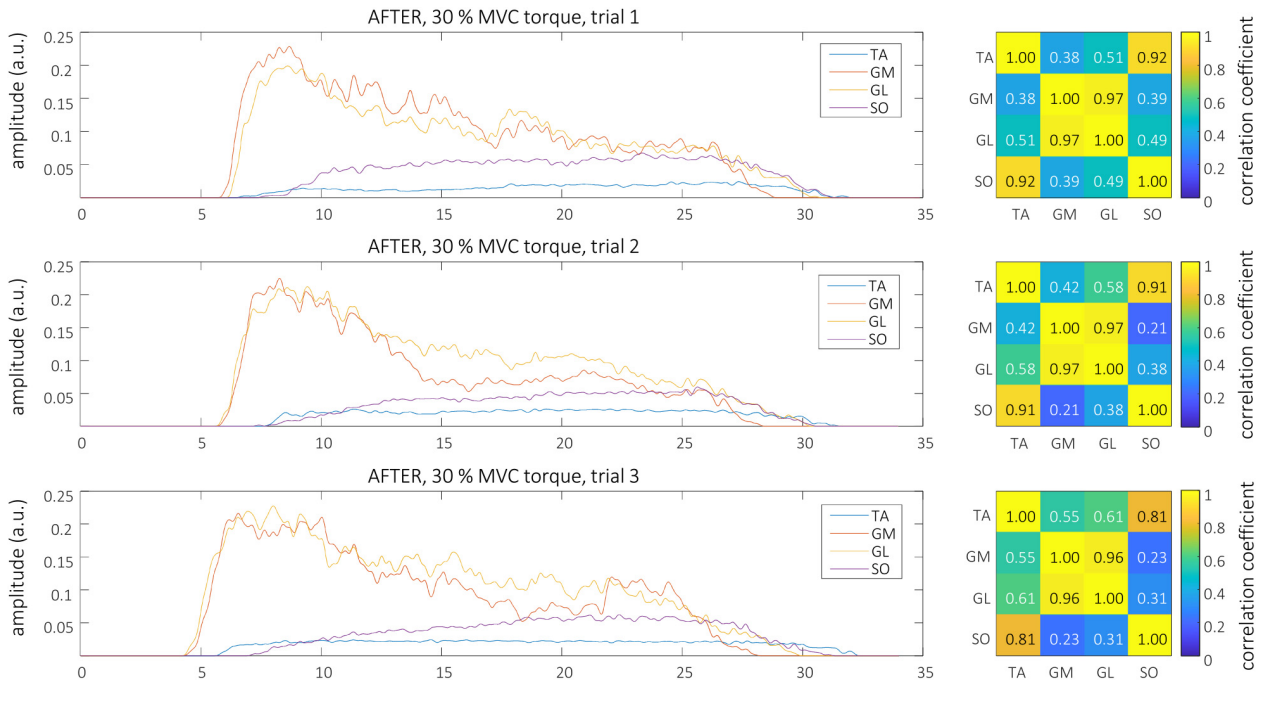

FIGURE 2 | Left, CSTs as calculated from the tibialis anterior (TA), gastrocnemius medialis (GM), gastrocnemius lateralis (GL), and soleus (SO) muscles of older participant (O1) during the three trials at 30% MVC torque after the bed rest. Right, The muscle coactivation as revealed by the cross-correlation analysis of CSTs of different muscles.

TABLE 1 | Number of motor units (Mean ± Standard Deviation) identified from different muscles in the BEFORE and AFTER sessions (PNR ≥ 28 dB).

	Older				Young			
Session	**TA**	**GM**	**GL**	**SO**	**TA**	**GM**	**GL**	**SO**
BEFORE, 30% MVC torque	8.6 ± 4.9	20.5 ± 9.7	14.6 ± 10.4	17.5 ± 5.9*	7.2 ± 4.9	20.5 ± 9.4	10.9 ± 4.9	12.2 ± 5.4*
AFTER, 30% MVC torque	6.3 ± 4.8	17.7 ± 9.8	18.3 ± 7.0	15.7 ± 4.8*	5.5 ± 3.5	17.1 ± 10.1	14.5 ± 7.0	12.3 ± 4.8*
BEFORE, 60% MVC torque	8.2 ± 4.7*	19.3 ± 10.8	11.7 ± 11.2	16.4 ± 8.0*	5.1 ± 3.5*	16.0 ± 15.6	6.4 ± 4.5	8.6 ± 5.5*
AFTER, 60% MVC torque	6.0 ± 3.7	16.6 ± 11.6	12.5 ± 8.0*	13.5 ± 6.9	5.6 ± 3.3	14.2 ± 6.7	7.2 ± 6.2*	12.8 ± 7.9

*TA, Tibialis anterior; GM, Gastrocnemius medialis; GL, Gastrocnemius lateralis; SO, Soleus; MVC, Maximum Voluntary Contraction. *Denotes significantly different values in older and young participants (Kruskal-Wallis test, $p < 0.05$).*

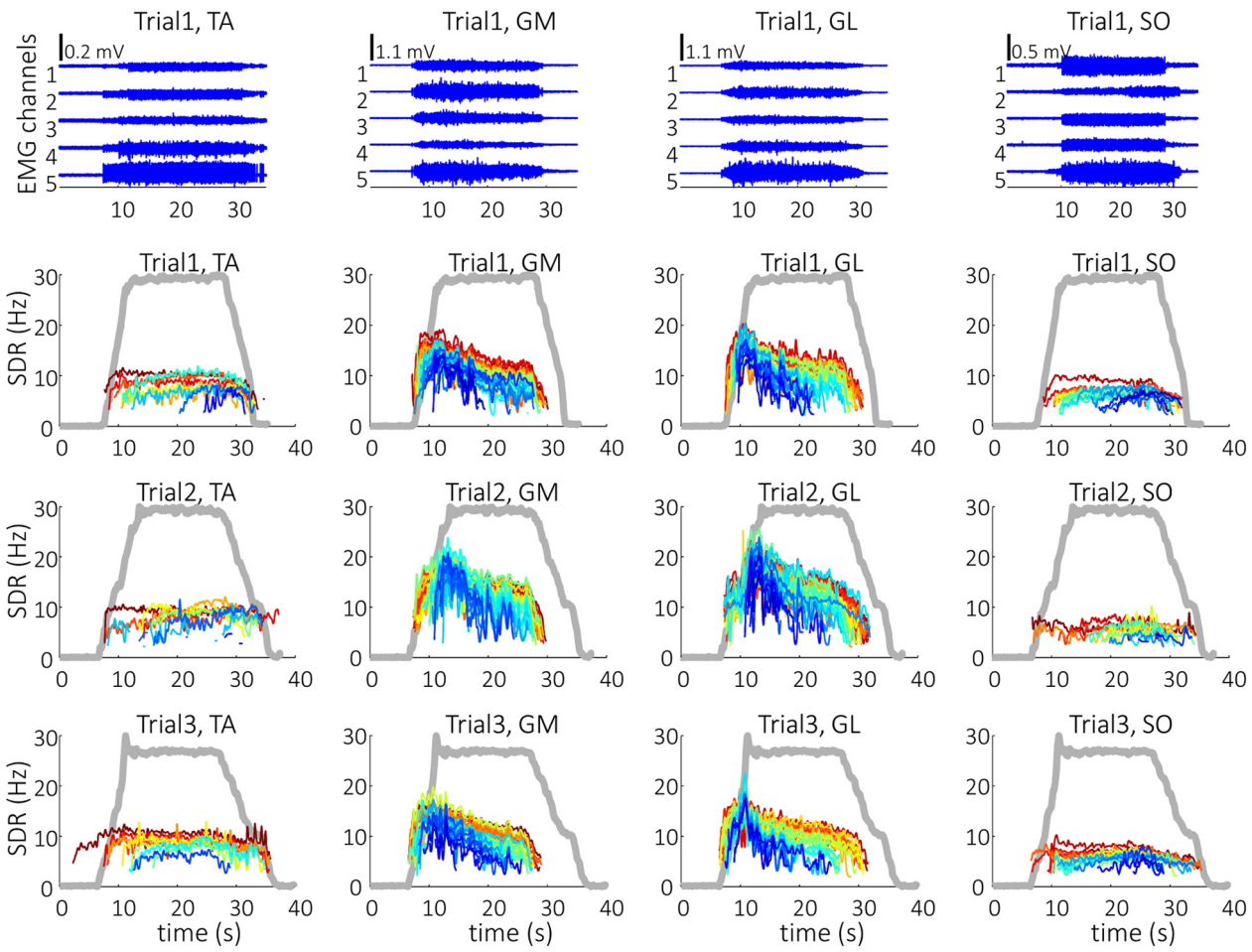

FIGURE 3 | Single differential hdEMG channels (top panels) and smoothed discharge rates (SDR) of individual motor units (panels in the three bottom rows), as identified from the hdEMG signals of older participant (O1). The three trials were performed before the bed rest at 30% MVC torque. TA, Tibialis anterior; GM, Gastrocnemius medialis; GL, Gastrocnemius lateralis; SO, Soleus. The thick gray line represents the measured muscle torque.

Root Mean Square Differences Between Cross-Correlations

Intra-person RMS differences between cross-correlations of CSTs are depicted in **Figure 6** (left panels). We calculated the RMS differences for two intra-session comparisons (BEFORE and AFTER) and for one inter-session (BEFORE-AFTER) combination. The RMS differences were normally distributed, and assumptions of homogeneity and sphericity were not violated. Therefore, we performed three-way Repeated Measures ANOVA analysis (between subject factors: Age, within subject factors: Session combination, contraction level). We found large significant effects for the factors session combination [$F(2, 26) = 10.888$, $p < 0.001$, $\omega^2 = 0.177$] and contraction level [$F(1, 13) = 8.278$, $p = 0.013$, $\omega^2 = 0.173$], but not for age. All interaction effects were not significant. *Post hoc* comparisons with Holm-Bonferroni corrections revealed higher

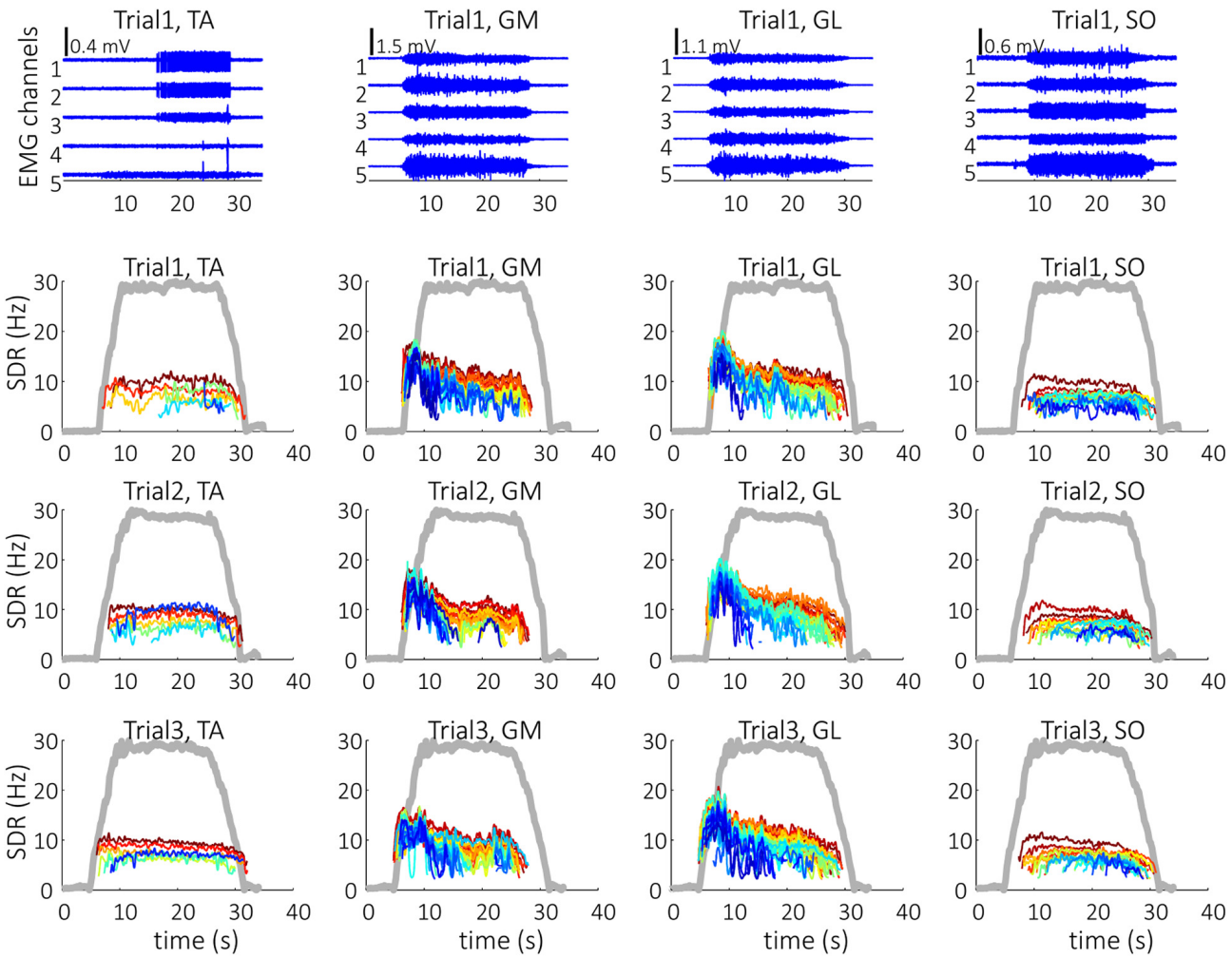

FIGURE 4 | Single differential hdEMG channels (top panels) and smoothed discharge rates (SDR) of individual motor units (panels in the three bottom rows), as identified from the hdEMG signals of older participant (O1). The three trials were performed after the bed rest at 30% MVC torque. TA, Tibialis anterior; GM, Gastrocnemius medialis; GL, Gastrocnemius lateralis; SO, Soleus; The thick gray line represents the measured muscle torque.

inter-session RMS differences than intra-session RMS differences (BEFORE-AFTER vs. BEFORE: $p = 0.014$, BEFORE-AFTER vs. AFTER: $p < 0.001$). *Post hoc* comparison for contraction levels showed that the RMS differences were smaller at 60% than at 30% MVC torque ($p = 0.013$). An additional simple main effect test (limited pairwise comparison) for the session combination factor showed that the inter-session RMS differences of older participants were higher than the intra-session at both 30% ($p = 0.013$) and 60% MVC torque ($p = 0.029$), whereas no difference was significant in young. *Post hoc* statistical powers for reported significant RMS differences between CSTs' cross-correlation coefficients ranged from 77 to 100%.

Analysis of the inter-person RMS differences between the cross-correlations of CSTs (**Figure 6**, right panels) followed the same procedure as the analysis of intra-person differences. Since the results were normally distributed, we performed a three-way Repeated Measures ANOVA analysis (between subject factors: Age, within subject factors: Session combination, contraction level). In both inter- and intra-session comparisons we found large significant effects for the main factor contraction level [intra-session: $F(1, 47) = 47.658$, $p < 0.001$, $\omega^2 = 0.228$; inter-session: $F(1, 47) = 42.044$, $p < 0.001$, $\omega^2 = 0.238$]. We found medium-sized significant effects for two-way interaction contraction level * age [intra-session: $F(1, 47) = 12.847$, $p < 0.001$, $\omega^2 = 0.07$; inter-session: $F(1, 47) = 11.751$, $p = 0.001$, $\omega^2 = 0.076$] and three-way interaction session combination * contraction level * age [intra-session: $F(1, 47) = 16.242$, $p < 0.001$, $\omega^2 = 0.07$; inter-session: $F(1.81, 85.062) = 10.568$, $p < 0.001$, $\omega^2 = 0.053$]. Intra-session *post hoc* comparisons revealed differences between the older and young at 60% MVC torque in the BEFORE ($p = 0.004$), but not in the AFTER session (the older had a lower RMS difference). After the bed rest the RMS differences at 60% MVC torque decreased in the young ($p = 0.005$), but not in the older. In addition, the older demonstrated lower RMS differences at 60% MVC than at 30% MVC torque levels for both BEFORE ($p < 0.001$) and AFTER ($p = 0.002$). In young participants the

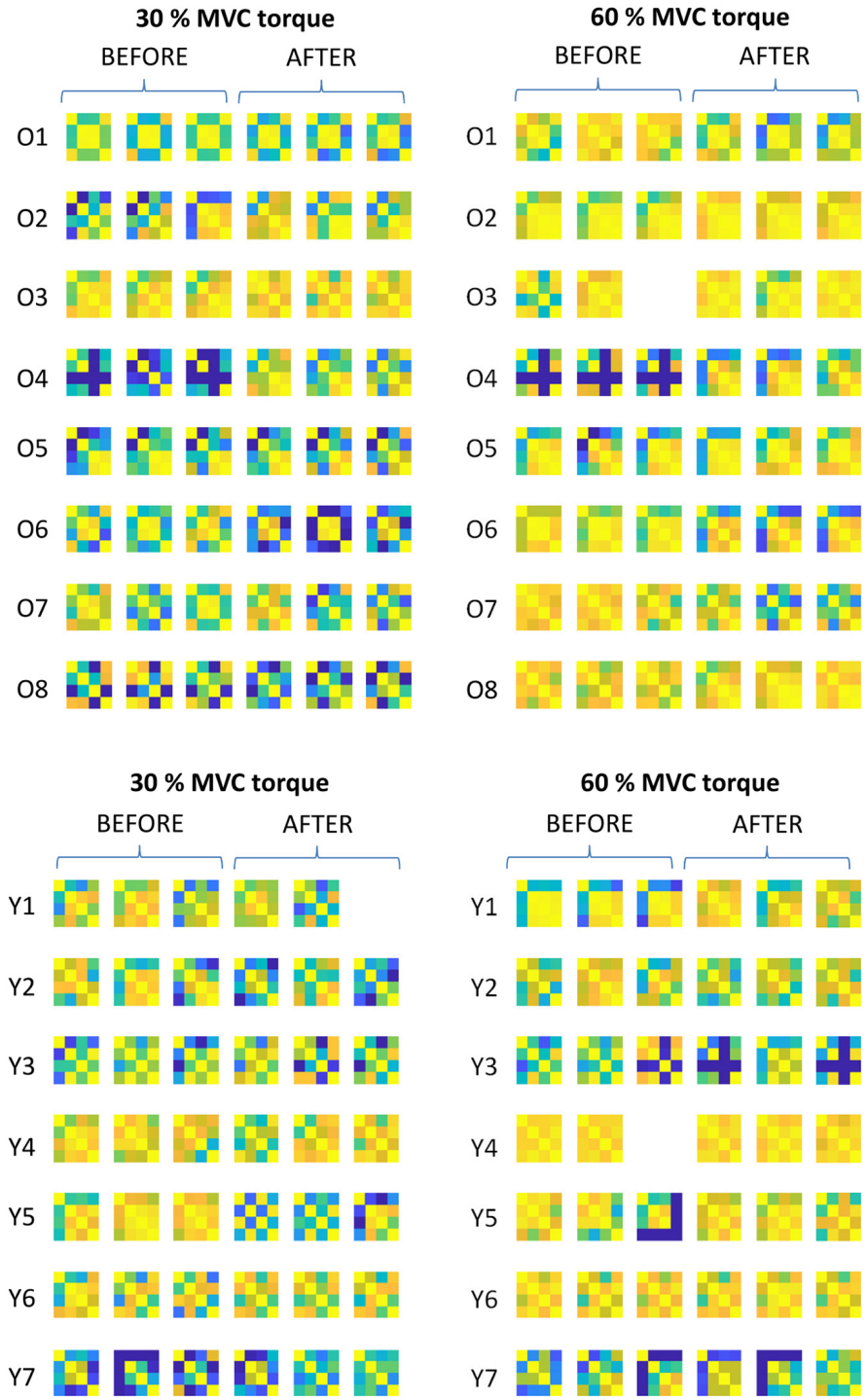

FIGURE 5 | Comparison of the muscle coactivation patterns in older (Oi) and young (Yi) participants across different trials at 30 and 60% MVC torque before (BEFORE) and after (AFTER) the bed rest. The muscle coactivation patterns are coded by pairwise cross-correlation of the cumulative spike trains of different muscles, in the same way as in the right panels of **Figures 1**, **2**. Due to technical problems during the measurements one trial is missing in the O3, Y1, and Y4 participants.

RMS differences were lower at 30% MVC than at 60% MVC torque levels only AFTER ($p = 0.018$), but not BEFORE the bed rest (**Figure 6**, right panels).

Smoothed Discharge Rate

Normal distribution of the mean SDR values was not rejected. Therefore, we performed the four-way Repeated Measures

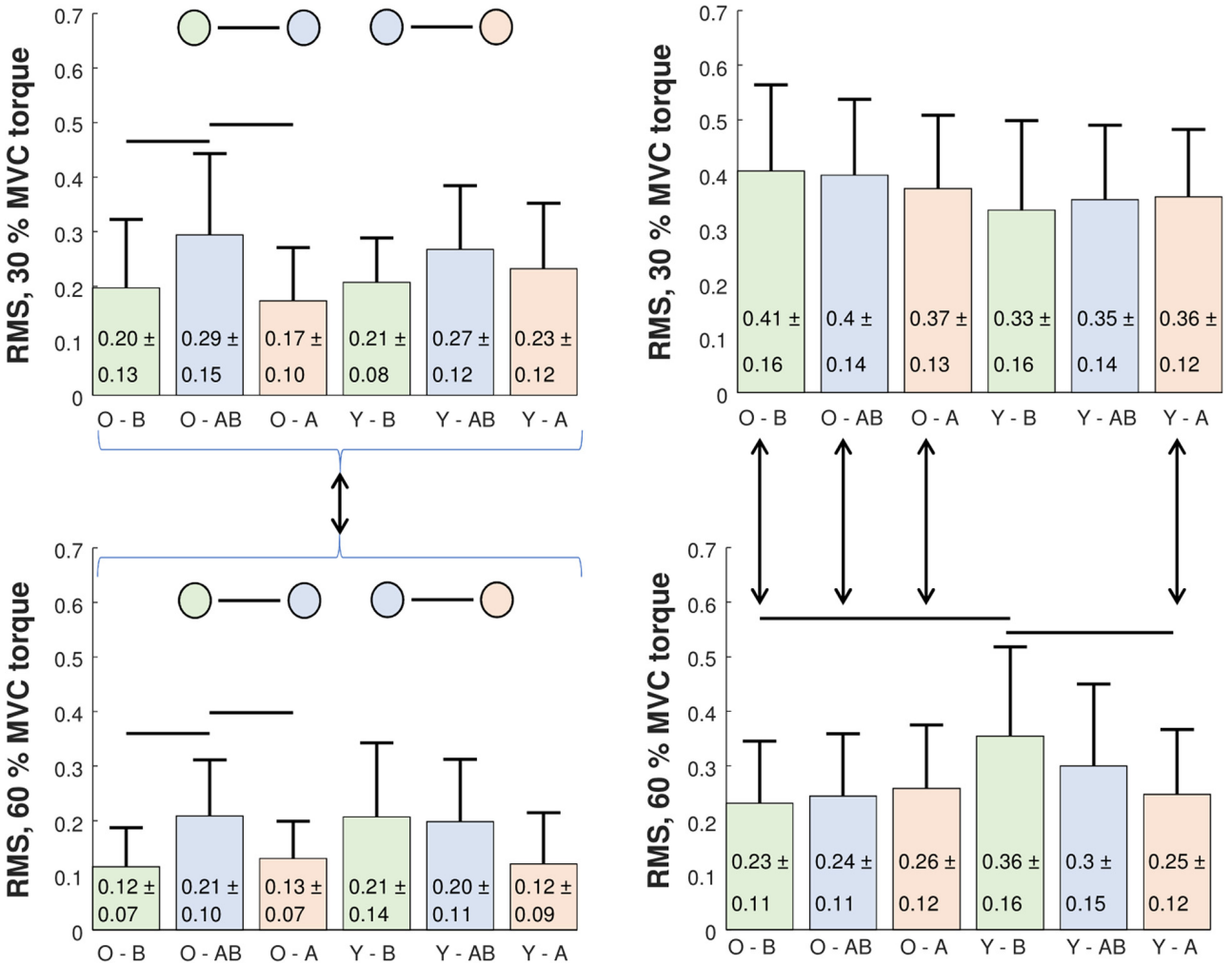

FIGURE 6 | Comparison of intra-person (left panels) and inter-person (right panels) RMS difference of cumulative spike trains' cross-correlation coefficients in older (O) and young (Y) participants at 30% (upper panels) and 60% MVC torque (lower panels). RMS differences were calculated across different trials before (B) and after (A) the bed rest (intra-session comparison), and between the trials of before and after bed rest sessions (AB, inter-session comparison). Statistically significant differences were estimated by a three-way Repeated Measures ANOVA test and are denoted by black lines (see the text for a detailed explanation).

ANOVA comparison (between subject factors: Age, within subject factors: Session, contraction level, muscle). We found large significant effects for all three main factors: Session [$F(1, 12) = 12.460$, $p = 0.004$, $\omega^2 = 0.131$, BEFORE has higher mean SDR], contraction level [$F(1, 12) = 30.984$, $p < 0.001$, $\omega^2 = 0.511$, mean SDR is higher at 60% MVC] and muscle [$F(3, 36) = 7.565$, $p < 0.001$, $\omega^2 = 0.263$], but no significant interactions. *Post hoc* comparison between muscles showed that SO had consistently lower mean SDR when compared to TA ($p = 0.029$), GM ($p < 0.001$), or GL ($p = 0.012$). As we were not able to calculate the four-way ANOVA *post hoc* statistical powers in ANOVA_Power software, we calculated three-way ANOVA *post hoc* powers separately for each contraction level. In accordance with the relatively high inter-person differences observed in this study (**Figure 5**), *post hoc* statistical powers for significant factors in SDRs ranged from 40 to 100% (at 30% MVC torque) and from 23 to 81% (at 60% MVC torque), suggesting that lager cohorts of participants are required to reliably assess the changes of SDRs.

Figure 7 depicts the comparison between SDRs in individual muscles of the young and older participants. For orientation purposes and comparison with other studies that studied individual muscles, we also show the results of the one-way ANOVA test. In the GM and GL muscles, the MU discharge rates were always higher in the older than in the young participants, regardless of the measuring session or contraction level. The opposite was true for the SO muscle, where the discharge rates were higher in the young than in the older participants, except at the 60% MVC torque in AFTER session. In the TA muscle, young participants demonstrated higher discharge rates than older at 30% MVC torque in AFTER and at 60% MVC torque in BEFORE.

Figure 8 depicts adaptations of the SDRs in individual muscles of individual participants. When tested with one-way ANOVA, the SDRs after the bed rest mostly decreased or did not change

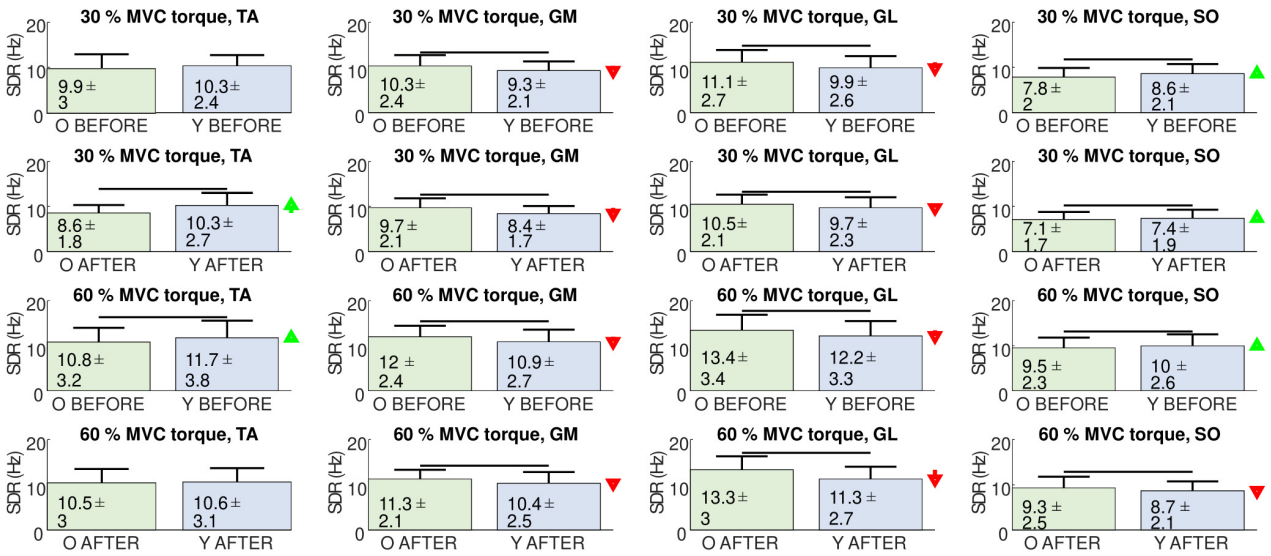

FIGURE 7 | Comparison of smoothed motor unit discharge rates (SDR, Mean ± SD) in the tibialis anterior (TA), gastrocnemius medialis (GM), gastrocnemius lateralis (GL), and soleus (SO) muscles between older (O), and young (Y) participants before (BEFORE), and after (AFTER) the bed rest. The red and green arrows indicate significant decrease and increase of SDR, respectively, at AFTER when compared to BEFORE (one-way ANOVA test, $p < 0.05$).

significantly, though several cases of increases in SDR were also observed. This agrees with the individual changes of coactivation patterns depicted in **Figure 5**, further demonstrating the person-specific adaptations of load sharing among the GM, GL, and SO muscles after the bed rest.

DISCUSSION

We identified and compared the discharge patterns in the GM, GL, SO, and TA muscles of eight older and seven young participants before and after 14 days of horizontal bed rest. We demonstrated that the changes of MU discharge rates and muscle coactivation patterns during submaximal isometric plantar flexion after the bed rest are person-specific, and depend on the level of plantar flexion. As discussed in the following paragraphs, our results agree at least partially with many other studies of MU discharge rates in older and young persons (Connelly et al., 1999; Kallio et al., 2012; Castronovo et al., 2018), but also extend them with the analysis across different muscles.

In our study, the number of investigated MUs was relatively high. In total, 3,196, 2,165, 2,453, and 1,179 MU discharge patterns were analyzed in the GM, GL, SO, and TA muscles, respectively. Their quality was assured by selecting the MUs with high PNR (Holobar et al., 2014), and by inspecting the discharge patterns carefully. Noteworthy, the number of identified MUs did not differ significantly across the measurement sessions (before vs. after the bed rest), whereas differences among older and young participants were detected in a limited number of cases (**Table 1**). This suggests relatively high repeatability of the MU identification in this study.

Although the activation of the TA muscle was not strictly expected, the TA was frequently active during the hold phase of plantar flexion, suggesting that the participants were trying to stabilize the ankle joint. This might be task specific (the participants were instructed to maintain a stable torque during the hold phase). Importantly, since the CKC-based EMG decomposition is biased toward superficial and large MUs (Frančič and Holobar, 2021), we can state with high probability that the activity observed at the skin surface above the TA muscle did not originate from deeper muscles, and was not due to the muscle crosstalk.

The identified MU discharge patterns were used to analyze and compare the MU discharge rates and muscle coactivation patterns mutually. When accumulated across the participants and across the muscles, the MU discharge rates decreased after the bed rest ($p = 0.004$, $\omega^2 = 0.131$). As expected, the MU discharge rates increased with the contraction levels, and the GL and GM muscles demonstrated higher discharge rates than the SO. In agreement with the diversity of results from other studies that demonstrated decreased MU discharge rates or no significant changes with aging (Connelly et al., 1999; Erim et al., 1999; Vaillancourt et al., 2003; Kallio et al., 2012; Watanabe et al., 2016; Castronovo et al., 2018), the MU discharge rates in our study showed mixed differences between the participants and muscles. When tested with one-way ANOVA, the older participants demonstrated higher MU discharge rates in the GL and GM muscles than the young, regardless of the contraction level or the measuring session (**Figure 7**). This trend was reversed in the TA muscle, which played the role of antagonist, stabilizing the ankle joint in the studied isometric plantar flexion. At 30% of MVC torque the MU discharge rates in the TA were lower in older than in young participants after the bed rest, but not before. However, at 60% of MVC, the MU discharge rates in the TA were lower in the older than in the young participants before the bed rest, but not after. This agrees with the results

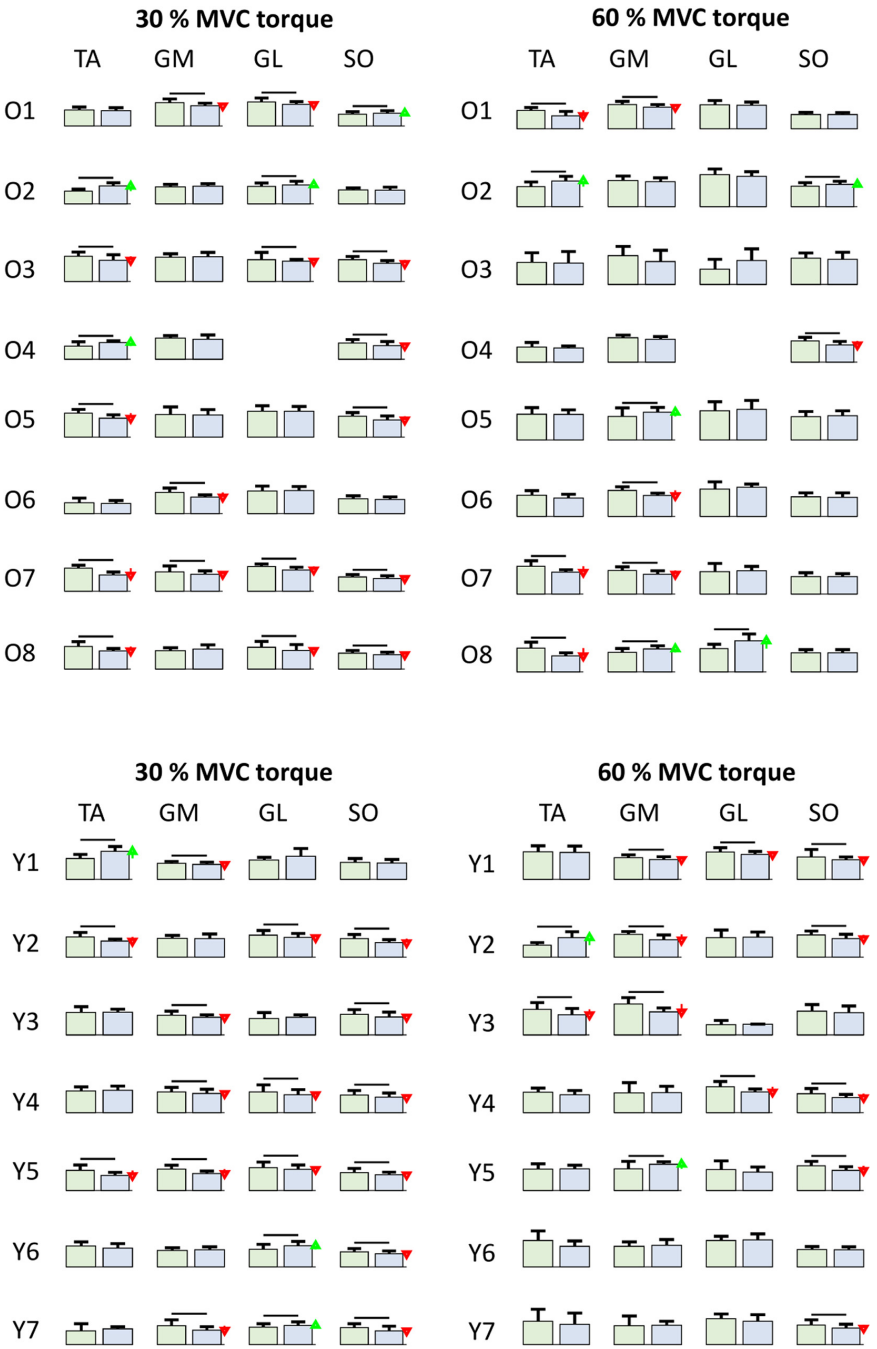

FIGURE 8 | Comparison of smoothed motor unit discharge rates (SDR, Mean ± SD) in individual older (Oi rows, top) and young (Yi rows, bottom) participants for different muscles (columns) at 30 and 60% MVC torque between BEFORE (left green bars) and AFTER (right blue bars). The red and green arrows indicate significant decrease and increase of SDR, respectively, at AFTER when compared to BEFORE (one-way ANOVA test, $p < 0.05$). TA, Tibialis anterior; GM, Gastrocnemius medialis; GL, Gastrocnemius lateralis; SO, Soleus.

of the previous study (Castronovo et al., 2018), where, despite a relatively high number of identified MUs, no association of MU discharge rates with age was observed in the TA muscle during dorsi flexion.

In a previous study by Kallio et al. (2012), the MU discharge rates of the SO muscle were lower in older than in young people, though the differences were not always statistically significant. In our analysis of the SO muscle, the discharge rates between the older and young did not differ extensively, though when tested by one-way ANOVA the differences were significant. During 30% MVC torque, the older participants demonstrated lower discharge rates than the young, both before and after the bed

rest. This was also true at 60% MVC torque before the bed rest, whereas after the bed rest the young participants exhibited lower discharge rates than the older ones (**Figure 7**). This again shows the complexity of interpretation of MU discharge rates on the level of individual muscles, and exposes the need for the person-specific and across muscle assessment of adaptations in muscle control strategies.

Indeed, the detailed analysis revealed individual responses of the participants to the bed rest (**Figure 8**). In most of the participants, but not all, the MU discharge rates decreased after the bed rest in at least one muscle, but the combination of muscles in which discharge rates decreased was different in different participants. For example, after the bed rest, three older participants decreased MU discharge rates at 30% MVC torque in GM, whereas, in five participants, the differences were not significant (**Figure 8**). Similar diversity of responses was also evident in the other muscles, for both 30 and 60% MVC torques. Interestingly, in the SO muscle of young participants the discharge rates never increased. Six out of 7 participants at 30% MVC torque, and 5 out of 7 participants at 60% MVC torque had decreased MU discharge rates, whereas in the others, the changes were not significant (**Figure 8**). These results are at least in partial agreement with the results of the immobilization study on young participants published by Gondin et al. (2004), where decrease of RMS value of bipolar EMG, normalized to respective M-waves, was measured in the SO muscle. The same values were also decreased in the gastrocnemii muscles, although the changes were not significant (Gondin et al., 2004). On the other hand, in the 36 year old participant studied by Duchateau (1995), EMG activity during MVC torque was reduced to a greater extent in the GL (−51%) than in the SO (−32%) muscle, whereas the decrease of the maximal M-wave amplitude was more prominent in the SO (−28%) than in the GL (−12%). Our study confirmed the changes in MU discharge rates, but the responses were heterogeneous and person specific.

To illuminate these differences among different participants better, we calculated the correlation coefficients between the CSTs from GM, GL, SO, and TA before and after the bed rest. In older participants the level of coactivation increased with the MVC torque level in both sessions, before and after the bed rest, whereas in the young this trend was observed only after the bed rest. The differences in muscle coactivation patterns were assessed further by calculating the inter- and intra-person and inter- and intra-session RMS difference of the cross-correlation coefficients of CSTs (**Figure 6**). In the intra-person comparison, inter-session variability was higher than intra-session variability, both before and after the bed rest. Also noteworthy, the intra-session variability was lower at 60% than at 30% MVC torque level (**Figure 6**). At 60% MVC torque, the young participants had higher inter-person variability of coactivation than the older ones, but this variability decreased after the bed rest. In the older group, the inter-person variability was consistently lower at 60% than at 30% MVC torque, but in the young participants inter-person variability became lower at 60% than at 30% MVC torque only after the bed rest (**Figure 6**). This suggests the potential decrease of inter-person differences in plantar flexion control strategies with age.

Our study has several limitations. First, the number of investigated participants that underwent the 14-day bed rest protocol is relatively low, but is comparable to many other studies that compared young vs. older participants (Erim et al., 1999, 20 participants; Connelly et al., 1999, 12 participants; Vaillancourt et al., 2003, 30 participants; Kallio et al., 2012, 17 participants; Castronovo et al., 2018, 20 participants) as well as to other bed rest studies where the number of participants ranged from 6 to 16 (Di Girolamo et al., 2021). This is partially justified by the complexity and stress of the prolonged bed rest that needs to be carried out in a hospital setting with 24-h medical inspection and care. Nevertheless, further investigations on larger cohorts of participants are required to confirm the findings reported herein. Despite this limitation, the number of investigated MUs was relatively large, assuring the high representativeness of the investigated MU discharge rates and CSTs (Farina et al., 2014). Second, to guarantee enough identified MUs, we focused our study on a relatively simple task, comprising isometric plantar flexions with the hold phase targeting only two different contraction levels. More complex tasks would likely expose the differences in cognitive, motor and sensory system interactions of older and young participants, but would also likely increase the heterogeneity of person-specific muscle control strategies, both before and after the bed rest. Also important, MU identification is more prone to methodological errors in dynamic conditions than in isometric conditions. Due to the relatively high complexity of the bed rest protocol, and, consequently, relatively low number of participants, we avoided more complex tasks in our study. Third, we limited our analysis to submaximal voluntary contractions. Increasing the contraction level would likely lead to very high coactivation levels of the investigated muscles. Fourth, to keep the experimental protocol short and to avoid the significant effect of muscle fatigue, we measured only three repetitions of each contraction level. More thorough analysis of repeatability of the observed coactivation patterns across a larger number of experimental recordings is left for future work. Finally, our group of older participants had a mean age of 58.4 ± 3.3 years, whereas the expression "older" is usually used for people of 65 years of age or above. Although this discrepancy might influence the extent of the observed differences, it likely does not change the observation that the adaptations are person specific.

CONCLUSION

In conclusion, we demonstrated person-specific changes of MU discharge rates and muscle coactivation patterns during submaximal isometric plantar flexion in both older and young participants after the bed rest. Several differences were observed among the older and young participants. At higher MVC torque levels before the bed rest, young participants demonstrated higher inter-person variability of muscle coactivation patterns than the older, but, after the bed rest, this variability decreased to a level that was comparable to the older participants. Further

studies on larger cohorts of participants are required to illuminate the physiological mechanisms behind the observed changes, but our results readily demonstrate that precaution is needed when analyzing the statistical differences in older and young persons, as the inter-person differences of muscle coactivations that are revealed by hdEMG decomposition endure in aging and after immobilization.

DATA AVAILABILITY STATEMENT

The datasets presented in this article are not readily available because our data was acquired a few years ago, before the GDPR came into force and before open science initiative was developed to the current stage. Unfortunately, this is reflected in our formulation of open data availability statements in the informed consent that the participants signed, which doesn't mention the possibility of public sharing of the gathered data.

ETHICS STATEMENT

The studies involving human participants were reviewed and approved by the Republic of Slovenia National Medical Ethics Committee. The participants provided their written informed consent to participate in this study.

AUTHOR CONTRIBUTIONS

AH, BŠ, MG, and RP contributed to the conception and design of the study and to the data acquisition. MD, AH, GS, and NM decomposed the hdEMG signals. MD, AH, BŠ, and UM performed the analysis of the results and wrote the first draft of the manuscript. All authors contributed to manuscript revision, and read and approved the submitted version.

FUNDING

This study was a part of the research project PANGeA (Physical Activity and Nutrition for Quality Ageing), supported by a Grant Cross-Border Cooperation Program Slovenia, Italy 2007–2013, Grant No. 042–2/2009. This study was also supported by the Slovenian Research Agency (Projects J2-7357, J2-1731, and L7 9421 and Program funding P2-0041).

ACKNOWLEDGMENTS

We would like to thank the participants in the study, the staff of the Orthopedic Hospital Valdoltra (Ankaran, Slovenia), all members of the research team, as well as the students of Applied Kinesiology of the University of Primorska, who contributed to the smooth undertaking of the study.

REFERENCES

Aeles, J., Horst, F., Lapuschkin, S., Lacourpaille, L., and Hug, F. (2021). Revealing the unique features of each individual's muscle activation signatures. *J. Royal Soc. Interf.* 18:20200770. doi: 10.1098/rsif.2020.0770

Castronovo, A. M., Mrachacz-Kersting, N., Stevenson, A. J. T., Holobar, A., Enoka, R. M., and Farina, D. (2018). Decrease in force steadiness with aging is associated with increased power of the common but not independent input to motor neurons. *J. Neurophysiol.* 120, 1616–1624. doi: 10.1152/jn.00093.2018

Cohen, J. W., Vieira, T., Ivanova, T. D., Cerone, G. L., and Garland, S. J. (2021). Maintenance of standing posture during multi-directional leaning demands the recruitment of task specific motor units in the ankle plantarflexors. *Exp. Brain Res.* 239, 2569–2581. doi: 10.1007/s00221-021-06154-0

Connelly, D. M., Rice, C. L., Roos, M. R., and Vandervoort, A. A. (1999). Motor unit firing rates and contractile properties in tibialis anterior of young and old men. *J. Appl. Physiol.* 87, 843–852. doi: 10.1152/jappl.1999.87.2.843

Cutting, J. E., and Kozlowski, L. T. (1977). Recognizing friends by their walk: gait perception without familiarity cues. *Bull. Psychon. Soc.* 9, 353–356. doi: 10.3758/BF03337021

d'Avella, A., Bizzi, E., and Saltiel, P. (2003). Combinations of muscle synergies in the construction of a natural motor behavior. *Nat. Neurosci.* 6, 300–308. doi: 10.1038/nn1010

d'Avella, A., Giese, M., Ivanenko, Y., Flash, T., and Schack, T. (2015). Editorial: Modularity in motor control: from muscle synergies to cognitive action representation. *Front. Comput. Neurosci.* 9:126. doi: 10.3389/fncom.2015.00126

Davis, L. A., Alenazy, M. S., Almuklass, A. M., Feeney, D., Vieira, T., Botter, A., et al. (2020). Force control during submaximal isometric contractions is associated with walking performance in persons with multiple sclerosis. *J. Neurophysiol.* 123, 2191–2200. doi: 10.1152/jn.00085.2020

De Luca, C. J. (1985). Control properties of motor units. *J. Experim. Biol.* 115, 125–136.

de Rugy, A., Loeb, G. E., and Carroll, T. J. (2012). Muscle coordination is habitual rather than optimal. *J. Neurosci.* 32, 7384–7391. doi: 10.1523/JNEUROSCI.5792-11.2012

de Souza, L. M. L., Cabral, H. V., de Oliveira, L. F., and Vieira, T. M. (2018). Motor units in vastus lateralis and in different vastus medialis regions show different firing properties during low-level, isometric knee extension contraction. *Hum. Mov. Sci.* 58, 307–314. doi: 10.1016/j.humov.2017.12.012

Di Girolamo, F. G., Fiotti, N., Milanović, Z., Situlin, R., Mearelli, F., Vinci, P., et al. (2021). The aging muscle in experimental bed rest: a systematic review and meta-analysis. *Front. Nutrit.* 8:633987. doi: 10.3389/fnut.2021.633987

Duchateau, J. (1995). Bed rest induces neural and contractile adaptations in triceps surae. *Med. Sci. Sports Exerc.* 27, 1581–1589.

Erim, Z., Beg, M. F., Burke, D. T., and de Luca, C. J. (1999). Effects of aging on motor-unit control properties. *J. Neurophysiol.* 82, 2081–2091. doi: 10.1152/jn.1999.82.5.2081

Farina, D., Negro, F., and Dideriksen, J. L. (2014). The effective neural drive to muscles is the common synaptic input to motor neurons. *J. Physiol.* 592, 3427–3441. doi: 10.1113/jphysiol.2014.273581

Frančič, A., and Holobar, A. (2021). On the reuse of motor unit filters in high density surface electromyograms recorded at different contraction levels. *IEEE Access* 9, 115227–115236. doi: 10.1109/ACCESS.2021.3104762

Glaser, V., and Holobar, A. (2018). Motor unit identification from high-density surface electromyograms in repeated dynamic muscle contractions. *IEEE Trans. Neural Syst. Rehab. Eng.* 27, 66–75. doi: 10.1109/TNSRE.2018.2885283

Gondin, J., Guette, M., Maffiuletti, N., and Martin, A. (2004). Neural activation of the triceps surae is impaired following 2 weeks of immobilization. *Eur. J. Appl. Physiol.* 93, 359–365. doi: 10.1007/s00421-004-1225-z

Héroux, M. E., Dakin, C. J., Luu, B. L., Inglis, J. T., and Blouin, J.-S. (2014). Absence of lateral gastrocnemius activity and differential motor unit behavior in soleus and medial gastrocnemius during standing balance. *J. Appl. Physiol.* 116, 140–148. doi: 10.1152/japplphysiol.00906.2013

Holobar, A., and Farina, D. (2021). Noninvasive neural interfacing with wearable muscle sensors: combining convolutive blind source separation methods and

deep learning techniques for neural decoding. *IEEE Signal Proc. Magaz.* 38, 103–118. doi: 10.1109/MSP.2021.3057051

Holobar, A., Minetto, M. A., and Farina, D. (2014). Accurate identification of motor unit discharge patterns from high-density surface EMG and validation with a novel signal-based performance metric. *J. Neural Eng.* 11:016008. doi: 10.1088/1741-2560/11/1/016008

Holobar, A., and Zazula, D. (2007). Multichannel blind source separation using convolution kernel compensation. *IEEE Trans. Signal Proc.* 55, 4487–4496. doi: 10.1109/TSP.2007.896108

Horst, F., Mildner, M., and Schöllhorn, W. I. (2017). One-year persistence of individual gait patterns identified in a follow-up study—a call for individualized diagnose and therapy. *Gait Post.* 58, 476–480. doi: 10.1016/j.gaitpost.2017.09.003

Hug, F., Vogel, C., Tucker, K., Dorel, S., Deschamps, T., LeCarpentier, E., et al. (2019). Individuals have unique muscle activation signatures as revealed during gait and pedaling. *J. Appl. Physiol.* 127, 1165–1174. doi: 10.1152/japplphysiol.01101.2018

Kallio, J., Søgaard, K., Avela, J., Komi, P., Selänne, H., and Linnamo, V. (2012). Age-related decreases in motor unit discharge rate and force control during isometric plantar flexion. *J. Electromyogr. Kinesiol.* 22, 983–989. doi: 10.1016/j.jelekin.2012.05.009

Koren, K. (2015). *Biomechanical and geometrical adaptation of skeletal muscle and its muscle fibers on 14-day bed rest and active rehabilitation in elderly subjects*. Koper: University of Primorska.

Kramberger, M., and Holobar, A. (2021). On the prediction of motor unit filter changes in blind source separation of high-density surface electromyograms during dynamic muscle contractions. *IEEE Access* 9, 103533–103540. doi: 10.1109/ACCESS.2021.3099015

Kranjec, J., and Holobar, A. (2019). Improved assessment of muscle excitation from surface electromyograms in isometric muscle contractions. *IEEE Trans. Neural Syst. Rehab. Eng.* 27, 1483–1491. doi: 10.1109/TNSRE.2019.2922453

Lakens, D., and Caldwell, A. R. (2019). Simulation-based power-analysis for factorial anova designs. *PsyArXiv* doi: 10.31234/osf.io/baxsf

Marusic, U., Naric0i, M., Simunic, B., Pisot, R., and Ritzmann, R. (2021). Nonuniform loss of muscle strength and atrophy during bed rest: a systematic review. *J. Appl. Physiol.* 131, 194–206. doi: 10.1152/japplphysiol.00363.2020

Monti, E., Reggiani, C., Franchi, M. V., Toniolo, L., Sandri, M., Armani, A., et al. (2021). Neuromuscular junction instability and altered intracellular calcium handling as early determinants of force loss during unloading in humans. *J. Physiol.* 599, 3037–3061. doi: 10.1113/JP281365

Mulder, E. R., Gerrits, K. H. L., Kleine, B. U., Rittweger, J., Felsenberg, D., de Haan, A., et al. (2009). High-density surface EMG study on the time course of central nervous and peripheral neuromuscular changes during 8 weeks of bed rest with or without resistive vibration exercise. *J. Electromyogr. Kinesiol.* 19, 208–218. doi: 10.1016/j.jelekin.2007.04.002

Narici, M., and Cerretelli, P. (1998). Changes in human muscle architecture in disuse-atrophy evaluated by ultrasound imaging. *J. Grav. Physiol.* 5, 73–74.

Negro, F., Holobar, A., and Farina, D. (2009). Fluctuations in isometric muscle force can be described by one linear projection of low-frequency components of motor unit discharge rates. *J. Physiol.* 587, 5925–5938. doi: 10.1113/jphysiol.2009.178509

Pišot, R., Marušič, U., Biolo, G., Mazzucco, S., Lazzer, S., Grassi, B., et al. (2016). Greater loss in muscle mass and function but smaller metabolic alterations in older compared with younger men following 2 wk of bed rest and recovery. *J. Appl. Physiol.* 120, 922–929. doi: 10.1152/japplphysiol.00858.2015

Potočnik, B., Divjak, M., Urh, F., Frančič, A., Kranjec, J., Šavc, M., et al. (2020). Estimation of muscle co-activations in wrist rehabilitation after stroke is sensitive to motor unit distribution and action potential shapes. *IEEE Trans. Neural Syst. Rehab. Eng.* 28, 1208–1215. doi: 10.1109/TNSRE.2020.2980440

Rejc, E., Floreani, M., Taboga, P., Botter, A., Toniolo, L., Cancellara, L., et al. (2018). Loss of maximal explosive power of lower limbs after 2 weeks of disuse and incomplete recovery after retraining in older adults. *J. Physiol.* 596, 647–665. doi: 10.1113/JP274772

Šavc, M., Glaser, V., Kranjec, J., Cikajlo, I., Matjačič, Z., and Holobar, A. (2018). Comparison of convolutive kernel compensation and non-negative matrix factorization of surface electromyograms. *IEEE Trans. Neural Syst. Rehab. Eng.* 26, 1935–1944. doi: 10.1109/TNSRE.2018.2869426

Šavc, M., and Holobar, A. (2021). Non-Negative matrix factorization of simulated high density surface electromyograms reflects both muscle excitation and muscle shortening. *IEEE Access* 9, 70548–70555. doi: 10.1109/ACCESS.2021.3078644

Tanzarella, S., Muceli, S., Santello, M., and Farina, D. (2021). Synergistic Organization of neural inputs from spinal motor neurons to extrinsic and intrinsic hand muscles. *J. Neurosci.* 41, 6878–6891. doi: 10.1523/JNEUROSCI.0419-21.2021

Tresch, M. C., Cheung, V. C. K., and dAvella, A. (2006). Matrix factorization algorithms for the identification of muscle synergies: evaluation on simulated and experimental data sets. *J. Neurophysiol.* 95, 2199–2212. doi: 10.1152/jn.00222.2005

Vaillancourt, D. E., Larsson, L., and Newell, K. M. (2003). Effects of aging on force variability, single motor unit discharge patterns, and the structure of 10, 20, and 40 Hz EMG activity. *Neurobiol. Aging* 24, 25–35. doi: 10.1016/s0197-4580(02)00014-3

Vieira, T. M., and Botter, A. (2021). The accurate assessment of muscle excitation requires the detection of multiple surface electromyograms. *Exer. Sport Sci. Rev.* 49, 23–34. doi: 10.1249/JES.0000000000000240

Vieira, T. M., Botter, A., Minetto, M. A., and Hodson-Tole, E. F. (2015). Spatial variation of compound muscle action potentials across human gastrocnemius medialis. *J. Neurophysiol.* 114, 1617–1627. doi: 10.1152/jn.00221.2015

Vieira, T. M., Loram, I. D., Muceli, S., Merletti, R., and Farina, D. (2011). Postural activation of the human medial gastrocnemius muscle: are the muscle units spatially localised? *J. Physiol.* 589, 431–443. doi: 10.1113/jphysiol.2010.201806

Vieira, T. M., Wakeling, J. M., and HodsonTole, E. F. (2016). Is there sufficient evidence to claim muscle units are not localised and functionally grouped within the human gastrocnemius? *J. Physiol.* 594, 1953–1954. doi: 10.1113/JP271866

Vinti, M., Gracies, J. M., Gazzoni, M., and Vieira, T. (2018). Localised sampling of myoelectric activity may provide biased estimates of cocontraction for gastrocnemius though not for soleus and tibialis anterior muscles. *J. Electromyogr. Kinesiol.* 38, 34–43. doi: 10.1016/j.jelekin.2017.11.003

Watanabe, K., Holobar, A., Kouzaki, M., Ogawa, M., Akima, H., and Moritani, T. (2016). Age-related changes in motor unit firing pattern of vastus lateralis muscle during low-moderate contraction. *Age* 38, 1–14. doi: 10.1007/s11357-016-9915-0

Conflict of Interest: The authors declare that the research was conducted in the absence of any commercial or financial relationships that could be construed as a potential conflict of interest.

Publisher's Note: All claims expressed in this article are solely those of the authors and do not necessarily represent those of their affiliated organizations, or those of the publisher, the editors and the reviewers. Any product that may be evaluated in this article, or claim that may be made by its manufacturer, is not guaranteed or endorsed by the publisher.

frontiers in Physiology

ORIGINAL RESEARCH
published: 01 March 2022
doi: 10.3389/fphys.2022.792576

Altered Gastrocnemius Contractile Behavior in Former Achilles Tendon Rupture Patients During Walking

Benjamin Stäudle[1,2], Olivier Seynnes[3], Guido Laps[4], Gert-Peter Brüggemann[5] and Kirsten Albracht[1,2]*

[1] Faculty of Medical Engineering and Technomathematics, Aachen University of Applied Sciences, Aachen, Germany, [2] Institute of Movement and Neurosciences, German Sport University Cologne, Cologne, Germany, [3] Department of Physical Performance, Norwegian School of Sport Sciences, Oslo, Norway, [4] Orthopädie am Gürzenich, Cologne, Germany, [5] Institute of Biomechanics and Orthopedics, German Sport University Cologne, Cologne, Germany

Achilles tendon rupture (ATR) remains associated with functional limitations years after injury. Architectural remodeling of the gastrocnemius medialis (GM) muscle is typically observed in the affected leg and may compensate force deficits caused by a longer tendon. Yet patients seem to retain functional limitations during—low-force—walking gait. To explore the potential limits imposed by the remodeled GM muscle-tendon unit (MTU) on walking gait, we examined the contractile behavior of muscle fascicles during the stance phase. In a cross-sectional design, we studied nine former patients (males; age: 45 ± 9 years; height: 180 ± 7 cm; weight: 83 ± 6 kg) with a history of complete unilateral ATR, approximately 4 years post-surgery. Using ultrasonography, GM tendon morphology, muscle architecture at rest, and fascicular behavior were assessed during walking at 1.5 $m \cdot s^{-1}$ on a treadmill. Walking patterns were recorded with a motion capture system. The unaffected leg served as control. Lower limbs kinematics were largely similar between legs during walking. Typical features of ATR-related MTU remodeling were observed during the stance sub-phases corresponding to series elastic element (SEE) lengthening (energy storage) and SEE shortening (energy release), with shorter GM fascicles (36 and 36%, respectively) and greater pennation angles (8° and 12°, respectively). However, relative to the optimal fascicle length for force production, fascicles operated at comparable length in both legs. Similarly, when expressed relative to optimal fascicle length, fascicle contraction velocity was not different between sides, except at the time-point of peak series elastic element (SEE) length, where it was 39 ± 49% lower in the affected leg. Concomitantly, fascicles rotation during contraction was greater in the affected leg during the whole stance-phase, and architectural gear ratios (AGR) was larger during SEE lengthening. Under the present testing conditions, former ATR patients had recovered a relatively symmetrical walking gait pattern. Differences in seen AGR seem to accommodate the profound changes in MTU architecture, limiting the required fascicle shortening velocity. Overall, the contractile behavior of the GM fascicles does not restrict length- or velocity-dependent force potentials during this locomotor task.

Keywords: tendon rupture, muscle fascicle behavior, walking gait, force generation, ultrasound imaging

OPEN ACCESS

Edited by:
Christoph Centner, University of Freiburg, Germany

Reviewed by:
Fábio Juner Lanferdini, Federal University of Santa Catarina, Brazil
Martino V. Franchi, University of Padua, Italy
Markus Tilp, University of Graz, Austria
Jeam Marcel Geremia, Federal University of Rio Grande do Sul, Brazil

****Correspondence:***
Benjamin Stäudle
staeudle@fh-aachen.de

Specialty section:
This article was submitted to Exercise Physiology, a section of the journal Frontiers in Physiology

Received: *10 October 2021*
Accepted: *01 February 2022*
Published: *01 March 2022*

Citation:
Stäudle B, Seynnes O, Laps G, Brüggemann G-P and Albracht K (2022) Altered Gastrocnemius Contractile Behavior in Former Achilles Tendon Rupture Patients During Walking. Front. Physiol. 13:792576. doi: 10.3389/fphys.2022.792576

INTRODUCTION

Recovery from Achilles tendon rupture (ATR) is a tedious process that results in permanent functional deficits in the majority of patients (Nilsson-Helander et al., 2010; Heikkinen et al., 2017). Such deficits are characterized by a weakness in end-range plantarflexion (Mullaney et al., 2006) and limited heel raise height (Silbernagel et al., 2012), and are often reflected by deficiencies during locomotor tasks (Willy et al., 2017). Gait deficiencies appear to be commensurate with movement velocity (Willy et al., 2017; Jandacka et al., 2018) and may therefore be related to the force-velocity relation of the affected muscles. Nonetheless, slow movements, — which require lower force levels — seem also impaired in most (Tengman and Riad, 2013; Agres et al., 2015; Willy et al., 2017; Speedtsberg et al., 2019) but not all investigated cases (Jandacka et al., 2017). The links between such deficits and the remodeling of the muscle-tendon unit (MTU) following ATR are, to date, poorly understood.

Long after recovery and regardless of treatment strategy, the MTU of ATR patients is characterized by a longer tendon (Silbernagel et al., 2012; Peng et al., 2019; Svensson et al., 2019). Recent studies suggest that the increased tendon stiffness (Agres et al., 2015; Stäudle et al., 2021) and shorter gastrocnemius medialis (GM) muscle fascicles (Baxter et al., 2018; Peng et al., 2019; Svensson et al., 2019) typically seen in ATR patients may compensate for their longer tendons, albeit incompletely (Stäudle et al., 2021). Using a musculoskeletal model to simulate maximum isometric contractions at various joint angles, we have shown that the shorter GM fascicles in the affected leg enables sarcomeres to operate close to their optimal length, but at the expense of a narrowed range for active force generation (Stäudle et al., 2021). The insights gained from these findings are, however, insufficient for predicting triceps surae mechanics in dynamic situations, where force-velocity conditions may set additional constraints.

As sarcomeres operate close to their optimal length during walking (Ishikawa et al., 2007), length-dependent deficits in muscle strength are expected to be rather small in ATR patients due to corresponding shorter fascicle lengths throughout the walking stance phase. Whereas, when considering the force-velocity relation of a muscle, shorter fascicles are expected to produce less force than longer ones at the same velocity because of their lower number of in-series sarcomeres (Hill, 1953; Bahler et al., 1968). This point may be critical in the case of ATR patients during walking, because of their shorter GM fascicle length and because of the force-limiting role of contractile velocity in the walking gait (Neptune and Sasaki, 2005; Farris and Sawicki, 2012). As the behavior of the remodeled muscle fascicles of ATR patients during walking gait has not yet been investigated and its impact on force generation is unclear, the purpose of this study was to investigate the hypothesis of altered contractile behavior of the GM causing a velocity-based deficit during walking in ATR patients. We expected the shorter GM fascicles of the affected leg to operate at a comparable length range but at a higher contractile velocity, relative to their optimal length, than the fascicles of the unaffected leg. Using combined ultrasonography and motion capture methods, we measured GM muscle mechanics in former ATR patients (more than 2 years post-surgery) walking at 1.5 m s^{-1}.

Abbreviations: AGR, architectural gear ratio; ATR, Achilles tendon rupture; FT, fast twitch; ICC, intra-class correlation coefficient; GM, gastrocnemius medialis; MTU, muscle-tendon unit; SEE, series elastic element.

MATERIALS AND METHODS

Subjects

Male patients (20–60 years) were recruited for this study if they had suffered a complete ATR that had been treated surgically within 7 days after injury and were at least 2 years post-surgery. Subjects were excluded if they had a concomitant soleus muscle tear, sural nerve injury, or recurrent or bilateral ATR. The "Physical Activity Readiness Questionnaire" (Thomas et al., 1992) was used to exclude volunteers with cardiovascular or musculoskeletal disorders. The institutional review board of the German Sport University Cologne approved the study (approval number: 12/72), and all subjects provided written informed consent prior to voluntary participation.

This study is part of a comprehensive investigation on ATR patients' functional deficits. For this purpose, sample size calculations were based on ATR patients' strength deficits, as described previously (Stäudle et al., 2021). The *a priori* power analysis suggested a minimum sample size of 10 subjects.

Furthermore, GM tendon length, fascicle length, pennation angle and muscle thickness with a resting muscle had already been included in the previous study (Stäudle et al., 2021).

Study Design and Experimental Protocol

A cross-sectional design was used for this study. Data acquisition took place according to a pseudo randomized order between the affected and unaffected leg, while the unaffected leg served as control for matched comparison. During the first of two testing sessions (**Figure 1**), GM tendon length, fascicle length, pennation angle and muscle thickness were examined using ultrasonography with the subjects lying prone, with a resting muscle and ankle and knee joint angles in anatomical position (0°), as described previously (Stäudle et al., 2021). During the second session, subjects were familiarized to the treadmill by walking for about 5 min at 1.5 m·s^{-1} (h/p cosmos pulsar 4.0, 2.2 kW, Traunstein, Germany) using their own running shoes. Kinematic and ultrasonographic data were thereafter collected from each leg during six consecutive stance phases.

Motion Capture of the Legs

A motion capture system (eight infrared cameras) sampling at 100 Hz (Vicon, Vicon Motion Systems Ltd., Oxford, United Kingdom) was used to capture knee and ankle joint kinematics. Anatomical landmarks were labeled *via* reflective markers representing the subjects' greater trochanter, lateral femur condyle, lateral malleolus, calcaneus, and second metatarsal head. A static reference was captured with the ankle

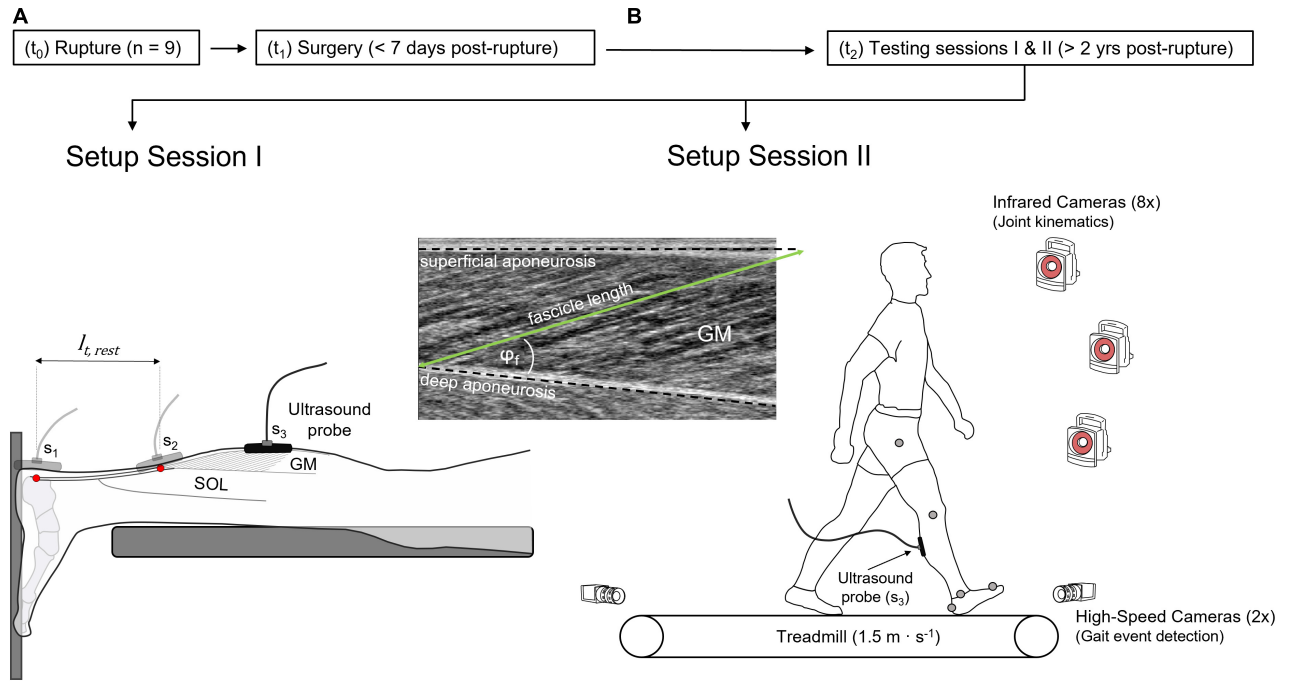

FIGURE 1 | Experimental design. **(A)** Setup to determine gastrocnemius medialis (GM) tendon length and muscle architecture, showing the scanning location S_1 and S_2 of the ultrasound probe, visualizing the calcaneal insertion and the myotendinous junction of the GM tendon (red dots), respectively, defining GM tendon resting length ($l_{t,rest}$). Scanning location 3 (S_3, GM mid-belly) visualizes GM muscle architecture in resting muscle **(A)** and during walking trials **(B)**, detailed by the ultrasound image. The treadmill setup **(B)** includes the motion capture system and the high-speed cameras. t_0: time-point of rupture, t_1: time-point of surgery, t_2: time-point of measurements, φ_f: pennation angle.

and knee joints in anatomical position to define 0°. For gait event detection (touch-down, toe-off), two additional high-speed cameras (Basler, 100 Hz, Ahrensburg, Germany) were positioned anteriorly and posteriorly to the treadmill belt.

Measurements of Muscle Fascicle Behavior

During walking, B-mode ultrasound (Prosound α7, ALOKA, Tokyo, Japan) image sequences (73 Hz) were recorded using a t-shaped 6 cm linear array transducer (UST-5713T, 13 MHz) fixed in a custom-made cast to the mid-belly of the GM muscle *via* self-adhesive bandages. For time-synchronization, a rectangular voltage pulse was generated and sent to all data capturing devices.

Ultrasonography is a frequently used method to quantify muscle architecture under dynamic conditions (Cronin and Lichtwark, 2013) and shows good reliability within session for fascicle length and pennation angle in the present dataset (intraclass correlation coefficient: 0.99). In previous studies using similar methods, our group measured good inter-rater reliability with an intraclass correlation coefficient of 0.97 for pennation angle (Pohle-Fröhlich et al., 2020) and good reliability between days represented by a coefficient of multiple correlation of 0.93 for fascicle length and 0.87 for pennation angle (Aggeloussis et al., 2010).

A semi-automatic tracking algorithm (UltraTrack Software, version 4.2) was used to quantify GM muscle architecture. A dominant fascicle was drawn over a visible fascicle fragment and tracked across all frames. Additionally, superficial and deep aponeuroses were segmented and tracked. Fascicle length was defined as the distance between the insertions of the fascicles on the superficial and deep aponeuroses (Farris et al., 2016; Farris and Lichtwark, 2016).

In the rare exception where the transducer's 6 cm width field of view failed to display the entire tracked fascicle (**Figure 1**), the missing portion was manually extrapolated, assuming that the fascicles and aponeurosis extend linearly. Linear extrapolation is associated with an error of less than 6% during maximal contractions of the GM muscle (Muramatsu et al., 2002). The pennation angle was defined as the angle between the muscle fascicle and the deep aponeurosis. Changes in series elastic element (SEE) length were estimated by subtracting muscle shortening amplitude from changes in MTU length. To this end, muscle shortening patterns were obtained from the length of the geometric projection of fascicles onto the axis of the deeper aponeurosis (Fukunaga et al., 2001). The length of the GM MTU was determined *via* a multiple linear regression equation using normative data based on joint angles and shank length (Hawkins and Hull, 1990).

Data Processing

A custom-made script (MATLAB R2020b, The MathWorks, Inc., Natick, MA, United States) was used to analyze the data. Fascicle length and pennation angle were smoothed with a 5th order

Butterworth lowpass filter at a 10 Hz cut-off frequency. Data were then time-normalized by being resampled to 101 data points and then averaged per stance. Muscle fascicle velocities were calculated as the time derivative of the respective lengths using the central difference method (Robertson et al., 2013). Marker trajectories of the kinematic measurement were smoothed with a Woltring filter (Generalized Cross Validation, smoothing: 10) (Vicon Nexus 2.2.2, Vicon Motion Systems Ltd., Oxford, United Kingdom).

All outcome parameters were obtained at the time-point of peak SEE length and calculated as average values during stance sub-phases of SEE lengthening and shortening. SEE lengthening was defined as the duration between initial ground contact and peak SEE length, the latter presumably indicating maximal SEE loading. SEE shortening was defined as the remaining duration to toe-off.

Kinematic parameters were also examined at additional time-points, to obtain an exhaustive characterization of potential changes in gait pattern. Thus, ankle and knee joint angles were analyzed at touch-down and toe-off, peak ankle joint dorsiflexion, and the first knee joint flexion angle local maximum. The range of motion of each joint was defined as the difference between the angles' minima and maxima.

Variables that characterize fascicle behavior were also studied, including operating fascicle length, fascicle velocity, and pennation angle. In addition, fascicle and muscle shortening amplitudes, changes in pennation angle and architectural gear ratio (AGR) were analyzed for each of the two sub-phases. A modified version of the AGR (Brainerd and Azizi, 2005) was calculated as the ratio between muscle shortening amplitude along the axis of the deeper aponeurosis [calculated as the product of fascicle length by the cosine of the pennation angle (Fukunaga et al., 2001)] and fascicle shortening amplitude during the SEE sub-phases of walking (Werkhausen et al., 2019).

In addition to absolute values, the average operating fascicle length was expressed relative to optimal fascicle length and termed normalized operating fascicle length. Average fascicle velocity was expressed relative to the velocity of one optimal fascicle length per second and termed normalized fascicle velocity. Optimal fascicle length was estimated from resting fascicle length and normative data of sarcomere length using the following equation:

$$l_{f,o} = \frac{l_{f,rest}}{l_{s,rest}} \cdot l_{s,o}, \tag{1}$$

where $l_{f,rest}$ is the fascicle length in resting condition (anatomically neutral position of the knee and ankle joint, 0°), $l_{s,rest}$ the sarcomere length at the identical joint angles reported by Sanchez et al. (2015) (3.09 μm), and $l_{s,o}$ the optimal sarcomere length of 2.725 μm defined by the mean value of the plateau region of the human sarcomere force-length relation (2.64–2.81 μm) (Herzog et al., 1990; Ward et al., 2009).

To illustrate the fraction of maximal GM force produced during walking, force potentials were estimated relative to operating length (length-dependent force potential) or velocity (velocity-dependent force potential). The length-dependent force potential was obtained using the default active-force-length curve of OpenSim based on quintic Bezier splines (Millard et al., 2013; Seth et al., 2018). As outlined in the OpenSim API guide (Millard, 2021), default parameters were chosen that the curve approximated the theoretical active-force-length curve of human sarcomeres (Nigg and Herzog, 1994) with the descending limb adapted from *in vitro* human fiber data (Gollapudi and Lin, 2009).

A dimensionless velocity-dependent force potential was obtained using the Hill-equation (Hill, 1938) for concentric contractions, relative values of force, velocity, and Hill's constant *a* (Zajac, 1989) as follows:

$$f_v\left(v'_f\right) = \frac{\left(1 - \frac{v'_f}{v'_{max}}\right)}{1 + \left(\frac{v'_f}{v'_{max}}\right) \cdot \frac{1}{a_{rel}}}, \text{with } v'_{max} = v_{max} \cdot \left(l_{f,o} \cdot s^{-1}\right)^{-1}. \tag{2}$$

v_{max} is the GM muscle's maximum shortening velocity, estimated as multiples of optimal fascicle length per second and considering the GM fraction of fast twitch fibers (Winters and Stark, 1988) as follows:

$$v_{max} = (2 + 8 \cdot FT) \cdot \left(l_{f,o} \cdot s^{-1}\right), \tag{3}$$

where the fraction of fast twitch (FT) fibers for the GM muscle was assumed to be 49.2% (Johnson et al., 1973). The normalized Hill constant a_{rel} was calculated from 0.1 + 0.4FT (Winters and Stark, 1988; Bohm et al., 2019), yielding 0.297.

Statistical Analysis

Two tailed paired *t*-tests or Wilcoxon signed-rank tests were used to identify differences between the legs using Prism (version 7.04, GraphPad Software, Inc., San Diego, CA, United States). Prior to these tests, data were checked for normal distribution (Shapiro–Wilk normality test). Values are reported as means ± standard deviations (M ± SD) and the level of statistical significance was set to $\alpha \leq 0.05$. A statistical software package [G*Power version 3.1.9.6 (Faul et al., 2007)] was used to calculate absolute effect sizes, which were defined as small (0.2), moderate (0.5), or large (0.8), as appropriate (Cohen, 1988). An equivalent to effect sizes for signed rank tests was obtained by dividing the sum of the signed ranks by the total rank sum (matched pairs rank-biserial correlation) (Cureton, 1956; Kerby, 2014).

RESULTS

Out of 59 former ATR patients who responded to advertisements at a medical center ($n = 45$) or in media announcements ($n = 14$), 14 were recruited for this study. Of the remainder, 23 patients did not meet inclusion criteria, eight had moved, and 14 declined to participate. Nine of the 14 recruited subjects performed all tests and were included in the present data. The data from the five remaining subjects could not be obtained because of incomplete ultrasound scans ($n = 2$) or schedule conflicts ($n = 3$).

The subjects (age: 44.7 ± 9.1 years; height: 180 ± 7 cm; weight: 82.8 ± 5.9 kg) had been operated with either a modified Bunnel, a Kessler end-to-end or a Dresdner Instrument (minimal invasive) 3.4 ± 1.8 days after rupture and, 4.4 ± 2.1 years prior to the study, on average. Structural differences in muscles and tendons were observed in the affected legs, with shorter GM muscle fascicles [30.8 ± 10.8%, $t(8) = 7.28$, $p < 0.001$, $d_z = 2.42$], greater pennation angles [5 ± 3°, $t(8) = 5.08$, $p = 0.001$, $d_z = 1.69$], reduced muscle thickness [9.8 ± 12.4%, $t(8) = 2.40$, $p = 0.043$, $d_z = 0.80$], and longer GM tendons [13.9 ± 11.7%, $t(8) = 3.73$, $p = 0.006$, $d_z = 1.25$] (**Supplementary Table 1**).

Kinematics

Figure 2 represents the knee and ankle joint angles and their corresponding angular velocities during stance. Except for a less plantarflexed averaged ankle joint angle during SEE shortening [3 ± 4°, $t(8) = 2.34$, $p = 0.048$, $d_z = 0.78$] and a slower ankle angular velocity at peak SEE length [21.5 ± 25.2%, $t(8) = 2.41$, $p = 0.043$, $d_z = 0.80$], the analyzed kinematic or spatio-temporal parameters did not show any significant differences (**Figure 2**, **Table 1**, and **Supplementary Table 2**). On average, the step frequency was 119 ± 5 steps·min^{-1}.

Gastrocnemius Medialis Muscle Fascicle Length and Pennation Angle During Walking

The timing of maximum SEE elongation was used to separate the stance phase into SEE lengthening and shortening sub-phases. This time-point did not differ between the affected and unaffected leg [80.9 ± 2.2% vs. 82.3 ± 1.1%, $t(8) = 1.76$, $p = 0.116$, $d_z = 0.59$].

During SEE lengthening and shortening sub-phases, the average operating fascicle length was shorter in the affected leg (36.2 ± 8.5% and 36.3 ± 10.0%, respectively), which was consistent with a shorter operating fascicle length at peak SEE length in the same leg (36.2 ± 10.6%) (**Table 2** and **Figure 3A**). Shortening amplitudes did not differ significantly during the lengthening sub-phase, whereas smaller shortening amplitudes were observed during the shortening sub-phase in the affected leg (26.0 ± 32.2%) (**Table 3**). However, after normalization to optimal length, the average operating fascicle length did not differ

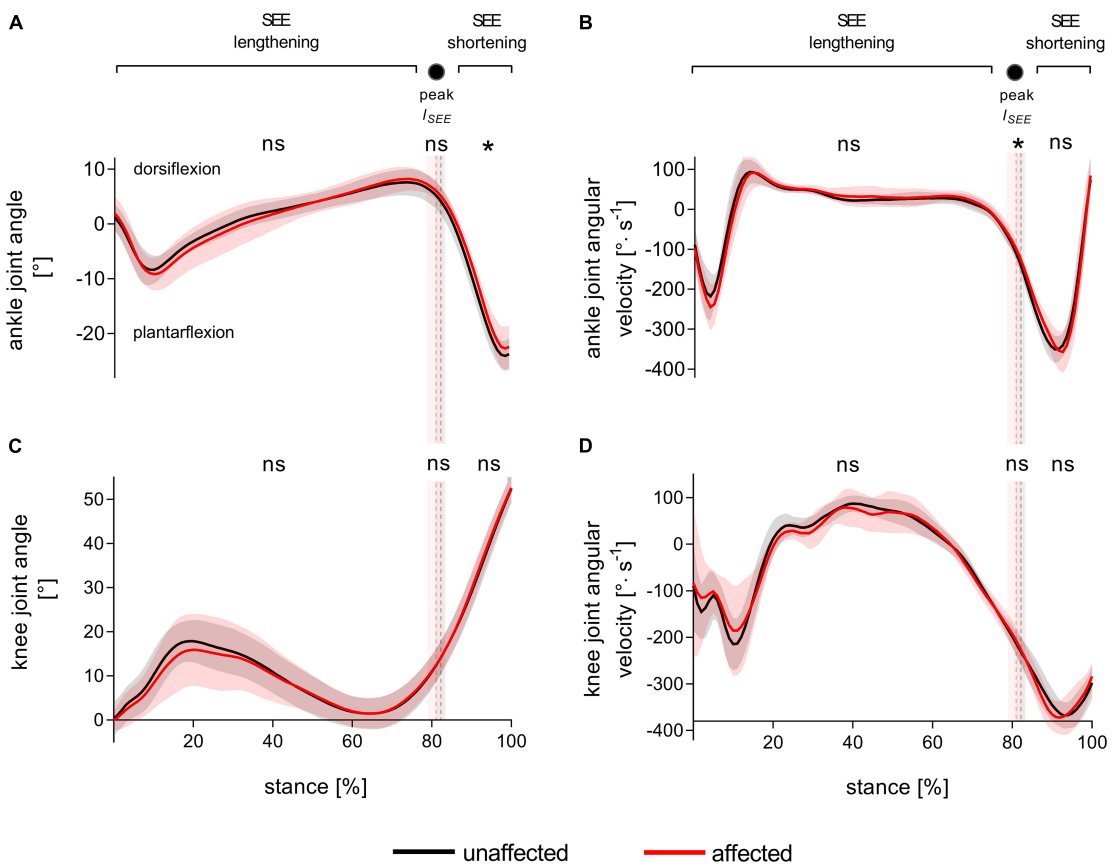

FIGURE 2 | Ankle **(A)** and knee **(C)** joint angles and corresponding angular velocities **(B,D)** during walking stance. The solid black and red lines, with their corresponding shaded areas [standard deviation (SD)], represent mean traces for the unaffected and affected leg, respectively. The dashed vertical lines with their corresponding shaded areas (SD) represent the mean time points of peak series elastic element (SEE) length (peak l_{SEE}) separating the SEE lengthening and shortening sub-phases. Statistical testing was run on average values during the SEE lengthening and shortening sub-phases, and on single data points at peak SEE length. *$p < 0.05$, significant side-to-side difference, ns: non-significant.

TABLE 1 | Leg kinematics and spatio-temporal parameters during walking stance.

Parameters		Affected		Unaffected		Diff		95% CI	Test statistic	*P*	Cohen's d_z
		M	SD	*M*	SD	*M*	SD				
Ankle joint	Range of motion (°)	32 (8)^w		32 (6)^w		0 (3)^w		–	*W* = −9 (18, −27)	0.652	*r* = 0.20^w
	Touch-down angle (°)	2 (4)^w		2 (4)^w		0 (5)^w		–	*W* = 3 (24, −21)	0.910	*r* = 0.07^w
	Toe off angle (°)	−22	4	−24	3	1	3	−1 to 4	*t*(8) = 1.22	0.256	0.41
	Max.-dorsiflexion (°)	8	2	8	2	1	3	−1 to 3	*t*(8) = 0.70	0.504	0.23
Knee joint	Range of motion (°)	54	6	54	7	0	5	−4 to 3	*t*(8) = 0.11	0.917	0.04
	Touch-down angle (°)	0	2	0	4	0	3	−3 to 2	*t*(8) = 0.36	0.732	0.12
	Toe-off angle (°)	53	3	52	3	0	3	−2 to 3	*t*(8) = 0.19	0.854	0.06
	Flexion (1st peak) (°)	16 (9)^w		18 (8)^w		0 (8)^w		-	*W* = −9 (18, −27)	0.652	*r* = 0.20^w
Stance duration	(s)	0.66	0.03	0.65	0.04	0.00	0.05	−0.03 to 0.04	*t*(8) = 0.14	0.890	0.05
Step length	(cm)	53.0 (6.0)^w		52.0 (4.0)^w		0 (1.5)^w		–	*W* = 11 (13, −2)	0.250	*r* = 0.73^w

M, mean; SD, standard deviation; CI, confidence interval; ^{w}, Wilcoxon signed rank test applied and values are expressed as median (interquartile range); W, sum of signed ranks (sum of positive, sum of negative ranks); r, matched pairs rank-biserial correlation.

TABLE 2 | Architectural parameters of the gastrocnemius medialis muscle during walking stance.

Parameters	Stance sub-phase or time-point	Affected		Unaffected		Diff		95% CI	Test statistic	*P*	Cohen's d_z
		M	SD	M	SD	M	SD				
l_f (mm)	SEE lengthening	33.3	6.6	52.2	7.7	−18.8	5.1	−22.7 to −14.9	*t*(8) = 11.10	< 0.001	3.71
	peak l_{SEE}	30.0	6.6	47.0	7.5	−17.0	5.5	−21.2 to −12.7	*t*(8) = 9.27	< 0.001	3.10
	SEE shortening	27.4	5.9	43.0	7.3	−15.6	5.2	−19.6 to −11.6	*t*(8) = 8.93	< 0.001	2.98
v_f (mm·s^{-1})	SEE lengthening	−16.3	4.9	−19.6	2.5	3.3	5.6	−1 to 7.6	*t*(8) = 1.79	0.112	0.59
	peak l_{SEE}	−22.4	17.3	−54.2	26.7	31.9	25.4	12.3 to 51.4	*t*(8) = 3.76	0.006	1.26
	SEE shortening	−44.2	18.4	−69.0	23.2	24.8	21.7	8.2 to 41.5	*t*(8) = 3.44	0.009	1.14
φ_f (°)	SEE lengthening	32	4	24	3	8	3	6 to 11	*t*(8) = 7.55	< 0.001	2.51
	peak l_{SEE}	37	5	27	5	10	4	7 to 13	*t*(8) = 6.67	< 0.001	2.22
	SEE shortening	40	6	27	5	12	4	9 to 16	*t*(8) = 8.56	< 0.001	2.84
$\tilde{l}_f$ ($l_{f,o}$)	SEE lengthening	0.88	0.09	0.95	0.12	−0.07	0.11	−0.15 to 0.01	*t*(8) = 2.10	0.069	0.70
	peak l_{SEE}	0.79	0.10	0.86	0.11	−0.07	0.10	−0.15 to 0.01	*t*(8) = 1.99	0.081	0.67
	SEE shortening	0.72	0.09	0.79	0.11	−0.06	0.10	−0.14 to 0.01	*t*(8) = 1.95	0.087	0.65
$\tilde{v}_f$ ($l_{f,o} \cdot s^{-1}$)	SEE lengthening	0.44	0.15	0.36	0.06	0.08	0.15	−0.04 to 0.20	*t*(8) = 1.59	0.150	0.53
	peak l_{SEE}	0.58	0.43	0.98	0.44	−0.39	0.49	−0.77 to −0.01	*t*(8) = 2.38	0.045	0.79
	SEE shortening	1.15	0.42	1.28	0.47	−0.13	0.40	−0.44 to 0.17	*t*(8) = 1.01	0.344	0.34
$f_l(\tilde{l}_f)$	SEE lengthening	0.93	0.06	0.96	0.07	−0.03	0.08	−0.09 to 0.03	*t*(8) = 1.03	0.332	0.34
	peak l_{SEE}	0.85	0.11	0.90	0.15	−0.05	0.11	−0.13 to 0.03	*t*(8) = 1.41	0.195	0.47
	SEE shortening	0.75	0.14	0.82	0.21	−0.07	0.16	−0.19 to 0.05	*t*(8) = 1.31	0.228	0.44
$f_v(\tilde{v}_f)$	SEE lengthening	0.74	0.07	0.78	0.03	−0.04	0.07	−0.09 to 0.02	*t*(8) = 1.50	0.173	0.50
	peak l_{SEE}	0.70	0.17	0.56	0.13	0.15	0.18	0.01 to 0.28	*t*(8) = 2.52	0.036	0.84
	SEE shortening	0.50	0.12	0.47	0.12	0.03	0.12	−0.06 to 0.13	*t*(8) = 0.81	0.439	0.27

M, mean; SD, standard deviation; CI, confidence interval; SEE, series elastic element; peak l_{SEE}, time-point of peak SEE length; l_f, operating fascicle length; v_f, fascicle velocity; φ_f, pennation angle; $\tilde{l}_f$, normalized operating fascicle length; $\tilde{v}_f$, normalized fascicle velocity; $f_l(\tilde{l}_f)$, length-dependent force potential; $f_v(\tilde{v}_f)$, velocity-dependent force potential.

between legs in either of the stance sub-phases or peak SEE length (**Table 2** and **Figure 4A**), nor did the average length-dependent force potential (**Table 2** and **Figure 5A**).

Average fascicle velocity did not differ between legs during the lengthening sub-phase, but differences were present during the SEE shortening phase (31.6 ± 28.3% lower in the affected leg, **Table 2** and **Figure 3C**). To the time-point of peak SEE length, fascicle velocity was lower (56.5 ± 28.0%) (**Table 2** and **Figure 3C**). No side-to-side differences were detected when velocities were expressed relative to optimal length in either sub-phase (**Table 2** and **Figure 4B**), but being lower in the effected leg to the time-point of peak SEE length (39.2 ± 49.4%) (**Table 2** and **Figure 4B**).

Likewise, the velocity-dependent force potential did not differ between legs during either sub-phase, while a greater velocity-dependent force potential was observed for the affected leg at the

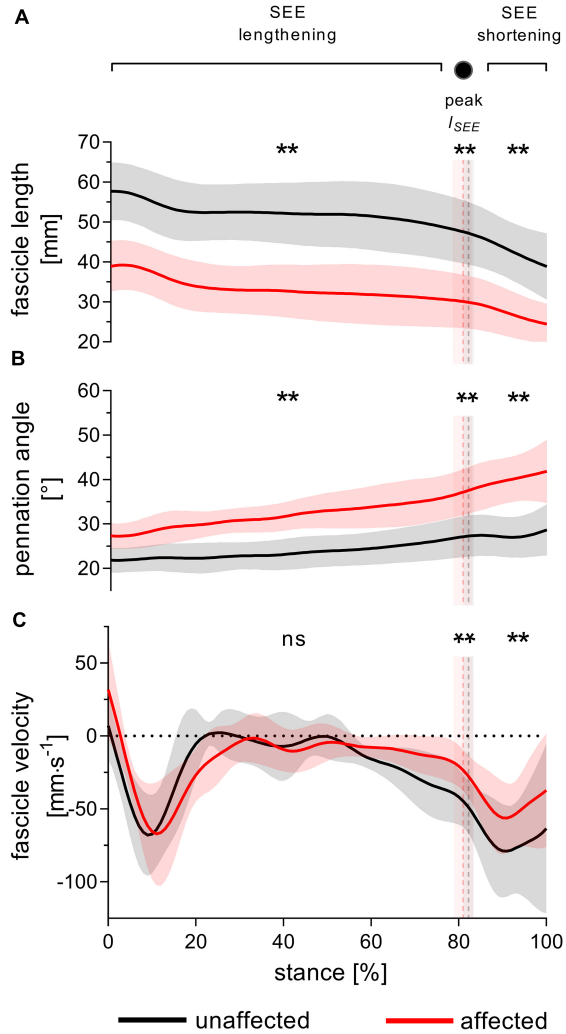

FIGURE 3 | Gastrocnemius medialis operating fascicle length **(A)**, pennation angle **(B)** and fascicle velocity **(C)** during walking stance. The solid black and red lines, with their corresponding shaded areas [standard deviation (SD)], represent mean traces for the unaffected and affected leg, respectively. The dashed vertical lines with their corresponding shaded areas (SD) represent the mean time points of peak series elastic element (SEE) length (peak l_{SEE}) separating the SEE lengthening and shortening sub-phases. Statistical testing was run on average values during SEE lengthening and shortening sub-phases, and on single data points at peak SEE length. $^{**}p < 0.01$, significant side-to-side difference; ns: non-significant.

discrete time-point of peak SEE length (14.8 ± 17.7%) (**Table 2** and **Figure 5B**).

The average pennation angle was greater in the affected leg during SEE lengthening and shortening (8 ± 3° and 12 ± 4°, respectively), which was consistent with a greater pennation angle at peak SEE length time-point in the same leg (10 ± 4°) (**Table 2** and **Figure 3B**). Greater changes in pennation angle were also found in the affected leg during SEE lengthening (4 ± 4°) and shortening (3 ± 3°) sub-phases (**Table 3**). Representative ultrasound images of the affected and unaffected GM at different time-points during ground contact are presented in the **Supplementary Figure 1**.

Muscle shortening amplitude did not differ between the legs in either sub-phase, while the AGR was greater in the affected leg during the SEE lengthening (8.7 ± 4.9%), but not during the SEE shortening sub-phase (**Table 3**).

DISCUSSION

This study aimed to understand how the behavior of the MTU is altered in former ATR patients during walking, to accommodate the longer Achilles tendon and shorter GM fascicles caused by the injury. Despite the drastic changes in the MTU architecture of the affected leg, gross walking parameters were not found to be dissimilar between the legs. The GM fascicle behavior was different between the affected and unaffected legs, however, unfavorable contractile conditions for force production during stance were not observed. Relative to their shorter length, the operating length of the affected fascicles was preserved, and the shortening velocity did not differ or was actually lower than in the healthy leg at the time of peak force production (as estimated from the timing of peak SEE length). These results indicate that under the tested walking conditions, the MTU recovery in former ATR patients may be sufficient to enable symmetrical walking gait. In addition, they suggest that long after recovery, GM fascicle behavior does not limit force generation potential and that remaining functional deficits during walking are attributable to other factors.

Leg Kinematics During Walking

The similar ankle and knee joint kinematics between the affected and unaffected legs indicate that the ATR patients had recovered a symmetrical gait pattern during treadmill walking. Two exceptions were found with a less plantarflexed average ankle joint angle during the push-off sub-phase and a lower angular velocity of that joint in the affected leg at the instant of peak SEE length. Since no side-to-side difference in angular excursion was detected during SEE shortening, the functional significance of a more dorsiflexed angle during the push-off of the affected leg is elusive. These differences may be congruent with several, but not all (Jandacka et al., 2018), reports documenting small kinematic differences in patients with similar characteristics. Several authors investigating leg kinematics during overground walking found greater dorsiflexion angles in the affected leg than in the unaffected leg at touch-down (∼1°) (Tengman and Riad, 2013; Speedtsberg et al., 2019), at toe-off (∼4°) (Willy et al., 2017), and at peak joint flexion (∼1–4°) (Don et al., 2007; Tengman and Riad, 2013; Agres et al., 2015; Speedtsberg et al., 2019). Such alterations in ankle joint kinematics, particularly greater dorsiflexion angles, could be related to the lengthened tendon caused by ATR (Agres et al., 2015). For this reason, side-to-side differences in joint kinematics may be proportional to the degree of MTU remodeling—and slackness reduction—characterizing individual recovery. Of note, the contrasting experimental modalities (walking on a treadmill or overground) between studies may have set slight differences in gait requirements,

TABLE 3 | Changes in muscle architecture of the gastrocnemius medialis muscle during the series elastic element (SEE) lengthening and shortening sub-phases.

Parameters	Stance sub-phase	Affected		Unaffected		Diff		95% CI	Test statistic	*P*	Cohen's d_z
		M	SD	M	SD	M	SD				
Δl_f (mm)	SEE lengthening	8.9	2.7	10.7	1.3	−1.8	2.8	−4 to 0.4	$t(8) = 1.93$	0.090	0.64
	SEE shortening	5.6	2.0	8.1	2.2	−2.5	2.8	−4.7 to −0.4	$t(8) = 2.68$	0.028	0.89
$\Delta\varphi_f$ (°)	SEE lengthening	10	4	5	2	4	4	2 to 7	$t(8) = 3.74$	0.006	1.24
	SEE shortening	5	3	1	2	3	3	1 to 6	$t(8) = 3.19$	0.013	1.06
Δl_m (mm)	SEE lengthening	10.5	2.9	11.8	1.7	−1.3	3.3	−3.83 to 1.3	$t(8) = 1.14$	0.289	0.38
	SEE shortening	5.7	1.7	7.6	2.0	−1.9	2.7	−3.9 to 0.2	$t(8) = 2.12$	0.067	0.71
AGR	SEE lengthening	1.19	0.05	1.09	0.04	0.09	0.05	0.06 to 0.14	$t(8) = 5.50$	< 0.001	1.83
	SEE shortening	1.08	0.23	0.93	0.07	0.15	0.22	−0.02 to 0.32	$t(8) = 1.96$	0.085	0.66

M, mean; SD, standard deviation; CI, confidence interval; Δl_f, fascicle shortening amplitude; $\Delta\varphi_f$, change in pennation angle; Δl_m, muscle shortening amplitude (geometric fascicle projection); AGR, architectural gear ratio; AGR was calculated as the ratio between the muscle shortening amplitudes and fascicle shortening amplitudes.

arguably less challenging in the present study. Walking on a treadmill seems indeed to reduce ground reaction forces compared to walking overground (Riley et al., 2007; Parvataneni et al., 2009), which may have lowered the GM force requirements for our patients. Regardless, the present results suggest that the remaining side-to-side differences in kinematics are small and that the gross walking pattern is relatively symmetrical. They also suggest that any difference in fascicle behavior is likely not related to dissimilarities in joint configuration.

The Gastrocnemius Medialis Fascicle Behavior Does Not Seem to Limit Force Production During Walking Stance

In support of our hypothesis, the operating GM fascicle length of the affected leg did not seem to limit potential force production. If fascicle length normalized to optimal length reflects sarcomere length, the sarcomeres of the affected leg appeared to work in a region of their force-length relation similar to that in the unaffected leg. These observations reinforce the notion that fascicle remodeling in ATR patients is achieved *via* a reduction in sarcomeres in series, as previously shown in animal studies on muscles immobilized at short lengths (Williams and Goldspink, 1973).

Unlike their operating length, we expected the fascicles of the affected leg to operate in an unfavorable region of their force-velocity relationship, explaining some of the functional limitations previously observed during walking. In fact, our data demonstrate that for most of the stance phase, fascicles do not operate at different normalized velocities between the legs. Conversely, affected fascicles operate in a more favorable region of their force-velocity relationship at peak SEE length, which is supported by a 15 ± 18% higher velocity-dependent force potential.

The observation of a slower contractile velocity also seems consistent with the slower ankle joint angular velocity at the time of peak SEE length. Such a reduction was likely not caused by an altered amount of fascicle shortening, since we did not find any difference in this parameter during the lengthening sub-phase. Therefore, it is difficult to elucidate the mechanisms responsible for the unchanged or reduced velocity from the present data.

One architectural factor may explain how the shorter fascicles of the affected leg could avoid contracting at a higher velocity than in the healthy leg: their rotation about their insertion point (i.e., change in pennation angle). This parameter being larger (4 ± 4°) in the affected leg may have limited the required fascicle contraction amplitude for a given muscle shortening, thereby providing a greater AGR. The present data support this interpretation, with a 9 ± 5% greater AGR in the affected leg during SEE lengthening. Thus, the contribution of the fascicle rotation to total muscle shortening during the SEE lengthening sub-phase accounted 16 ± 4% (1.6 ± 0.4 mm) on the affected leg and just 9 ± 4% (1.0 ± 0.5 mm) in the unaffected leg.

Variable AGR in general provides a mechanism to modulate performance during mechanically diverse functions (Azizi et al., 2008). The greater pennation angle after MTU remodeling of ATR patients may also promote fascicle rotation (Brainerd and Azizi, 2005), supporting architectural gearing. Architectural gearing may, therefore, constitute another adaptive mechanism in ATR patients, allowing maintaining the required muscle shortening velocity with a reduced fascicle velocity.

In the same line of thought, the altered mechanical properties of the GM tendon observed in ATR patients (Agres et al., 2015; Geremia et al., 2015; Stäudle et al., 2021) may also affect the contractile behavior of the muscle fascicles, *via* the effect of in series compliance on fascicle operating length and contraction velocity. We hypothesize that an increased stiffness counteracts the larger strain expected in the longer tendons of the affected side. This trade-off may thus limit the shortening of muscle fibers, while more compliant tendons would promote the opposite behavior. Since fascicular velocity was maintained or decreased on the affected side despite longer tendons, tendon stiffness was likely higher in the present patients, which could represent another adaptive mechanism in ATR patients to maintain function.

Functional Implications

The present findings indicate that affected GM sarcomeres still operate within a favorable length range and at favorable velocities for force production during treadmill walking. This is particularly interesting, as, contrary to our hypothesis, fascicle behavior does not appear to explain the functional limitations observed in ATR patients during walking (Tengman and Riad, 2013; Willy et al., 2017; Speedtsberg et al., 2019).

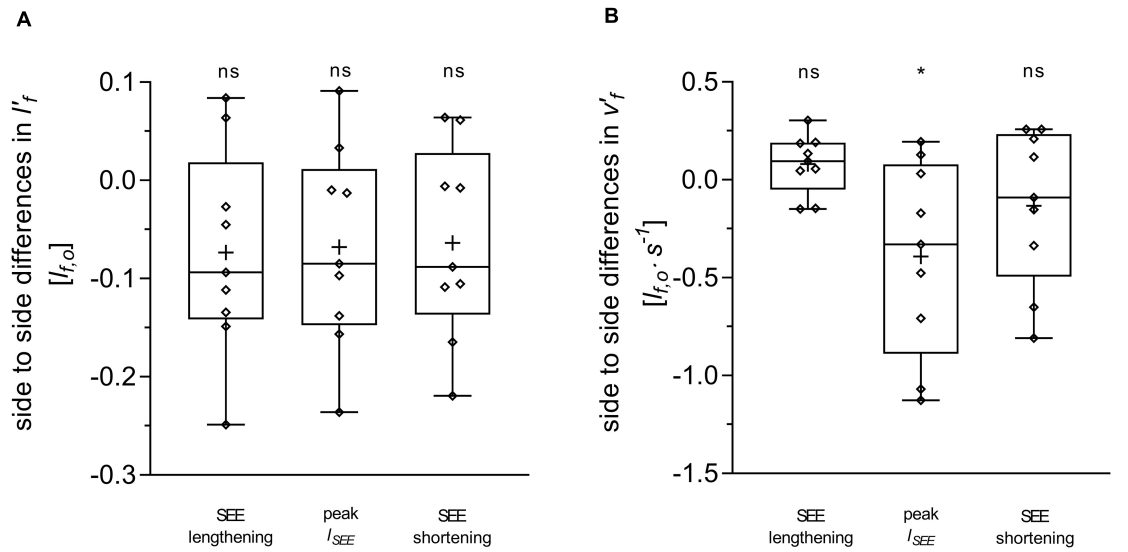

FIGURE 4 | Differences between the affected and unaffected legs in gastrocnemius medialis normalized fascicle length (l'_f) **(A)** and normalized fascicle velocity (v'_f) **(B)**. Statistical testing was run on average values during the series elastic element (SEE) lengthening and shortening sub-phases, and on single data points at peak SEE length (l_{SEE}). The lower and upper parts of the box plots represent the first and third quartile, respectively. The length of the whisker delineates the minimum and maximum values. The horizontal line in the box represents the median of the sample; +, sample mean; *$p < 0.05$, significant side-to-side difference; ns: non-significant.

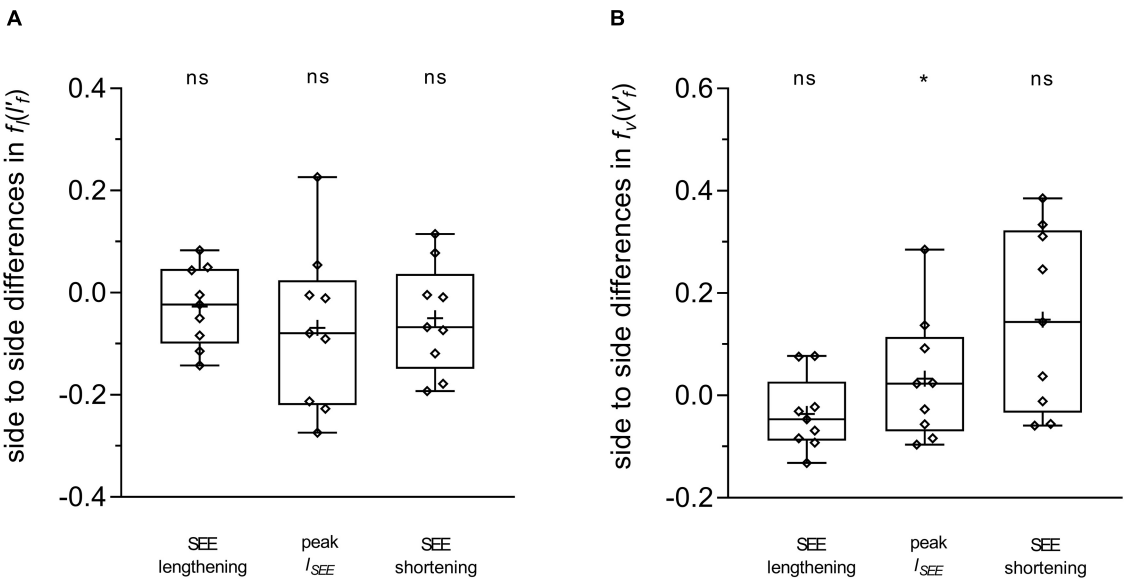

FIGURE 5 | Differences between the affected and unaffected legs in gastrocnemius medialis length-dependent [$f_l(l'_f)$] **(A)** and velocity-dependent [$f_v(v'_f)$] **(B)** force potential. Statistical testing was run on average values during the series elastic element (SEE) lengthening and shortening sub-phases, and on single data points at peak SEE length (l_{SEE}). The lower and upper parts of the box plots represent the first and third quartile, respectively. The length of the whisker delineates the minimum and maximum values. The horizontal line in the box represents the median of the sample; +, sample mean; *$p < 0.05$, significant side-to-side difference; ns: non-significant.

However, the question remains whether ATR patients can fully regain the plantar flexion force required for walking. Substantial atrophy (Heikkinen et al., 2017), as shown here by a 10 ± 12% reduction in GM thickness, is usually measured in the transversal plane of the affected fascicles, reflecting a reduced capacity for maximal force production compared to the unaffected leg. In the present experiment, the remodeled—smaller—GM muscle may have produced marginally less force during most of the stance phase. However, we contend that the force requirements of our walking experimental conditions were sufficiently low and met

by compensatory mechanisms without substantially affecting gait symmetry. Although this study was not designed to investigate such mechanisms, an increase in muscle activation such as that previously reported (Wenning et al., 2021) likely occurred here.

It follows that locomotor deficits may be force- and gait-dependent in ATR patients. This hypothesis is consistent with the data of Jandacka et al. (2018), who did not find functional deficit in ATR patients during overground walking, but observed such deficits in the affected leg during running. Future studies should systematically investigate the effects of gait velocity and ground reaction forces on fascicle behavior and force production capacity to describe muscle function in a more comprehensive manner.

Limitations

A few aspects deserve further consideration for the interpretation of the present data. The final sample size (n = 9) was lower than the sample size ($n \geq 10$) suggested after our *a priori* power analysis. Dropouts and exclusions of data of insufficient quality could not be prevented. However, the effect sizes of the differences discussed here are satisfactory; nevertheless, for completeness, the results should be verified in a future study against a matched control population with a greater sample size.

Furthermore, we used mean values of variables describing fascicular behavior. Although this approach omits testing differences at discrete time points, this choice was justified by two criteria. Firstly, it was our intention to capture substantial differences relative to tissue loading and unloading. Secondly, there was no obvious rationale to support the choice of discrete time points. Additionally, statistical parametric mapping analyses done *a posteriori* (**Supplementary Figure 2**; Bankosz and Winiarski, 2020) did not suggest that significant differences may have been masked by the present approach.

In general, the length- and velocity-dependent force potentials are based on the assumptions of biological consistency and best-fit approximations. Consequently, no model is exempt from inaccuracies. Our models could have been enhanced with additional data collection as previously described for the force-length relationship (de Brito Fontana and Herzog, 2016; Nikolaidou et al., 2017; Bohm et al., 2019, 2021) and the force-velocity relationship (Hauraix et al., 2015). Unfortunately, the large project encompassing this study did not allow additional measurements.

Similarly, for the calculations of the velocity-dependent force potential, maximum shortening velocity and normalized Hill constant (a_{rel}) were estimated based on normative data for fiber type distribution in GM muscles (type I fibers: 50.8%, type II fibers: 49.2%) (Johnson et al., 1973). As we cannot discard the possible influence of this parameter on side-to-side differences, speculating about the potential role of fiber type distribution in the present data should be avoided.

CONCLUSION

The results of this study indicate that sarcomere operating length and lower limbs kinematics are relatively preserved during walking in ATR patients more than 2 years post-surgery. Despite atrophy in the longitudinal and transversal planes of the affected GM muscle, fascicles were found to operate at contractile velocities comparable to or lower than those of the non-operated leg during the stance phase. An increased fascicle rotation during stance may contribute to preserving fascicle contractile velocity. Collectively, these results suggest that the contractile behavior of the GM muscle does not limit force production under the present walking condition and in ATR patients with a similar level of recovery.

DATA AVAILABILITY STATEMENT

The raw data supporting the conclusions of this article will be made available by the authors, without undue reservation.

ETHICS STATEMENT

The studies involving human participants were reviewed and approved by the institutional review board of the German Sport University Cologne. The patients/participants provided their written informed consent to participate in this study.

AUTHOR CONTRIBUTIONS

G-PB and KA conceptualized the research. BS, GL, G-PB, and KA designed the research. BS acquired the data. BS and KA analyzed the data. BS, OS, and KA interpreted the data and drafted the manuscript. BS, OS, GL, G-PB, and KA revised the manuscript. All authors approved the final manuscript.

SUPPLEMENTARY MATERIAL

The Supplementary Material for this article can be found online at: https://www.frontiersin.org/articles/10.3389/fphys.2022.792576/full#supplementary-material

REFERENCES

Aggeloussis, N., Giannakou, E., Albracht, K., and Arampatzis, A. (2010). Reproducibility of fascicle length and pennation angle of gastrocnemius medialis in human gait in vivo. *Gait Posture* 31, 73–77. doi: 10.1016/j.gaitpost.2009.08.249

Agres, A. N., Duda, G. N., Gehlen, T. J., Arampatzis, A., Taylor, W. R., and Manegold, S. (2015). Increased unilateral tendon stiffness and its effect on gait 2-6 years after Achilles tendon rupture. *Scand. J. Med. Sci. Sports* 25, 860–867. doi: 10.1111/sms.12456

Azizi, E., Brainerd, E. L., and Roberts, T. J. (2008). Variable gearing in pennate muscles. *Proc. Natl. Acad. Sci. U.S.A.* 105, 1745–1750. doi: 10.1073/pnas.0709212105

Bahler, A. S., Fales, J. T., and Zierler, K. L. (1968). The dynamic properties of mammalian skeletal muscle. *J. Gen. Physiol.* 51, 369–384. doi: 10.1085/jgp.51.3.369

Bankosz, Z., and Winiarski, S. (2020). Statistical parametric mapping reveals subtle gender differences in angular movements in table tennis topspin backhand. *Int. J. Environ. Res. Public Health* 17:6996. doi: 10.3390/ijerph17196996

Baxter, J. R., Hullfish, T. J., and Chao, W. (2018). Functional deficits may be explained by plantarflexor remodeling following Achilles tendon rupture repair: preliminary findings. *J. Biomech.* 79, 238–242. doi: 10.1016/j.jbiomech.2018.08.016

Bohm, S., Mersmann, F., Santuz, A., and Arampatzis, A. (2019). The force-length-velocity potential of the human soleus muscle is related to the energetic cost of running. *Proc. Biol. Sci.* 286:20192560. doi: 10.1098/rspb.2019.2560

Bohm, S., Mersmann, F., Santuz, A., and Arampatzis, A. (2021). Enthalpy efficiency of the soleus muscle contributes to improvements in running economy. *Proc. Biol. Sci.* 288:20202784. doi: 10.1098/rspb.2020.2784

Brainerd, E. L., and Azizi, E. (2005). Muscle fiber angle, segment bulging and architectural gear ratio in segmented musculature. *J. Exp. Biol.* 208, 3249–3261. doi: 10.1242/jeb.01770

Cohen, J. (1988). *Statistical Power Analysis for the Behavioral Sciences*. Amsterdam: Elsevier Science.

Cronin, N. J., and Lichtwark, G. (2013). The use of ultrasound to study muscle-tendon function in human posture and locomotion. *Gait Posture* 37, 305–312. doi: 10.1016/j.gaitpost.2012.07.024

Cureton, E. E. (1956). Rank-biserial correlation. *Psychometrika* 21, 287–290. doi: 10.1007/bf02289138

de Brito Fontana, H., and Herzog, W. (2016). Vastus lateralis maximum force-generating potential occurs at optimal fascicle length regardless of activation level. *Eur. J. Appl. Physiol.* 116, 1267–1277. doi: 10.1007/s00421-016-3381-3

Don, R., Ranavolo, A., Cacchio, A., Serrao, M., Costabile, F., Iachelli, M., et al. (2007). Relationship between recovery of calf-muscle biomechanical properties and gait pattern following surgery for achilles tendon rupture. *Clin. Biomech. (Bristol, Avon)* 22, 211–220. doi: 10.1016/j.clinbiomech.2006.10.001

Farris, D. J., and Lichtwark, G. A. (2016). UltraTrack: software for semi-automated tracking of muscle fascicles in sequences of B-mode ultrasound images. *Comput. Methods Programs Biomed.* 128, 111–118. doi: 10.1016/j.cmpb.2016.02.016

Farris, D. J., and Sawicki, G. S. (2012). Human medial gastrocnemius force-velocity behavior shifts with locomotion speed and gait. *Proc. Natl. Acad. Sci. U.S.A.* 109, 977–982. doi: 10.1073/pnas.1107972109

Farris, D. J., Lichtwark, G. A., Brown, N. A., and Cresswell, A. G. (2016). The role of human ankle plantar flexor muscle-tendon interaction and architecture in maximal vertical jumping examined in vivo. *J. Exp. Biol.* 219, 528–534. doi: 10.1242/jeb.126854

Faul, F., Erdfelder, E., Lang, A. G., and Buchner, A. (2007). G*Power 3: a flexible statistical power analysis program for the social, behavioral, and biomedical sciences. *Behav. Res. Methods* 39, 175–191. doi: 10.3758/bf03193146

Fukunaga, T., Kubo, K., Kawakami, Y., Fukashiro, S., Kanehisa, H., and Maganaris, C. N. (2001). In vivo behaviour of human muscle tendon during walking. *Proc. Biol. Sci.* 268, 229–233. doi: 10.1098/rspb.2000.1361

Geremia, J. M., Bobbert, M. F., Casa Nova, M., Ott, R. D., Lemos Fde, A., Lupion Rde, O., et al. (2015). The structural and mechanical properties of the Achilles tendon 2 years after surgical repair. *Clin. Biomech. (Bristol, Avon)* 30, 485–492. doi: 10.1016/j.clinbiomech.2015.03.005

Gollapudi, S. K., and Lin, D. C. (2009). Experimental determination of sarcomere force-length relationship in type-I human skeletal muscle fibers. *J. Biomech.* 42, 2011–2016. doi: 10.1016/j.jbiomech.2009.06.013

Hauraix, H., Nordez, A., Guilhem, G., Rabita, G., and Dorel, S. (2015). In vivo maximal fascicle-shortening velocity during plantar flexion in humans. *J. Appl. Physiol. (1985)* 119, 1262–1271. doi: 10.1152/japplphysiol.00542.2015

Hawkins, D., and Hull, M. L. (1990). A method for determining lower extremity muscle-tendon lengths during flexion/extension movements. *J. Biomech.* 23, 487–494. doi: 10.1016/0021-9290(90)90304-l

Heikkinen, J., Lantto, I., Piilonen, J., Flinkkila, T., Ohtonen, P., Siira, P., et al. (2017). Tendon length, calf muscle atrophy, and strength deficit after acute achilles tendon rupture: long-term follow-up of patients in a previous study. *J. Bone Joint Surg. Am.* 99, 1509–1515. doi: 10.2106/JBJS.16.01491

Herzog, W., Abrahamse, S. K., and Ter Keurs, H. E. (1990). Theoretical determination of force-length relations of intact human skeletal muscles using the cross-bridge model. *Pflugers Arch.* 416, 113–119. doi: 10.1007/BF00370231

Hill, A. V. (1938). The heat of shortening and the dynamic constants of muscle. *Proc. R. Soc. Lond. Ser. B Biol. Sci.* 126, 136–195. doi: 10.1152/advan.00072.2005

Hill, A. V. (1953). The mechanics of active muscle. *Proc. R. Soc. Lond. B Biol. Sci.* 141, 104–117.

Ishikawa, M., Pakaslahti, J., and Komi, P. V. (2007). Medial gastrocnemius muscle behavior during human running and walking. *Gait Posture* 25, 380–384. doi: 10.1016/j.gaitpost.2006.05.002

Jandacka, D., Plesek, J., Skypala, J., Uchytil, J., Silvernail, J. F., and Hamill, J. (2018). Knee joint kinematics and kinetics during walking and running after surgical achilles tendon repair. *Orthop. J. Sports Med.* 6:2325967118779862. doi: 10.1177/2325967118779862

Jandacka, D., Silvernail, J. F., Uchytil, J., Zahradnik, D., Farana, R., and Hamill, J. (2017). Do athletes alter their running mechanics after an Achilles tendon rupture? *J. Foot Ankle Res.* 10:53. doi: 10.1186/s13047-017-0235-0

Johnson, M. A., Polgar, J., Weightman, D., and Appleton, D. (1973). Data on the distribution of fibre types in thirty-six human muscles. An autopsy study. *J. Neurol. Sci.* 18, 111–129. doi: 10.1016/0022-510x(73)90023-3

Kerby, D. S. (2014). The simple difference formula: an approach to teaching nonparametric correlation. *Compr. Psychol.* 3, 2165–2228.

Millard, M. (2021). *OpenSim:: ActiveForceLengthCurve Class Reference. In API Guide for C++ developers*. Available online at: https://simtk.org/api_docs/opensim/api_docs/classOpenSim_1_1ActiveForceLengthCurve.html (accessed September 15, 2021).

Millard, M., Uchida, T., Seth, A., and Delp, S. L. (2013). Flexing computational muscle: modeling and simulation of musculotendon dynamics. *J. Biomech. Eng.* 135:021005. doi: 10.1115/1.4023390

Mullaney, M. J., Mchugh, M. P., Tyler, T. F., Nicholas, S. J., and Lee, S. J. (2006). Weakness in end-range plantar flexion after Achilles tendon repair. *Am. J. Sports Med.* 34, 1120–1125. doi: 10.1177/0363546505284186

Muramatsu, T., Muraoka, T., Kawakami, Y., Shibayama, A., and Fukunaga, T. (2002). In vivo determination of fascicle curvature in contracting human skeletal muscles. *J. Appl. Physiol. (1985)* 92, 129–134. doi: 10.1152/jappl.2002.92.1.129

Neptune, R. R., and Sasaki, K. (2005). Ankle plantar flexor force production is an important determinant of the preferred walk-to-run transition speed. *J. Exp. Biol.* 208, 799–808. doi: 10.1242/jeb.01435

Nigg, B. M., and Herzog, W. (1994). *Biomechanics Of The Musculo-Skeletal System*. Hoboken, NJ: Wiley.

Nikolaidou, M. E., Marzilger, R., Bohm, S., Mersmann, F., and Arampatzis, A. (2017). Operating length and velocity of human *M. vastus* lateralis fascicles during vertical jumping. *R. Soc. Open Sci.* 4:170185. doi: 10.1098/rsos.170185

Nilsson-Helander, K., Silbernagel, K. G., Thomee, R., Faxen, E., Olsson, N., Eriksson, B. I., et al. (2010). Acute achilles tendon rupture: a randomized, controlled study comparing surgical and nonsurgical treatments using validated outcome measures. *Am. J. Sports Med.* 38, 2186–2193. doi: 10.1177/0363546510376052

Parvataneni, K., Ploeg, L., Olney, S. J., and Brouwer, B. (2009). Kinematic, kinetic and metabolic parameters of treadmill versus overground walking in healthy older adults. *Clin. Biomech. (Bristol, Avon)* 24, 95–100. doi: 10.1016/j.clinbiomech.2008.07.002

Peng, W. C., Chao, Y. H., Fu, A. S. N., Fong, S. S. M., Rolf, C., Chiang, H., et al. (2019). Muscular morphomechanical characteristics after an achilles repair. *Foot Ankle Int.* 40, 568–577. doi: 10.1177/1071100718822537

Pohle-Fröhlich, R., Dalitz, C., Richter, C., Hahnen, T., Stäudle, B., and Albracht, K. (2020). "Estimation of muscle fascicle orientation in ultrasonic images," in *Proceedings of the 15th International Joint conference on Computer Vision, Imaging and computer Graphics Theory and Applications*, Valletta, 79–86.

Riley, P. O., Paolini, G., Della Croce, U., Paylo, K. W., and Kerrigan, D. C. (2007). A kinematic and kinetic comparison of overground and treadmill walking in healthy subjects. *Gait Posture* 26, 17–24. doi: 10.1016/j.gaitpost.2006.07.003

Robertson, D. G. E., Caldwell, G. E., Hamill, J., Kamen, G., and Whittlesey, S. (2013). *Research Methods in Biomechanics*. Champaign, IL: Human Kinetics.

Sanchez, G. N., Sinha, S., Liske, H., Chen, X., Nguyen, V., Delp, S. L., et al. (2015). In vivo imaging of human sarcomere twitch dynamics in individual motor units. *Neuron* 88, 1109–1120. doi: 10.1016/j.neuron.2015.11.022

Seth, A., Hicks, J. L., Uchida, T. K., Habib, A., Dembia, C. L., Dunne, J. J., et al. (2018). OpenSim: simulating musculoskeletal dynamics and

neuromuscular control to study human and animal movement. *PLoS Comput. Biol.* 14:e1006223. doi: 10.1371/journal.pcbi.1006223

Silbernagel, K. G., Steele, R., and Manal, K. (2012). Deficits in heel-rise height and achilles tendon elongation occur in patients recovering from an Achilles tendon rupture. *Am. J. Sports Med.* 40, 1564–1571. doi: 10.1177/0363546512447926

Speedtsberg, M. B., Kastoft, R., Barfod, K. W., Penny, J. O., and Bencke, J. (2019). Gait function and postural control 4.5 years after nonoperative dynamic treatment of acute achilles tendon ruptures. *Orthop. J. Sports Med.* 7:2325967119854324. doi: 10.1177/2325967119854324

Stäudle, B., Seynnes, O., Laps, G., Goll, F., Bruggemann, G. P., and Albracht, K. (2021). Recovery from achilles tendon repair: a combination of postsurgery outcomes and insufficient remodeling of muscle and tendon. *Med. Sci. Sports Exerc.* 53, 1356–1366. doi: 10.1249/MSS.0000000000002592

Svensson, R. B., Couppé, C., Agergaard, A.-S., Josefsen, C. O., Jensen, M. H., Weisskirchner Barfod, K., et al. (2019). Persistent functional loss following ruptured Achilles tendon is associated with reduced gastrocnemius muscle fascicle length, elongated gastrocnemius and soleus tendon, and reduced muscle cross-sectional area. *Transl. Sports Med.* 2, 316–324. doi: 10.1002/tsm2.103

Tengman, T., and Riad, J. (2013). Three-dimensional gait analysis following achilles tendon rupture with nonsurgical treatment reveals long-term deficiencies in muscle strength and function. *Orthop. J. Sports Med.* 1:2325967113504734. doi: 10.1177/2325967113504734

Thomas, S., Reading, J., and Shephard, R. J. (1992). Revision of the physical activity readiness questionnaire (PAR-Q). *Can. J. Sport Sci.* 17, 338–345.

Ward, S. R., Eng, C. M., Smallwood, L. H., and Lieber, R. L. (2009). Are current measurements of lower extremity muscle architecture accurate? *Clin. Orthop. Relat. Res.* 467, 1074–1082. doi: 10.1007/s11999-008-0594-8

Wenning, M., Mauch, M., Heitner, A., Lienhard, J., Ritzmann, R., and Paul, J. (2021). Neuromechanical activation of triceps surae muscle remains altered at 3.5 years following open surgical repair of acute Achilles tendon rupture. *Knee Surg. Sports Traumatol. Arthrosc.* 29, 2517–2527. doi: 10.1007/s00167-021-06512-z

Werkhausen, A., Cronin, N. J., Albracht, K., Paulsen, G., Larsen, A. V., Bojsen-Moller, J., et al. (2019). Training-induced increase in Achilles tendon stiffness affects tendon strain pattern during running. *PeerJ* 7:e6764. doi: 10.7717/peerj.6764

Williams, P. E., and Goldspink, G. (1973). The effect of immobilization on the longitudinal growth of striated muscle fibres. *J. Anat.* 116, 45–55.

Willy, R. W., Brorsson, A., Powell, H. C., Willson, J. D., Tranberg, R., and Gravare Silbernagel, K. (2017). Elevated knee joint kinetics and reduced ankle kinetics are present during jogging and hopping after achilles tendon ruptures. *Am. J. Sports Med.* 45, 1124–1133. doi: 10.1177/0363546516685055

Winters, J. M., and Stark, L. (1988). Estimated mechanical properties of synergistic muscles involved in movements of a variety of human joints. *J. Biomech.* 21, 1027–1041. doi: 10.1016/0021-9290(88)90249-7

Zajac, F. E. (1989). Muscle and tendon: properties, models, scaling, and application to biomechanics and motor control. *Crit. Rev. Biomed. Eng.* 17, 359–411.

Conflict of Interest: The authors declare that the research was conducted in the absence of any commercial or financial relationships that could be construed as a potential conflict of interest.

Advantages of publishing in Frontiers

OPEN ACCESS
Articles are free to read for greatest visibility and readership

FAST PUBLICATION
Around 90 days from submission to decision

HIGH QUALITY PEER-REVIEW
Rigorous, collaborative, and constructive peer-review

TRANSPARENT PEER-REVIEW
Editors and reviewers acknowledged by name on published articles

Frontiers
Avenue du Tribunal-Fédéral 34
1005 Lausanne | Switzerland

Visit us: www.frontiersin.org
Contact us: frontiersin.org/about/contact

REPRODUCIBILITY OF RESEARCH
Support open data and methods to enhance research reproducibility

DIGITAL PUBLISHING
Articles designed for optimal readership across devices

FOLLOW US
@frontiersin

IMPACT METRICS
Advanced article metrics track visibility across digital media

EXTENSIVE PROMOTION
Marketing and promotion of impactful research

LOOP RESEARCH NETWORK
Our network increases your article's readership